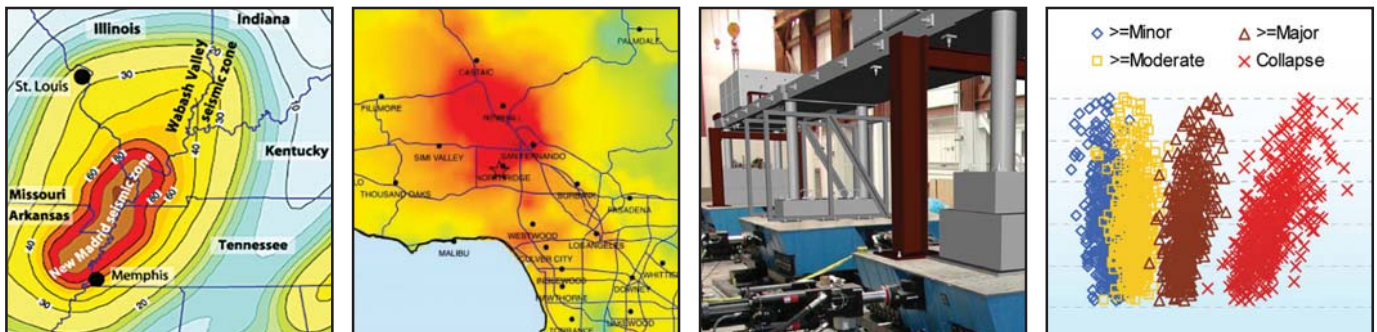


# Fragility Considerations in Highway Bridge Design

by  
**M. Shinozuka, S. Banerjee and S.-H. Kim**



Technical Report MCEER-07-0023

December 14, 2007

## NOTICE

This report was prepared by the University of California Irvine as a result of research sponsored by MCEER through a contract from the Federal Highway Administration. Neither MCEER, associates of MCEER, its sponsors, the University of California Irvine, nor any person acting on their behalf:

- a. makes any warranty, express or implied, with respect to the use of any information, apparatus, method, or process disclosed in this report or that such use may not infringe upon privately owned rights; or
- b. assumes any liabilities of whatsoever kind with respect to the use of, or the damage resulting from the use of, any information, apparatus, method, or process disclosed in this report.

Any opinions, findings, and conclusions or recommendations expressed in this publication are those of the author(s) and do not necessarily reflect the views of MCEER or the Federal Highway Administration.

---

## Fragility Considerations in Highway Bridge Design

by

M. Shinozuka,<sup>1</sup> S. Banerjee<sup>2</sup> and S-H. Kim<sup>3</sup>

Publication Date: December 14, 2007

Submittal Date: November 25, 2007

Technical Report MCEER-07-0023

Task Number 094-B-1.5

FHWA Contract Number DTFH61-98-C-00094

Contract Officer's Technical Representative: W. Phillip Yen, Ph.D., P.E. HRDI-7  
Senior Research Structural Engineer/Seismic Research Program Manager  
Federal Highway Administration

- 1 Distinguished Professor and Chair, Department of Civil and Environmental Engineering, University of California Irvine
- 2 Post-Doctoral Researcher, Department of Civil and Environmental Engineering, University of California Irvine
- 3 Former Graduate Student, Department of Civil and Environmental Engineering, University of California Irvine

MCEER

University at Buffalo, The State University of New York

Red Jacket Quadrangle, Buffalo, NY 14261

Phone: (716) 645-3391; Fax (716) 645-3399

E-mail: [mceer@buffalo.edu](mailto:mceer@buffalo.edu); WWW Site: <http://mceer.buffalo.edu>

---



## Preface

The Multidisciplinary Center for Earthquake Engineering Research (MCEER) is a national center of excellence in advanced technology applications that is dedicated to the reduction of earthquake losses nationwide. Headquartered at the University at Buffalo, State University of New York, the Center was originally established by the National Science Foundation in 1986, as the National Center for Earthquake Engineering Research (NCEER).

Comprising a consortium of researchers from numerous disciplines and institutions throughout the United States, the Center's mission is to reduce earthquake losses through research and the application of advanced technologies that improve engineering, pre-earthquake planning and post-earthquake recovery strategies. Toward this end, the Center coordinates a nationwide program of multidisciplinary team research, education and outreach activities.

MCEER's research is conducted under the sponsorship of two major federal agencies, the National Science Foundation (NSF) and the Federal Highway Administration (FHWA), and the State of New York. Significant support is also derived from the Federal Emergency Management Agency (FEMA), other state governments, academic institutions, foreign governments and private industry.

The Center's Highway Project develops improved seismic design, evaluation, and retrofit methodologies and strategies for new and existing bridges and other highway structures, and for assessing the seismic performance of highway systems. The FHWA has sponsored three major contracts with MCEER under the Highway Project, two of which were initiated in 1992 and the third in 1998.

Of the two 1992 studies, one performed a series of tasks intended to improve seismic design practices for new highway bridges, tunnels, and retaining structures (MCEER Project 112). The other study focused on methodologies and approaches for assessing and improving the seismic performance of existing "typical" highway bridges and other highway system components including tunnels, retaining structures, slopes, culverts, and pavements (MCEER Project 106). These studies were conducted to:

- assess the seismic vulnerability of highway systems, structures, and components;
- develop concepts for retrofitting vulnerable highway structures and components;
- develop improved design and analysis methodologies for bridges, tunnels, and retaining structures, which include consideration of soil-structure interaction mechanisms and their influence on structural response; and
- develop, update, and recommend improved seismic design and performance criteria for new highway systems and structures.

The 1998 study, “Seismic Vulnerability of the Highway System” (FHWA Contract DTFH61-98-C-00094; known as MCEER Project 094), was initiated with the objective of performing studies to improve the seismic performance of bridge types not covered under Projects 106 or 112, and to provide extensions to system performance assessments for highway systems. Specific subjects covered under Project 094 include:

- development of formal loss estimation technologies and methodologies for highway systems;
- analysis, design, detailing, and retrofitting technologies for special bridges, including those with flexible superstructures (e.g., trusses), those supported by steel tower substructures, and cable-supported bridges (e.g., suspension and cable-stayed bridges);
- seismic response modification device technologies (e.g., hysteretic dampers, isolation bearings); and
- soil behavior, foundation behavior, and ground motion studies for large bridges.

In addition, Project 094 includes a series of special studies, addressing topics that range from non-destructive assessment of retrofitted bridge components to supporting studies intended to assist in educating the bridge engineering profession on the implementation of new seismic design and retrofitting strategies.

*This report integrates statistical and analytical methods for the seismic performance evaluation of highway transportation networks. Bridge damageability is expressed in the form of fragility curves, represented by two-parameter lognormal distribution functions, in which fragility parameters are estimated through the maximum likelihood procedure. Empirical fragility curves are developed utilizing bridge damage data obtained from past earthquakes, particularly the 1994 Northridge earthquake. They are then used to construct a mechanistic model which calibrates analytical damage states with empirical damage data so that analysis becomes consistent with past experience. Using these calibrated threshold damage states, analytical fragility curves are generated through nonlinear static and dynamic procedures for typical bridges in the transportation network in Los Angeles and Orange counties. The application of fragility curves in the performance-based design of bridges is demonstrated and a design acceptance criteria is suggested that verifies the target performance level of a newly designed bridge under a prescribed level of seismic hazard.*

## ABSTRACT

This report integrates statistical and analytical methods for the prediction of seismic performance of highway transportation networks. For this purpose, an integrated framework involving the structural engineering module of multilayer simulation scheme is developed. This module is a key component of the performance simulation of such spatially distributed systems. In the analysis, it is assumed that bridges are the only components of the network system vulnerable to earthquake ground motion. Because of the predictive nature of the analysis, ground motion intensity at bridge sites can be described at best in terms of PGA, PGV, or SA. The frequency domain information of the bridges may not be readily available for most of the bridges. Also, the nonlinear range of dynamic response behavior is involved for the damage prediction. Therefore, even the SA information is not directly useful for predicting the state of damage of a large number of bridges (two thousands of them for Los Angeles County) under also a large number (typically 50) of scenario earthquakes. This is the reason for employing the fragility curve approach to develop the state of damage of the network components in a large spatially distributed seismic hazard footprint.

Bridge seismic damageability at various damage conditions is expressed in the form of fragility curves associated with the states of minor, moderate, major and collapse damage, mechanistically defined in terms of the extent of ductility rotation of bridge columns at the bottom and top. These fragility curves are defined by two-parameter lognormal distribution functions in which parameters (referred to as fragility parameters) are estimated with the aid of the maximum likelihood procedure. This study considers standard reinforced concrete bridges in southern California, and describes the characteristics of bridges and surrounding soil in terms of skew angle, single or multiple span, and soil conciliations (hard, medium, or soft). Empirical fragility curves of more than 2000 RC bridges are developed utilizing bridge damage data obtained from past earthquakes, particularly the 1994 Northridge earthquake. Numerical simulation of bridge seismic response is carried out by developing nonlinear finite element models of five standard RC bridges. In these models, bilinear rotational springs are introduced at each column end that represents the hysteretic nature of energy dissipation of column plastic hinge regions. A mechanistic model is developed to calibrate analytical damage with empirical damage data so that analysis becomes consistent with past experience. This calibration results in the threshold damage limits, which are further utilized to generate analytical fragility curves. In addition, enhancement in bridge seismic characteristics due to retrofit is demonstrated by comparing analytical fragility curves developed for these five bridges before and after retrofitting them with steel jackets. These five analytical bridges represent different bridge classes for retrofit purpose as they are consisting of columns with various cross-sections such as circular, rectangular, and oblong.

Furthermore, this report demonstrates the application of fragility curves in the performance-based seismic design of bridges. On the basis of statistical and analytical tools discussed here, a design acceptance criterion is suggested that can verify the target performance level of a newly designed bridge under a prescribed level of seismic hazard.





## **ACKNOWLEDGMENT**

This study was supported by the Federal Highway Administration under contracts DTFH61-92-C-00106 and DTFH61-98-C-00094 through the Multidisciplinary Center for Earthquake Engineering Research (MCEER) in Buffalo, NY.



## TABLE OF CONTENTS

SECTION	TITLE	PAGE
<b>1</b>	<b>INTRODUCTION</b>	<b>1</b>
<b>2</b>	<b>STATISTICAL ANALYSIS OF FRAGILITY CURVES</b>	<b>5</b>
2.1	Fragility Curves for Structural Sub-Sets of Caltrans' Bridges	5
2.1.1	Method 1 and Method 2	5
2.1.2	Method 3	20
2.1.3	Development of Fragility Curves using Weibull Distribution	25
2.2	Test of Goodness of Fit	26
2.2.1	Method 1	26
2.2.2	Method 2	29
2.3	Estimation of Confidence Intervals	30
<b>3</b>	<b>MODEL-BASED UNCERTAINTY ANALYSIS OF FRAGILITY CURVES</b>	<b>37</b>
3.1	Realization of Parameters: Monte Carlo Simulation	39
3.1.1	Realization Based on Method 1	39
3.1.2	Realization Based on Method 2	39
3.2	Confidence Interval	40
3.2.1	Confidence Interval Based on Method 1	40
3.2.2	Confidence Interval Based on Method 2	44
3.3	Summary	47
<b>4</b>	<b>DEVELOPMENT OF ANALYTICAL FRAGILITY CURVES</b>	<b>49</b>
4.1	Time History Analysis of Bridges	49
4.1.1	Analytical Fragility Curves in Longitudinal Direction	49
4.1.2	Analytical Fragility Curves in Transverse Direction	54
4.2	Fragility Curve Development using Capacity Spectrum Method (CSM)	56
4.2.1	Fragility Analysis in Longitudinal Direction	56
4.2.2	Fragility Analysis in Transverse Direction	57
4.2.3	Comparison of Analytical Fragility Curves	58
4.3	Fragility Enhancement after Column Retrofit	60
4.4	Calibration of Analytical Fragility Curves with Damage Data	66
4.4.1	Comparison of Analytical Fragility Curves with Empirical Data	66
4.4.2	Estimation of Ductility Capacities at Various Damage States	67
4.5	Effect of Ground Motion Directionality on Fragility Characteristics of Bridges	70
4.5.1	Case I: Fragility Curves for two Orthogonal Components	71
4.5.2	Case II: Fragility Curves for one Inclined Component	74

## **TABLE OF CONTENTS (CONT'D)**

<b>SECTION</b>	<b>TITLE</b>	<b>PAGE</b>
<b>5</b>	<b>ANALYTICAL FRAGILITY CURVES OF MEMPHIS BRIDGES</b>	<b>77</b>
<b>6</b>	<b>COMPARISON OF FRAGILITY CURVES</b>	<b>85</b>
	6.1 Comparison of Analytical Fragility Curves with other Fragility Curves	85
	6.2 Comparison of Empirical Fragility Curves with HAZUS	91
<b>7</b>	<b>VERIFICATION OF BRIDGE DAMAGE STATE DEFINITIONS THROUGH EXPERIMENTAL DATA</b>	<b>93</b>
	7.1 Experimental Study	93
	7.1.1 Low and High Amplitude Tests	94
	7.1.2 Bridge Response and Progressive Damage in Columns	95
	7.2 Comparison between Experimental and Analytical Result	96
	7.2.1 Bridge Damage States	96
	7.2.2 Moment-Rotation Analysis	98
	7.2.3 Rotational Ductility of Bridge Columns at Various Damage States	100
	7.2.4 Comparison of Threshold Damage Limits	102
	7.3 Discussion of Results	103
<b>8</b>	<b>DEVELOPMENT OF DESIGN STRATEGY</b>	<b>105</b>
<b>9</b>	<b>CONCLUSIONS</b>	<b>109</b>
<b>10</b>	<b>REFERENCES</b>	<b>111</b>
	<b>APPENDIX A</b>	<b>115</b>
	<b>APPENDIX B</b>	<b>123</b>
	<b>APPENDIX C</b>	<b>147</b>

## LIST OF ILLUSTRATIONS

FIGURE	TITLE	PAGE
1-1	Method of Evaluating Performance of Highway Network System	2
2-1	Fragility Curves for a Second Level Subset (Caltrans' Bridges; Single Span) by Method 2	10
2-2	Fragility Curves for a Second Level Subset (Caltrans' Bridges; Multiple Span) by Method 2	10
2-3	Fragility Curves for a Second Level Subset (Caltrans' Bridges; Soil A) by Method 2	11
2-4	Fragility Curves for a Second Level Subset (Caltrans' Bridges; Soil B) by Method 2	11
2-5	Fragility Curves for a Second Level Subset (Caltrans' Bridges; Soil C) by Method 2	12
2-6	Fragility Curves for a Second Level Subset (Caltrans' Bridges; skew $\leq 20$ ) by Method 2	12
2-7	Fragility Curves for a Second Level Subset (Caltrans' Bridges; $20 < \text{skew} \leq 60$ ) by Method 2	13
2-8	Fragility Curves for a Second Level Subset (Caltrans' Bridges; skew $> 60$ ) by Method 2	13
2-9	Fragility Curves for a Fourth Level Subset (Caltrans' Bridges; single span/ $0 \leq \text{skew} \leq 20$ /soil A) by Method 2	14
2-10	Fragility Curves for a Fourth Level Subset (Caltrans' Bridges; single span/ $0 \leq \text{skew} \leq 20$ /soil B) by Method 2	14
2-11	Fragility Curves for a Fourth Level Subset (Caltrans' Bridges; single span/ $0 \leq \text{skew} \leq 20$ /soil C) by Method 2	15
2-12	Fragility Curves for a Fourth Level Subset (Caltrans' Bridges; single span/ $20 < \text{skew} \leq 60$ /soil C) by Method 2	15
2-13	Fragility Curves for a Fourth Level Subset (Caltrans' Bridges; single span/ $60 < \text{skew}$ /soil C) by Method 2	16
2-14	Fragility Curves for a Fourth Level Subset (Caltrans' Bridges; multiple span/ $0 \leq \text{skew} \leq 20$ /soil A) by Method 2	16
2-15	Fragility Curves for a Fourth Level Subset (Caltrans' Bridges; multiple span/ $0 \leq \text{skew} \leq 20$ /soil C) by Method 2	17
2-16	Fragility Curves for a Fourth Level Subset (Caltrans' Bridges; multiple span/ $20 < \text{skew} \leq 60$ /soil A) by Method 2	17
2-17	Fragility Curves for a Fourth Level Subset (Caltrans' Bridges; multiple span/ $20 < \text{skew} \leq 60$ /soil B) by Method 2	18
2-18	Fragility Curves for a Fourth Level Subset (Caltrans' Bridges; multiple span/ $20 < \text{skew} \leq 60$ /soil C) by Method 2	18
2-19	Fragility Curves for a Fourth Level Subset (Caltrans' Bridges; multiple span/ $60 < \text{skew}$ /soil A) by Method 2	19
2-20	Fragility Curves for a Fourth Level Subset (Caltrans' Bridges; multiple span/ $60 < \text{skew}$ /soil B) by Method 2	19

## LIST OF ILLUSTRATIONS (CONT'D)

FIGURE	TITLE	PAGE
2-21	Fragility Curves for a Fourth Level Subset (Caltrans' Bridges; multiple span/60 < skew/soil C) by Method 2	20
2-22	Fragility Curve for Caltrans' Bridges developed in Method 1 and Method 3 and Input Damage Data (Method 3) with 'At least Minor' Damage	21
2-23	Fragility Curve for Caltrans' Bridges developed in Method 1 and Method 3 and Input Damage Data (Method 3) with 'At least Moderate' Damage	21
2-24	Fragility Curve for Caltrans' Bridges developed in Method 1 and Method 3 and Input Damage Data (Method 3) with 'At least Major' Damage	22
2-25	Fragility Curve for Caltrans' Bridges developed in Method 1 and Method 3 and Input Damage Data (Method 3) with 'Collapse'	22
2-26	Fragility Curve for Caltrans' Bridges developed in Method 2 and Method 3 and Input Damage Data (Method 3) with 'At least Minor' Damage	23
2-27	Fragility Curve for Caltrans' Bridges developed in Method 2 and Method 3 and Input Damage Data (Method 3) with 'At least Moderate' Damage	23
2-28	Fragility Curve for Caltrans' Bridges developed in Method 2 and Method 3 and Input Damage Data (Method 3) with 'At least Major' Damage	24
2-29	Fragility Curve for Caltrans' Bridges developed in Method 2 and Method 3 and Input Damage Data (Method 3) with 'Collapse'	24
2-30	Fragility Curve for Caltrans' Bridges developed in Method 1 using Weibull Distribution	26
2-31	Validity of Asymptotic Normality of Statistic $Y^2$ (Caltrans' Bridges with at least Minor Damage/Method 1)	27
2-32	Validity of Asymptotic Normality of Statistic $Y^2$ (Caltrans' Bridges with at least Moderate Damage/Method 1)	27
2-33	Validity of Asymptotic Normality of Statistic $Y^2$ (Caltrans' Bridges with at least Major Damage/Method 1)	28
2-34	Validity of Asymptotic Normality of Statistic $Y^2$ (Caltrans' Bridges with Collapse Damage/Method 1)	28
2-35	Validity of Asymptotic Normality of Statistic $Y^2$ (Caltrans' Bridges/Method 2)	29
2-36	Two-Dimensional Plot of 500 Sets of Simulated Realizations of Medians ( $\hat{C}_1, \hat{C}_2, \hat{C}_3, \hat{C}_4$ ) and Log-Standard Deviations $\hat{\xi}$	31
2-37	Log-Normal Plot of Realizations of 500 Realizations of (Caltrans' Bridges/Method 2)	31
2-38	Log-Normal Plot of Realizations of 500 Realizations of $\hat{C}_2$ (Caltrans' Bridges/Method 2)	32
2-39	Log-Normal Plot of Realizations of 500 Realizations of $\hat{C}_3$ (Caltrans' Bridges/Method 2)	32
2-40	Log-Normal Plot of Realizations of 500 Realizations of $\hat{C}_4$ (Caltrans' Bridges/Method 2)	33

## LIST OF ILLUSTRATIONS (CONT'D)

FIGURE	TITLE	PAGE
2-41	Log-Normal Plot of Realizations of 500 Realizations of $\hat{\xi}$ (Caltrans' Bridges/Method 2)	33
2-42	Fragility Curves for State of at least Minor Damage with 95%, 50% and 5% Statistical Confidence (Caltrans' Bridges/Method 2)	34
2-43	Fragility Curves for State of at least Moderate Damage with 95%, 50% and 5% Statistical Confidence (Caltrans' Bridges/Method 2)	34
2-44	Fragility Curves for State of at least Major Damage with 95%, 50% and 5% Statistical Confidence (Caltrans' Bridges/Method 2)	35
2-45	Fragility Curves for State of Collapse Damage with 95%, 50% and 5% Statistical Confidence (Caltrans' Bridges/Method 2)	35
2-46	Combined Plot of Fragility Curves for Caltrans' Bridges with 95%, 50% and 5% Statistical Confidence (Method 2)	36
3-1	Fragility curves ( $c^{60} = c^{30} = 0.55g$ , $\zeta^{60} = \zeta^{30} = 0.83$ )	38
3-2	Distribution of Simulated $c$ and $\zeta$ (Method 1)	41
3-3	Lognormal Plot of 500 Realizations of $c$	42
3-4	Statistical Uncertainty in terms of Sample Size (Method 1)	43
3-5	Confidence Bands Comparison	44
3-6	Distribution of Simulated $c_i$ and $\zeta$ (Method 2)	45
3-7	Statistical Uncertainty in terms of Sample Size (Method 2)	46
4-1	Elevation of Sample Bridges	50
4-2	Fragility Curves of Bridge 1 for Five Damage States	51
4-3	Fragility Curves of Bridge 2 for Five Damage States	51
4-4	Fragility Curves of Bridge 3 for Five Damage States	52
4-5	Fragility Curves of Bridge 4 for Five Damage States	52
4-6	Fragility Curves of Bridge 5 for Five Damage States	53
4-7	Fragility Curves of Bridge 2 Considering Abutment Stiffness	53
4-8	Fragility Curves of Bridge 1 for Five Damage States for Abutment Stiffness 14.57 kN/m	54
4-9	Fragility Curves of Bridge 2 for Five Damage States for Abutment Stiffness 14.57 kN/m	55
4-10	Fragility Curves of Bridge 1 for Five Damage States for Abutment Stiffness 7287.68 kN/m	55
4-11	Fragility Curves of Bridge 2 for Five Damage States for Abutment Stiffness 29150.73 kN/m	56
4-12	Fragility Curves of Bridge 2 in Longitudinal Direction from CSM	57
4-13	Fragility Curves of Bridge 2 in Transverse Direction from CSM	57
4-14	Comparison of Fragility Curves of Bridge 2 in Longitudinal Direction	58
4-15	Comparison of Fragility Curves of Bridge 2 in Transverse Direction	59
4-16	Fragility Curves of Bridge 2	61

## LIST OF ILLUSTRATIONS (CONT'D)

FIGURE	TITLE	PAGE
4-17	Fragility Curves of Bridge 3	62
4-18	Fragility Curves of Bridge 4	63
4-19	Fragility Curves of Bridge 5	64
4-20	Enhancement Curve for Circular Columns with Steel Jacketing	65
4-21	Enhancement Curve for Oblong Columns with Steel Jacketing	65
4-22	Enhancement Curve for Rectangular Columns with Steel Jacketing	65
4-23	Enhancement Curve for Five Sample Bridges with Steel Jacketing	65
4-24	Comparison of Empirical and Analytical Fragility Curves of Bridge 2	66
4-25	Empirical and Calibrated Analytical Fragility Curves at Minor Damage	68
4-26	Empirical and Calibrated Analytical Fragility Curves at Moderate Damage	69
4-27	Rotational Ductility Capacities at Various Damage States	70
4-28	Trajectory of Ground Acceleration Time Histories of El Centro Earthquake, 1940	71
4-29	Fragility Curves of Bridge 2 for State of Minor Damage (Case I)	72
4-30	Fragility Curves of Bridge 2 for State of Moderate Damage (Case I)	73
4-31	Fragility Curves of Bridge 2 for State of Major Damage (Case I)	73
4-32	Fragility Curves of Bridge 2 for State of Minor Damage (Case II)	75
4-33	Fragility Curves of Bridge 2 for State of Moderate Damage (Case II)	75
4-34	Fragility Curves of Bridge 2 for State of Major Damage (Case II)	76
5-1	A Representative Memphis Bridge	80
5-2	New Madrid Seismic Zone and Marked Tree, AR	81
5-3	Typical Ground Acceleration Time Histories in the Memphis Area	81
5-4	Average Spectral Accelerations in the Memphis Area	82
5-5	Fragility Curves for Memphis Bridges M1 and M2	82
5-6	Fragility Curve for Bridge M1 with Major Damage and Input Damage Data	83
5-7	Fragility Curve for Bridge M1 with at least Minor Damage and Input Damage Data	83
5-8	Comparison of Fragility Curves based on Sample Size 80 and 60 (Bridge M1 with at least Minor Damage)	84
5-9	Comparison of Fragility Curves based on Sample Size 80 and 60 (Bridge M1 with Major Damage)	84
6-1	Comparison of Fragility Curves of Bridge 2 at Minor Damage	86
6-2	Comparison of Fragility Curves of Bridge 2 at Moderate Damage	87
6-3	Comparison of Fragility Curves of Bridge 2 at Major Damage	87
6-4	Comparison of Fragility Curves of Bridge 4 at Minor Damage	88
6-5	Comparison of Fragility Curves of Bridge 4 at Moderate Damage	88
6-6	Comparison of Fragility Curves of Bridge 4 at Major Damage	89
6-7	Comparison of Fragility Curves of Bridge 5 at Minor Damage	89



## LIST OF ILLUSTRATIONS (CONT'D)

FIGURE	TITLE	PAGE
6-8	Comparison of Fragility Curves of Bridge 5 at Moderate Damage	90
6-9	Comparison of Fragility Curves of Bridge 5 at Major Damage	90
6-10	Comparison of Modification Factors for Different Skew Angles	92
6-11	Comparison of Modification Factors for Different Numbers of Bridge Spans	92
7-1	Experimental Model of a Two-Span Reinforced Concrete Bridge (Johnson et al. 2006)	94
7-2	Experimental Bridge Model on Shake Tables (Johnson et al. 2006)	94
7-3	Moment-Rotation Curve of Bent 1 and 3	99
7-4	Moment-Rotation Curve of Bent 2	100
7-5	Estimated Rotational Ductilities from Experimental Data	102
7-6	Rotational Ductilities Representing Threshold Limits of Bridge Damage	103
8-1	Performance Levels of Bridge under Seismic Excitation	105
8-2	Flow Chart: Method 1	106
8-3	Flow Chart: Method 2	106
8-4	Flow Chart: Method 3	108



## LIST OF TABLES

TABLE	TITLE	PAGE
2-1	Median and Log-Standard Deviation of Sample Sub-Divisions of Caltrans Bridges	7
2-2	Fragility Parameters using Weibull Distribution Function	25
2-3	$P_{Y^2}$ Values for Goodness of Fit	29
3-1	Variation of Simulated Median Values (Method 2)	46
3-2	Confidence Band of Fragility Median Values (Method 2)	46
4-1	Fragility Parameters (Median Values in g) for Empirical and Calibrated Analytical Fragility Curves	68
4-2	Lower Bound of Calibrated Rotational Ductility of Bridges	69
4-3	Fragility Parameters of Bridge 2 at Different $\theta$ for Two Orthogonal Components of Ground Motion (Case I)	72
4-4	Fragility Parameters of Bridge 2 at Different $\theta$ for One Inclined Component of Ground Motion (Case II)	74
6-1	Median Spectral Accelerations (SA)	86
6-2	Empirical Fragility Parameters of Caltrans' Bridges with Different Skewness	91
6-3	Empirical Fragility Parameters of Caltrans' Bridges with Different Numbers of Span	91
7-1	High Amplitude Tests and Target PGAs	95
7-2	Description of Bridge Damage States as Observed from the Experiment	96
7-3	Recorded Curvatures at Column Ends and Corresponding Damage Levels	97
7-4	Rotational Ductility of Bridge Columns at Different Damage Levels	101



# SECTION 1 INTRODUCTION

As is well known, risk assessment of infrastructure systems plays an increasingly important role in their plan, design, maintenance, retrofit and life-cycle cost evaluation taking into consideration their damageability under natural, technological and man-made hazards. The 1994 Northridge earthquake and other destructive earthquakes showed that bridges are one of the most vulnerable components of a highway network system subjected to earthquake ground motion. For this reason, bridge damageability information in a succinct form such as fragility curves is needed to pursue the seismic risk assessment of a highway transportation network consisting of as many as thousands of bridges that can be affected by a high magnitude earthquake within and near the area the network serves.

The current project represents part of a research project for the development of seismic risk assessment methodologies integrating such disciplines as engineering seismology, mechanics, geotechnical and structural engineering, statistical and probabilistic analysis, economics, and social science. Figure 1-1 shows the method used for seismic performance evaluation of a highway network system. In this study, Caltrans' (California Department of Transportation's) highway transportation network, spanning Los Angeles and Orange Counties, is used as a testbed. In the scope of this current report, the evaluation of bridge damageability utilizing nonlinear static and dynamic procedures and the development of fragility curves to apply in bridge design methodology are discussed. This research helps to judiciously estimate the seismic impact on the performance of the highway transportation network and its post-event functionality, and to determine bridge retrofit strategies and estimate the socio-economic benefit accrued from the seismic retrofit.

In past few years, many researchers have performed bridge fragility analysis following a number of different approaches (Hwang and Huo, 1994, Fukushima et al., 1996, Kai and Fukushima, 1996, Singhal and Kiremidjian, 1998, Basoz and Kiremidjian 1998, Mander and Basoz, 1999, Shinozuka et al., 2000a, Karim and Yamazaki, 2001, Gardoni et al., 2002, Shinozuka et al., 2003, Choi et al., 2004). Here, analytical fragility curves corresponding to each damage state are expressed in the form of a two-parameter lognormal distribution function as given in Shinozuka et al. (2003). These two-parameters (referred to as fragility parameters) are estimated through a maximum likelihood method. In this context, it should be noted that any monotonically increasing function can be used to develop fragility curves.

In the initial part, this study introduces statistical procedures appropriate for the development of fragility curves under the assumption that they can be represented by two-parameter lognormal distribution functions with the unknown median and log-standard deviation. Following this, empirical fragility curves are developed by utilizing 1994 Northridge earthquake damage data obtained by Caltrans inspection of more than 2,000 affected bridges in the two counties immediately after the event. Additionally, statistical procedures for testing goodness of fit of the fragility curves and of estimating the confidence intervals of the fragility parameters are also discussed.

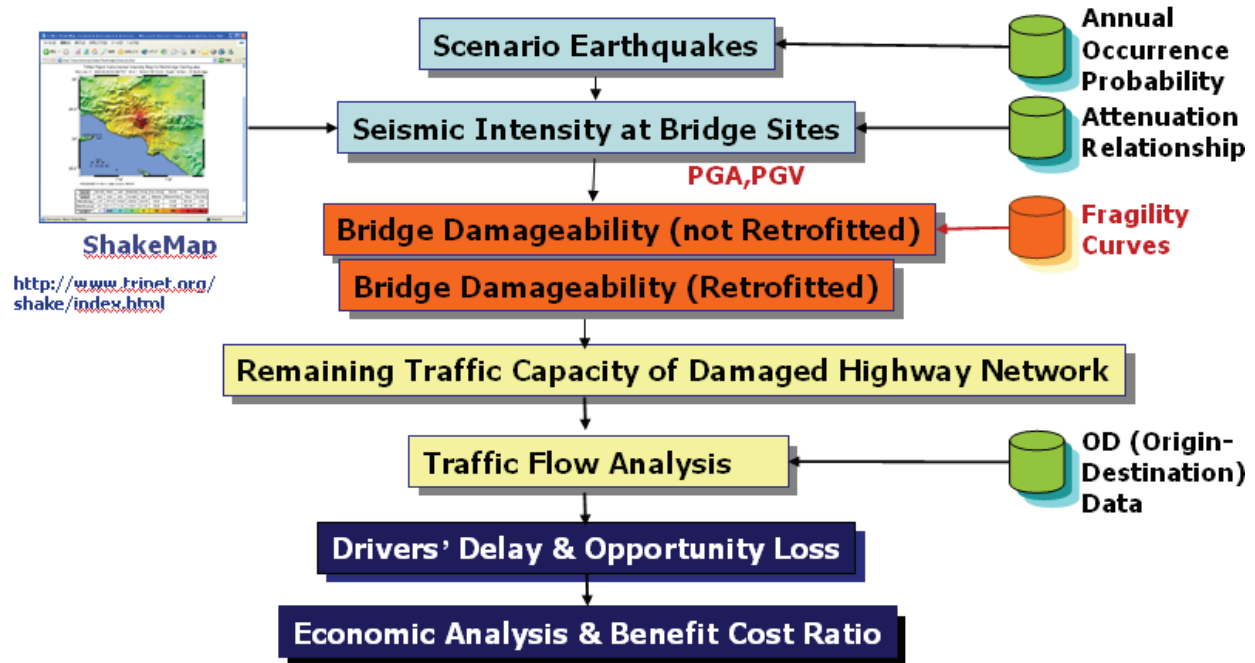


**FIGURE 1-1 Method of Evaluating Performance of Highway Network System**

In the following part of this report, analytical models are constructed for bridge systems in southern California in terms of finite element method integrating appropriate nonlinear elements to represent plastic hinge formation at bridge column ends, failure of expansion joints and unseating of bridge decks. Also, the possibility of having premature shear failure in the bridge column that may lead to the collapse of the bridge is investigated. Then, nonlinear time history analysis is carried out in order to investigate the mechanism of dynamic progressive failure of these bridges under earthquake ground motions. This research provides a better understanding of and insight to the global performance of bridges to seismic ground motion. In addition, this study also provides an approach for the seismic performance assessment of older bridges retrofitted by steel jacketing of bridge columns. Result shows a considerable improvement in the seismic performance of existing bridges.

This research integrates probabilistic, statistical and mechanistic aspects of bridge damageability in the form of traditional two-parameter lognormal fragility curve in order to quantify bridge damage states in terms of rotational ductility of bridge columns. For this purpose, a mechanistic damage model is developed that can be calibrated with empirical seismic damage data. In fact, analytical fragility curves are obtained from the nonlinear time history analysis in calibration with the 1994 Northridge earthquake damage data obtained by Caltrans inspecting more than 2000 affected bridges in Los Angeles, Ventura and Orange counties immediately after the event. These analytical fragility curves are given as functions of seismic intensity parameter at each bridge site such as SA, PGA, SI, etc. Hence, this makes it possible to carry out Monte Carlo simulation of the states of bridge damage for all the bridges in a highway network in the region expected to be impacted by any of scenario earthquakes representing the regional seismic hazard reported by USGS. This Monte Carlo simulation procedure provides a basic critical step for seismic risk assessment and loss estimation of highway transportation systems, or for that matter, many other civil infrastructure network systems.

In parallel with nonlinear time history analysis, nonlinear static analysis is also performed making use of the Capacity Spectrum Method (CSM) to assess the seismic performance of bridges. This method is more practice-oriented, and therefore, attracted more interest and support from the profession. This research proposed one simplified CSM approach for bridge analysis alternatives to the current design procedure in practice for building structures (ATC-40, 1996). The overall structural capacity is evaluated considering dynamic characteristics of the bridge and the effect of its higher modes of vibration. While estimating seismic demands, inelastic spectrum of earthquake ground motion which takes in consideration of structural damping is generated. Structural performance is estimated through the interaction of capacity spectrum of the structure and inelastic spectrum of earthquake ground motion. The validity of this proposed technique is verified through a very favorable comparison of the analytical results obtained from nonlinear time history analysis and FEMA's technical manual, "HAZUS" (currently in practice to evaluate earthquake loss estimation). Hence, this research provides a more practical alternative to the nonlinear time history analysis in assessing the seismic performance of bridges. Furthermore, on the basis of suggested CSM, a general guideline for bridge design verification is recommended that integrates bridge damage states with ground motion return periods.

This project also aims to estimate the effect of ground motion directionally on fragility characteristics of highway bridges. As we know, the ground motion trajectory in the corresponding multi-dimensional space results in time variant principal axes of the motion and defies any meaningful definition of directionality of the motion. Indeed, it is very difficult to incorporate the multi-dimensional effect of the ground motion in the design and response analysis of structures. In this context, this research presents one simplified approach in which the structure can be designed to ensure the safety under single or a pair of independent orthogonal ground motions traveling horizontally with an arbitrary direction to structural axis. This approach is used to generate fragility curves under a set of single and orthogonal pairs of ground motion components having different inclinations with longitudinal bridge axis. Results depict that ground motion directionality plays an important role in the estimation of maximum seismic demand. Further research is underway utilizing more rigorous finite-element analysis which will verify the accuracy of this simplified approach. The word directionality used here is different from "directivity" used in seismology to mean a specific characteristic of seismic fault movement.

Finally, a design acceptance criterion is developed on the basis of bridge performance under a prescribed level of earthquake ground motion. In this part, fragility information is used in order to calibrate threshold performance levels at different damage states. Thus, making use of statistical and analytical tools, newly designed and existing bridges can be analyzed and verified to identify whether or not the target performance level is achieved.





## SECTION 2

### STATISTICAL ANALYSIS OF FRAGILITY CURVES

It is assumed that the empirical fragility curves can be expressed in the form of two-parameter lognormal distribution functions, and developed as functions of peak ground acceleration (PGA) representing the intensity of the seismic ground motion. For the development of empirical fragility curves, the damage reports are usually utilized to establish the relationship between the ground motion intensity and the damage state of each bridge. In this present study the damage report for the Caltrans' bridges under the Northridge event, where the extent of damage is classified into the state of no, minor, moderate and major damage in addition to the state of collapse. The report did not provide explicit physical definitions of these damage states. This inspection report is used when a damage state is assigned to each bridge in the analysis that follows. The detail theoretical background of statistical analysis such as parameter estimation, hypotheses testing and confidence interval estimation related to the fragility curves are taken from Shinozuka et al. 2003 and presented in Appendix A.

#### 2.1 Fragility Curves for Structural Sub-Sets of Caltrans' Bridges

##### 2.1.1 Method 1 and Method 2

The sample of the Caltrans' bridges is sub-divided into a number of sub-sets in accordance with the pertinent bridge attributes and their combinations. This should be done in such a way that each sub-sample can be considered to be drawn from the corresponding sub-population which is more homogeneous than the initial population. In this regard, it is recognized each bridge can easily be associated with one of the following three distinct attributes; (A) It is either single span (S) or multiple span (M) bridge, (B) it is built on either hard soil ( $S_1$ ), medium soil ( $S_2$ ) or soft soil ( $S_3$ ) in the definition of UBC 93, and (C) it has a skew angle  $\theta_1$  (less than  $20^\circ$ ),  $\theta_2$  (between  $20^\circ$  and  $60^\circ$ ) or  $\theta_3$  (larger than  $60^\circ$ ). The sample can then be sub-divided into a number of sub-sets. To begin with, one might consider the first level hypothesis that the entire sample is taken from a statistically homogenous population of bridges. The second level sub-sets are created by dividing the sample either (A) into two groups of bridges, one with single spans and the other with multiple spans, (B) into three groups, the first with soil condition  $S_1$ , the second with  $S_2$  and the third with  $S_3$ , or (C) into three groups depending on the skew angles  $\theta_1$ ,  $\theta_2$  and  $\theta_3$ . The third level sub-sets consists of either (D) 6 groups each with a particular combination between (S, M) and ( $S_1, S_2, S_3$ ), (E) 6 groups each with a combination between (S, M) and ( $\theta_1, \theta_2, \theta_3$ ), or (F) 9 groups each with a combination between ( $\theta_1, \theta_2, \theta_3$ ) and ( $S_1, S_2, S_3$ ). Finally, the fourth level sub-sets comprises of 18 groups each with a combination of the attributes (S, M), ( $S_1, S_2, S_3$ ) and ( $\theta_1, \theta_2, \theta_3$ ).

As alluded to in the preceding paragraph, the higher the level of sub-sets, more statistically homogeneous the corresponding sub-population is compared with the population at the level at least one rank lower. For example, each sample of the fourth level sub-sets is taken from the population with identical span, skewness and soil characteristics as they are defined here. While this by no means implies that the corresponding population is purely homogeneous, it is much

more homogeneous in engineering sense than the population corresponding to the first, second or even third level sub-sets.

Theoretical background of fragility curve development using method 1 and 2 are discussed in detail in Appendix A. Fragility parameters for different levels of subsets are given in Table 2-1. The families of fragility curves corresponding to the second and fourth level subsets are plotted in figures 2-1~2-8 and 2-9~2-21, respectively. Fragility curves associated with some damage states are missing from the plots for some subsets that do not have bridges suffering from these damage states. The families of fragility curves shown in figures 2-1~2-21 play a pivotal role in the seismic performance assessment of the expressway network in the Los Angeles area.

**TABLE 2-1 Median and Log-Standard Deviation of Sample Sub-Divisions of Caltrans Bridges**

(a) First Level (Composite)

	Median	Log. St. Dev.
Min	0.83	0.82
Mod	1.07	0.82
Maj	1.76	0.82
Col	3.96	0.82

(b) Second Level (Span)

		Median	Log. St. Dev.			Median	Log. St. Dev.
Single	Min	1.22	0.78	Multiple	Min	0.72	0.72
	Mod	1.60	0.78		Mod	0.92	0.92
	Maj	2.65	0.78		Maj	1.51	1.51
	Col	N/A	0.78		Col	3.26	3.26

(c) Second Level (Skew)

(d) Second Level (Soil)

		Median	Log. St. Dev.			Median	Log. St. Dev.
Sk1 0°~20°	Min	0.99	0.95	Soil A	Min	1.35	0.94
	Mod	1.38	0.95		Mod	1.79	0.94
	Maj	2.52	0.95		Maj	2.62	0.94
	Col	5.15	0.95		Col	N/A	0.94
Sk2 21°~60°	Min	0.71	0.73	Soil B	Min	0.97	0.94
	Mod	0.87	0.73		Mod	1.36	0.94
	Maj	1.38	0.73		Maj	2.19	0.94
	Col	3.93	0.73		Col	N/A	0.94
Sk3 >60°	Min	0.50	0.59	Soil C	Min	0.79	0.79
	Mod	0.63	0.59		Mod	1.01	0.79
	Maj	0.93	0.59		Maj	1.70	0.79
	Col	1.69	0.59		Col	3.57	0.79

**TABLE 2-1 Median and Log-Standard Deviation of Sample Sub-Divisions of Caltrans Bridges (Cont'd)**

(e) Third Level (Span/Skew)

	Median	Log. St. Dev.	Median	Log. St. Dev.	Median	Log. St. Dev.
	Single/Sk1		Single/Sk2		Single/Sk3	
Min	2.15	0.98	0.73	0.43	0.48	0.52
Mod	3.42	0.98	0.82	0.43	0.57	0.52
Maj	6.41	0.98	1.13	0.43	0.85	0.52
Col	N/A	0.98	N/A	0.43	N/A	0.52
	Multiple/Sk1		Multiple/Sk2		Multiple/Sk3	
Min	1.03	0.93	0.70	0.83	0.47	0.51
Mod	1.46	0.93	0.88	0.83	0.56	0.51
Maj	2.75	0.93	1.48	0.83	0.80	0.51
Col	5.80	0.93	4.63	0.83	1.35	0.51

(f) Third Level (Skew\Soil)

	Median	Log. St. Dev.	Median	Log. St. Dev.	Median	Log. St. Dev.
	Sk1/Soil A		Sk1/Soil B		Sk1/Soil C	
Min	1.69	0.69	1.36	0.76	1.01	0.85
Mod	1.96	0.69	N/A	N/A	1.38	0.85
Maj	N/A	0.69	N/A	N/A	2.44	0.85
Col	N/A	0.69	N/A	N/A	4.97	0.85
	Sk2/Soil A		Sk2/Soil B		Sk2/Soil C	
Min	0.84	0.5	0.54	0.53	0.68	0.76
Mod	0.91	0.5	0.68	0.53	0.84	0.76
Maj	1.01	0.5	0.8	0.53	1.48	0.76
Col	N/A	0.5	N/A	0.53	4.01	0.76
	Sk3/Soil A		Sk3/Soil B		Sk3/Soil C	
Min	0.54	0.66	0.34	0.24	0.52	0.61
Mod	0.69	0.66	0.43	0.24	0.65	0.61
Maj	1.06	0.66	0.72	0.24	0.94	0.61
Col	N/A	0.66	N/A	0.24	1.64	0.61

**TABLE 2-1 Median and Log-Standard Deviation of Sample Sub-Divisions of Caltrans Bridges (Cont'd)**

(g) Third Level (Span\Soil)

	Median	Log. St. Dev.	Median	Log. St. Dev.	Median	Log. St. Dev.
	Single/Soil A		Single/Soil B		Single/Soil C	
Min	1.1	0.86	1.1	0.78	0.97	0.65
Mod	N/A	0.86	N/A	0.78	1.21	0.65
Maj	N/A	0.86	N/A	0.78	1.90	0.65
Col	N/A	0.86	N/A	0.78	N/A	0.65
	Multiple/Soil A		Multiple/Soil B		Multiple/Soil C	
Min	1.06	0.9	0.59	0.51	0.71	0.78
Mod	1.36	0.9	0.72	0.51	0.91	0.78
Maj	2.03	0.9	0.99	0.51	1.53	0.78
Col	N/A	0.9	N/A	0.51	3.13	0.78

(h) Forth Level (Span/Skew/Soil)

Case \ Damage	Min	Mod	Maj	Col	Log. Std. Dev.
S/0-20/a	0.71	N/A	N/A	N/A	0.20
S/0-20/b	0.61	N/A	N/A	N/A	0.41
S/0-20/c	1.23	1.49	2.29	N/A	0.57
S/20-60/a	N/A	N/A	N/A	N/A	N/A
S/20-60/b	N/A	N/A	N/A	N/A	N/A
S/20-60/c	0.62	0.70	0.98	N/A	0.39
S/60-90/a	N/A	N/A	N/A	N/A	N/A
S/60-90/b	N/A	N/A	N/A	N/A	N/A
S/60-90/c	0.56	1.08	2.04	N/A	0.83
M/0-20/a	1.16	1.38	N/A	N/A	0.80
M/0-20/b	N/A	N/A	N/A	N/A	N/A
M/0-20/c	0.84	1.16	2.05	4.06	0.81
M/20-60/a	0.59	0.59	0.72	N/A	0.41
M/20-60/b	0.50	0.64	0.64	N/A	0.48
M/20-60/c	0.69	0.88	1.64	4.63	0.85
M/60-90/a	0.39	0.48	0.70	N/A	0.43
M/60-90/b	0.34	0.43	0.72	N/A	0.25
M/60-90/c	0.50	0.57	0.81	1.33	0.53

Note: S = Single Span; M = Multiple Span; a = Soil A; b = Soil B; c = Soil C; Number: Skewness Angle

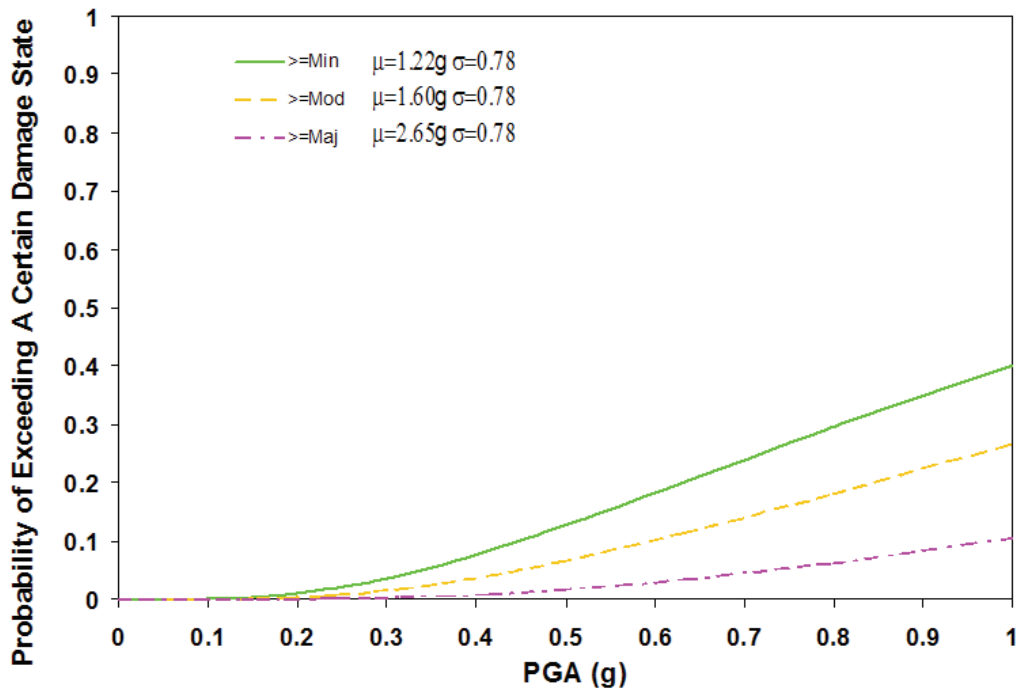


**FIGURE 2-1 Fragility Curves for a Second Level Subset (Caltrans' Bridges; Single Span) by Method 2**

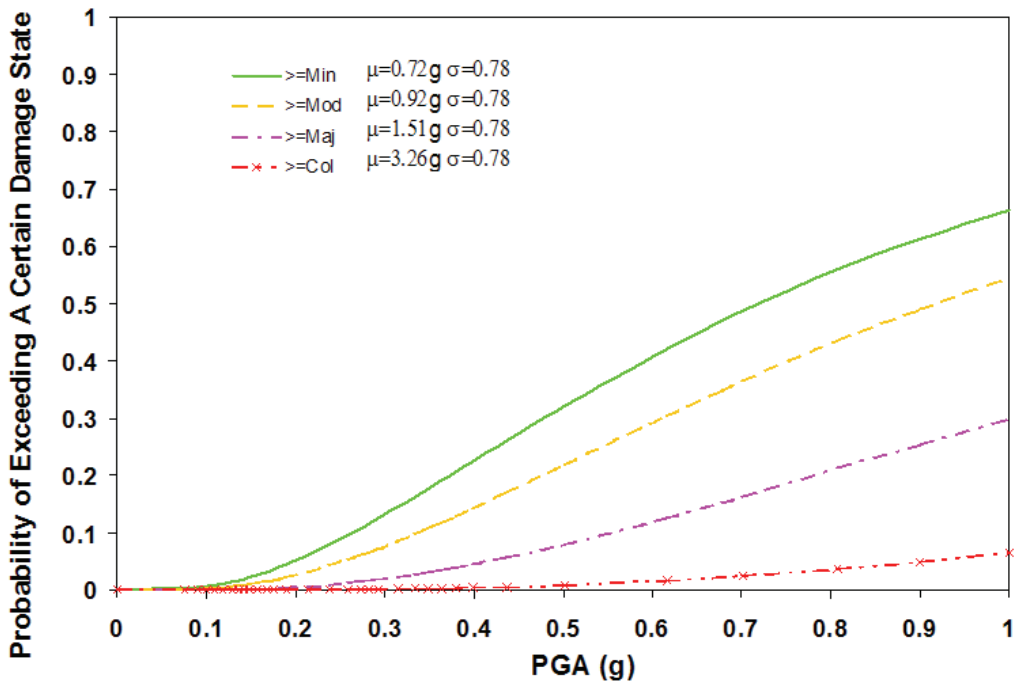


**FIGURE 2-2 Fragility Curves for a Second Level Subset (Caltrans' Bridges; Multiple Span) by Method 2**

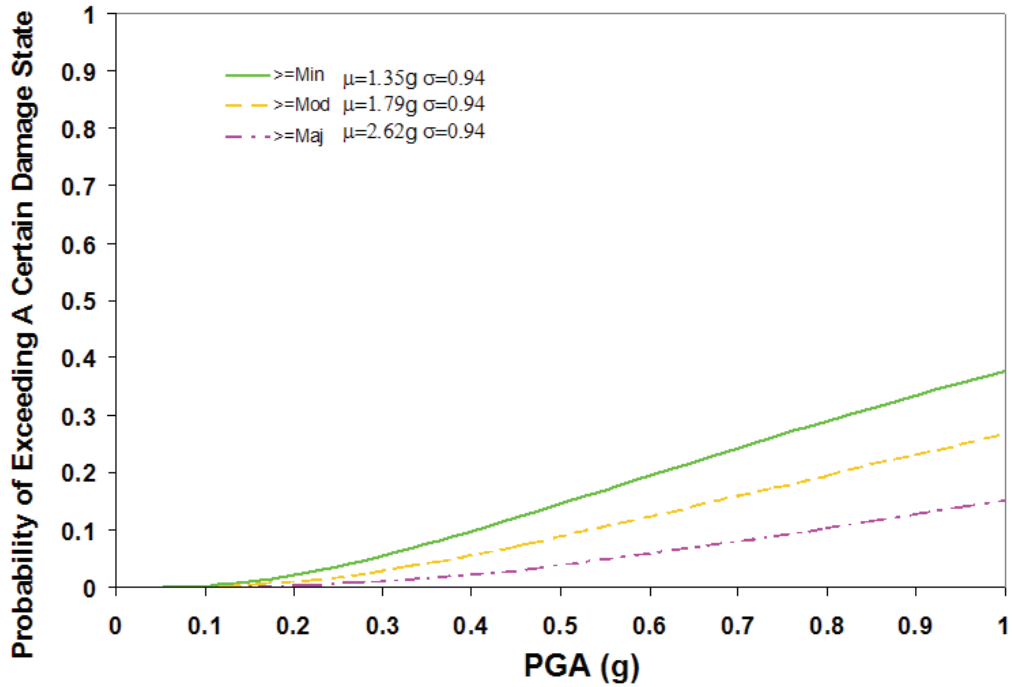


**FIGURE 2-3 Fragility Curves for a Second Level Subset (Caltrans' Bridges; Soil A) by Method 2**

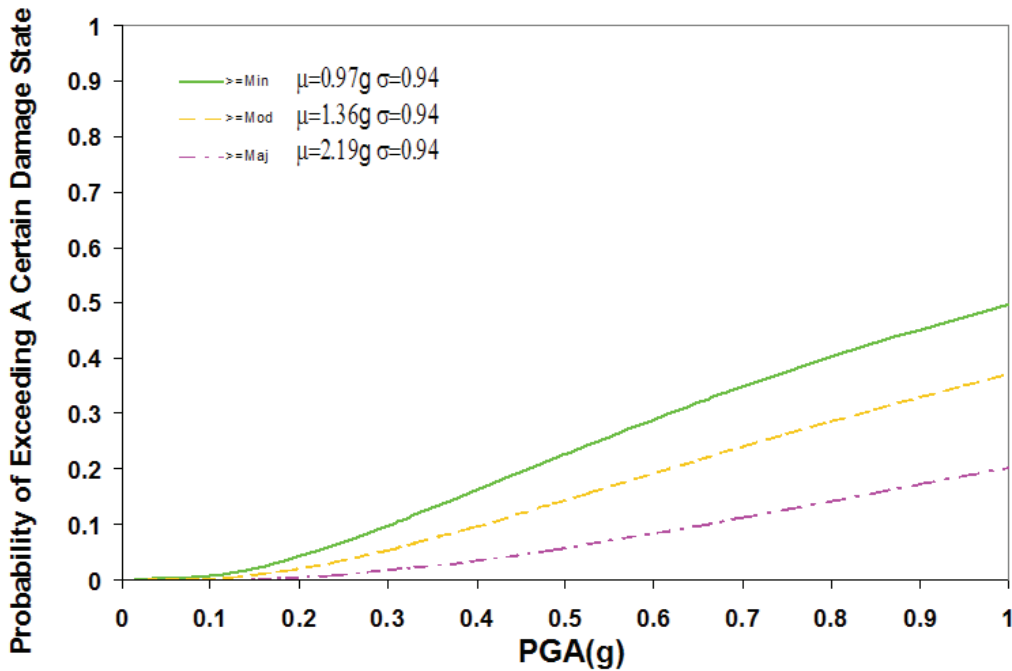


**FIGURE 2-4 Fragility Curves for a Second Level Subset (Caltrans' Bridges; Soil B) by Method 2**

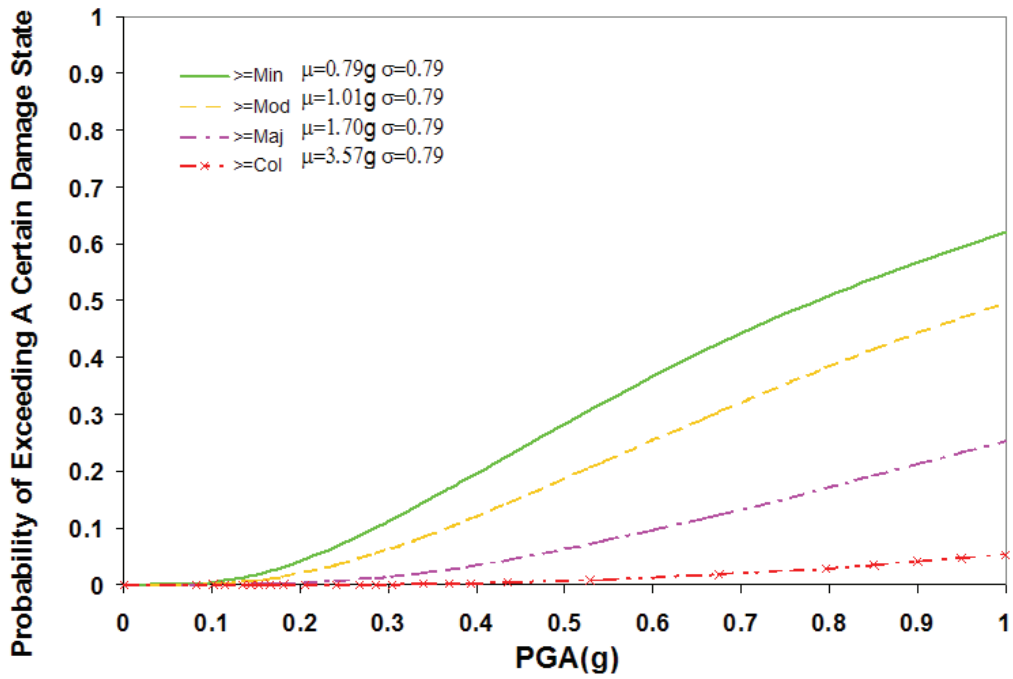


**FIGURE 2-5 Fragility Curves for a Second Level Subset (Caltrans' Bridges; Soil C) by Method 2**

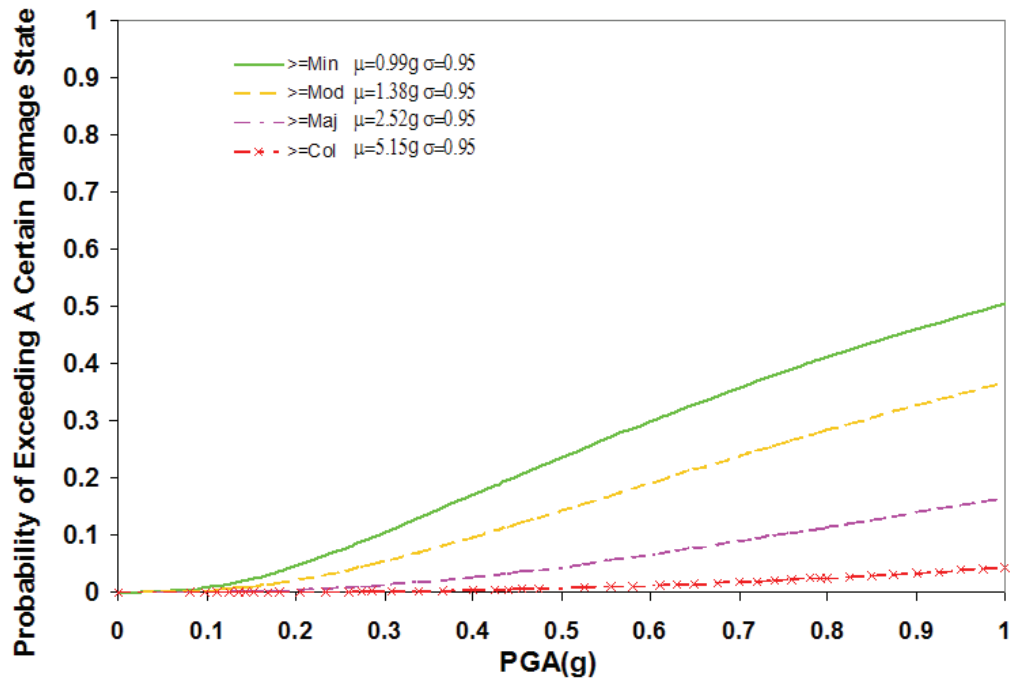


**FIGURE 2-6 Fragility Curves for a Second Level Subset (Caltrans' Bridges; Skew  $\leq 20$ ) by Method 2**



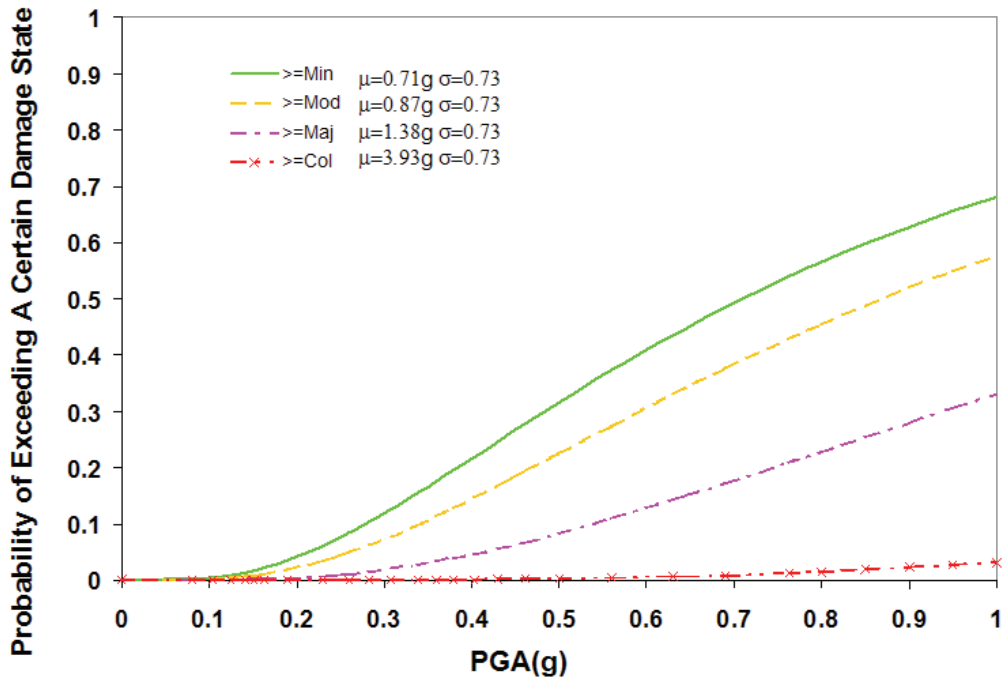


**FIGURE 2-7 Fragility Curves for a Second Level Subset (Caltrans' Bridges; 20 < Skew ≤ 60) by Method 2**

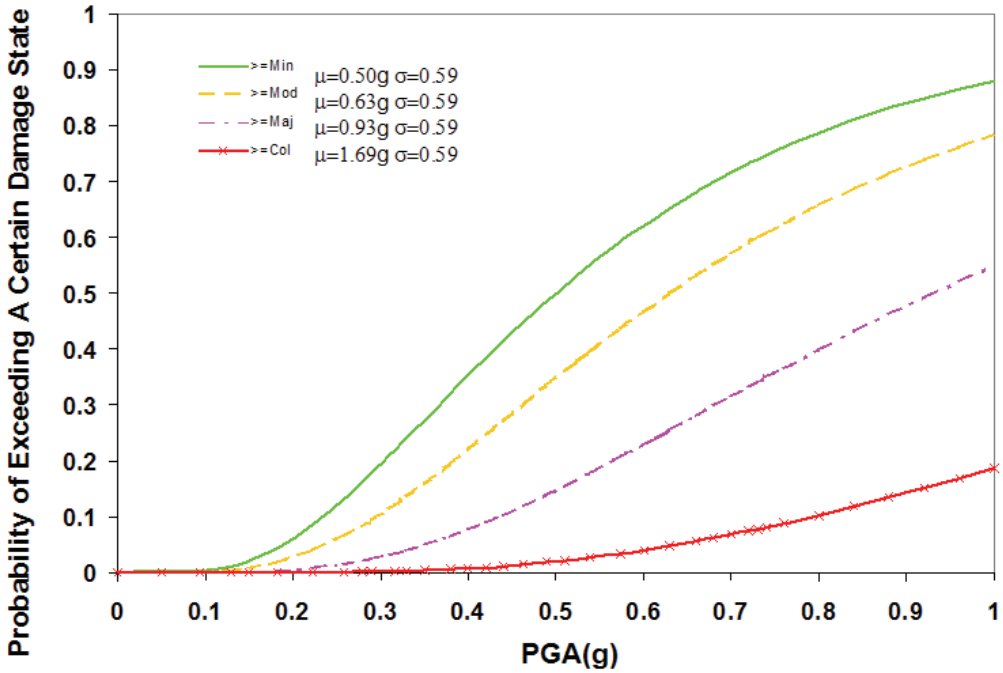


**FIGURE 2-8 Fragility Curves for a Second Level Subset (Caltrans' Bridges; Skew > 60) by Method 2**

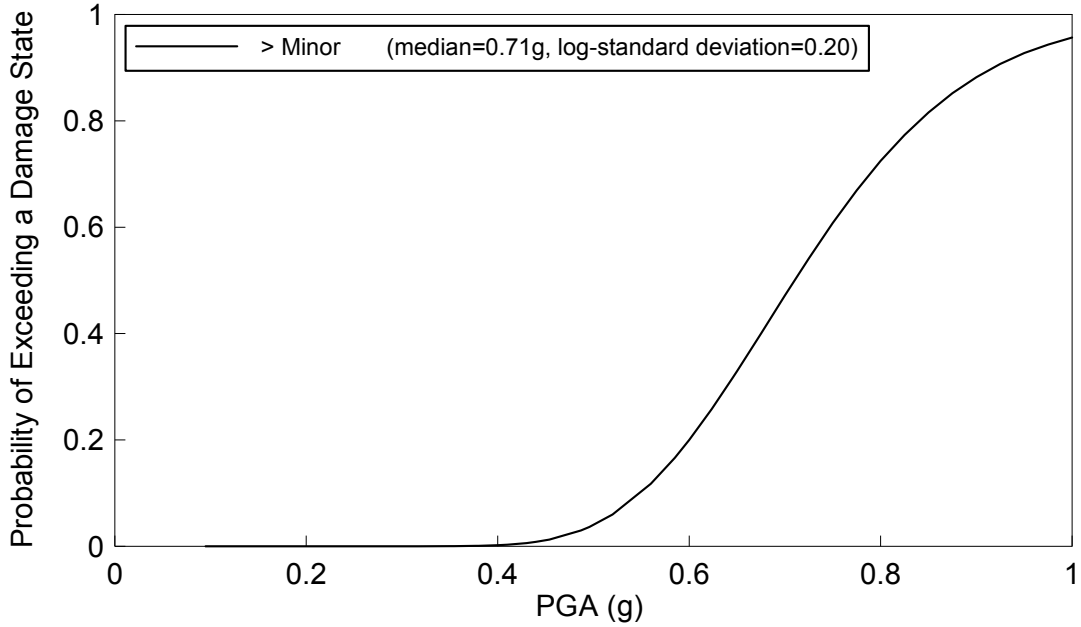


**FIGURE 2-9 Fragility Curves for a Fourth Level Subset (Caltrans' Bridges; single span/0 ≤ skew ≤ 20/soil A) by Method 2**

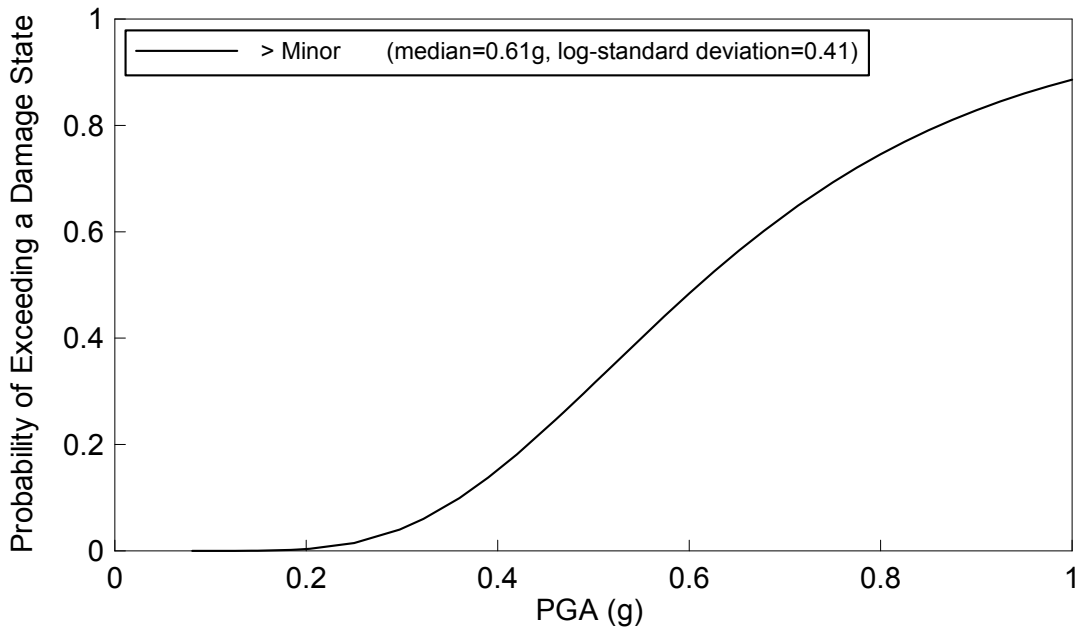


**FIGURE 2-10 Fragility Curves for a Fourth Level Subset (Caltrans' Bridges; single span/0 ≤ skew ≤ 20/soil B) by Method 2**

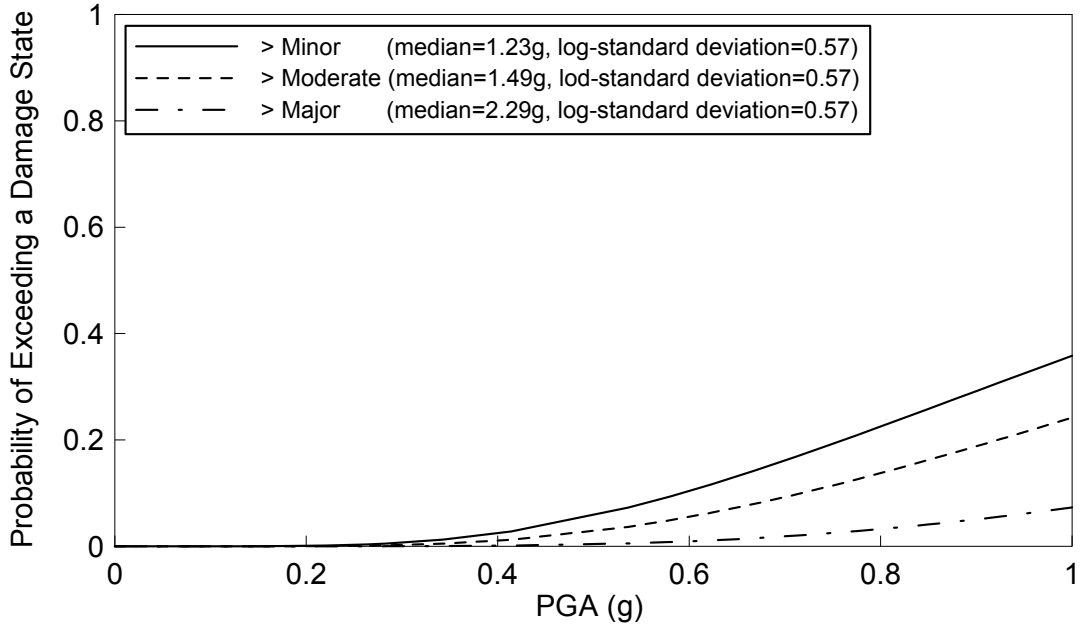


**FIGURE 2-11 Fragility Curves for a Fourth Level Subset (Caltrans' Bridges; single span/0 ≤ skew ≤ 20/soil C) by Method 2**

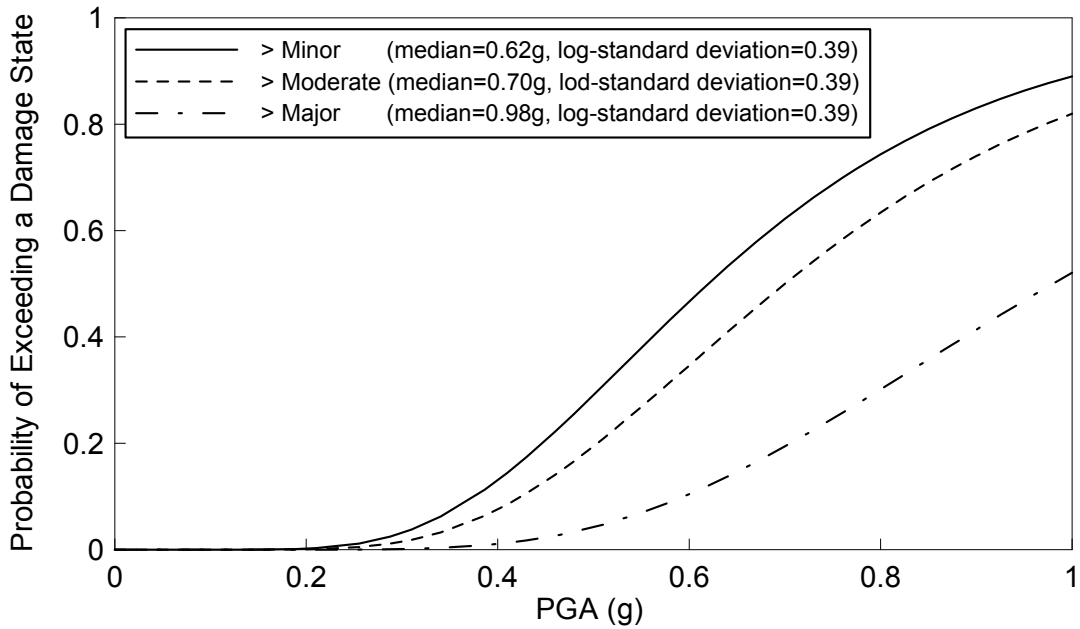


**FIGURE 2-12 Fragility Curves for a Fourth Level Subset (Caltrans' Bridges; single span/20 < skew ≤ 60/soil C) by Method 2**

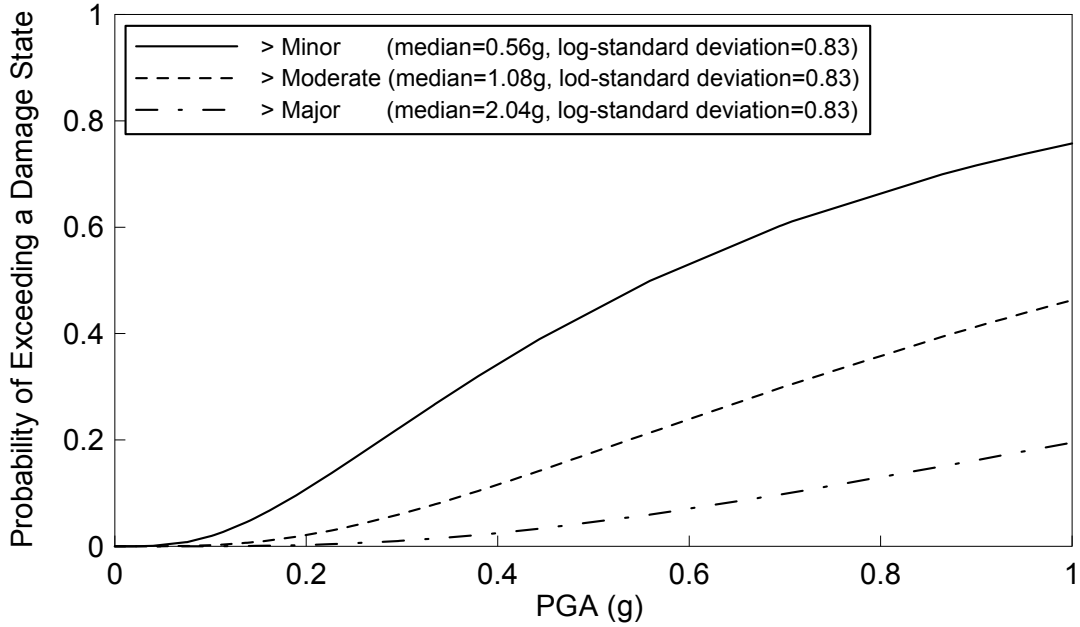


**FIGURE 2-13 Fragility Curves for a Fourth Level Subset (Caltrans' Bridges; single span/60 < skew/soil C) by Method 2**

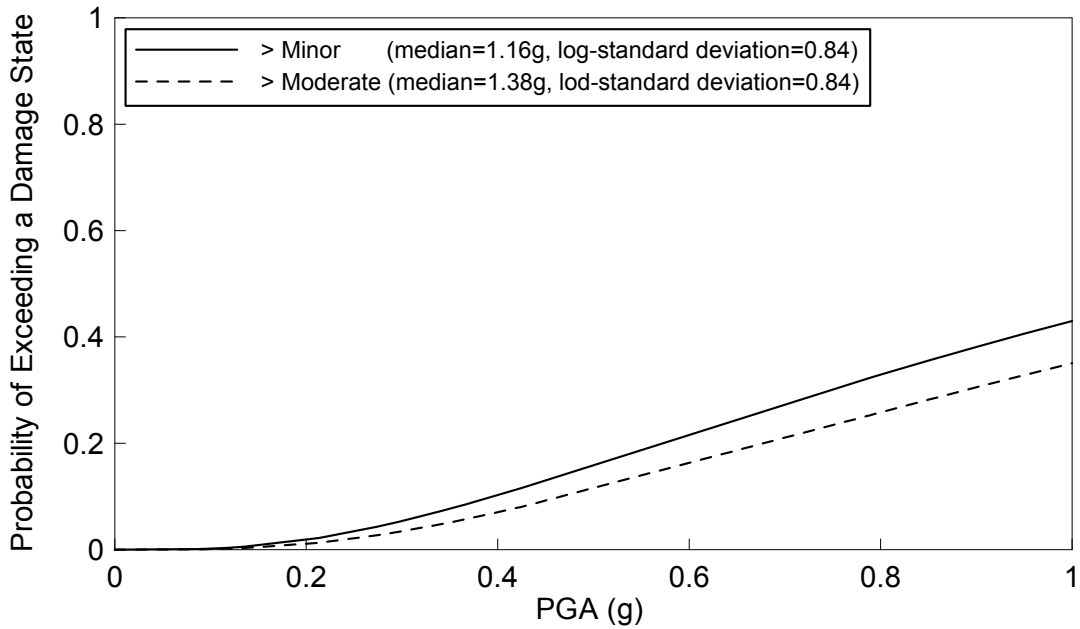


**FIGURE 2-14 Fragility Curves for a Fourth Level Subset (Caltrans' Bridges; multiple span/0 ≤ skew ≤ 20/soil A) by Method 2**

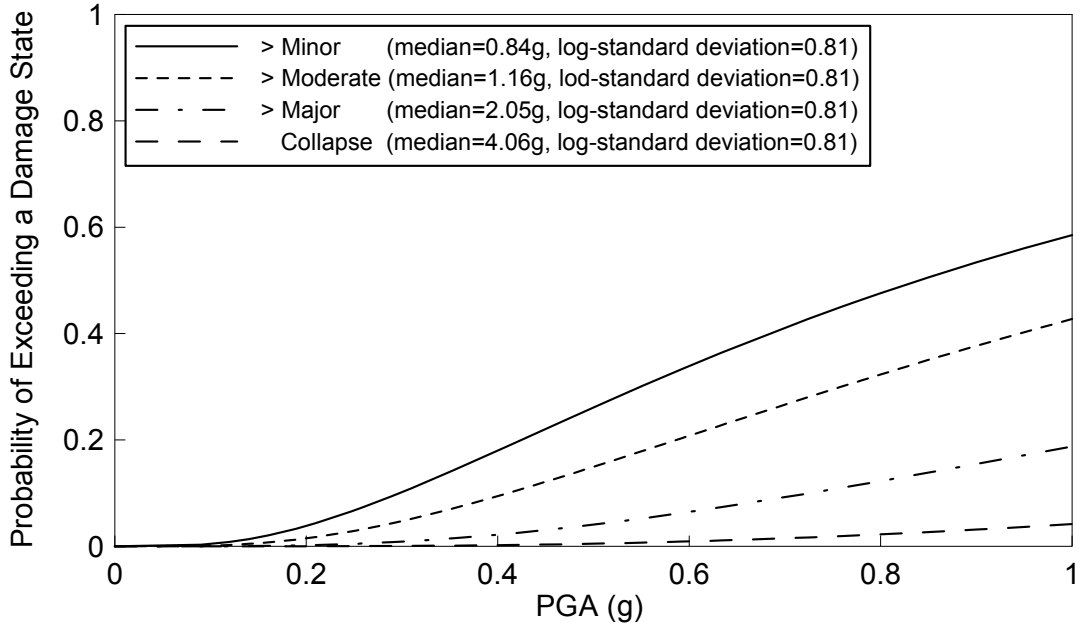


**FIGURE 2-15 Fragility Curves for a Fourth Level Subset (Caltrans' Bridges; multiple span/0 ≤ skew ≤ 20/soil C) by Method 2**

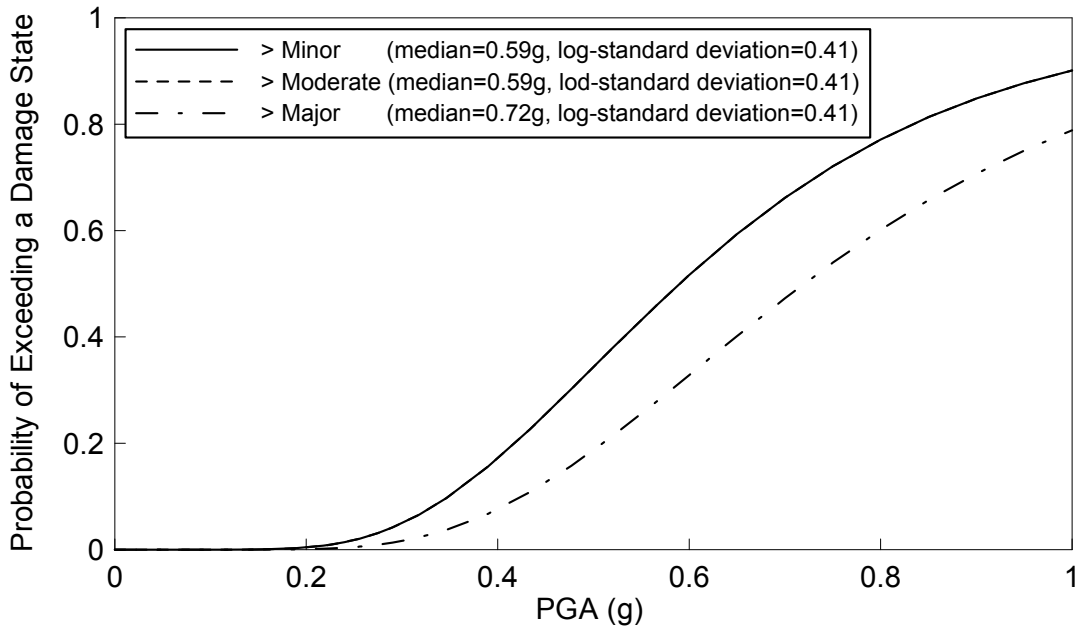


**FIGURE 2-16 Fragility Curves for a Fourth Level Subset (Caltrans' Bridges; multiple span/20 < skew ≤ 60/soil A) by Method 2**

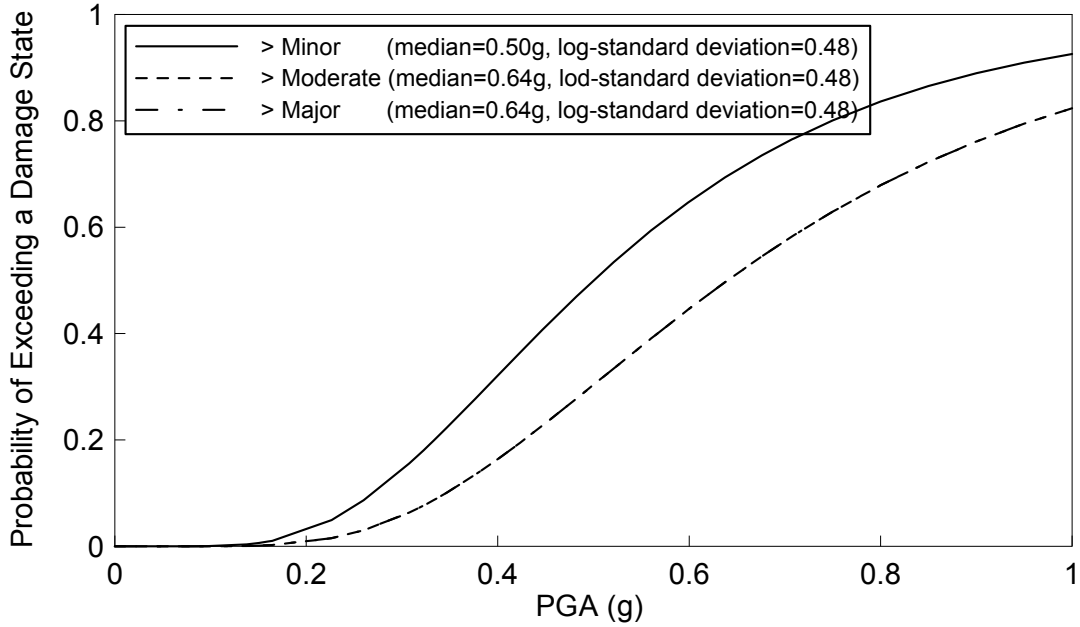


**FIGURE 2-17 Fragility Curves for a Fourth Level Subset (Caltrans' Bridges; multiple span/20 < skew ≤ 60/soil B) by Method 2**

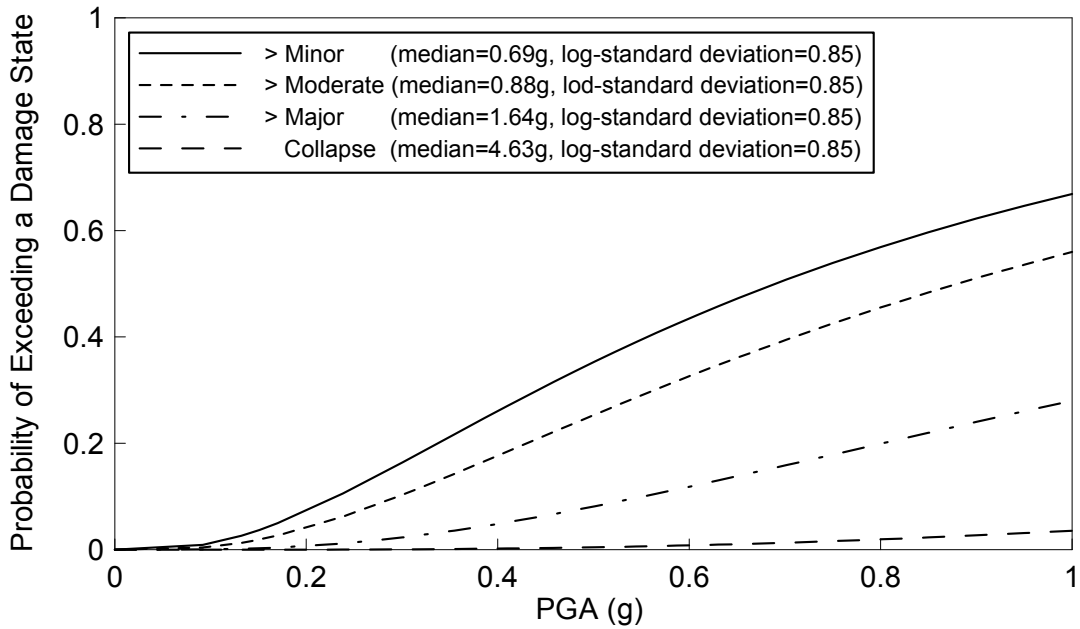


**FIGURE 2-18 Fragility Curves for a Fourth Level Subset (Caltrans' Bridges; multiple span/20 < skew ≤ 60/soil C) by Method 2**

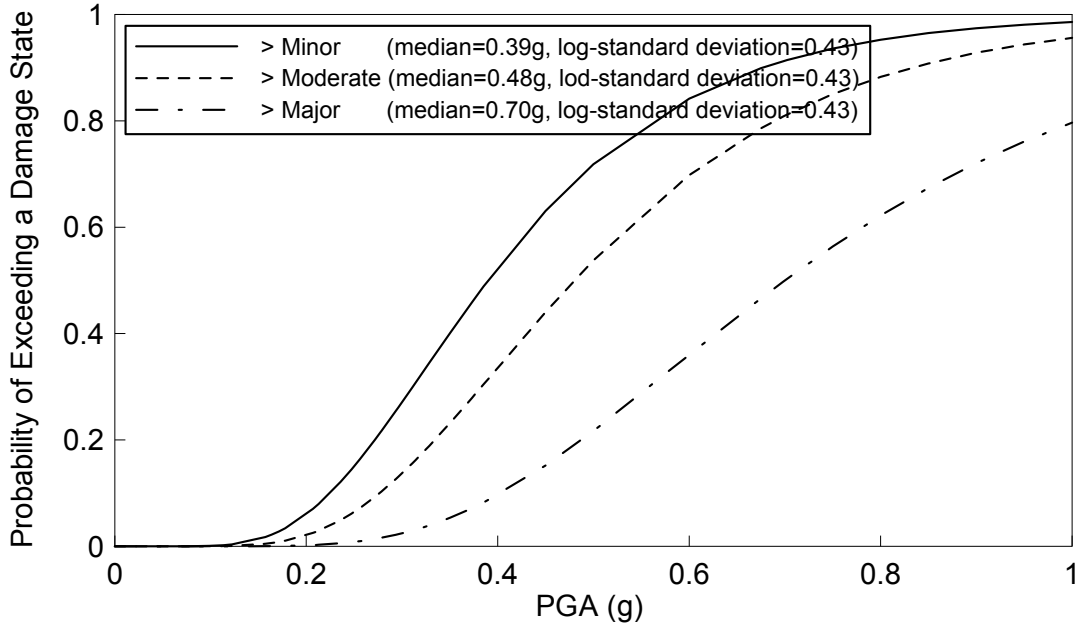


**FIGURE 2-19 Fragility Curves for a Fourth Level Subset (Caltrans' Bridges; multiple span/60 < skew/soil A) by Method 2**

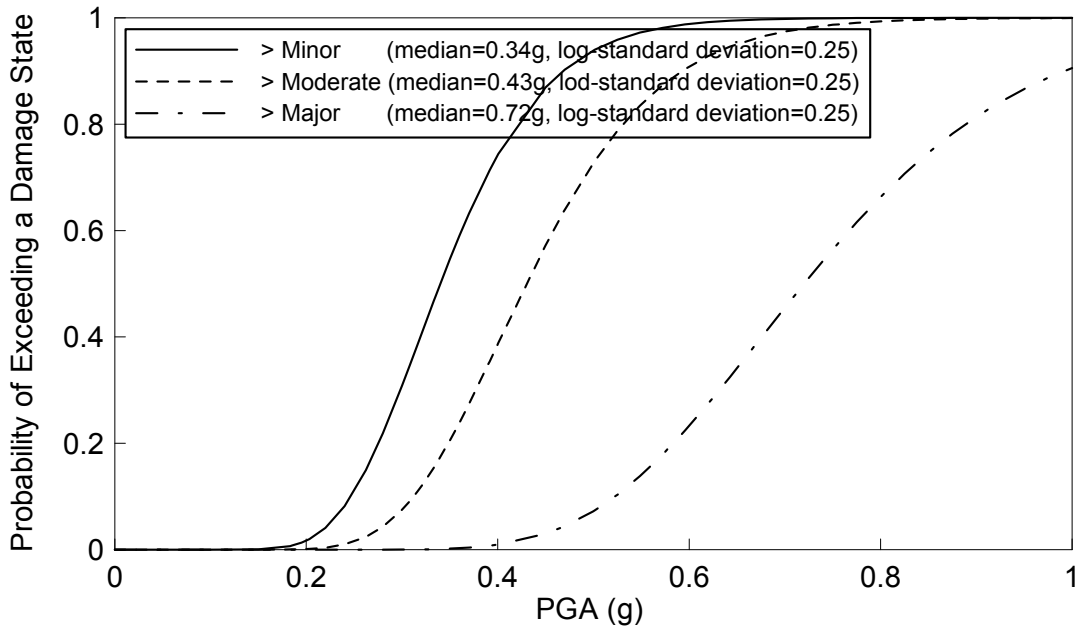


**FIGURE 2-20 Fragility Curves for a Fourth Level Subset (Caltrans' Bridges; multiple span/60 < skew/soil B) by Method 2**

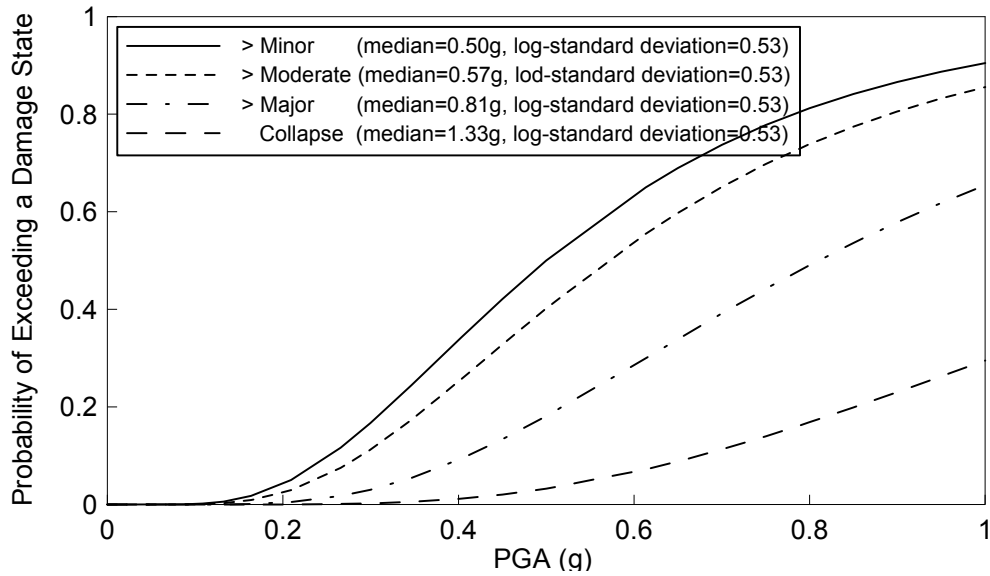


**FIGURE 2-21 Fragility Curves for a Fourth Level Subset (Caltrans' Bridges; multiple span/60 < skew/soil C) by Method 2**

### 2.1.2 Method 3

In Method 3, the bridge damage is rearranged according to the ascending order of PGA to demonstrate the statistical variation of data relative to the estimated fragility curves. The entire sample is sub-divided into certain number of groups. The number of the bridges that sustained certain damage state in a group is divided by the total number of bridges in the group and this ratio is used as a realization of fragility value at the PGA value representative of the group obtained by averaging PGA values assigned to the bridges in the group. The likelihood function for the present purpose is expressed as

$$L = \prod_{i=1}^n [F(a_i)]^{k_i} [1 - F(a_i)]^{(m_i - k_i)} \quad (2-1)$$

where,  $F(\cdot)$  represents the fragility curve for a specific state of damage,  $n$  is the number of bridge groups,  $a_i$  is the PGA value to which  $i$ th group of bridge is subjected,  $m_i$  is the total number of bridge in  $i$ th group and  $k_i$  is the number of damaged bridges among  $m_i$  in  $i$ th group of bridge. Under this condition, the fragility parameters can be obtained following (A-2) and (A-3).

In order to develop fragility curves in Method 3, the entire sample of 1998 damage data are sub-divided into 44 groups of 44 bridges (starting from bridges 1~44, bridges 45~88, and so on) with the last group having 62 bridges. Figures 2-22~2-25 show the four fragility curves obtained by Method 1 and Method 3. The black diamonds in these figures indicate the ratio of number of the bridges that sustained the state of damage under consideration in a group and the total number of bridges in the group (which is 44 except for the last group) and used as a realization of fragility value at the PGA value representative of the group obtained by averaging the smallest and the largest PGA value assigned to the bridges in the group. Figures 2-26~2-29 show the statistical variation of the same input data (Method 3) relative to the estimated fragility curves obtained by Method 2 with each curve plotted separately (though estimated together).



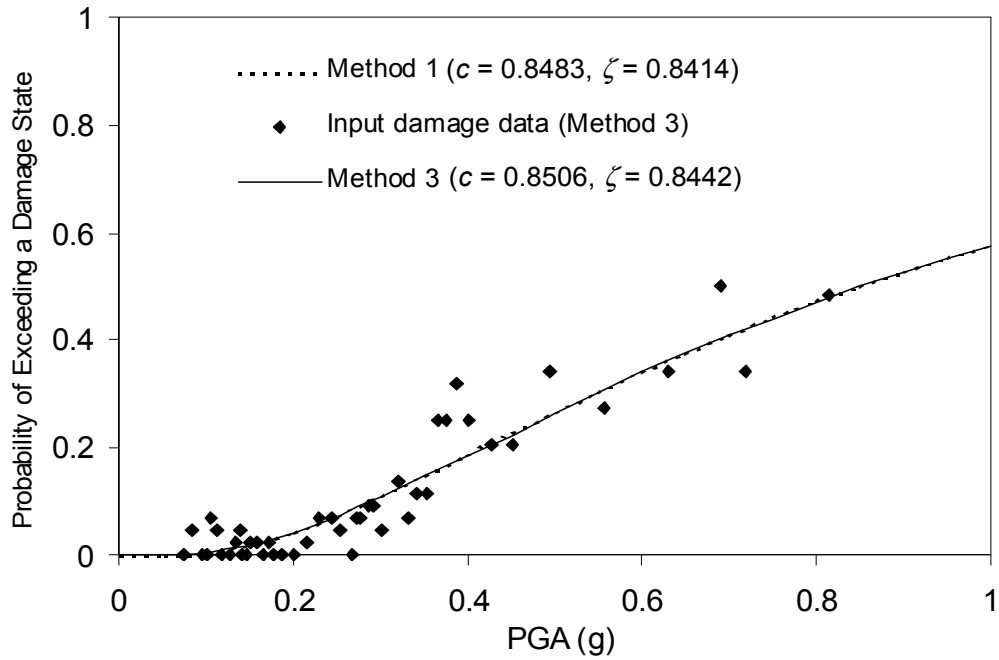


**FIGURE 2-22 Fragility Curve for Caltrans' Bridges developed in Method 1 and Method 3 and Input Damage Data (Method 3) with 'At least Minor' Damage**

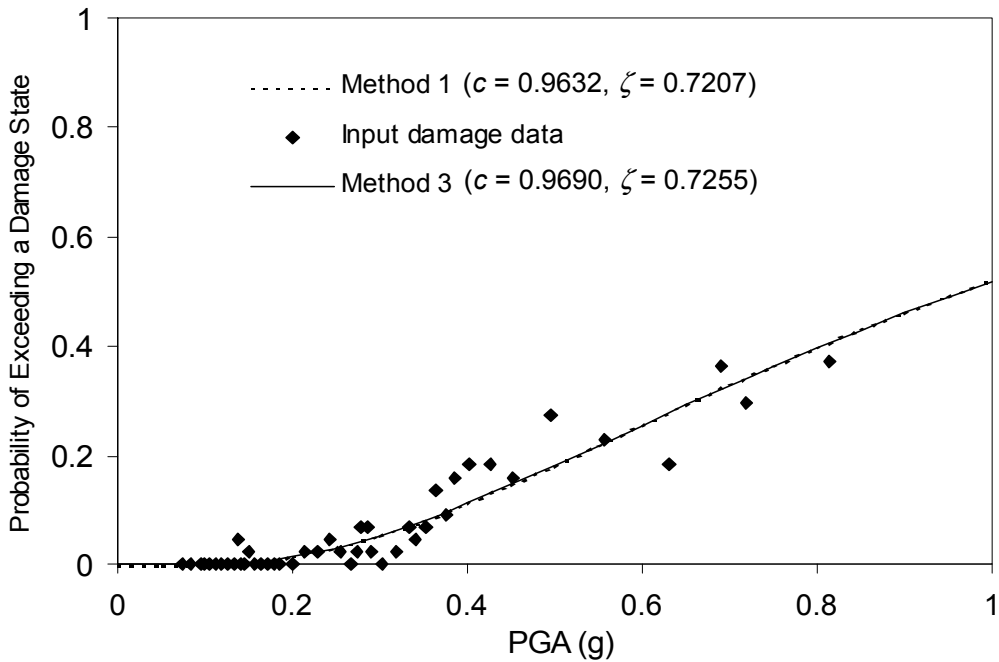


**FIGURE 2-23 Fragility Curve for Caltrans' Bridges developed in Method 1 and Method 3 and Input Damage Data (Method 3) with 'At least Moderate' Damage**

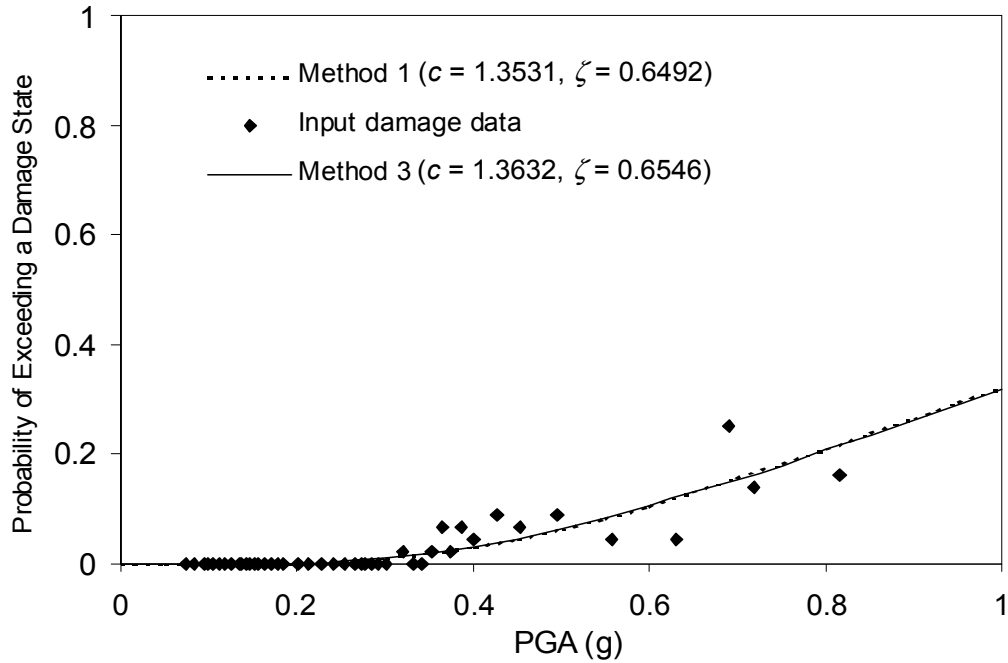


**FIGURE 2-24 Fragility Curve for Caltrans' Bridges developed in Method 1 and Method 3 and Input Damage Data (Method 3) with 'At least Major' Damage**

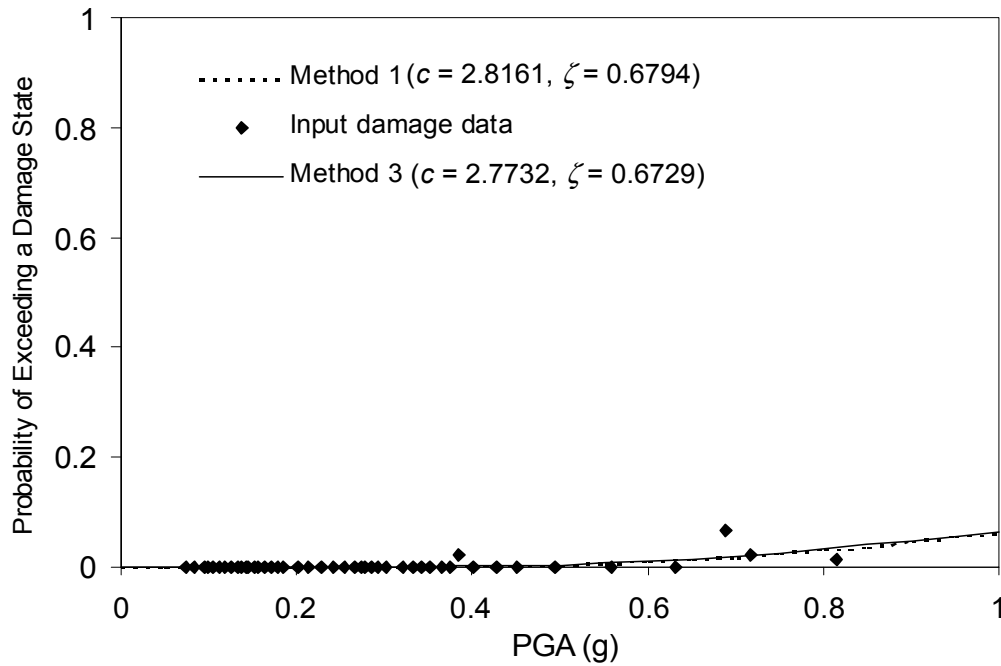


**FIGURE 2-25 Fragility Curve for Caltrans' Bridges developed in Method 1 and Method 3 and Input Damage Data (Method 3) with 'Collapse'**

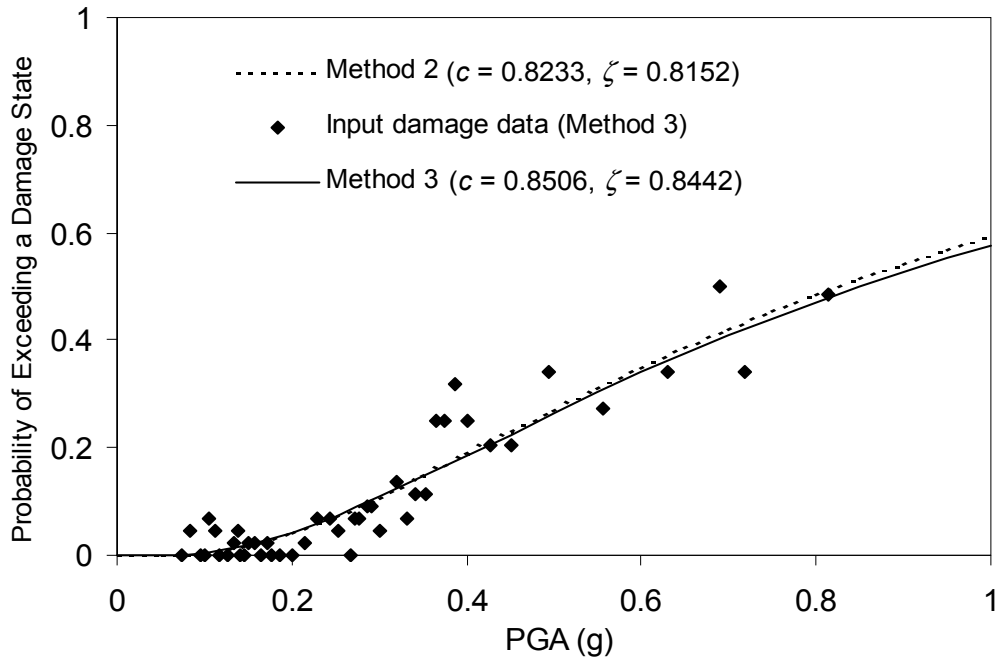


**FIGURE 2-26** Fragility Curve for Caltrans' Bridges developed in Method 2 and Method 3 and Input Damage Data (Method 3) with 'At least Minor' Damage

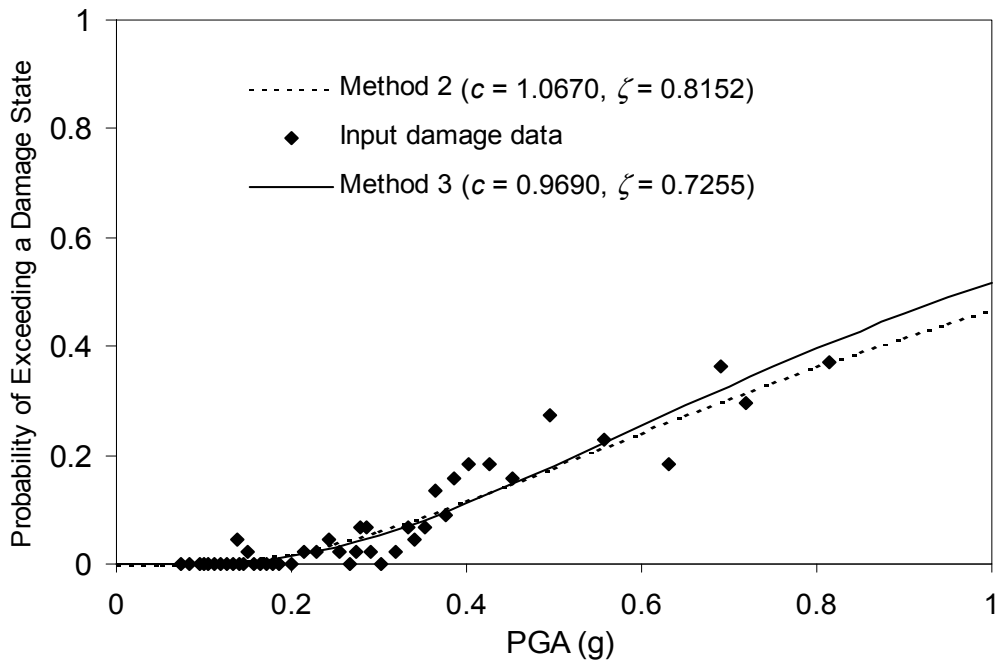


**FIGURE 2-27** Fragility Curve for Caltrans' Bridges developed in Method 2 and Method 3 and Input Damage Data (Method 3) with 'At least Moderate' Damage

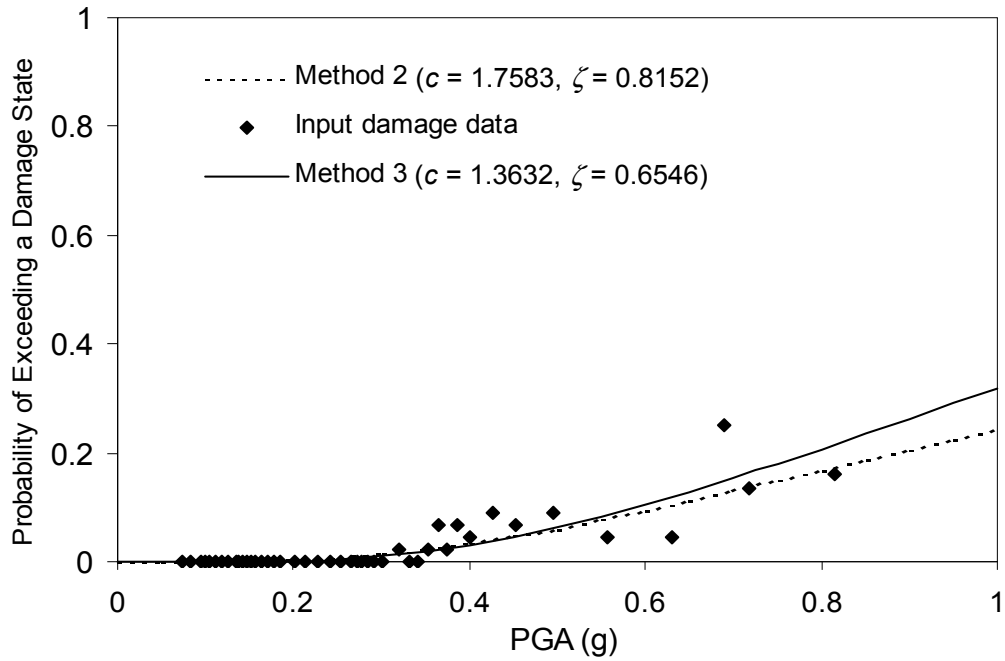


**FIGURE 2-28** Fragility Curve for Caltrans' Bridges developed in Method 2 and Method 3 and Input Damage Data (Method 3) with 'At least Major' Damage

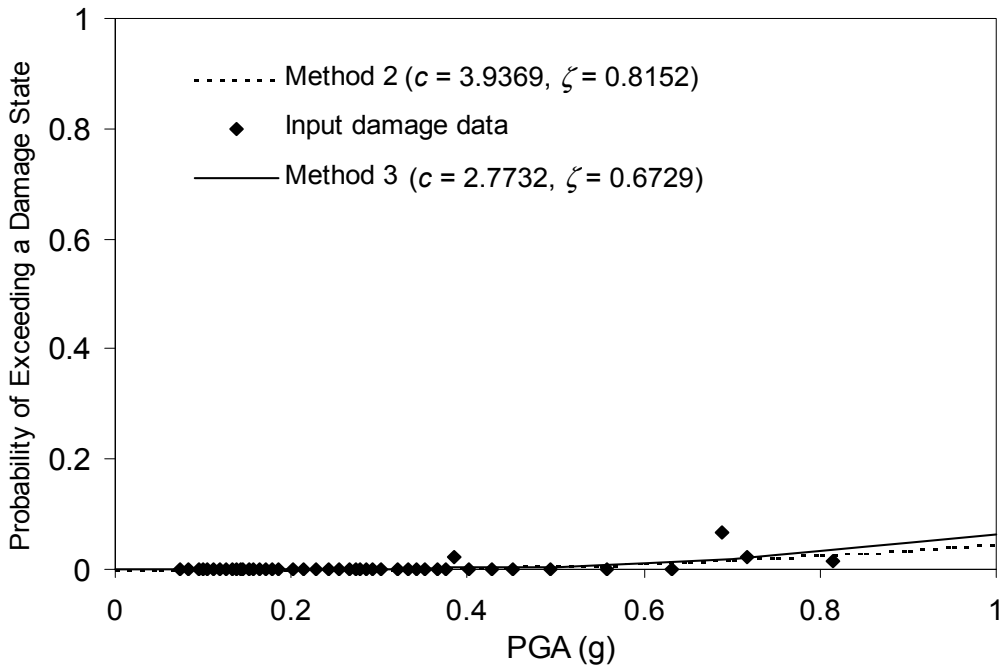


**FIGURE 2-29** Fragility Curve for Caltrans' Bridges developed in Method 2 and Method 3 and Input Damage Data (Method 3) with 'Collapse'

### 2.1.3 Development of Fragility Curves using Weibull Distribution

In preceding sections, fragility curves are developed using log-normal distribution function. However, any other distribution function such as weibull distribution can be used for this purpose as fragility curves are non-decreasing functions by definition. The current section develops fragility curves using weibull distribution in which the two-parameter distribution function is expressed as

$$F(a) = 1 - \exp\left[-\left(\frac{a}{b}\right)^c\right] \quad (2-2)$$

where  $a$  represents ground motion intensity (PGA),  $b$  and  $c$  are respectively location and shape parameters that can be obtained by maximizing the likelihood as shown below.

$$L = \prod_{i=1}^n [F(a_i)]^{x_i} [1 - F(a_i)]^{1-x_i} \quad (2-3)$$

$$\frac{\partial \ln L}{\partial b} = \frac{\partial \ln L}{\partial c} = 0 \quad (2-4)$$

In order to develop fragility curves, the same empirical data as used in Section 2.1.1 is utilized. Fragility parameters are obtained in Method 1 and listed in table 2-2. Figure 2-30 represents fragility curves in all damage states.

**TABLE 2-2 Fragility Parameters using Weibull Distribution Function**

Damage States	Parameters		Mean (g)	SD	Median (g)
	$b$	$c$			
At least minor	0.9186	2.0397	0.8138	0.4180	0.7675
At least moderate	1.0115	2.4513	0.8971	0.3907	0.8711
At least major	1.2555	3.1284	1.1232	0.3932	1.1166
Collapse	1.8502	4.0571	1.6784	0.4649	1.6904

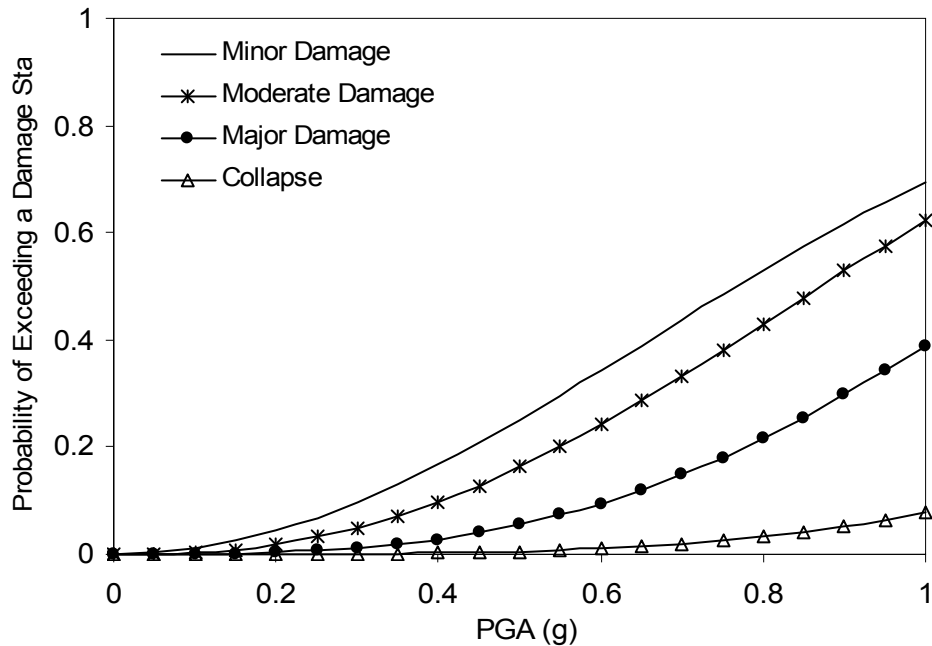


**FIGURE 2-30 Fragility Curve for Caltrans' Bridges developed in Method 1 using Weibull Distribution**

## 2.2 Test of Goodness of Fit

### 2.2.1 Method 1

According to Section A.2 in Appendix A, the  $P_{y^2}$  values for the fragility curve developed for Caltrans' bridges are computed as 0.38, 0.58, 0.56 and 0.50 for minor, moderate, major and collapse states, respectively. These values of  $P_{y^2}$  indicate that the hypotheses involved in all the cases cannot be discarded at the significance level of 10%. It is noted here that this method can test the goodness of fit of fragility curves only over the range of PGA where damage data sufficiently exist.

Figures 2-31~2-34 show the validity of the assumption of in (A-16) being asymptotically normal by means of plotting 100 simulated realizations of  $Y^2$  associated with the corresponding state of damage, respectively. This requires simulation of  $X_i$  at each  $a_i$  using  $p_i$  based on  $c_0$  and  $\zeta_0$  obtained from the empirically or analytically observed damage data for each state of damage. Upon simulating all  $X_i$  for all  $a_i$  and obtaining their realizations  $x_i$ , (A-19) is evaluated. This process is repeated  $n$  times ( $n=100$  here) to produce 100 realizations of  $Y^2$ , each representing one set of simulation of  $x_i$  ( $i = 1, 2, \dots, N$ ). This sample of  $y^2$  is indeed plotted in figures 2-31~2-34 for the corresponding states of damage using the normal probability paper; the dashed line represents the least square fit of the sample, while the solid line indicates the theoretical normal distribution with the mean and standard deviation given by (A-17) and (A-18) respectively for the fragility curves for Caltrans' bridges.

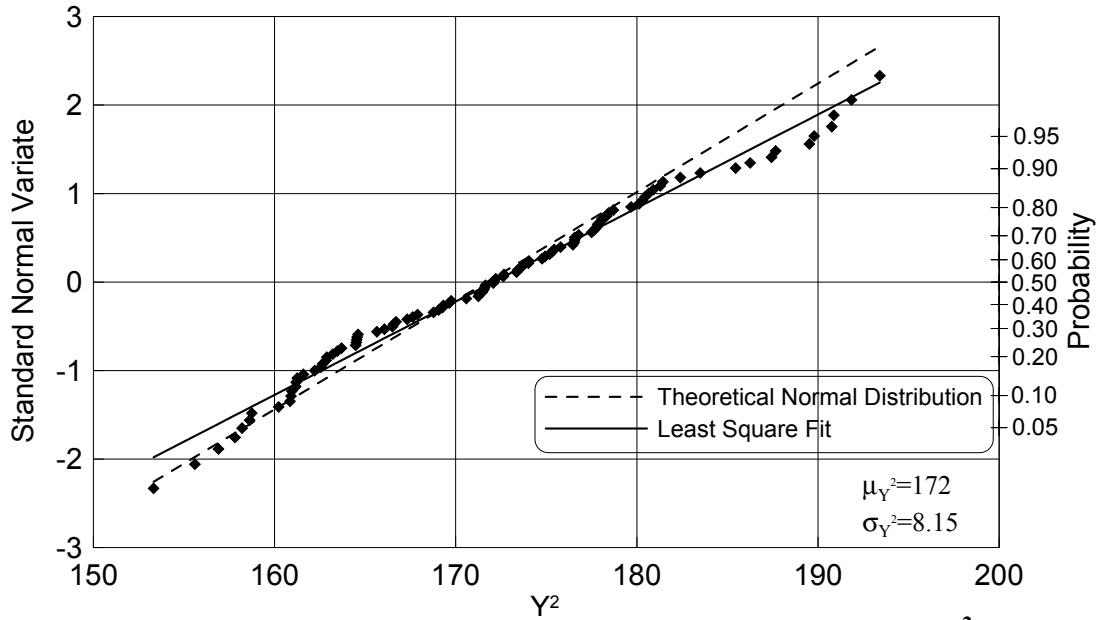


**FIGURE 2-31 Validity of Asymptotic Normality of Statistic  $Y^2$   
(Caltrans' Bridges with at least Minor Damage/Method 1)**

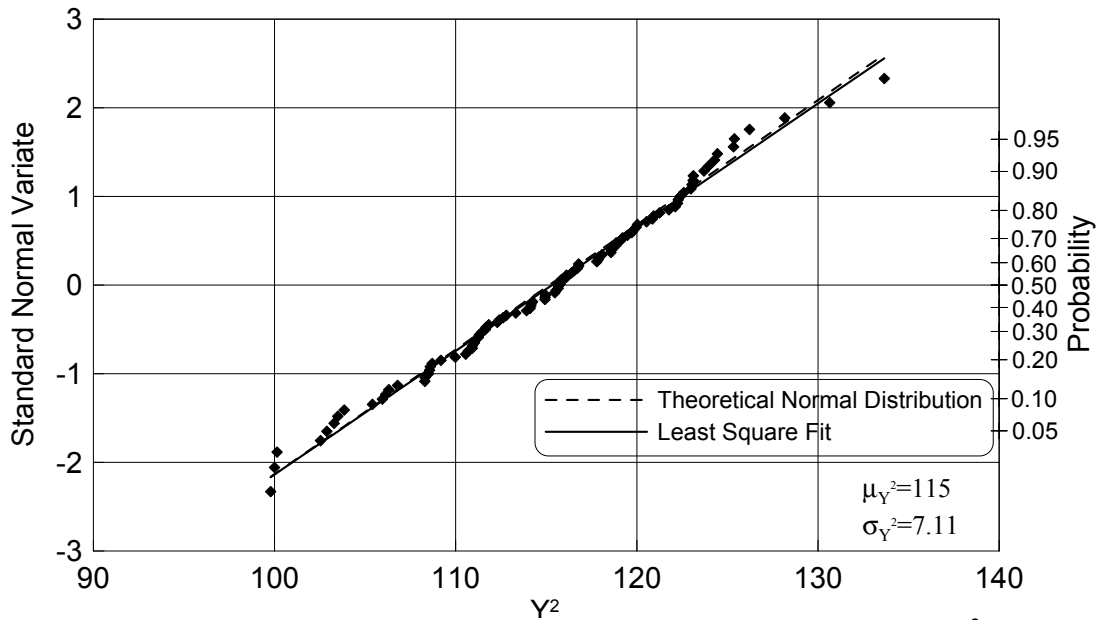


**FIGURE 2-32 Validity of Asymptotic Normality of Statistic  $Y^2$   
(Caltrans' Bridges with at least Moderate Damage/Method 1)**

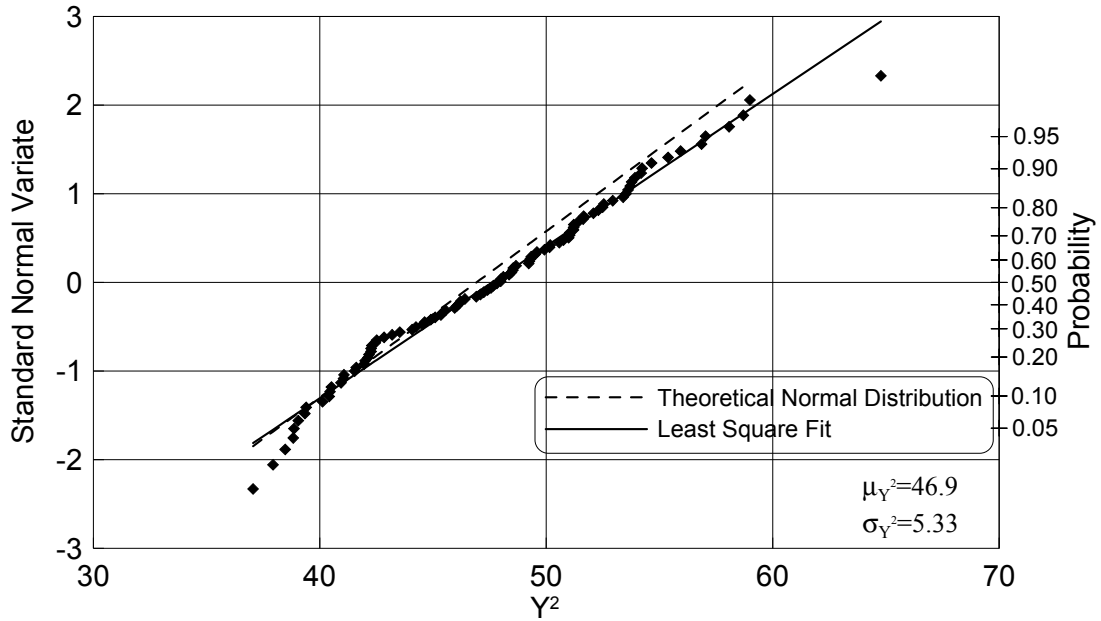


**FIGURE 2-33 Validity of Asymptotic Normality of Statistic  $Y^2$   
(Caltrans' Bridges with at least Major Damage/Method 1)**

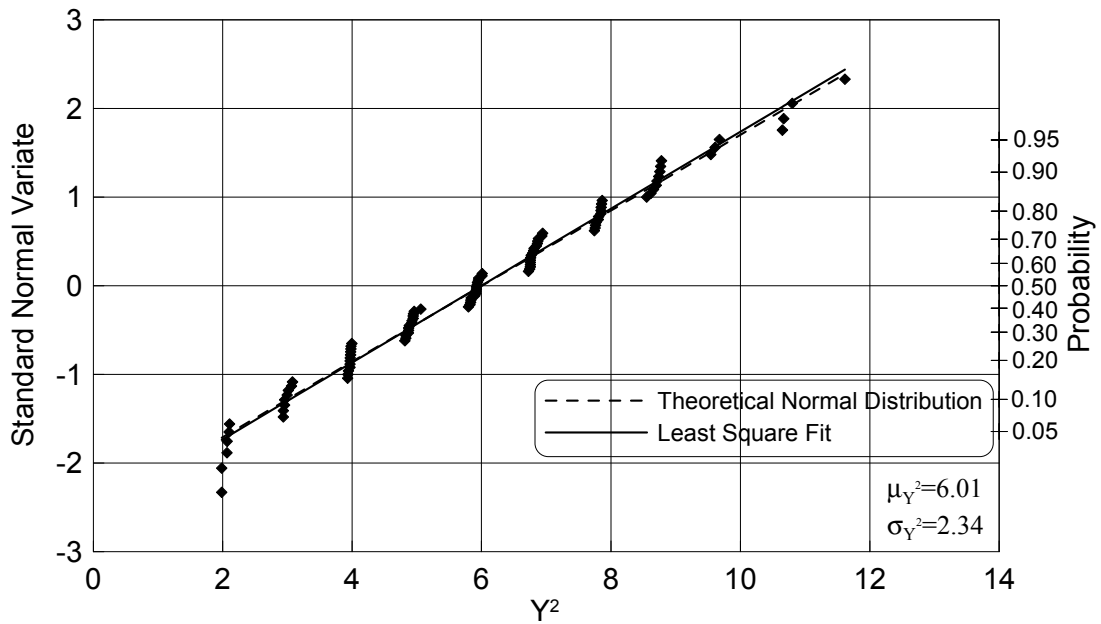


**FIGURE 2-34 Validity of Asymptotic Normality of Statistic  $Y^2$   
(Caltrans' Bridges with Collapse Damage/Method 1)**



This analysis is also conducted for weibull distribution and obtained values for  $P_{y^2}$  are presented in table 2-3. These values indicate that the hypotheses involved in all the cases cannot be discarded at the significance level of 10%.

**Table 2-3  $P_{y^2}$  Values for Goodness of Fit**

Damage States	Log-normal	Weibull
Minor	0.38	0.59
Moderate	0.58	0.69
Major	0.56	0.599
Collapse	0.50	0.51

### 2.2.2 Method 2

The  $P_{y^2}$  value for the fragility curves developed for Caltrans' bridges in Method 2 is computed to be 0.45. This value is sufficiently small so that the family of fragility curves simultaneously estimated cannot be discarded in the case of Caltrans' bridges at the significance level of 10%. The validity of asymptotic normality is also checked by simulating 100 realizations of  $Y^2$  in (5-12), each realization representing one set of simulation of  $x_{ik}$  ( $i = 1, 2, \dots, N; k = 1, 2, \dots, m$ ) with  $N = 1998$  and  $m = 5$ . The 100 realizations each for Caltrans' data are plotted in the normal probability papers as shown in figure 2-35. These plots clearly support the validity of asymptotic normality of  $Y^2$  in (A-24).

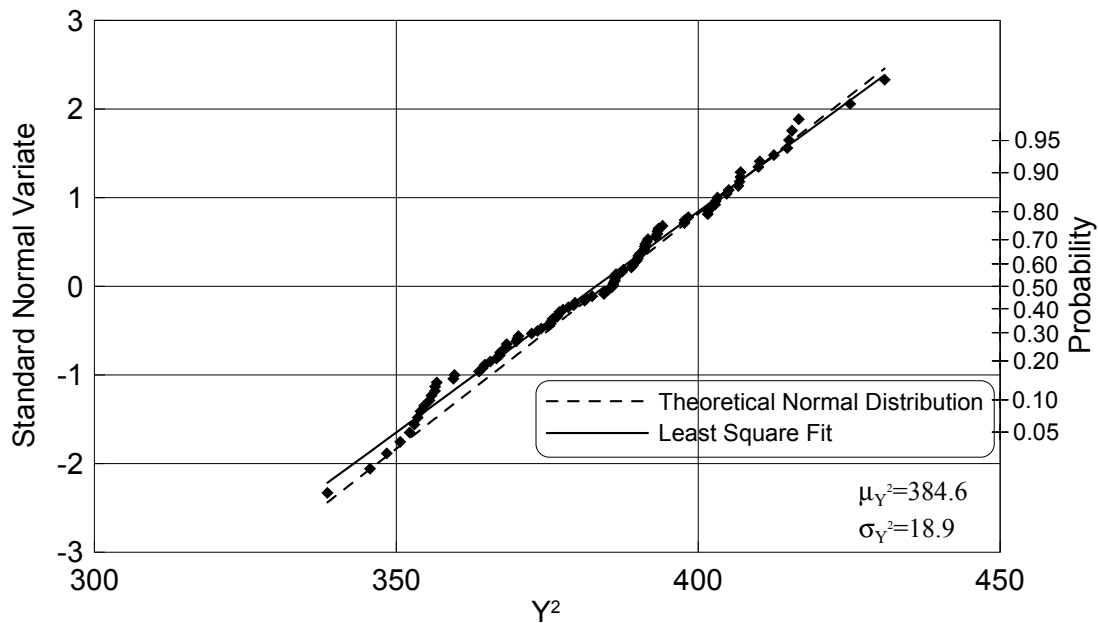


**FIGURE 2-35 Validity of Asymptotic Normality of Statistic  $Y^2$  (Caltrans' Bridges/Method 2)**

### 2.3 Estimation of Confidence Interval

The estimators  $\hat{c}$  and  $\hat{\zeta}$  of  $c$  and  $\zeta$  cannot be explicitly given in terms of analytical form as they represent optimal solutions obtained numerically by maximizing the logarithmic likelihood function. From the uncertainty analysis point of view, however, it is most desirable to demonstrate the extent of the statistical variations of these estimators by generating their realizations with the aid of a Monte Carlo simulation procedure. The following example is worked out for the fragility parameters  $c_j$  ( $j=1, 2, 3, 4$ ) and  $\zeta$  of Caltrans' bridges estimated by Method 2 assuming that the sample is composite. The Monte Carlo procedure calls for the simulation of  $X_{ik}$  ( $i = 1, 2, \dots, N$  and  $k = 1, 2, \dots, 5$ ), based on the family of fragility curves with the parameters  $c_{j,0}$  ( $j=1, 2, 3, 4$ ) and  $\zeta_0$  obtained from the maximum likelihood method. This much is the same procedure as executed for the validation of asymptotic normality of  $Y^2$  under Method 2. In the present case, however, (A-12) must be solved for the maximum likelihood estimates  $c_{j,0}^*$  and  $\zeta_0^*$  using the simulated realizations  $x_{ik}$  of  $X_{ik}$  in (A-10) and (A-11). Repeating this process a large number of times (500 times in this case), one obtains 500 sets of realizations of  $\hat{c}_j$  and  $\hat{\zeta}$ . This study contends that the statistical variation of these realizations presents a first approximation for the statistical variation of  $\hat{c}_j$  and  $\hat{\zeta}$ . The nature of the maximum likelihood estimates  $\hat{c}_j$  (and hence  $\log \hat{c}_j$ ) and  $\hat{\zeta}$  dictates that they are jointly distributed normally as  $N \rightarrow \infty$  (i.e., asymptotically). For the ease of understanding, 500 sets of four points  $(c_{1,0}^*, \zeta_0^*)$ ,  $(c_{2,0}^*, \zeta_0^*)$ ,  $(c_{3,0}^*, \zeta_0^*)$ ,  $(c_{4,0}^*, \zeta_0^*)$  thus simulated are plotted in figure 2-36 respectively corresponding to the states of at least minor, at least moderate, at least major damage and collapse. Marginal distributions of  $c_{j,0}^*$  are also separately plotted on log-normal probability papers for different states of damage in figures 2-37, 2-38, 2-39 and 2-40, respectively. Medians indicated in these figures are in good agreements with the corresponding values (i.e.,  $c_{1,0}$ ,  $c_{2,0}$ ,  $c_{3,0}$ ,  $c_{4,0}$ ) in figure 2-10. Although  $\zeta^*$  is asymptotically normal, it is plotted on a log-normal paper in figure 2-41. The median value 0.81 indicated in figure 2-41 agrees very well with  $\zeta_0=0.8152$  shown in figure A-4 (Appendix A). Figures 2-37 ~ 2-41 show that marginal distributions of simulated parameter values fit quite well to log-normal distribution functions. Assuming the distribution of  $\hat{c}_j$  being lognormal, and identifying, from the results in figures 2-37 ~ 2-40, the 90% confidence interval associated with exceedance probabilities 95% and 5% of  $\hat{c}_j$ , the fragility curves of Caltrans' bridges with the four states of damage are given in figures 2-42 ~ 2-45, respectively together with the confidence information. In each of these figures, the curves on the left, at the center and on the right respectively represent the fragility curves with 95%, 50% and 5% confidence consistent with figures 2-37 ~ 2-40. As in the risk assessment procedure for the nuclear power plant (NRC, 1983), the log-standard deviation associated with 50% confidence in figure 2-41 (0.81 in this case) is used for the three curves in each figure, although it is possible to use 95% and 5% confidence value of  $\hat{\zeta}$  together with those of  $\hat{c}_j$ . This study contends as in PRA procedures Guide (NRC, 1983) that the use of 50%

confidence value of  $\hat{\xi}$  only is justifiable because the variation in  $\hat{c}_j$  has the first order effect on fragility values whereas that in  $\hat{\xi}$  has the second order effect in general. Figure 2-46 plots all these fragility curves at three levels of confidence for the ease of comparison.

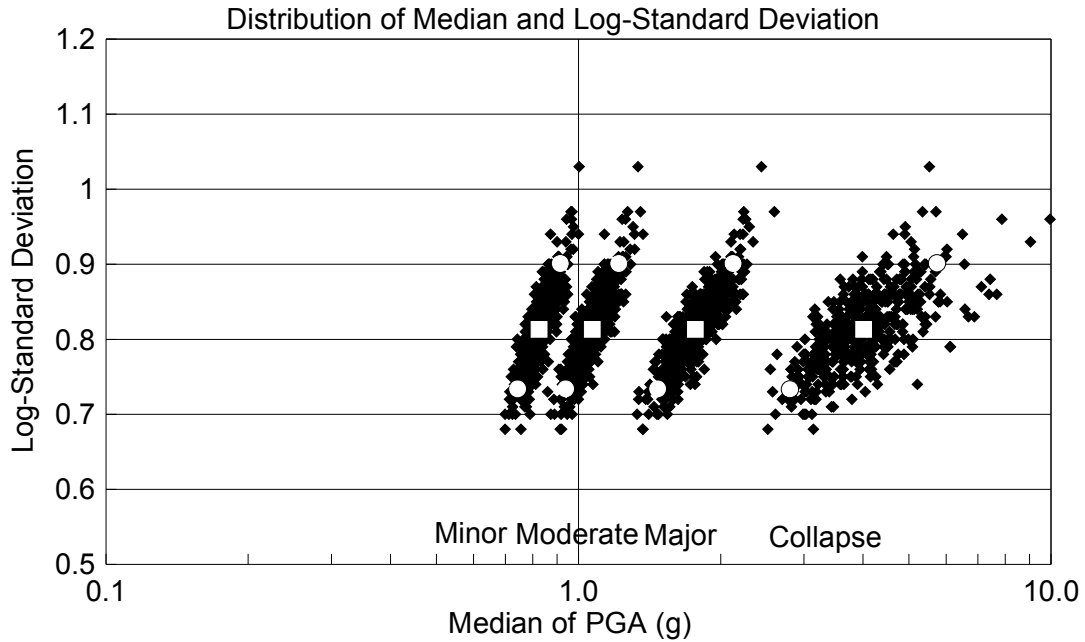


**FIGURE 2-36 Two-Dimensional Plot of 500 Sets of Simulated Realizations of Medians ( $\hat{C}_1, \hat{C}_2, \hat{C}_3, \hat{C}_4$ ) and Log-Standard Deviations  $\hat{\xi}$**

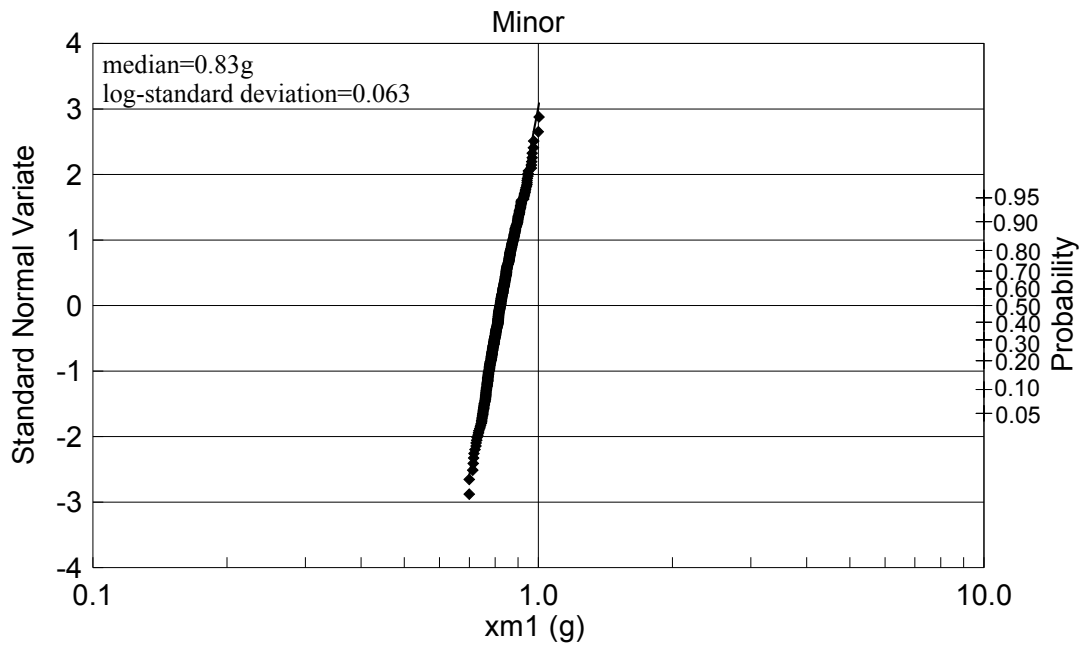


**FIGURE 2-37 Log-Normal Plot of Realizations of 500 Realizations of  $\hat{C}_1$  (Caltrans' Bridges/Method 2)**

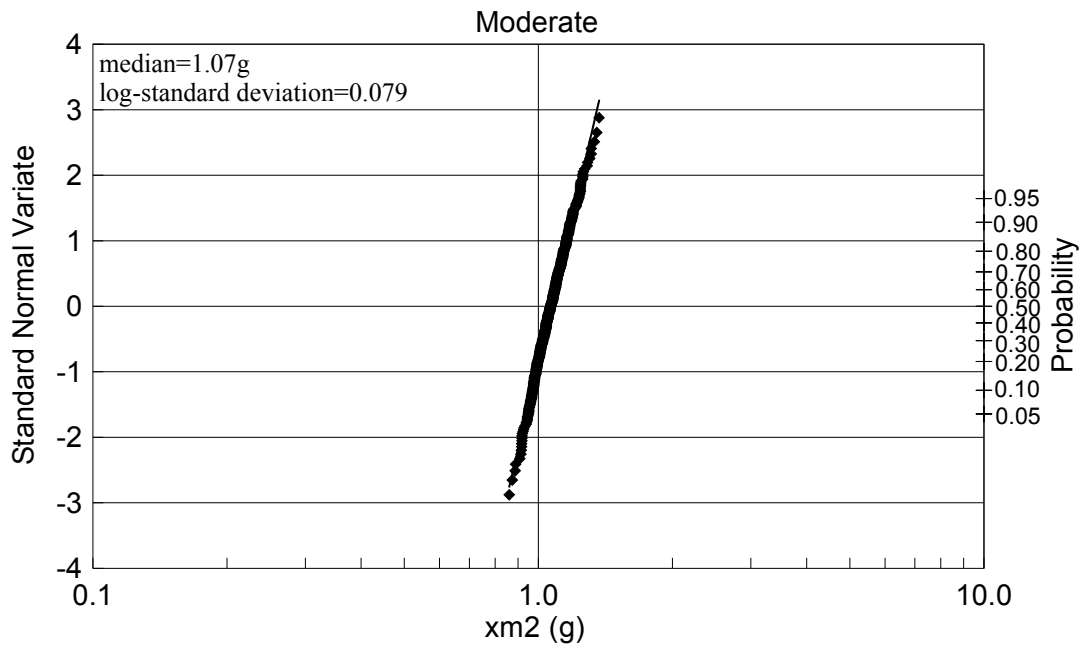


**FIGURE 2-38 Log-Normal Plot of Realizations of 500 Realizations of  $\hat{C}_2$  (Caltrans' Bridges/Method 2)**

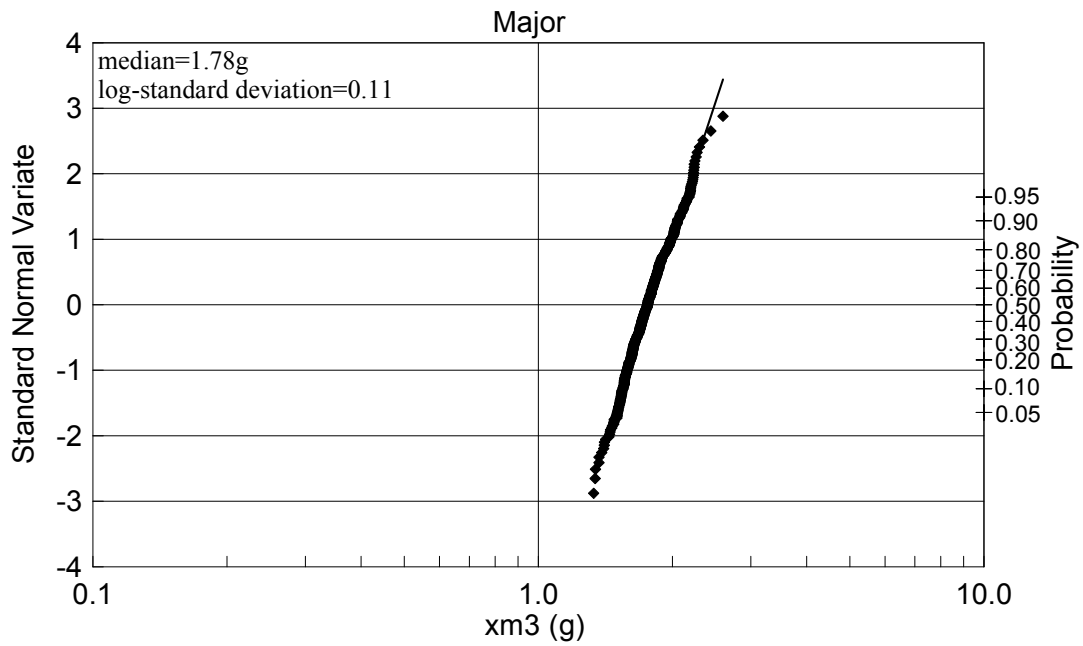


**FIGURE 2-39 Log-Normal Plot of Realizations of 500 Realizations of  $\hat{C}_3$  (Caltrans' Bridges/Method 2)**

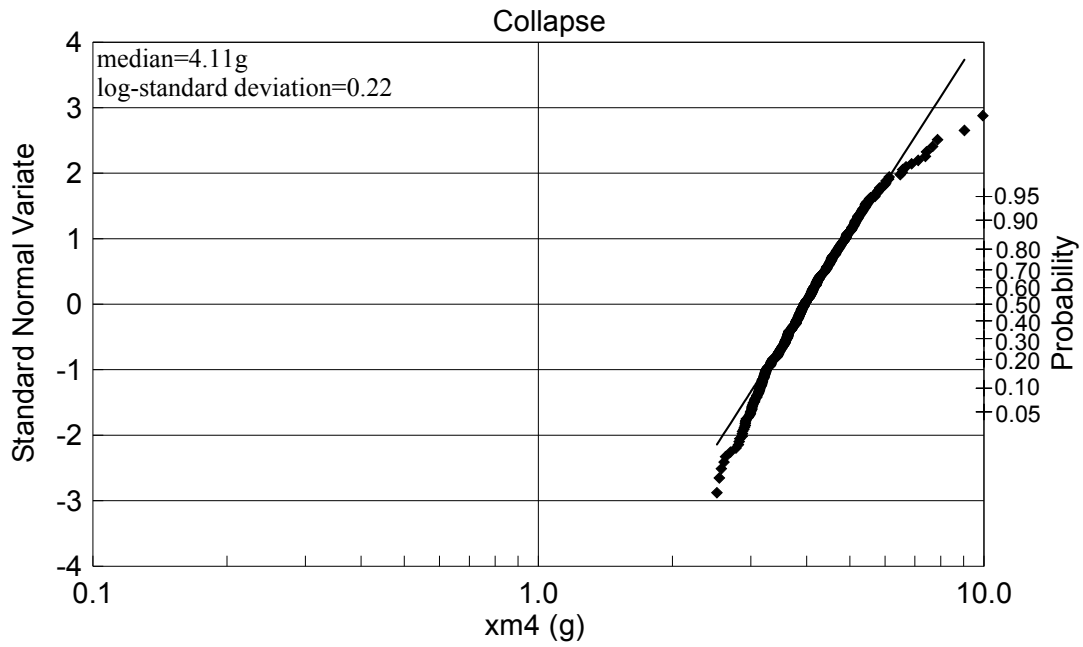


**FIGURE 2-40 Log-Normal Plot of Realizations of 500 Realizations of  $\hat{C}_4$  (Caltrans' Bridges/Method 2)**

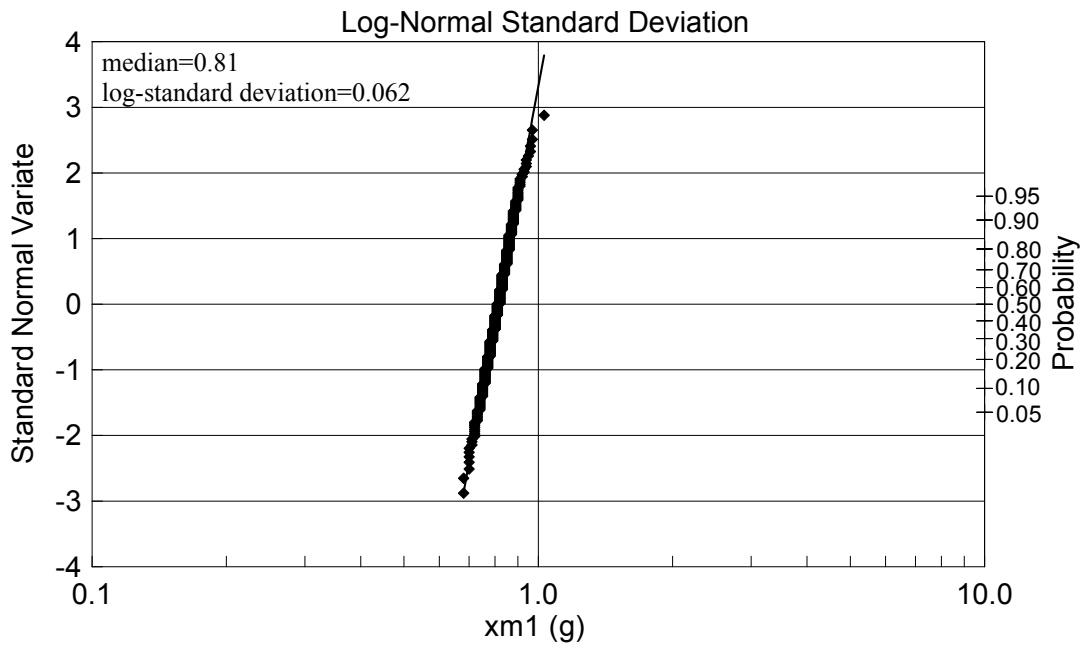


**FIGURE 2-41 Log-Normal Plot of Realizations of 500 Realizations of  $\hat{\xi}$  (Caltrans' Bridges/Method 2)**

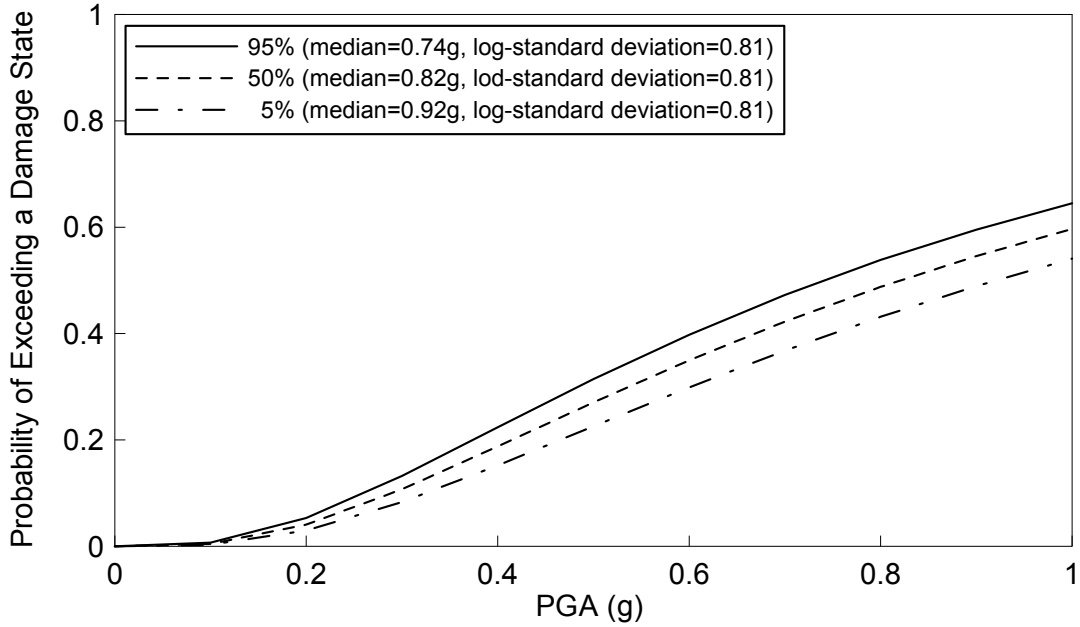


**FIGURE 2-42 Fragility Curves for State of at least Minor Damage with 95%, 50% and 5% Statistical Confidence (Caltrans' Bridges/Method 2)**

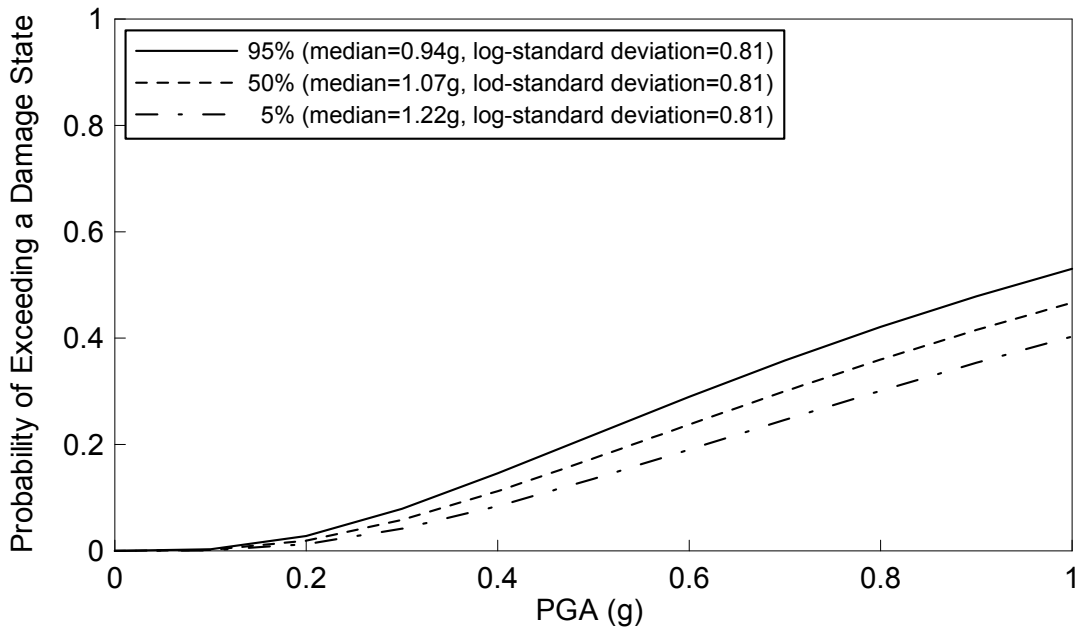


**FIGURE 2-43 Fragility Curves for State of at least Moderate Damage with 95%, 50% and 5% Statistical Confidence (Caltrans' Bridges/Method 2)**

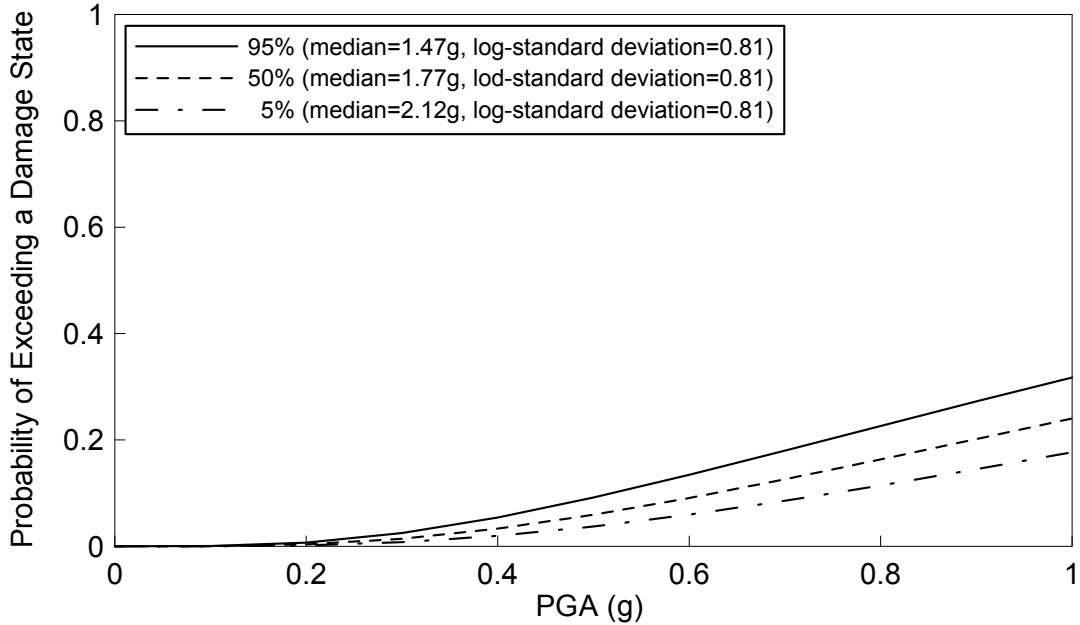


**FIGURE 2-44 Fragility Curves for State of at least Major Damage with 95%, 50% and 5% Statistical Confidence (Caltrans' Bridges/Method 2)**

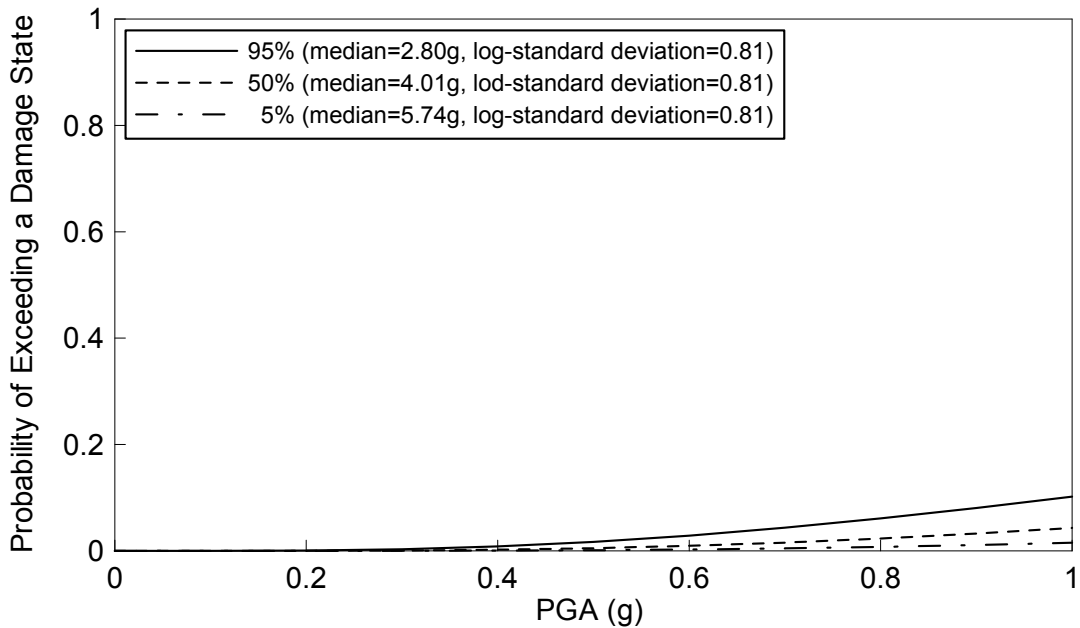


**FIGURE 2-45 Fragility Curves for State of Collapse Damage with 95%, 50% and 5% Statistical Confidence (Caltrans' Bridges/Method 2)**

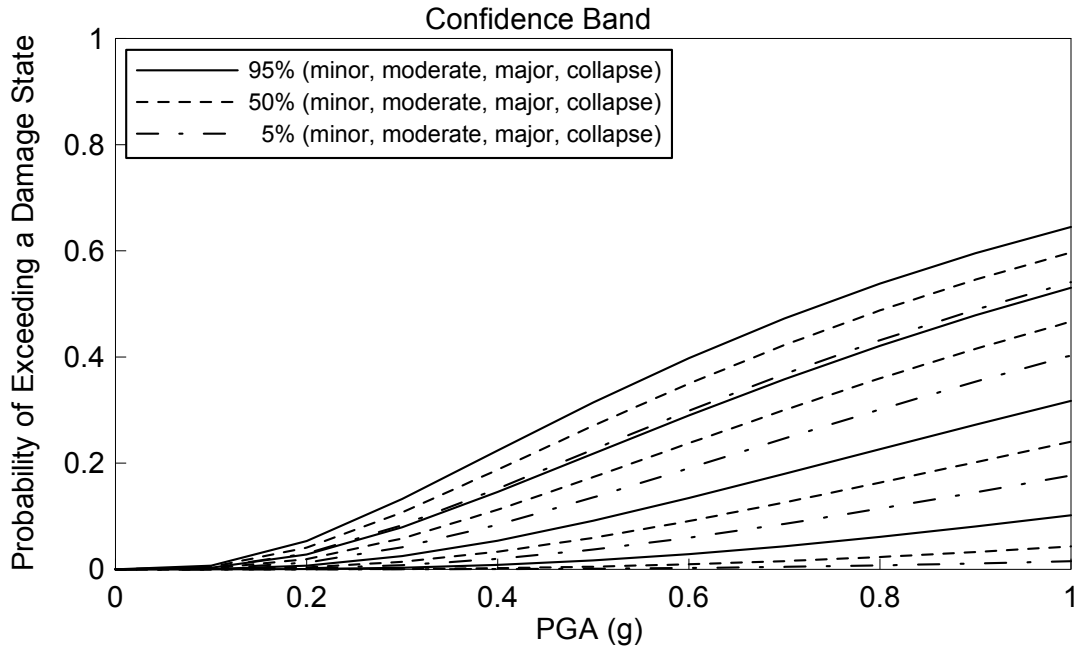


**FIGURE 2-46 Combined Plot of Fragility Curves for Caltrans' Bridges with 95%, 50% and 5% Statistical Confidence (Method 2)**



### SECTION 3

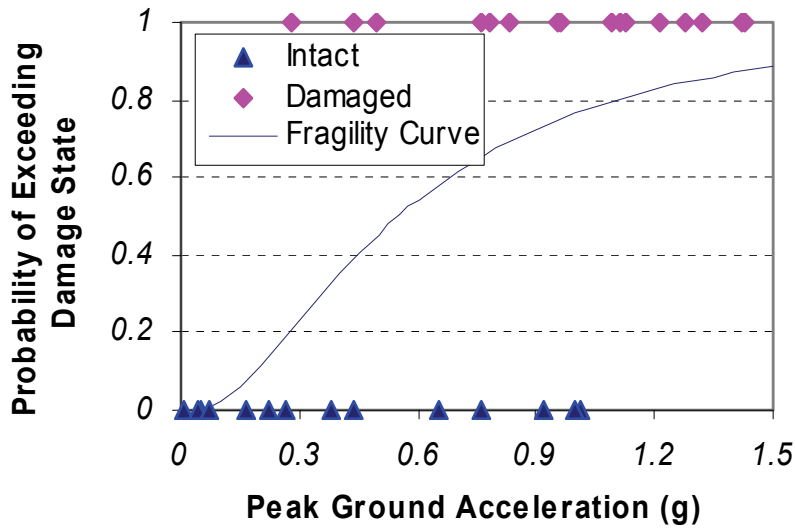
## MODEL-BASED UNCERTAINTY ANALYSIS OF FRAGILITY CURVES

Fragility model plays an essential role in predicting the seismic risk and states of damage of urban infrastructure systems after future earthquakes. Such information will then be used as input to evaluate the degraded performance of systems, and therefore, to estimate associated economic loss. Hence, accuracy in the fragility model has utmost importance for reliable a risk estimation. However, the uncertainty resulting from modeling and imperfect information is inevitably involved in the development of the fragility model. As this uncertainty propagates through the seismic risk analysis procedure, its contribution accumulates and eventually could produce a significant impact on the estimated final risk. Most of the current seismic risk analysis procedures can produce a “best” (point) estimate unless the whole process of risk assessment is not model-based. As the seismic risk analysis is an important tool for the decision-makers to evaluate various mitigation measures for most cost effective strategies for example, rational decision making requires that the level of uncertainty involved in the development of fragility curve be quantified and minimized as much as possible for a more reliable risk estimation.

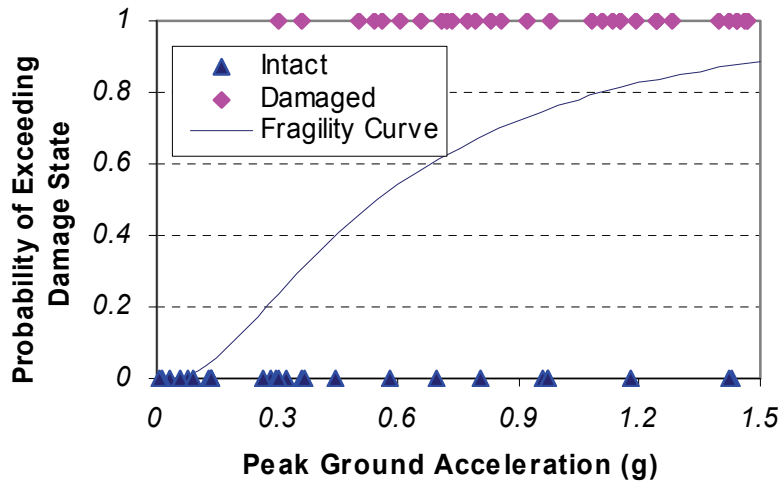
This chapter investigates the model-based uncertainty of the fragility curve in the most common form of lognormal distribution function. The fragility parameters are estimated by maximum likelihood method and a Monte Carlo simulation procedure is developed to obtain the associated uncertainty of the fragility curve. The simulation results quantitatively show the dependence of the uncertainty of the fragility parameters on sample size.

The fragility estimators,  $\hat{c}$  and  $\hat{\zeta}$  (in method 1) of the median and log-standard deviation can be obtained by performing the maximum likelihood method, based on the original fragility curve developed on the basis of damage data  $(x_i, a_i)$ . In figure 3-1, two identical fragility curves ( $c^{60} = c^{30} = 0.55g$ ,  $\zeta^{60} = \zeta^{30} = 0.83$ ) are obtained based on two sets of damage data of different sample size,  $N = 30$  or  $60$ .

Though these two different sets of damage data produce same fragility curves, the uncertainty of the fragility parameters cannot be implicitly expressed in terms of analytical format. In probabilistic risk analysis point of view, this uncertainty should be quantified and solved through Monte Carlo simulation procedure. In this procedure, realizations of the parameters are first obtained based on the originally estimates. Then the uncertainty of estimators is computed by asserting that the variation of these realizations represents the extent of the uncertainty of the estimators. The following section describes the process in detail.



(a) Sample Size = 30



(b) Sample Size = 60

**FIGURE 3-1 Fragility Curves ( $c^{60} = c^{30} = 0.55g$ ,  $\zeta^{60} = \zeta^{30} = 0.83$ )**

### 3.1 Realization of Parameters: Monte Carlo Simulation

#### 3.1.1 Realization Based on Method 1

Three steps are needed to generate a set of realizations of the parameter pair,  $c_e$  and  $\zeta_e$ . The first step is to identify a sample of damage data,  $(x_i^0, a_i^0)$  ( $i=1,2,\dots,N$ ). On the basis of the damage data,  $c_0$  and  $\zeta_0$  are estimated as point estimates which determines a fragility curve. The second step consists of the generation of damage data using this fragility curve just developed. In doing this, the value of ground motion intensity measure,  $a_i$ , is randomly generated independent of the parameters of the fragility curve, by assuming that they are uniformly distributed in a practical range (for example, 0-1.5g for PGA). For each  $a_i$ , a corresponding random number  $b_i$  is generated between 0 and 1. Depending on  $c_0$  and  $\zeta_0$ , the simulated damage state,  $x_i$  (1: damaged; 0: not damaged), at the ground motion level of  $a_i$ , is determined by

$$x_{i0} = \begin{cases} 1 & \text{if } b_i > \Phi\left(\frac{\ln(a_i/c_{01})}{\zeta_0}\right) \\ 0 & \text{else.} \end{cases} \quad (3-1)$$

In the third step, using the above maximum likelihood method, one set of realizations of the median value and log-standard deviation of the fragility curve can be obtained based on the  $N$  damage data pairs  $(a_i, x_i)$  ( $i=1,2,\dots,N$ ) simulated in the first step. Repeating the last two steps  $M$  times, a set of  $M$  realizations can be simulated.

#### 3.1.2 Realization Based on Method 2

If parameters of a group of fragility curves,  $c_{0j}$  ( $j=1,2,3,4$ ) and  $\zeta_0$  have estimated based on a sample of damage data  $(a_i^0, x_{ik}^0)$  ( $i=1,2,\dots,N; k=0,1,2,3,4$ ) by method 2, similar to procedure as in section 3.1.1 can be used to generate a set of realizations of the fragility parameter group, median values  $c_{ej}$  ( $j=1,2,3,4$ ) and  $\zeta_e$ . Again, simulated damage data should first be generated using estimated  $c_{0j}$  ( $j=1,2,3,4$ ) and  $\zeta_0$ . In doing so, the value of ground motion intensity measure,  $a_i$ , is again randomly generated and independent of the parameters of the fragility curves, by assuming that it is uniformly distributed in a practical range (for example, 0-1.5g for PGA). For each  $a_i$ , a corresponding random number  $b_i$  is generated between 0 and 1. Depending on  $c_{0j}$  and  $\zeta_0$ , the simulated damage state,  $x_{ik}$ , at the ground motion level of  $a_i$ , is determined by

$$x_{i0} = \begin{cases} 1 & \text{if } b_i > \Phi\left(\frac{\ln(a_i/c_{01})}{\zeta_0}\right) \\ 0 & \text{else.} \end{cases} \quad (3-2)$$

$$x_{i1} = \begin{cases} 1 & \text{if } \Phi\left(\frac{\ln(a_i/c_{02})}{\zeta_0}\right) < b_i \leq \Phi\left(\frac{\ln(a_i/c_{01})}{\zeta_0}\right) \\ 0 & \text{else.} \end{cases} \quad (3-3)$$

$$x_{i2} = \begin{cases} 1 & \text{if } \Phi\left(\frac{\ln(a_i/c_{03})}{\zeta_0}\right) < b_i \leq \Phi\left(\frac{\ln(a_i/c_{02})}{\zeta_0}\right) \\ 0 & \text{else.} \end{cases} \quad (3-4)$$

$$x_{i3} = \begin{cases} 1 & \text{if } \Phi\left(\frac{\ln(a_i/c_{04})}{\zeta_0}\right) < b_i \leq \Phi\left(\frac{\ln(a_i/c_{03})}{\zeta_0}\right) \\ 0 & \text{else.} \end{cases} \quad (3-5)$$

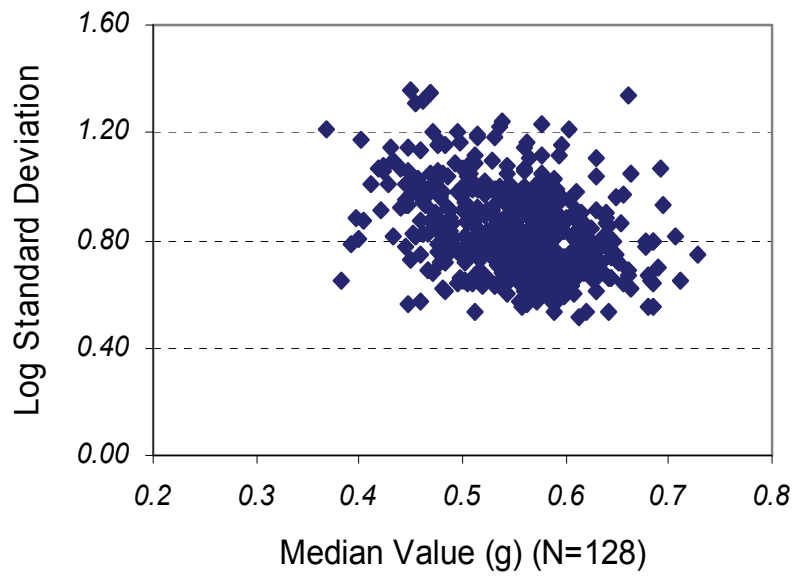
$$x_{i4} = \begin{cases} 1 & \text{if } b_i \leq \Phi\left(\frac{\ln(a_i/c_{04})}{\zeta_0}\right) \\ 0 & \text{else.} \end{cases} \quad (3-6)$$

In the third step, using the above maximum likelihood Method 2, one set of realizations of the median values and log-standard deviation of the fragility curves can be obtained based on the  $N$  damage data pairs  $(a_i, x_{ik})$  ( $i = 1, 2, \dots, N$ ;  $k = 0, 1, 2, 3, 4$ ) simulated in the first step. Repeating the last two steps  $M$  times, a set of  $M$  realizations of fragility parameters can also be simulated as in section 3.1.1.

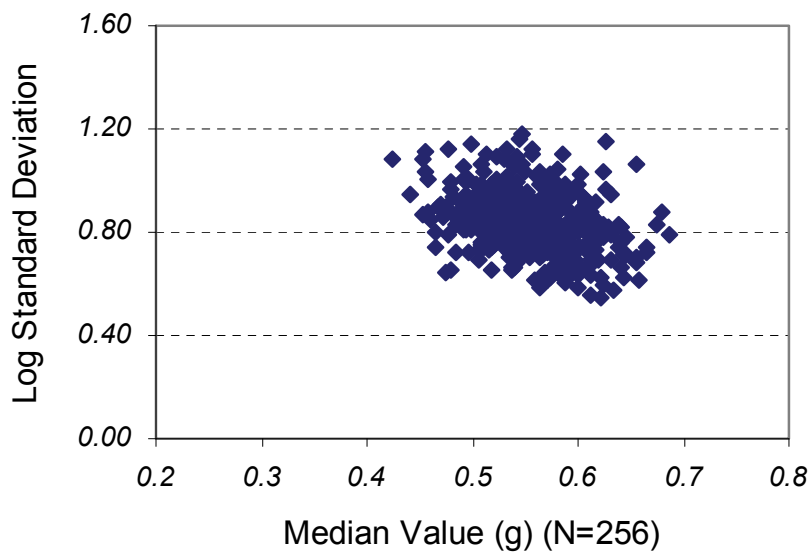
## 3.2 Confidence Interval

### 3.2.1 Confidence Interval Based on Method 1

The nature of the maximum likelihood estimates  $c_e$  (hence  $\ln c_e$ ) and  $\zeta_e$  dictates that they are jointly distributed normally as  $N \rightarrow \infty$  (i.e., asymptotically). The 500 sets of realizations are plotted for either case of sample size,  $N = 128$  and  $N = 256$  (figures 3-2(a) and 3-2(b)). These realizations are simulated from the same original estimates,  $c_0 = 0.55g$  and  $\zeta_0 = 0.83$  by repeating the above Monte Carlo procedure. Figure 3-2 graphically demonstrates that the realizations of the median value and log standard deviation in the case of  $N = 256$  are far more concentrated than that in the case of  $N = 128$ , and the variation of the realizations decreases as sample size  $N$  becomes larger. The marginal distributions of simulated  $c_e$  are also separately plotted on lognormal probability papers for the two sample cases (figures 3-3(a) and 3-3(b)). Median in either figure is in good agreements with the original estimate  $c_0$  with  $c_{m128} = c_{m256} = c_0 = 0.55g$ , where  $c_{m128}$  and  $c_{m256}$  are medians in the case of  $N = 128$  and  $256$ , respectively.

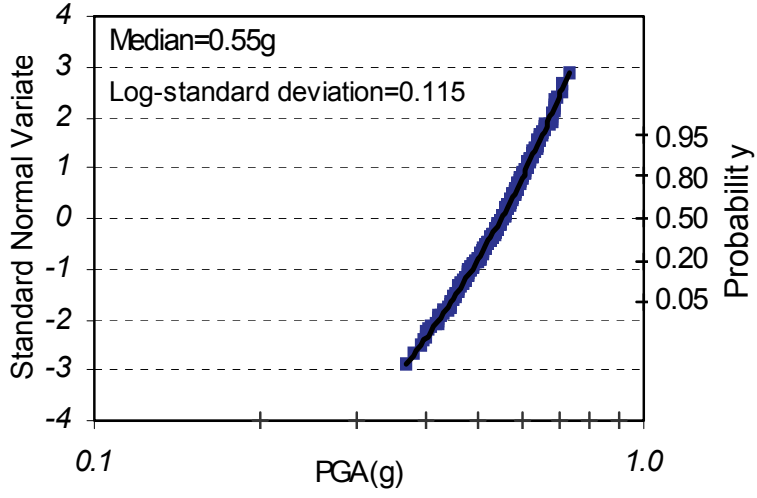


(a)

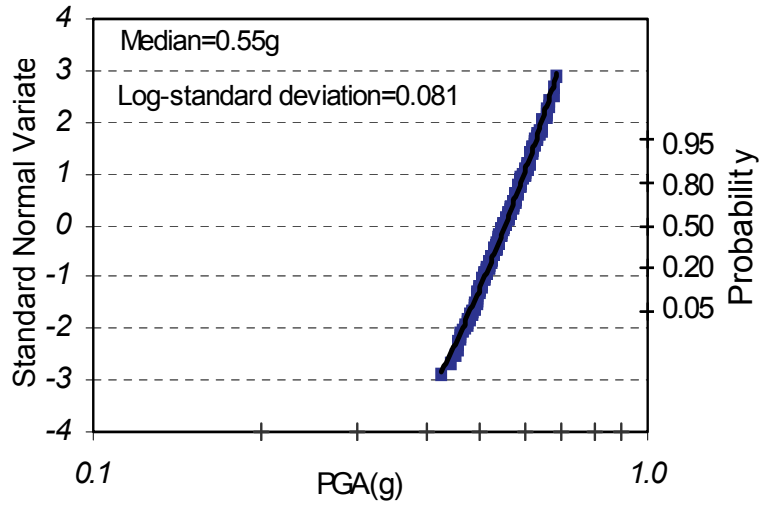


(b)

**FIGURE 3-2 Distribution of Simulated  $c$  and  $\zeta$  (Method 1)**



(a) N = 128



(b) N = 256

**FIGURE 3-3 Lognormal Plot of 500 Realizations of  $c$**

This study then contends that the variation of these realizations represents the statistical variation of the estimators  $\hat{c}$  and  $\hat{\zeta}$ . Assuming that the marginal distribution of  $\hat{c}$  is lognormal, one obtains  $\sigma_{\ln \hat{c}}$  and therefore  $\hat{c} = c_p$  associated with any exceedance probability of  $p\%$  of  $\hat{c}$ . The  $\zeta = \hat{\zeta}$  associated with  $c = \hat{c}_m$  is used for every  $\hat{c} = c_p$ , following the tradition of the risk assessment procedure for the nuclear power plant, which justifies that the variation in  $c$  has the first-order effect whereas that in  $\zeta$  has the second-order effect for ensuing risk analysis.

If original estimates,  $c_0 = 0.55g$  and  $\zeta_0 = 0.83$ , are resulting from sample size of  $N = 16, 24, 32, 64, 128$  and  $256$ , the corresponding  $\sigma_{\ln \hat{c}}$  can be similarly obtained. Figure 3-4 presents the quantitative relationship between  $\sigma_{\ln \hat{c}}$ , the statistical variation of the estimate  $\hat{c}$ , and sample size  $N$ , in which  $\sigma_{\ln \hat{c}}$  is approximately proportional to  $1/\sqrt{N}$ . Three groups of fragility curves, corresponding to  $c_p$  with confidence level of 5%, 50% and 95%, respectively, are plotted in figure 3-5 for sample size  $N = 16, 64$  and  $256$ . It can be clearly seen that the confidence band of the fragility curve narrows down as sample size increases.

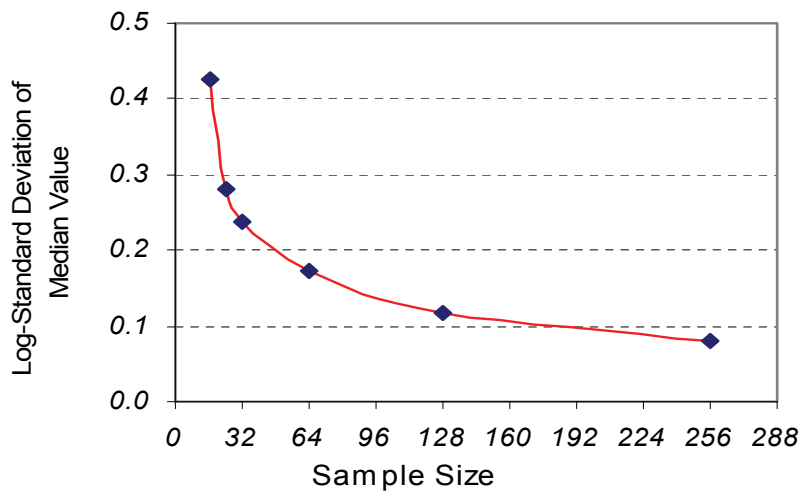


**FIGURE 3-4 Statistical Uncertainty in terms of Sample Size (Method 1)**

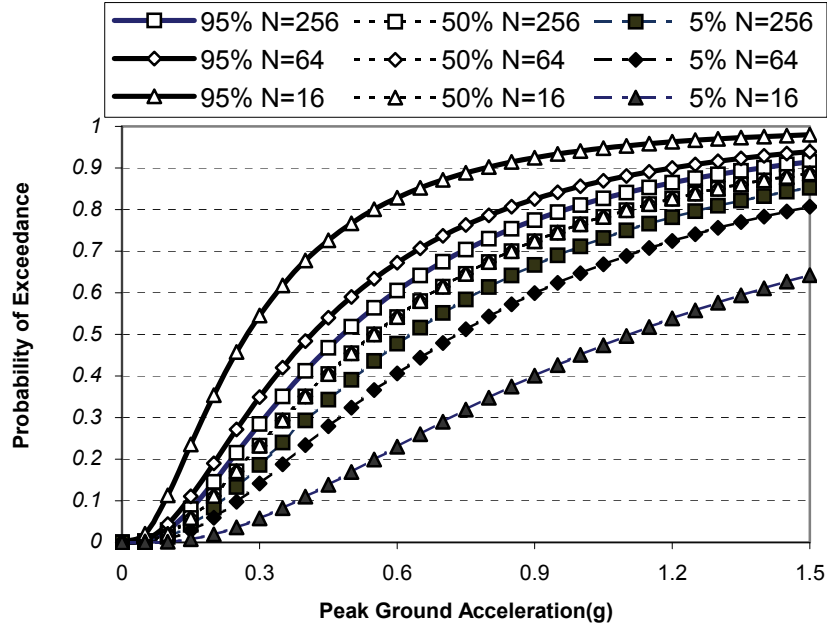


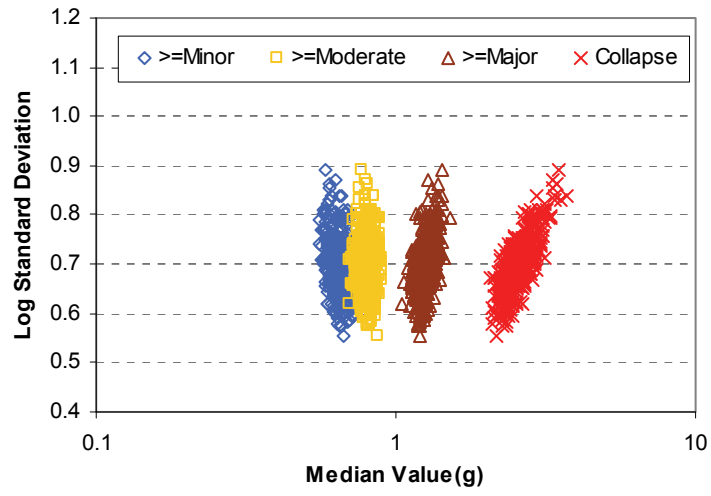
**FIGURE 3-5 Confidence Bands Comparison**

### 3.2.2 Confidence Interval Based on Method 2

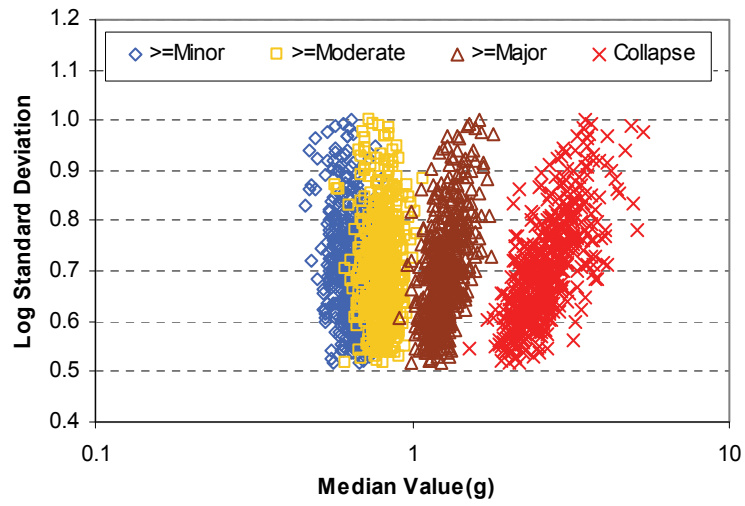
The nature of the maximum likelihood estimates  $c_{ej}$  (hence  $\ln c_{ej}$ ) and  $\zeta_e$  dictates that they are also jointly distributed normally as  $N \rightarrow \infty$  (i.e., asymptotically). The 500 sets of realizations are plotted for either case of sample size,  $N = 512$  and  $N = 256$  (figures 3-6(a) and 3-6(b)). These realizations are simulated from the same original estimates,  $c_{01} = 0.64g$ ,  $c_{02} = 0.80g$ ,  $c_{03} = 1.25g$ ,  $c_{04} = 2.55g$  and  $\zeta_0 = 0.70$  based on the historical bridge damage data collected from 1994 Northridge Earthquake by repeating the above Monte Carlo procedure. Figure 3-6 graphically demonstrates that the realizations of the median value and log standard deviation in the case of  $N = 512$  are far more concentrated than that in the case of  $N = 128$ , and the variation of the realizations decreases as sample size  $N$  becomes larger.

It then contends that the variation of these realizations represents the statistical variation of the estimators  $\hat{c}_j$  and  $\hat{\zeta}$ . Assuming that the marginal distribution of  $\hat{c}_j$  is lognormal, one obtains  $\sigma_{\ln \hat{c}_j}$  and therefore  $\hat{c}_j = c_{pj}$  associated with any exceedance probability of  $p\%$  of  $\hat{c}_j$ . The  $\zeta = \hat{\zeta}$  associated with  $c_j = \hat{c}_{mj}$  is used for every  $\hat{c}_j = c_{pj}$ . Based on this, table 3-1 lists the log-standard deviation of the simulated median values of the four fragility curves representing different damage states, when sample sizes are 64, 128, 256, 512 and 1024. The median values with confidence level of 5% and 95% probability of being exceeded (table 3-2) are calculated according to the variations in table 3-1. Finally, figure 3-7 represents the log-standard deviations of median values for different sample sizes.





(a) Sample Size = 512



(b) Sample Size = 128

**FIGURE 3-6 Distribution of Simulated  $c_i$  and  $\zeta$  (Method 2)**

**TABLE 3-1 Variation of Simulated Median Values (Method 2)**

Sample Size	Log-Standard Deviation of Median Value			
	At least minor	At least moderate	At least major	Collapse
1024	0.039	0.038	0.041	0.064
512	0.050	0.048	0.055	0.096
256	0.066	0.065	0.078	0.129
128	0.099	0.093	0.109	0.196
64	0.132	0.129	0.148	0.260

**TABLE 3-2 Confidence Band of Fragility Median Values (Method 2)**

Confidence Level	95% (g)					5% (g)				
	64	128	256	512	1024	64	128	256	512	1024
At least minor	0.515	0.544	0.574	0.589	0.602	0.795	0.753	0.713	0.695	0.681
At least moderate	0.648	0.687	0.719	0.740	0.757	0.988	0.932	0.890	0.865	0.845
At least major	0.980	1.044	1.099	1.142	1.170	1.594	1.496	1.421	1.368	1.336
Collapse	1.658	1.853	2.069	2.188	2.313	3.952	3.537	3.168	2.996	2.833

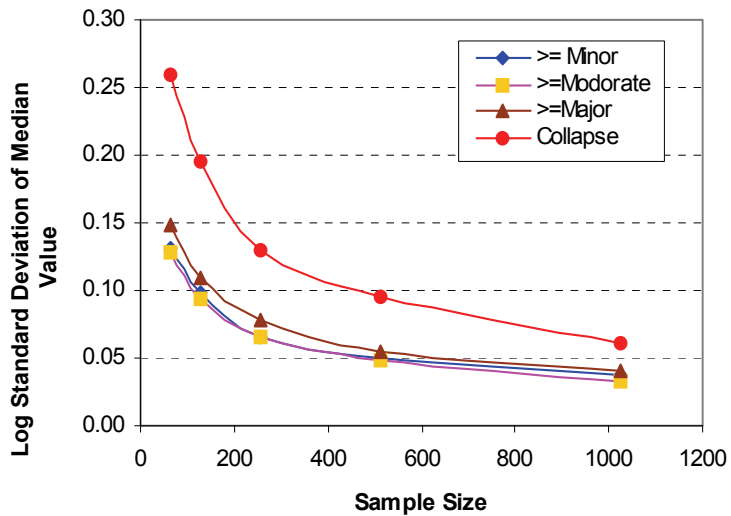


**FIGURE 3-7 Statistical Uncertainty in terms of Sample Size (Method 2)**

### 3.3 Summary

This chapter presents an innovative Monte Carlo simulation method for obtaining statistical uncertainty of fragility parameters. As these parameters are not available in analytical form, the extent of the statistical uncertainty of these two parameters can only be obtained numerically in a Monte Carlo simulation. The realization of the parameters is obtained by simulating a sample of damage data based on the fragility curves developed on the basis of the original estimate of these parameters  $c_0$  (or  $c_{i0}$ ) and  $\zeta_0$ . The statistical uncertainty is then approximately represented by the variation of a large number of realizations of these parameters. The simulation result clearly shows that as the sample size increases, the statistical variation of the parameters becomes smaller and the confidence band of the parameters narrows down in accordance with a factor of  $1/\sqrt{N}$  with  $N$  being the sample size. Thus obtained statistical uncertainty of fragility parameters can be used in the seismic risk analysis to achieve more reliable risk estimate for structural components and systems.



## **SECTION 4 DEVELOPMENT OF ANALYTICAL FRAGILITY CURVES**

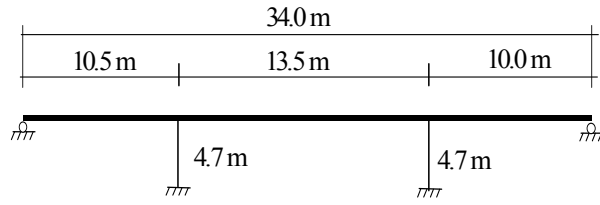
To examine the performance of bridges under seismic ground motions, finite element modeling of five (5) typical reinforced concrete bridges with various dimensions, configurations and site conditions in California is done and analyzed using commercially available structural analysis computer code. Figure 4-1 shows the schematic diagrams of these five bridges. To improve the seismic performance, these bridges are retrofitted using steel jacketing technique. The detail in finite element modeling of these bridges and retrofitting technique is given in Appendix B.

To generate analytical fragility curves, bridges are analyzed under 60 earthquake ground motion time histories in Los Angeles area. The details of selected ground motions, moment curvature analysis of bridge columns and bridge damage state definitions can also be found in Appendix B.

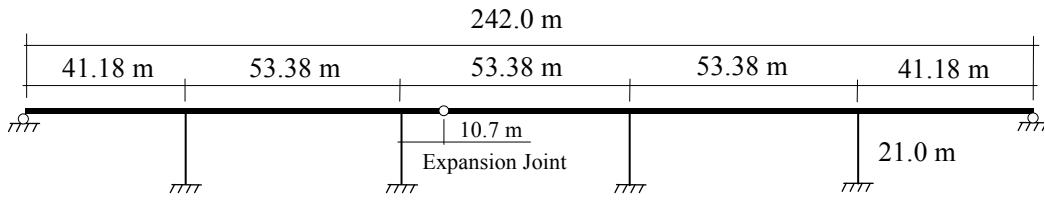
### **4.1 Time History Analysis of Bridges**

#### **4.1.1 Analytical Fragility Curves in Longitudinal Direction**

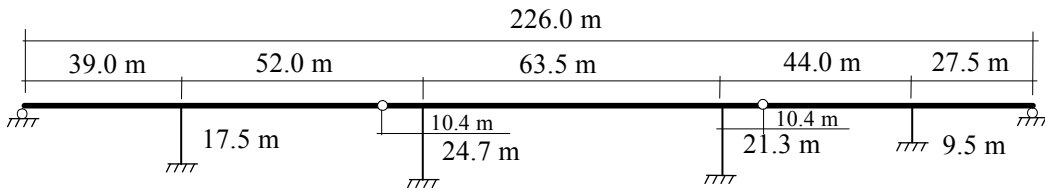
To construct analytical fragility curves of the example bridges, bridge models are analyzed under sixty (60) ground motion time histories. According to the damage states definition given by Dutta and Mander (1998), ductility demands at each damage states are calculated (Appendix B, Section B.5). Bridges are analyzed considering no resistance from embankment soil at abutment locations such that superstructure can move freely in longitudinal direction. Figures 4-2 to 4-6 show the analytical fragility curves of Bridge 1 to 5 respectively. This part does not consider the longitudinal stiffness of the abutments. This topic is discussed in the later part of this section.



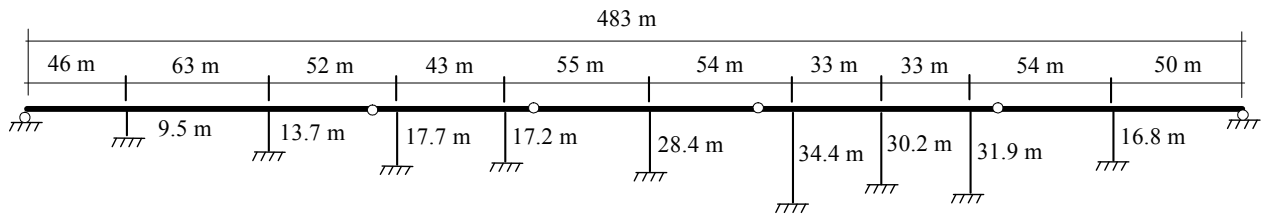
**(a) Bridge 1**



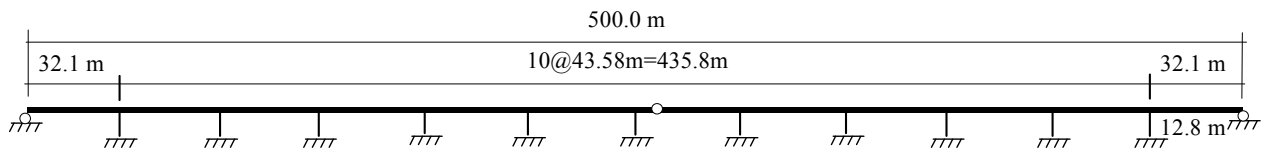
**(b) Bridge 2**



**(c) Bridge 3**



**(d) Bridge 4**



**(e) Bridge 5**

**FIGURE 4-1 Elevation of Sample Bridges**

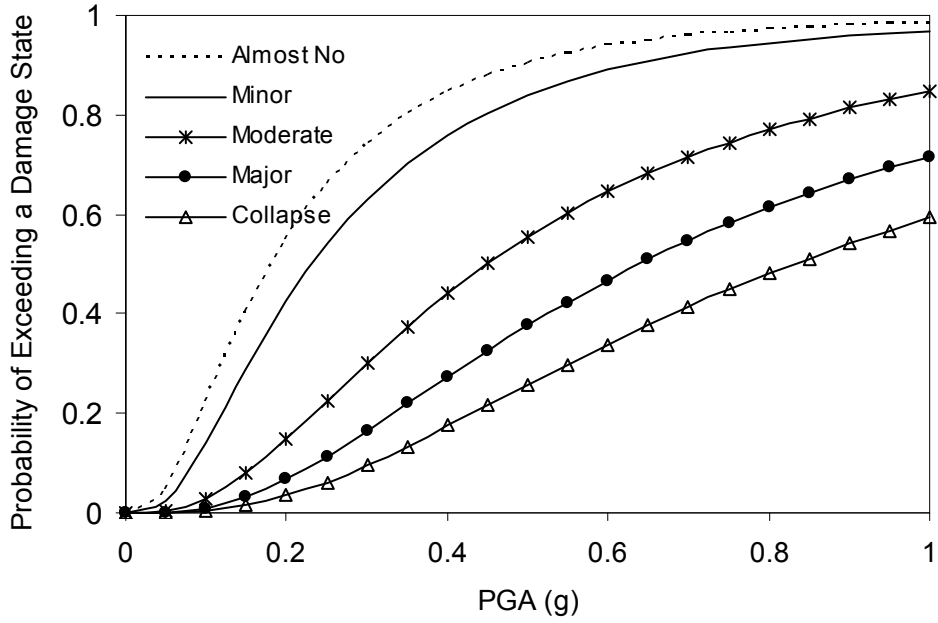


**FIGURE 4-2 Fragility Curves of Bridge 1 for Five Damage States**

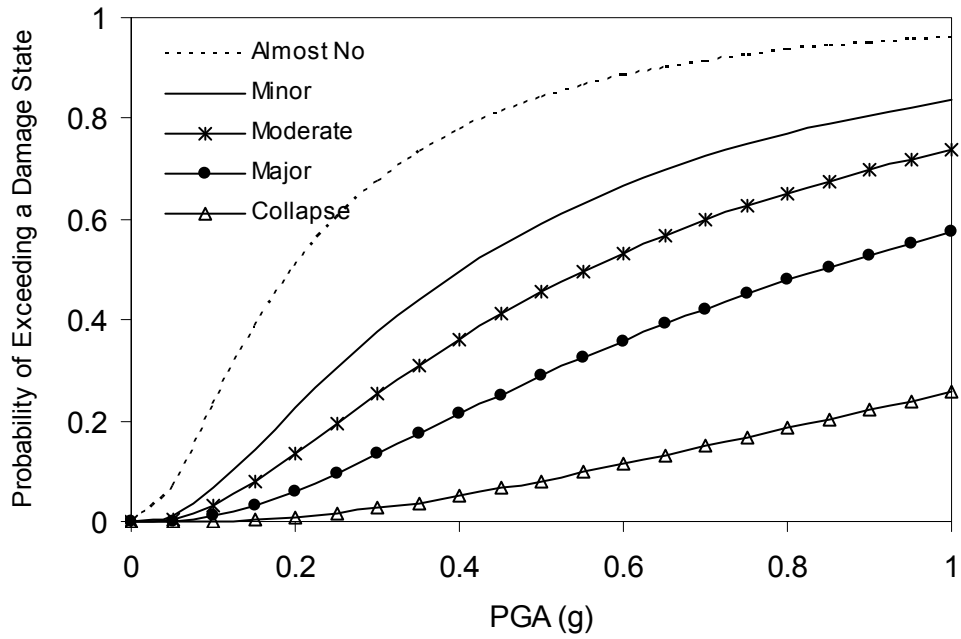


**FIGURE 4-3 Fragility Curves of Bridge 2 for Five Damage States**

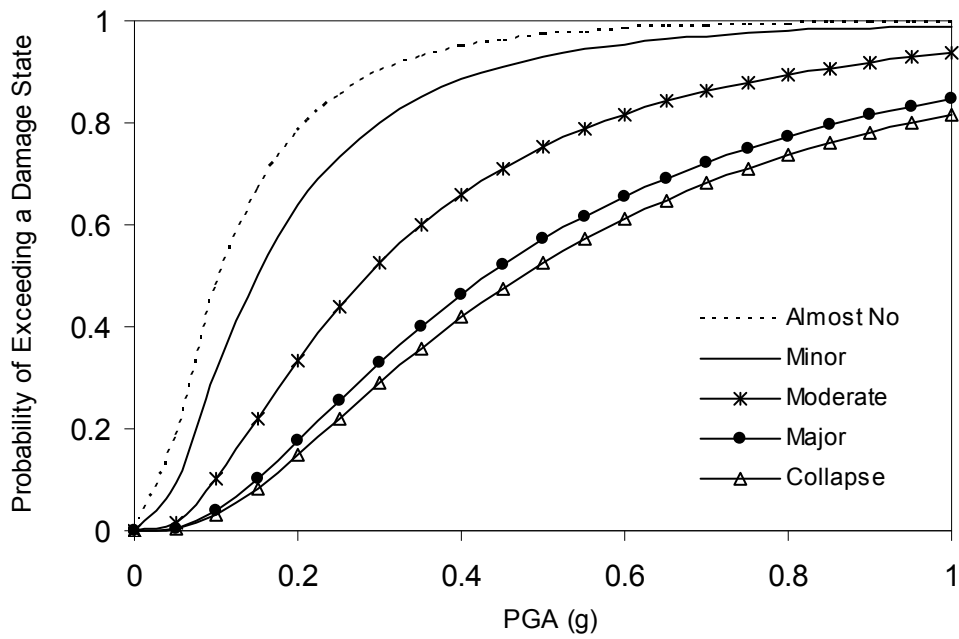


**FIGURE 4-4 Fragility Curves of Bridge 3 for Five Damage States**

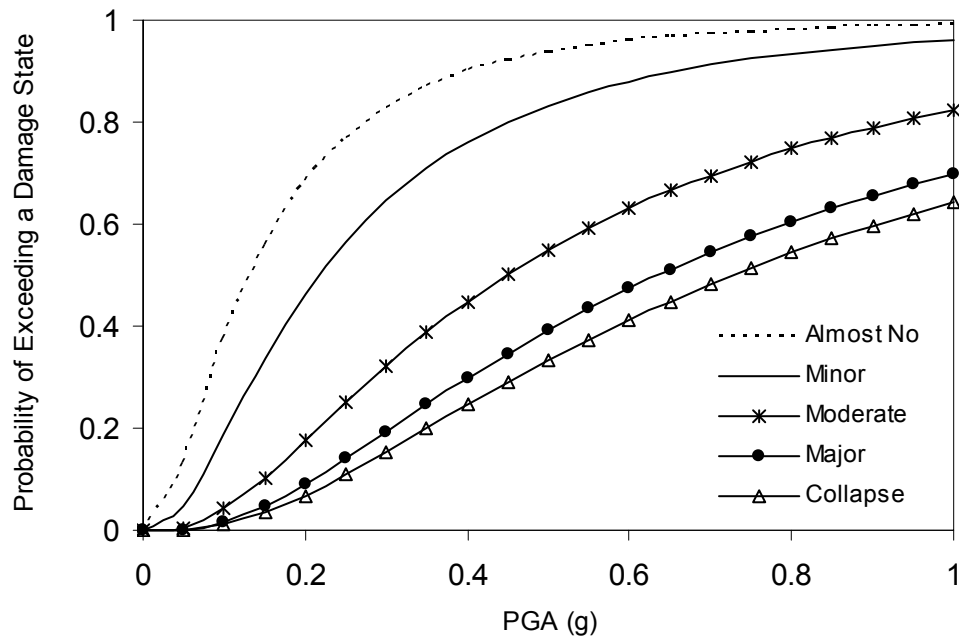


**FIGURE 4-5 Fragility Curves of Bridge 4 for Five Damage States**



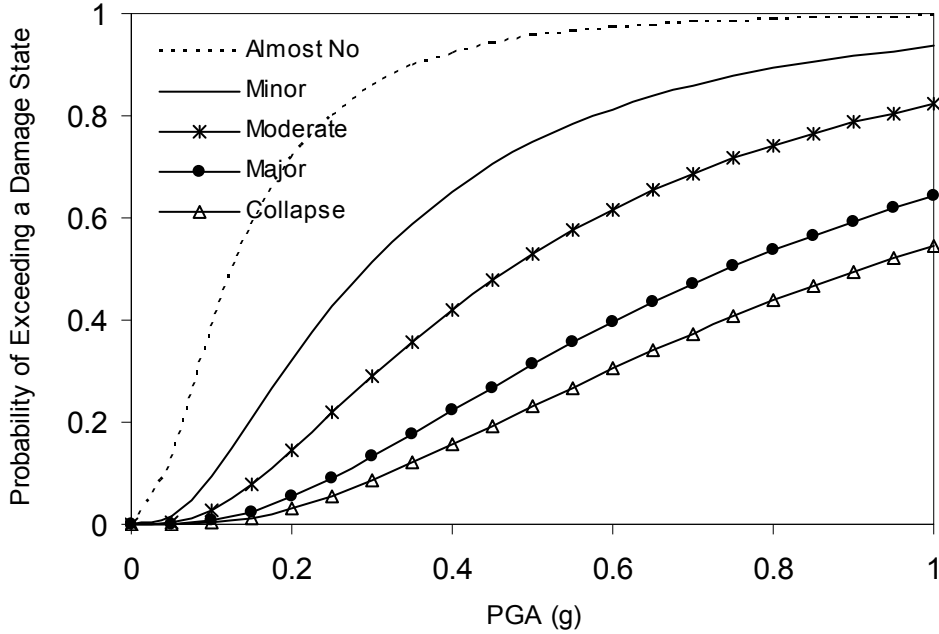


**FIGURE 4-6 Fragility Curves of Bridge 5 for Five Damage States**

To consider the resistance from embankment soil due to passive earth pressure at abutment locations, the connection between bridge deck and abutment is modeled as a gap element which is active only in compression. An initial gap of 0.0508 m (2 in) is provided in the gap element (Appendix B). Axial force develops due to pounding when the bridge deck strikes the abutment by losing initially provided gap. The analytical fragility curves are shown in figure 4-7.

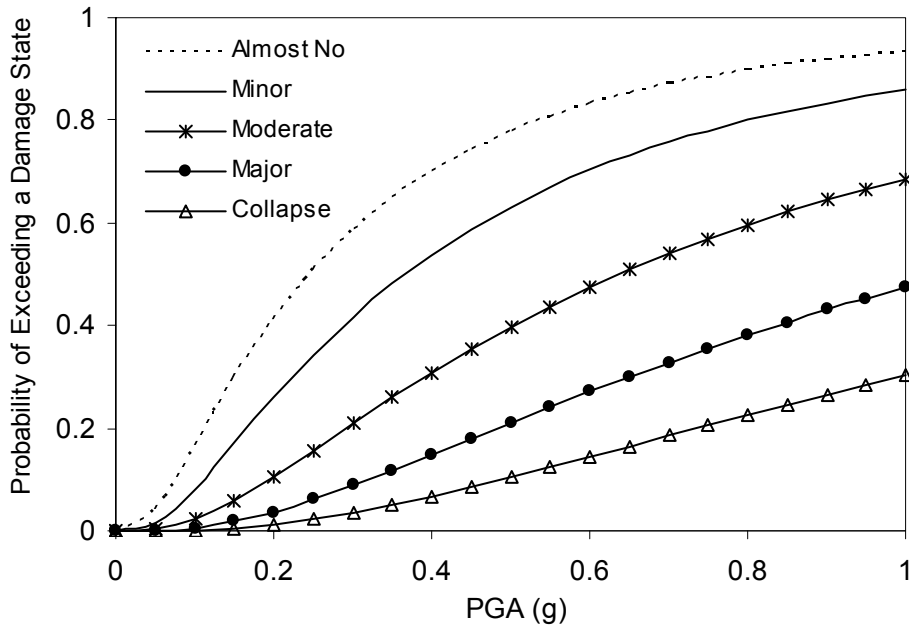


**FIGURE 4-7 Fragility Curves of Bridge 2 Considering Abutment Stiffness**

Comparison of figure 4-7 with figure 4-3 shows that there is no significant improvement of the fragility characteristics of Bridge 2 if the abutment stiffness in longitudinal direction is considered. Though it is very difficult to draw any conclusion depending on one test result, but the comparison procedure is general and applicable for all other bridges.

#### 4.1.2 Analytical Fragility Curves in Transverse Direction

Example bridges are analyzed in transverse direction under sixty (60) ground motion time histories with and without considering abutment stiffness in this direction. The damage state definitions are kept unaltered. For the first case with no abutment stiffness (zero resistance from backfill soil), bridge acts as a single degree of freedom system in transverse direction. Very low abutment stiffness (14.57 kN/m, nearly zero resistance from backfill soil) is considered in this case to analyze Bridge 1 and 2 under earthquake ground motions and corresponding fragility curves in transverse direction are plotted in figures 4-8 and 4-9. In the second case, lateral abutment stiffness of 7287.68 kN/m (500 kips/ft) and 29150.73 kN/m (2000 kips/ft), respectively for Bridge 1 and 2 are computed as per the recommendations given in Caltrans Seismic Design Criteria, V1.3 (2004). For this case figures 4-10 and 4-11 represent the transverse fragility curves of Bridge 1 and 2, respectively.

Comparison of fragility curves obtained for Bridge 1 and 2 from the above two cases show a considerable improvement in fragility characteristics due to the lateral resistance of backfill soil at abutment locations. In reality, it is rational to consider that the lateral movement of bridge is resisted by the wingwalls.

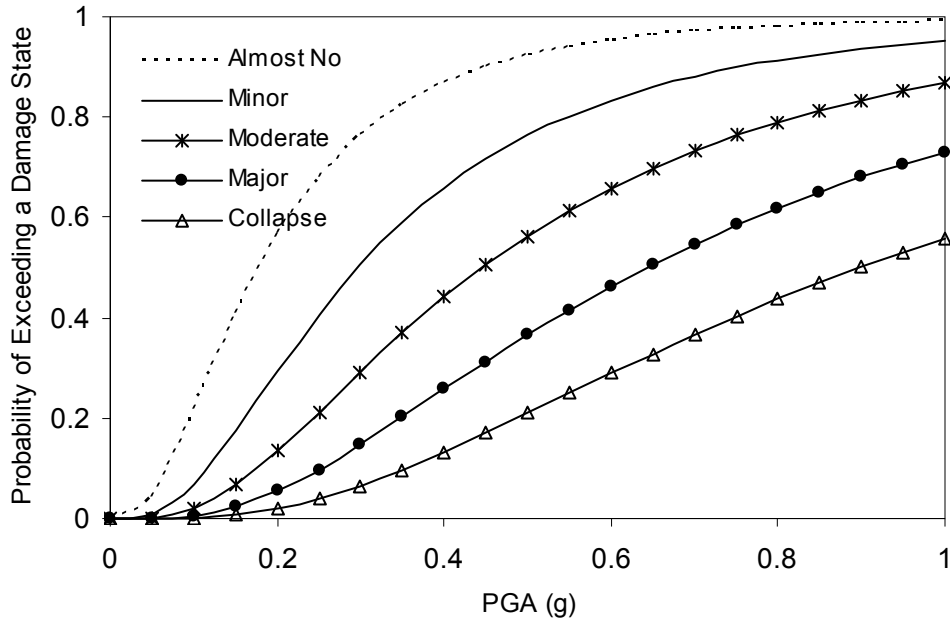


**FIGURE 4-8 Fragility Curves of Bridge 1 for Five Damage States for Abutment Stiffness 14.57 kN/m**

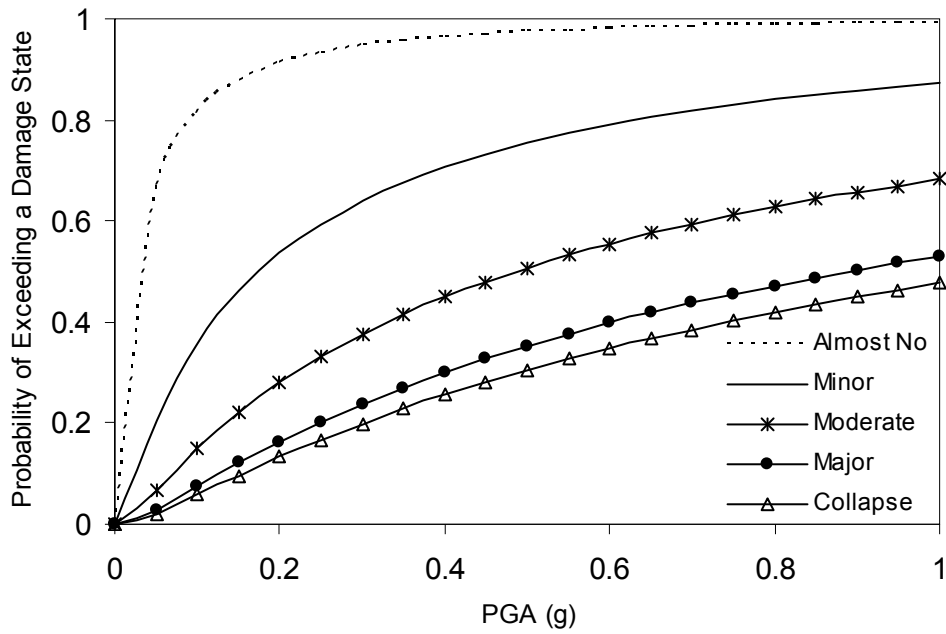


**FIGURE 4-9 Fragility Curves of Bridge 2 for Five Damage States for Abutment Stiffness 14.57 kN/m**

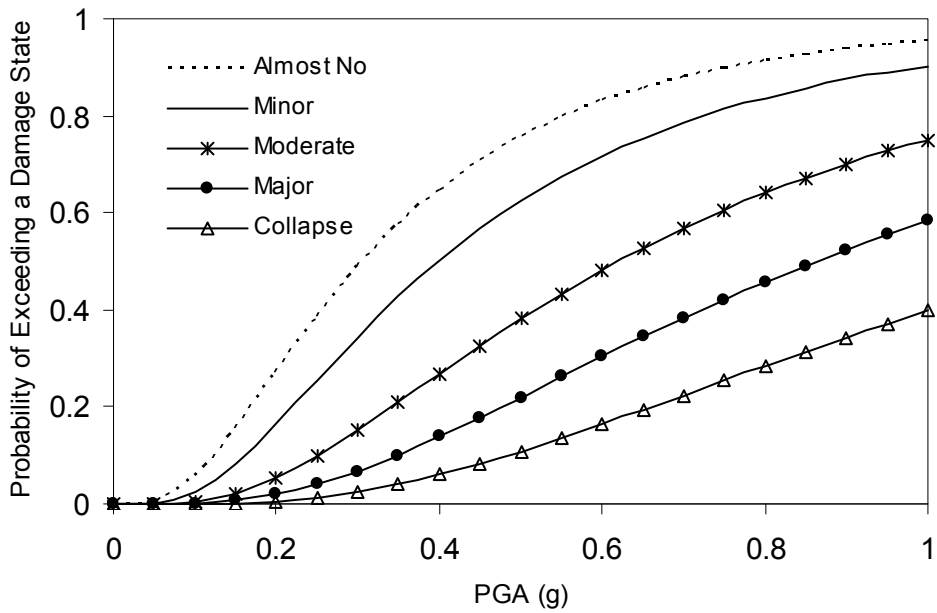


**FIGURE 4-10 Fragility Curves of Bridge 1 for Five Damage States for Abutment Stiffness 7287.68 kN/m**

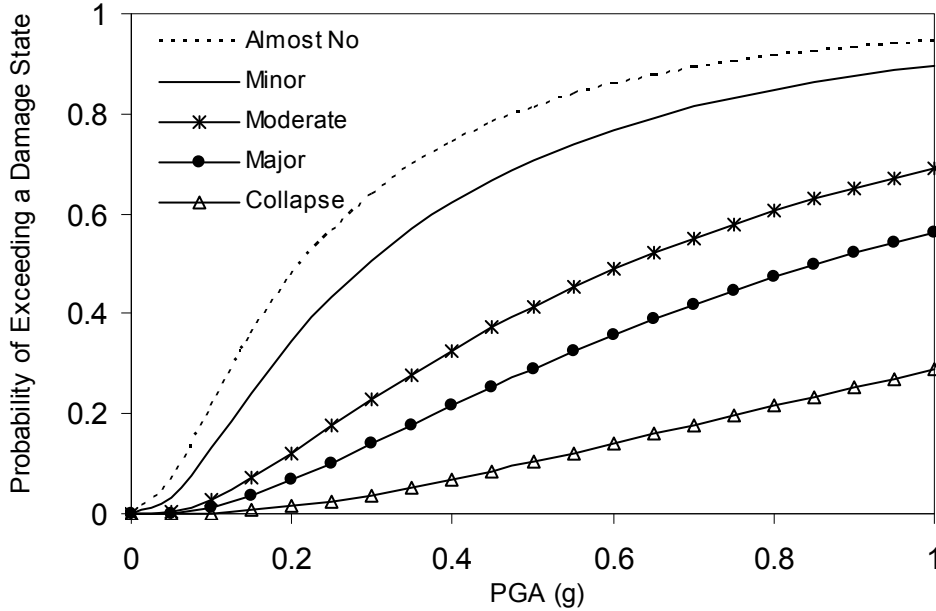


**FIGURE 4-11 Fragility Curves of Bridge 2 for Five Damage States for Abutment Stiffness 29150.73 kN/m**

## 4.2 Fragility Curve Development using Capacity Spectrum Method (CSM)

In this study, CSM is used to evaluate the seismic performance of Bridge 2 for sixty (60) ground acceleration time histories mentioned earlier. Two spectra, “Demand Spectrum” that represents intensity of the seismic ground motion to which bridges are subjected, and “Capacity Spectrum” that represents the bridges’ ability to resist the seismic demand and the “Performance Point” (i.e. the intersecting point of demand and capacity spectra) are the key elements in CSM. The detail theoretical background of this method is given in Appendix B, Section B.8.

### 4.2.1 Fragility Analysis in Longitudinal Direction

Rotations at plastic hinge regions of bridge columns are computed corresponding to the estimated displacements of the bridge girder,  $\Delta_{girder}$  (B-12) for all sixty ground motions, and used converted to rotational ductility demand. To be consistent with the analytical fragility curves developed utilizing time history analysis, the definition of damage states is kept unaltered. Figure 4-12 shows the fragility curves of Bridge 2 for all damage states.

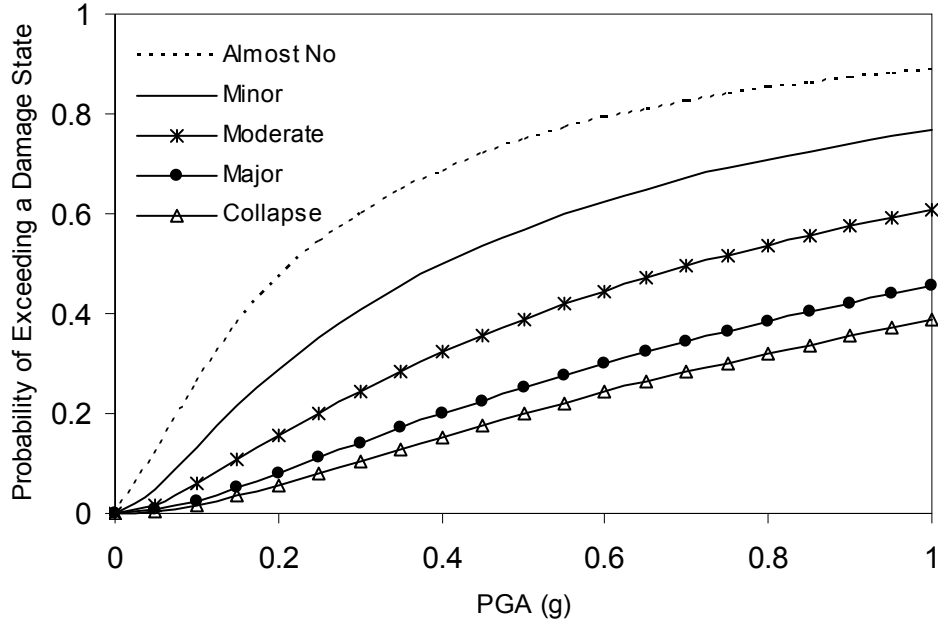


**FIGURE 4-12 Fragility Curves of Bridge 2 in Longitudinal Direction from CSM**

#### 4.2.2 Fragility Analysis in Transverse Direction

Fragility analysis in transverse direction of the bridge is performed following the same theory of CSM. Figure 4-13 shows the fragility curves of Bridge 2 for all damage states.

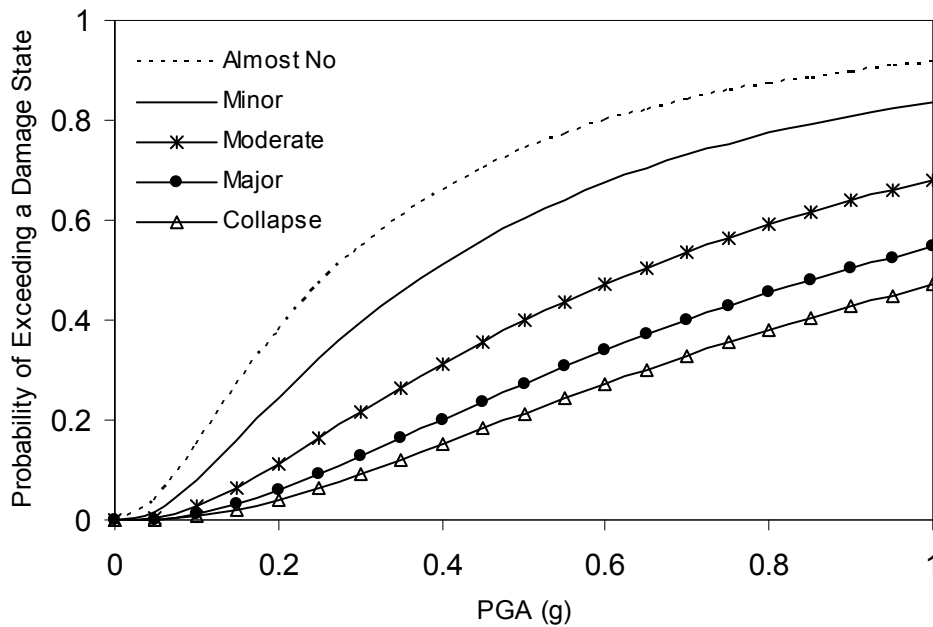


**FIGURE 4-13 Fragility Curves of Bridge 2 in Transverse Direction from CSM**

### 4.2.3 Comparison of Analytical Fragility Curves

To check the consistency of CSM, developed fragility curves in longitudinal and transverse directions are compared with those from time history analysis. Figures 4-14 and 4-15 show the comparison in 'Almost No', 'Minor', 'Moderate' and 'Major' damage states of Bridge 2 in longitudinal and transverse direction, respectively. Result indicates, in both directions analytical fragility curves derived from pushover analysis are in well accordance with those from time history analysis. Therefore this nonlinear static analysis method can be used as an alternative to nonlinear time history analysis in seismic vulnerability analysis of bridges.

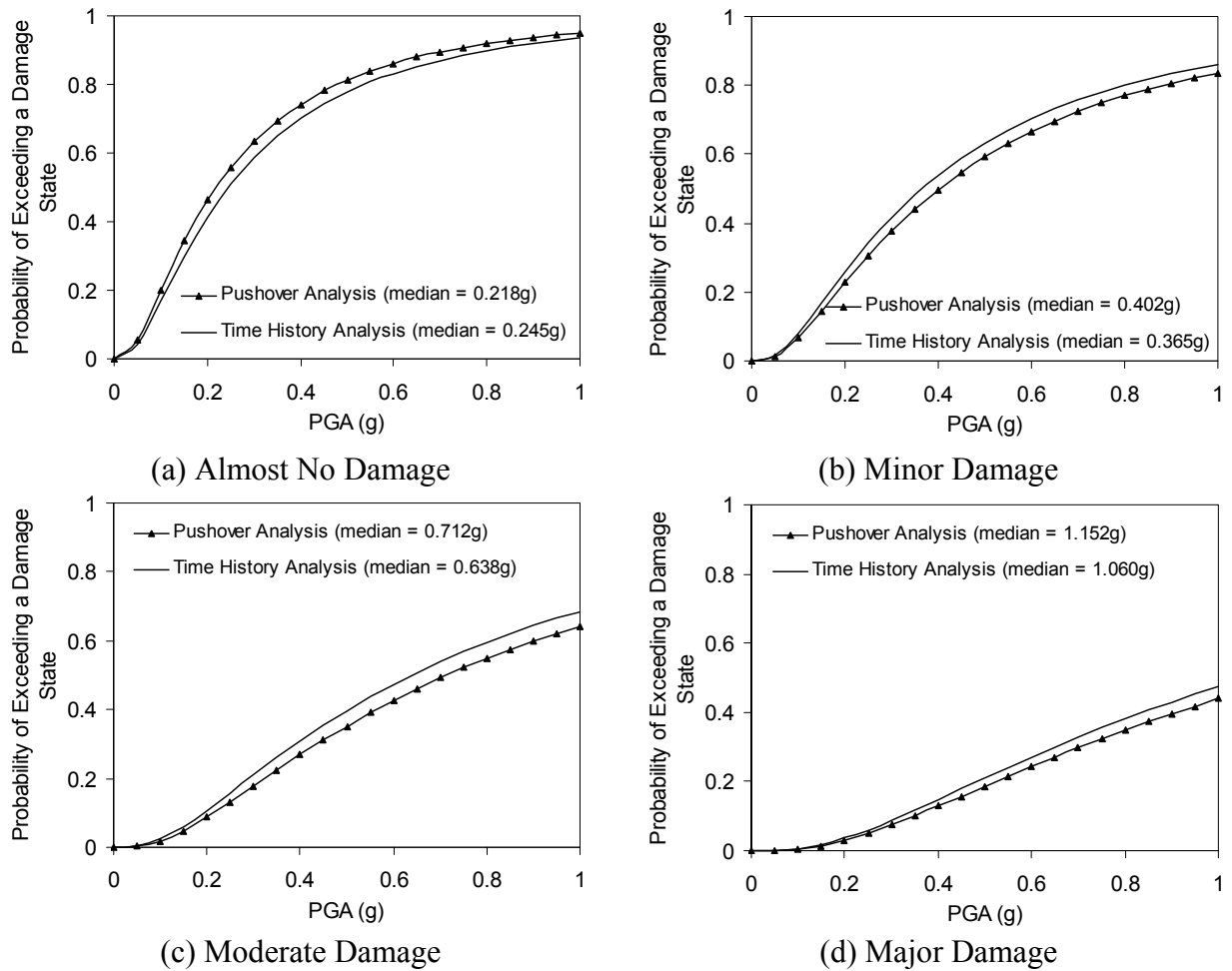
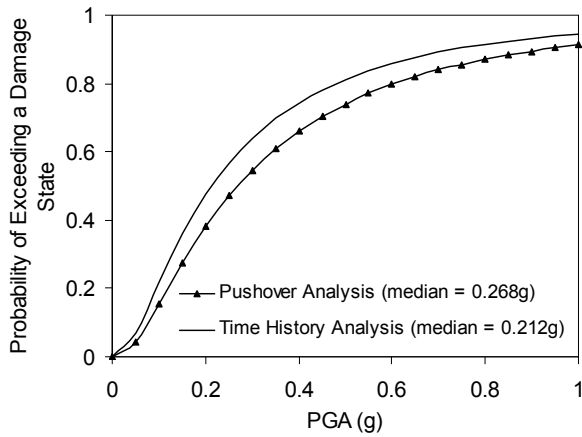
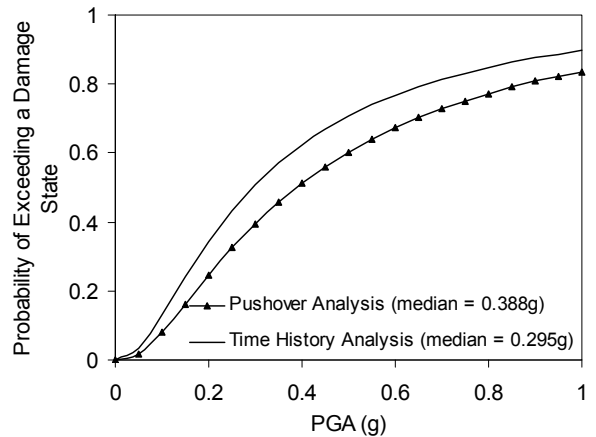


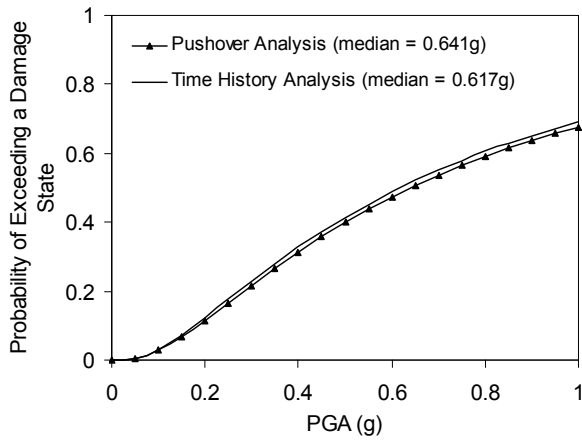
FIGURE 4-14 Comparison of Fragility Curves of Bridge 2 in Longitudinal Direction



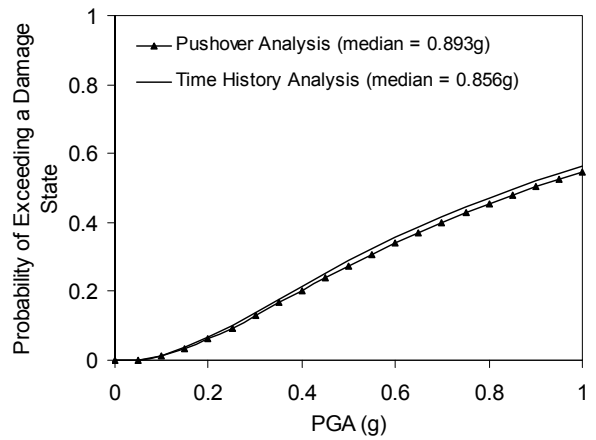
(a) Almost No Damage



(b) Minor Damage



(c) Moderate Damage



(d) Major Damage

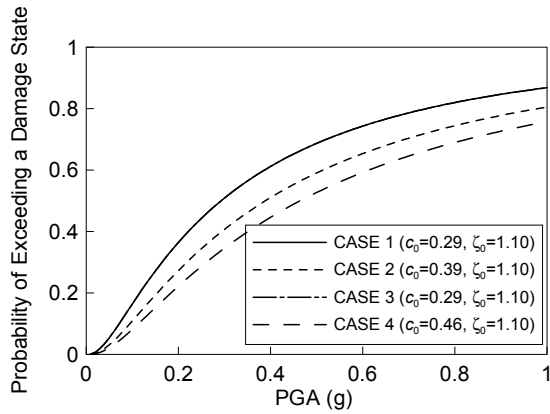
**FIGURE 4-15 Comparison of Fragility Curves of Bridge 2 in Transverse Direction**

### 4.3 Fragility Enhancement after Column Retrofit

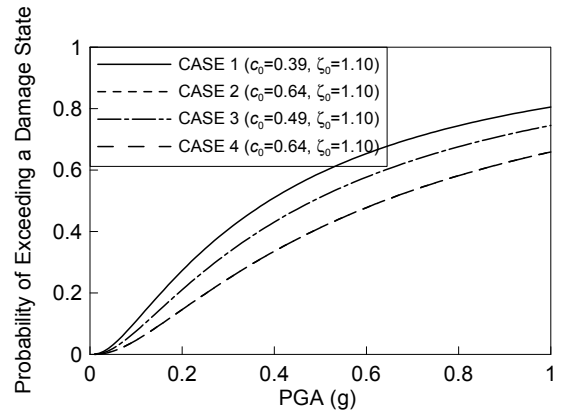
In order to investigate the effect of bridge retrofit by confining columns with steel jackets, fragility curves of each bridge after retrofit are developed and compared with that of before retrofit. Also, the effect of restrainer in the fragility characteristics of bridges is observed by analyzing the bridge with and without applying restrainer. Analyses are performed utilizing nonlinear time history analysis. The fragility curves for the four (4) sample bridges are plotted in figures 4-16, 4-17, 4-18 and 4-19, respectively. Each figure has four (4) curves for the following four (4) cases: CASE 1: without jacketing and without restrainer; CASE 2: with jacketing and without restrainer; CASE 3: without jacketing and with restrainer; CASE 4: with jacketing and with restrainer. It is noted that the log-standard deviation in each of figures 4-16, 4-17, 4-18 and 4-19 is obtained such that the fragility curves in each figure will not intersect each other.

Figures 4-20 ~ 4-23 show the enhancement in bridge fragility characteristics after retrofitting with steel jackets. Here, the enhancements are computed separately for different shapes of bridge columns. The percent increase in fragility parameter ( $c$ ) after retrofit with respect to the same before retrofit represent the “Enhancement” by definition. Figures 4-20, 4-21, 4-22 and 4-23 show average fragility enhancement of bridges with circular columns (Bridge 1 and 2), bridges with oblong columns (Bridge 3 and 5), bridge with rectangular columns (Bridge 4), and bridges with all types of columns (Bridge 1 ~ 5), respectively. An analytical function is interpolated and the “enhancement curve” is plotted on the basis of the least square fit. Five damage states are mentioned as indices,  $x = 1$ , to 5 and described on the figure.

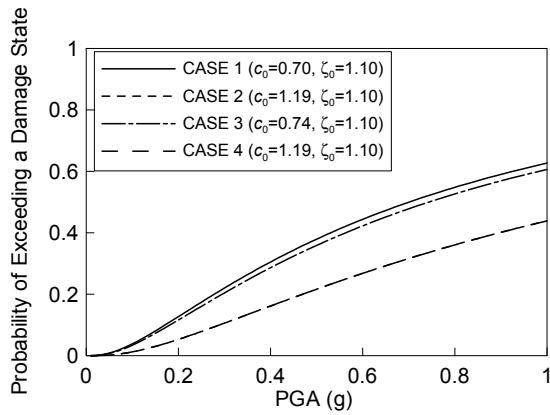




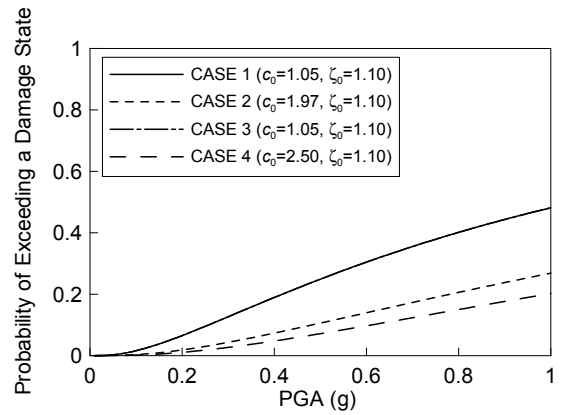
(a) Almost No Damage



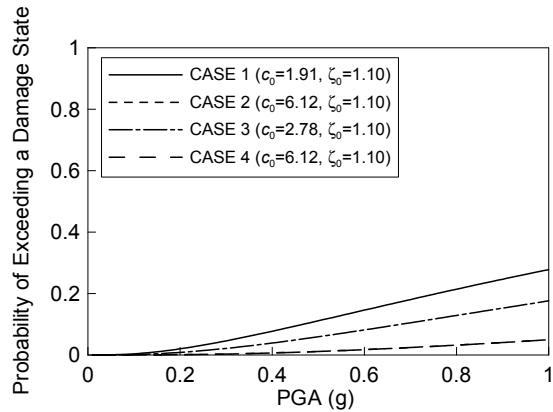
(b) Slight Damage



(c) Moderate Damage



(d) Extensive Damage



(e) Complete Collapse

**FIGURE 4-16 Fragility Curves of Bridge 2**

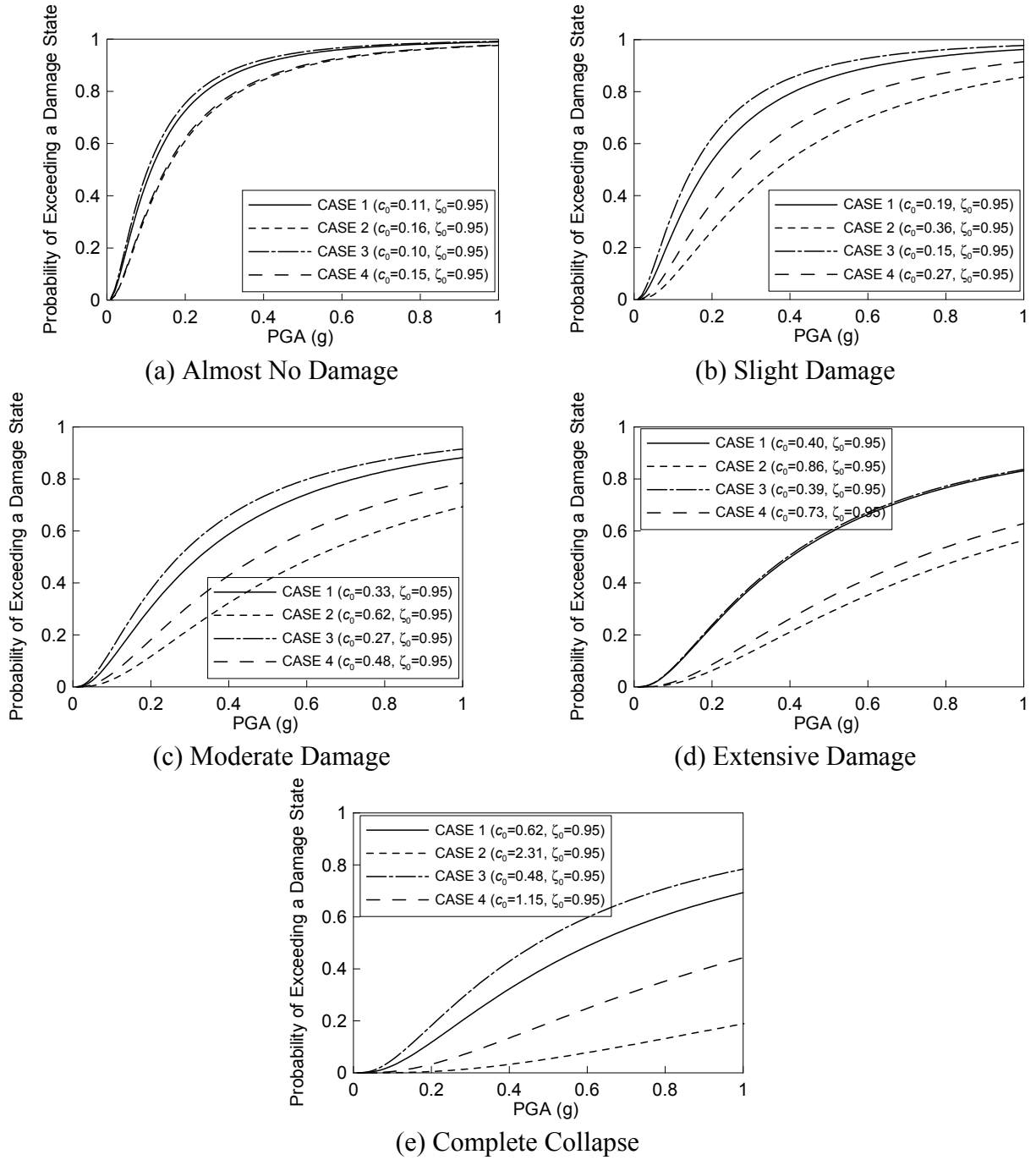


**FIGURE 4-17 Fragility Curves of Bridge 3**

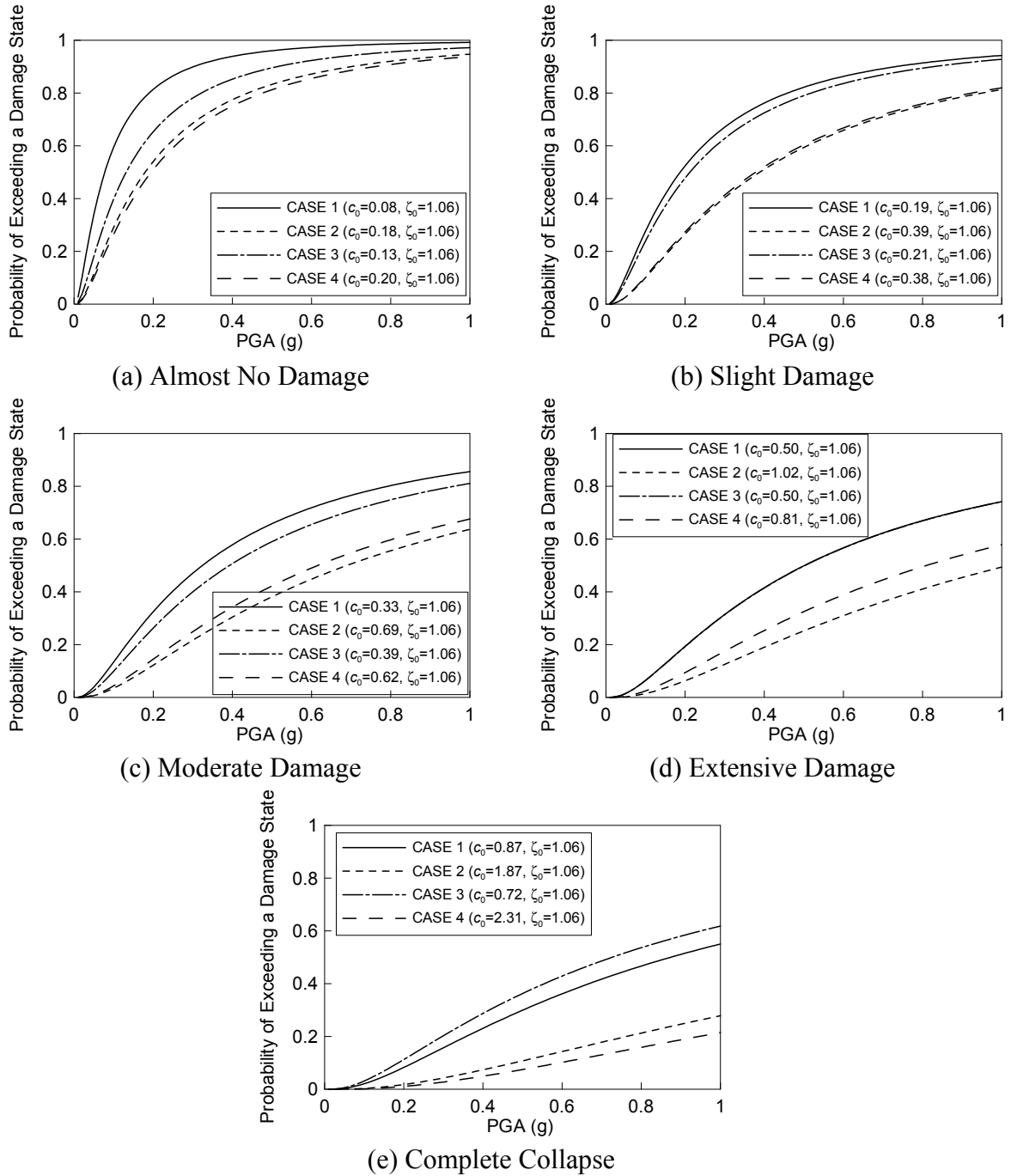


**FIGURE 4-18 Fragility Curves of Bridge 4**

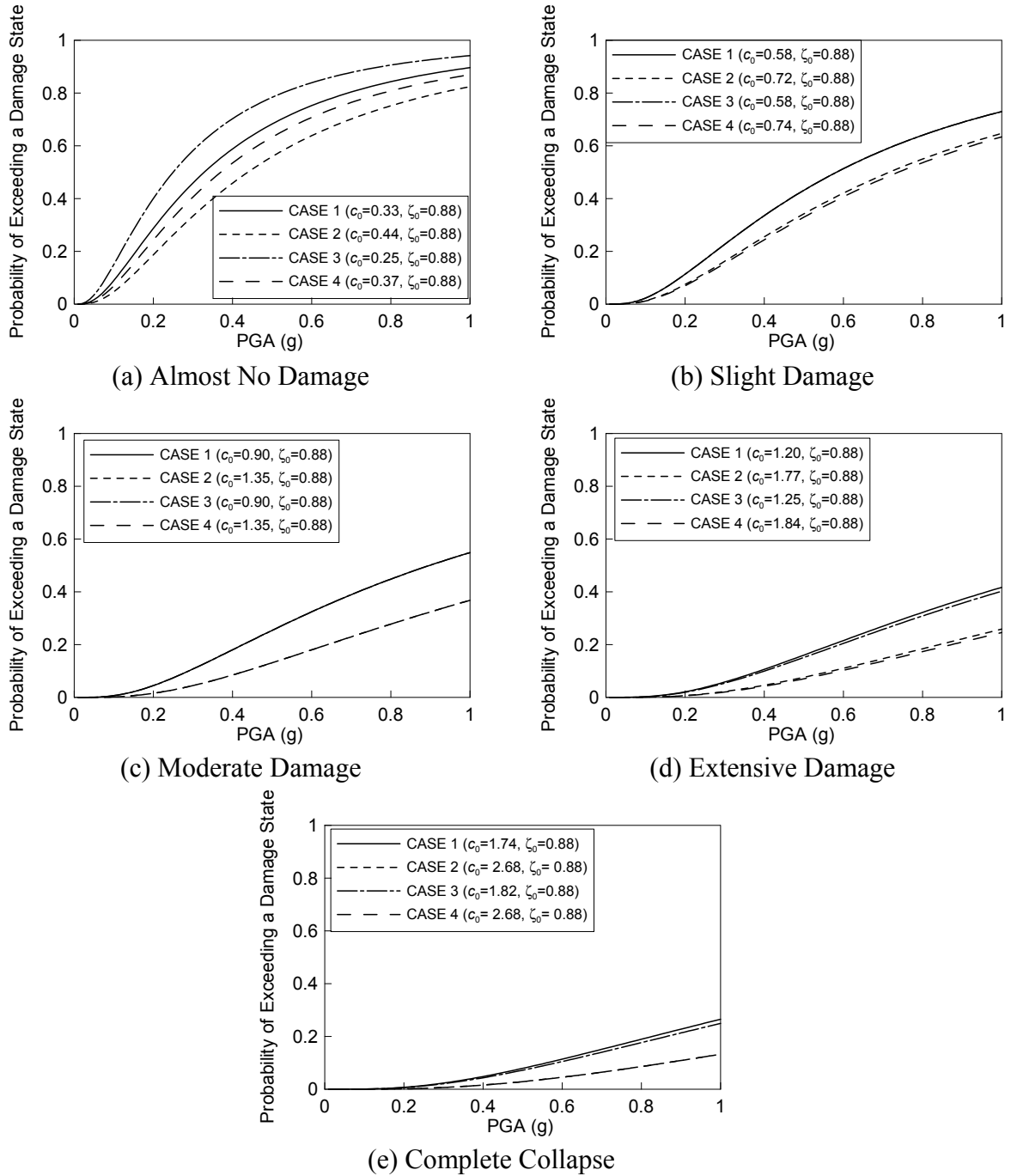


**FIGURE 4-19 Fragility Curves of Bridge 5**

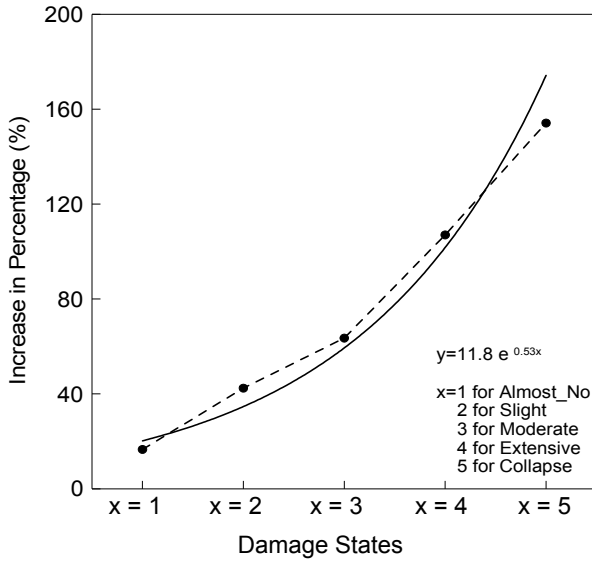


**FIGURE 4-20 Enhancement Curve for Circular Columns with Steel Jacketing**

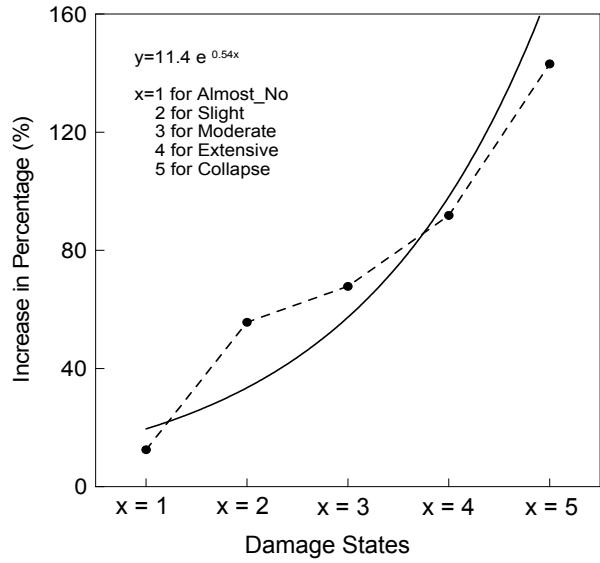


**FIGURE 4-21 Enhancement Curve for Oblong Columns with Steel Jacketing**

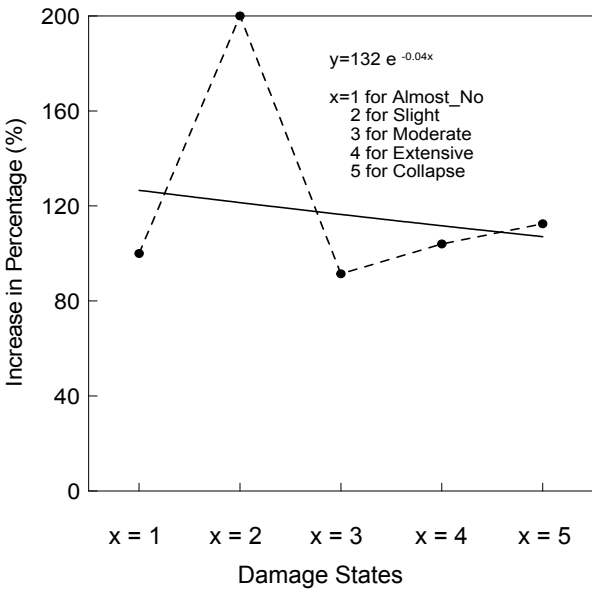


**FIGURE 4-22 Enhancement Curve for Rectangular Columns with Steel Jacketing**

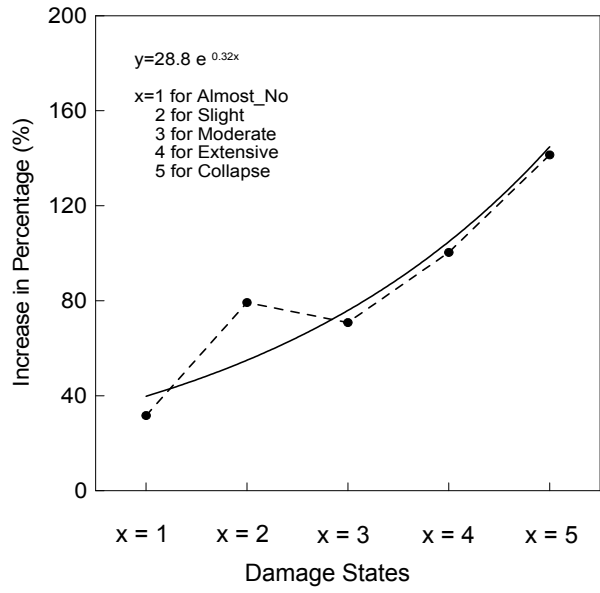


**FIGURE 4-23 Enhancement Curve for Five Sample Bridges with Steel Jacketing**

## 4.4 Calibration of Analytical Fragility Curves with Damage Data

### 4.4.1 Comparison of Analytical Fragility Curves with Empirical Data

The damage report of Caltrans' bridges under the Northridge earthquake serves as invaluable field experiments that the nature provided. For the analytical purpose, mechanistic model of bridge damage should be in accordance with that past earthquake damage data. Shinozuka et al. (2003) developed the empirical fragility curves for Caltrans' bridges for 1994 Northridge Earthquake and the bridge damage data associated with it. They sub-divided the sample of Caltrans' bridges into four levels of sub-sets in accordance with the relevant bridge attributes (i.e., number of spans, soil conditions, and bridge skew). In the present study, empirical fragility curves for a fourth level subset (considering 'multiple span', 'zero skew' and 'soil type C') are used to compare these curves with the analytically obtained fragility curves (figure 4-24). Comparison indicates that the analytical curves tend to be substantially conservative in the sense that bridges are more probable to suffer from a damage state than they are when empirical fragility curves suggest. For example, the probability that Bridge 2 will suffer from the state of at least moderate damage (figure 4-24) at a peak ground acceleration (PGA) of 0.4g is 37% obtained from analytical result, whereas the same is 20% obtained from empirical result. Similar discrepancies are observed for other bridges and other states of damage. However, these discrepancies are minimized for each pair of empirical and analytical fragility curves associated with the same state of damage. This is achieved by mechanistically adjusting the minimum rotational ductility value (to be used for the dynamic analysis) obtained from Dutta and Mander's drift limits (Dutta and Mander 1998) and by utilizing the least square optimization procedure as detailed in Appendix A (A-3).

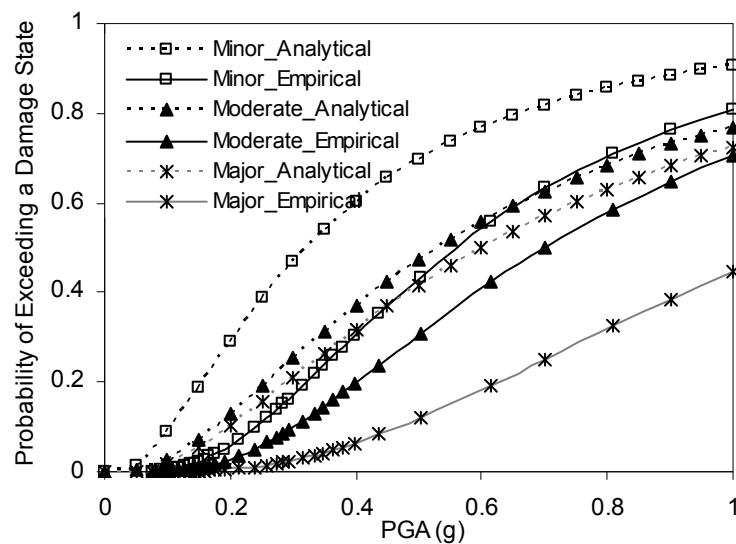


FIGURE 4-24 Comparison of Empirical and Analytical Fragility Curves of Bridge 2

#### 4.4.2 Estimation of Ductility Capacities at Various Damage States

Seismic response of bridges from nonlinear time history analysis (*SAP2000 Nonlinear* analysis) for sixty ground motions is used as input in this part of analysis. While comparing with empirical fragility curves, numerical analysis is done to get best-fit distribution, for minor, moderate and extensive damage states and their corresponding ductility capacities. The parameters (median and log-standard deviation) of each fragility curve are independently estimated by means of the maximum likelihood procedure as described in Appendix A. The two fragility parameters are computed as  $c_0$  and  $\zeta_0$  satisfying (A-3).

Second optimization is done to minimize the difference between parameters of empirical fragility curves (median,  $c_{emp}$  and log-standard deviation,  $\zeta_{emp}$ ) and those obtained in the analytical procedure (i.e.  $c_0$  and  $\zeta_0$ ). In order to capture the proper value of threshold ductility capacity at each damage state, which will produce the analytical fragility curves consistent with empirical curves, the above two optimization procedures are performed simultaneously. The entire procedure is carried out independently for Bridge 2, 4 and 5. Table 4-1 presents the median values ( $c$ ) for empirical fragility curves and calibrated analytical fragility curves. Result indicates that at minor and moderate damage states, calibrated median values are well in accordance with that from empirical fragility curves, although dispersion is observed in the major damage state for Bridges 4 and 5. This is because of the limited failure cases observed in major damage state while analyzing these example bridges under 60 ground motion time histories. Analysis with many severe ground motions that may cause major damage to Bridge 4 and 5 will produce better correspondence with empirical data. Figures 4-25 and 4-26 show the empirical fragility curves and calibrated fragility curves of three example bridges respectively for minor and moderate damage states.

Calibrated rotational ductility capacities for minor, moderate and major damage states of these three example bridges are presented in table 4-2. Figure 4-27 plots these calibrated rotational ductility capacities for different damage states in which indices 1, 2, and 3 stand for 'Minor Damage', 'Moderate Damage' and 'Major Damage' respectively. This figure indicates that in all damage states threshold rotational ductility for Bridge 4 and 5 almost overlap with each other while that for Bridge 2 lay far apart. A clear increasing trend is common for all bridges which can be represented on the basis of least square fit. It can be stated from this result that empirical fragility curve for more detailed bridge classification is needed in order to calibrate analytical result. For example, additional consideration of bridge length and number of span in current classification will enhance calibrated result significantly.

**TABLE 4-1 Fragility Parameters (Median Values in g) for Empirical and Calibrated Analytical Fragility Curves**

Damage States	Median Values (g)			
	Empirical Fragility Curves	Calibrated Analytical Fragility Curves		
		Bridge 2	Bridge 4	Bridge 5
Minor	0.56	0.56	0.53	0.54
Moderate	0.70	0.70	0.67	0.67
Major	1.09	1.06	0.73	0.83

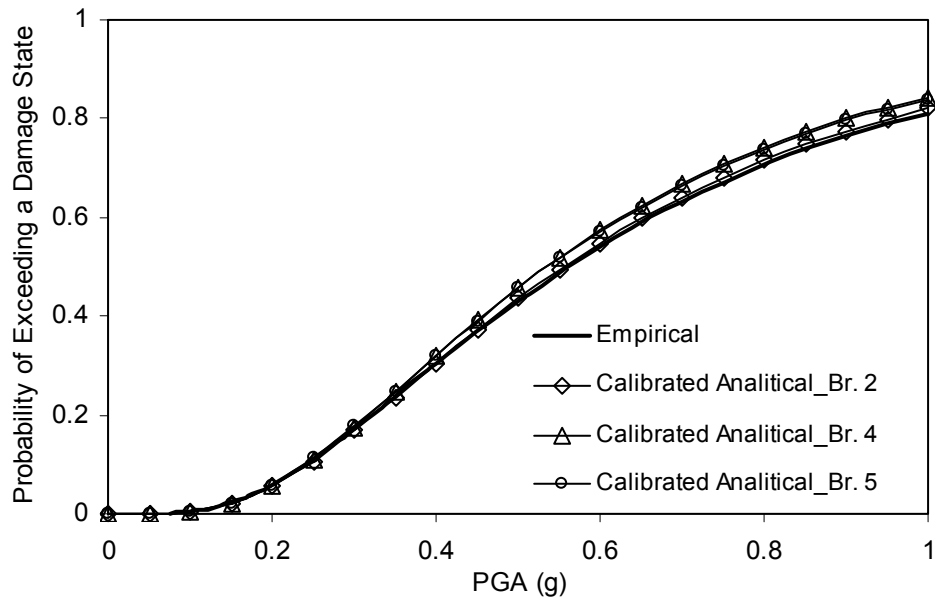


**FIGURE 4-25 Empirical and Calibrated Analytical Fragility Curves at Minor Damage**



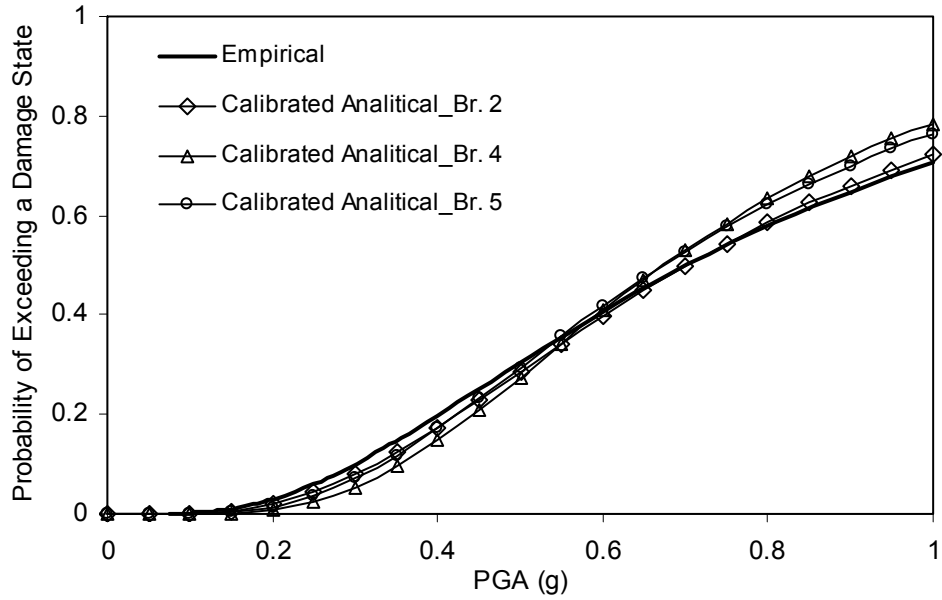


**FIGURE 4-26 Empirical and Calibrated Analytical Fragility Curves at Moderate Damage**

**TABLE 4-2 Lower Bound of Calibrated Rotational Ductility of Bridges**

Bridge No	Threshold Rotational Ductility at Different Damage States		
	Minor	Moderate	Major
2	3.39	4.75	8.43
4	6.43	9.02	12.35
5	5.93	9.06	12.18

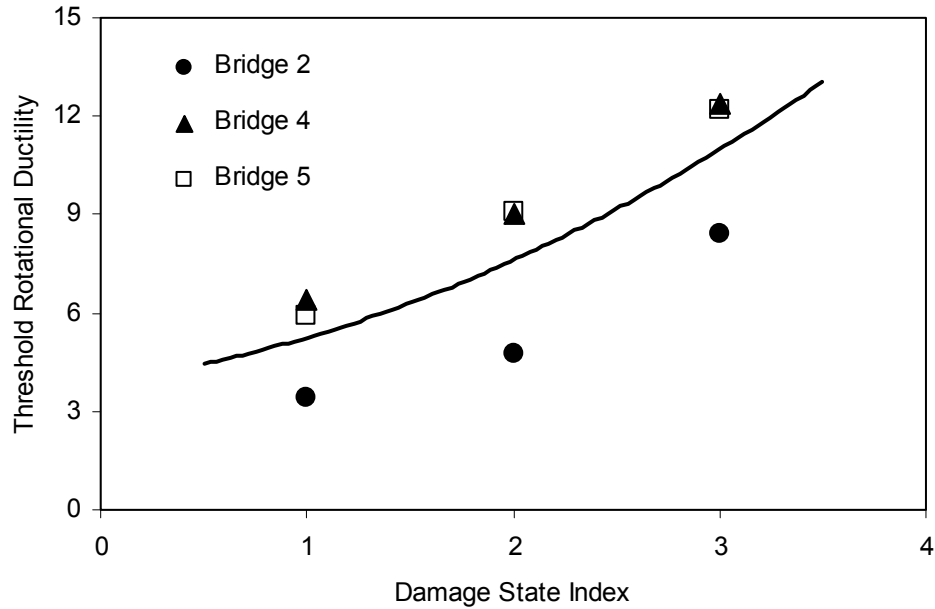


**FIGURE 4-27 Rotational Ductility Capacities at Various Damage States**

#### **4.5 Effect of Ground Motion Directionality on Fragility Characteristics of Bridges**

Most of the studies on the seismic performance of structures are conducted using earthquake ground motions acting along one of the principle axes of those structures. In general recorded ground motions have two components, N-S and E-W. Figure 4-28 shows the trajectory of an earthquake ground motion with two orthogonal components. Although it is possible to model the ground motion acceleration time history as a 2D or 3D vector random process (Shinozuka and Deodatis, 1996), the model results in time varying principal axis of the process. However, recognizing the fact that the directionality of the earthquake ground motion may have an important effect on structures, the current section represents a practice-oriented concept and procedure that follows the pioneering studies carried out earlier by other researchers using multi-components of earthquake ground motions. This procedure consists of rigorous nonlinear time history analysis where the effect of directionality is obtained and presented in the form of fragility curves. The detail theoretical background can be found in Appendix B, Section B.9. The word ‘directionality’ is used here as opposed to ‘directivity’ used in engineering seismology with a specific definition related to fault motion unique to that field.

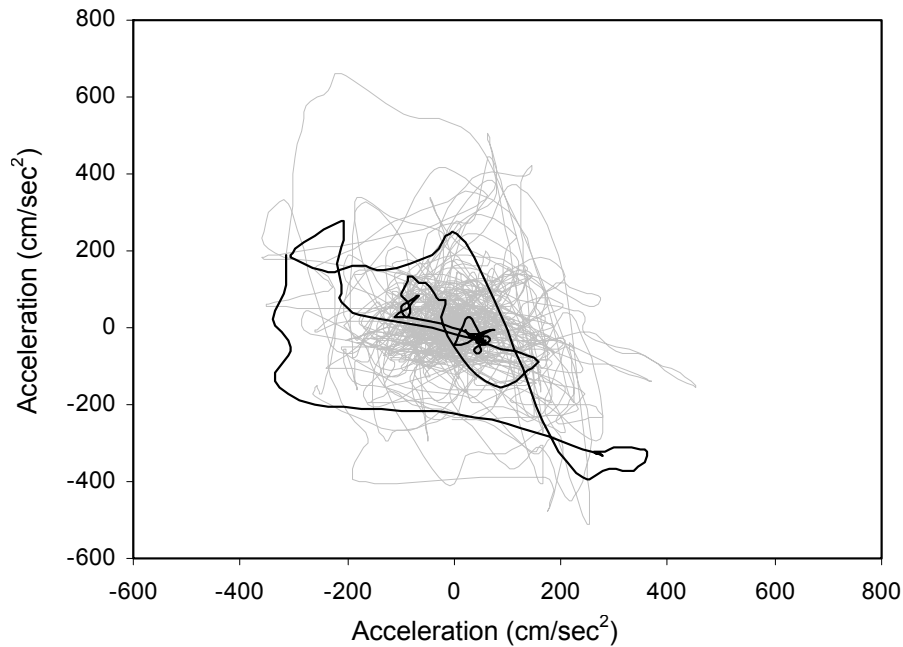


**FIGURE 4-28 Trajectory of Ground Acceleration Time Histories of El Centro Earthquake, 1940**

#### **4.5.1 Case I: Fragility Curves for two Orthogonal Components**

Maximum resultant rotations at all column ends of the bridge are computed utilizing (B-15) and (B-16) for two orthogonal components of ground motions for several values of  $\theta$ . The orthogonal components are considered such that each pair contains one strike-parallel (SP) and one strike-normal (SN) ground acceleration records of same earthquake. As the columns are circular in cross section, same nonlinear moment-curvature relationship is considered in all directions of column rotation. Following the procedure indicated in Appendix A, fragility curves are developed for different damage states of the bridge considering  $\theta$  as  $0^0$ ,  $15^0$ ,  $30^0$ ,  $45^0$ ,  $60^0$ ,  $75^0$  and  $90^0$  and estimated fragility parameter is tabulated in table 4-3. The comparison of fragility curves for different  $\theta$  values are plotted in Figures 4-29, 4-30 and 4-31, respectively for ‘Minor’, ‘Moderate’ and ‘Major’ damage levels. These results show that  $\theta$  does not have any significant influence on the fragility characteristics of Bridge 2 in any particular damage level.

**TABLE 4-3 Fragility Parameters of Bridge 2 at Different  $\theta$  for Two Orthogonal Components of Ground Motion (Case I)**

$\theta$ (Degree)	Fragility Parameters at Different Damage Levels		
	$c_{Minor}$ (g)	$c_{Moderate}$ (g)	$c_{Major}$ (g)
0	0.365	0.500	0.742
15	0.400	0.479	0.715
30	0.387	0.463	0.670
45	0.407	0.500	0.690
60	0.402	0.500	0.728
75	0.364	0.514	0.745
90	0.355	0.484	0.738

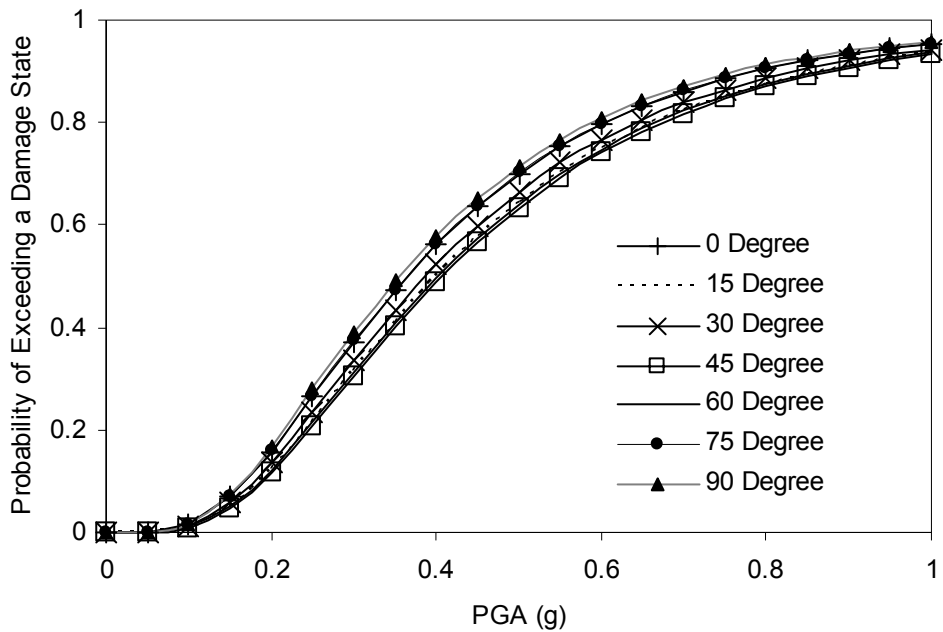


**FIGURE 4-29 Fragility Curves of Bridge 2 for State of Minor Damage (Case I)**

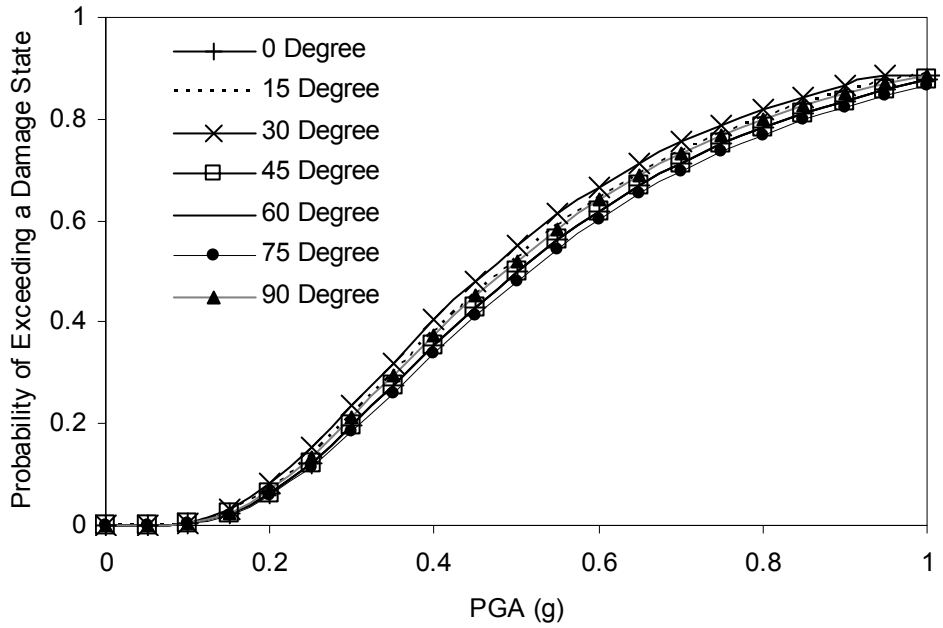


**FIGURE 4-30 Fragility Curves of Bridge 2 for State of Moderate Damage (Case I)**

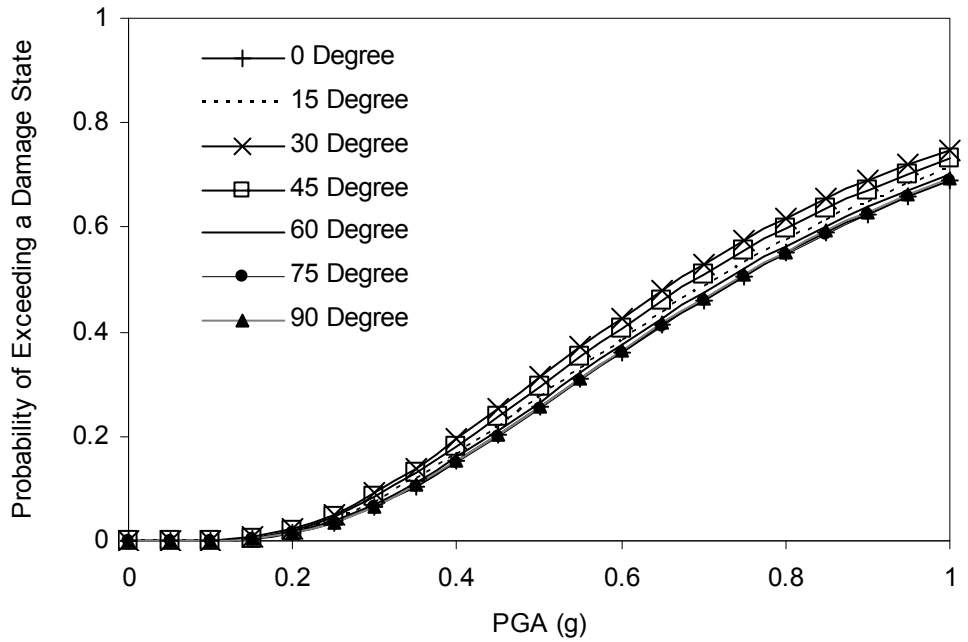


**FIGURE 4-31 Fragility Curves of Bridge 2 for State of Major Damage (Case I)**

#### 4.5.2 Case II: Fragility Curves for one Inclined Component

With the aid of (B-17), maximum resultant rotations at all column ends of the bridge are computed for different inclination ( $\theta$ ) of ground motions. Fragility curves are developed for five damage states of the bridge considering  $\theta$  as  $0^0$  (along the longitudinal direction),  $15^0$ ,  $30^0$ ,  $45^0$ ,  $60^0$ ,  $75^0$  and  $90^0$  (along the transverse direction) and estimated fragility parameter is tabulated in table 4-4. The comparison of fragility curves for different  $\theta$  values are plotted in Figures 4-32, 4-33 and 4-34, respectively for ‘Minor’, ‘Moderate’ and ‘Major’ damage levels. From this result, it is evident that when ground motions come along the longitudinal axis of the bridge (i.e.  $\theta = 0^0$ ), it has least probability of failure while the same is maximum for  $\theta = 45^0$ . Fragility curves for  $\theta = 90^0$  (along transverse direction) are more damaging than that for  $\theta = 45^0$  but weaker than those for  $\theta = 0^0$ . Similar trend is observed in all damage levels except for ‘Minor’ damage where the fragility curves in longitudinal and transverse directions represent same failure probability. Therefore, it can be stated that for one inclined component (case II), the ground motions have maximum impact on the example bridge for an inclination in between  $30^0$  to  $60^0$  with the longitudinal direction of the bridge.

**TABLE 4-4 Fragility Parameters of Bridge 2 at Different  $\theta$  for One Inclined Component of Ground Motion (Case II)**

$\theta$ (Degree)	Fragility Parameters at Different Damage Levels		
	$c_{Minor}$ (g)	$c_{Moderate}$ (g)	$c_{Major}$ (g)
0	0.560	0.707	1.060
15	0.476	0.557	0.822
30	0.435	0.517	0.742
45	0.407	0.517	0.742
60	0.435	0.517	0.760
75	0.490	0.579	0.778
90	0.560	0.617	0.856

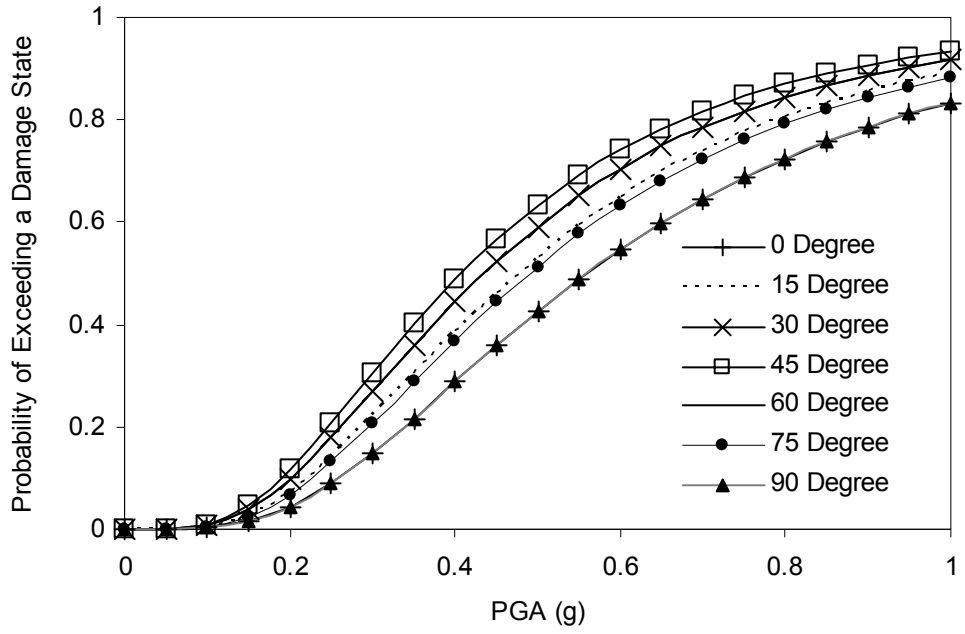


**FIGURE 4-32 Fragility Curves of Bridge 2 for State of Minor Damage (Case II)**

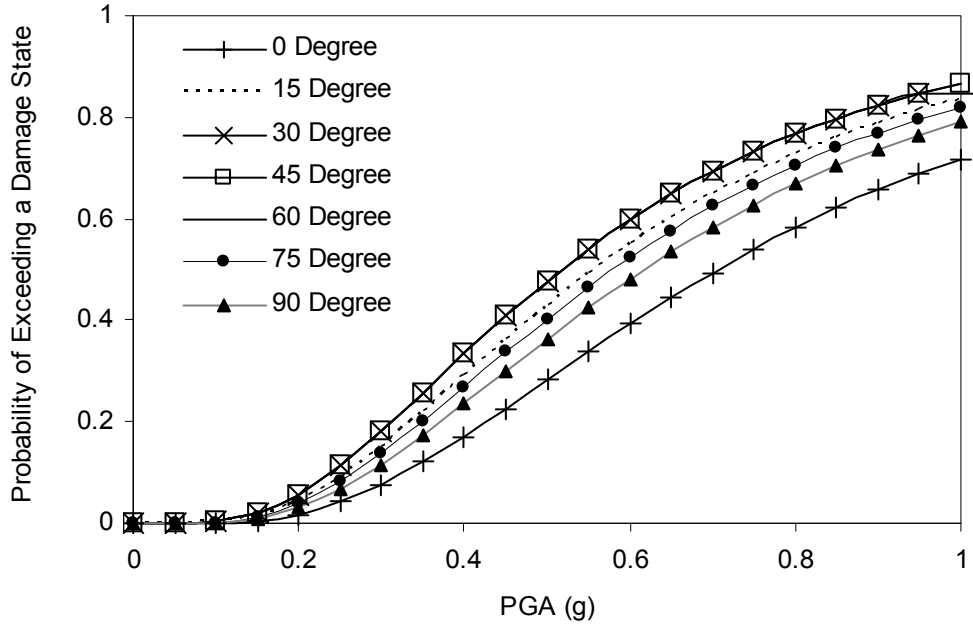


**FIGURE 4-33 Fragility Curves of Bridge 2 for State of Moderate Damage (Case II)**

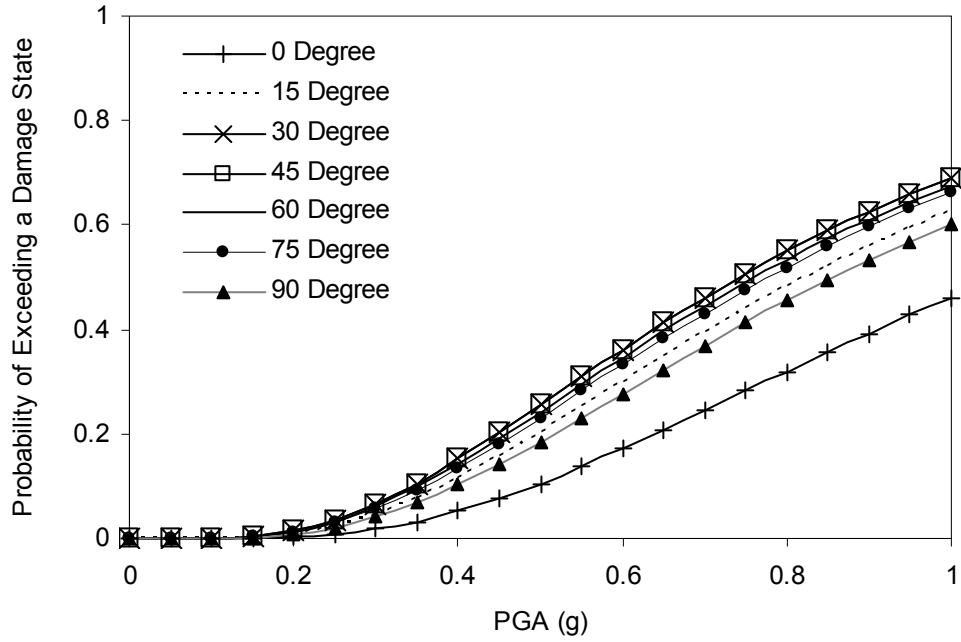


**FIGURE 4-34 Fragility Curves of Bridge 2 for State of Major Damage (Case II)**



## SECTION 5

### ANALYTICAL FRAGILITY CURVES OF MEMPHIS BRIDGES

To demonstrate the development of analytical fragility curves, two representative bridges with a precast prestressed continuous deck in the Memphis, Tennessee area studied by Jernigan and Hwang (1997) are used. The plan, elevation and column cross-section of Bridge M1 are depicted in figure 5-1. Geometry and configuration of Bridge M2 is similar to Bridge M1. Bridge M2 also has a precast prestressed continuous deck. However, the deck is supported by 2 abutments and 4 bents with 5 spans equal to 10.7 m (35'), 16.8 m (55'), 16.8 m (55'), 16.8 m (55') and 10.7 m (35'). Each bent has 3 columns 5.8 m (19') high with the same cross-sectional and reinforcing characteristics as those of Bridge M1. Following Jernigan and Hwang (1997), the strength  $f_c$  of 20.7 MPa (3000 psi) concrete used for the bridge is assumed to be best described by a normal distribution with a mean strength of 31.0 MPa (4500 psi) and a standard deviation of 6.2 MPa (900 psi), whereas the yield strength  $f_y$  of grade 40 reinforcing bars used in design is described by a lognormal distribution having a mean strength of 336.2 MPa (48.8 ksi) with a standard deviation of 36.0 MPa (5.22 ksi). Then, a sample of ten nominally identical but statistically different bridges are created by simulating ten realizations of  $f_c$  and  $f_y$  according to respective probability distribution functions assumed. Other parameters that could contribute to variability of structural response were not considered in the present analysis under the assumption that their contributions are disregarable.

For the seismic ground motion, the time histories generated by Hwang and Huo (1996) at the Center for Earthquake Research and Information, the University of Memphis are used. These time histories are generated by making use of the Fourier acceleration amplitude on the base rock derived under the assumption of a far-field point source by Boore (1983). In fact, the study area is located 40 km to 100 km from Marked Tree, Arkansas (see figure 5-2), the epicenter of the 1846 earthquake of magnitude of 6.5 and of all the scenario earthquakes considered in this study. Use of more widely distributed sources of seismic events that represent better the New Madrid seismic zone is a worthwhile subject of future study. Marked Tree is currently considered to define the southwestern edge of the New Madrid fault. Upon using seismologically consistent values for the parameters in the Boore and other related models and converting the Fourier amplitude to a power spectrum, corresponding histories are generated on the base rock by means of the spectral representation method by Shinozuka and Deodatis (1991). The seismic wave represented by these time histories is propagated through the surface layer to the ground surface by means of the SHAKE 91 computer code by Idriss and Sun (1992) and used, upon modulating in the time domain, for the response analysis. To minimize computational effort, samples of 10 time histories are randomly selected from 50 histories generated by Hwang and Huo (1996) for each of the following eight (8) combinations of M (magnitude) and R (epicentral distance); M = 6.5 with R = 80 km and 100 km, M = 7.0 with R = 60 km and 80 km, M=7.5 with R= 40 km and 60 km, and M = 8.0 with R = 40 km and 60 km.

Typical ground motion time histories for two extreme combinations M = 8.0 with R = 40 km and M = 6.5 with R = 100 km are shown in figure 5-3. For the purpose of response analysis, a

sample of ten time histories generated from each M and R combination is matched with a sample of ten bridges in a pseudo Latin Hypercube format; pseudo in the sense that the sample of ten bridges is the same for all the combinations of M and R. Hence, each statistical representation of Bridges M1 and M2 are subjected to 80 ground motion time histories. The spectral accelerations averaged over 10 acceleration time histories used in this study from each of the combinations  $M = 7.5$  for  $R = 40$  km, and 60 km are shown in figure 5-4 to provide an insight to the frequency content of these ground motion time histories.

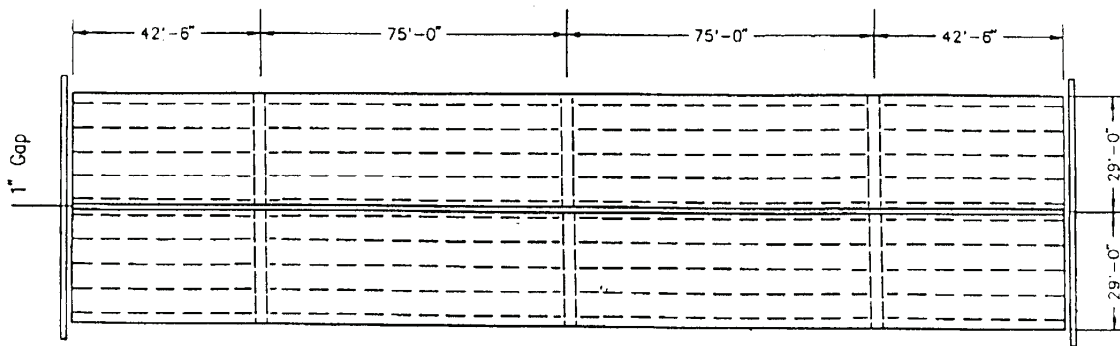
The present study utilizes the SAP 2000 finite element code, which is user-friendly particularly for bridge design and analysis, in order to simulate the state of damage of each structure under ground acceleration time history. This computer code can provide hysteretic elements that are in essence bilinear without strength or stiffness degeneration. The results from SAP 2000 code was validated for the bilinear behavior by analyzing the same problem using ANSYS computer code. Similarly, validation should be made using ANSYS, DIANA and other up-scale codes to account for bilinear hysteresis with strength and stiffness degradation in order to identify the extent of the approximation the SAP 2000 code provides. Such validation and adjustment would provide an analytical basis for possibly improving SAP 2000 results in a systematic fashion to derive more realistic fragility curves in an efficient fashion. This indeed is an interesting future study.

The states of damage considered for both Bridges M1 and M2 are major (all the columns subjected to ductility demand  $\geq 2$ ) and “at least minor” (all the columns subjected to ductility demand  $\geq 1$ ) under the longitudinal applications of ground motion. For the Memphis bridges, the median and log-standard deviation parameters for the log-normal fragility curves were estimated by Method 1. Figure 5-5 shows the fragility curves associated with these states of damage for Bridges M1 and M2. Eighty diamonds are plotted in figure 5-5 and also more clearly in figure 5-6 on the two horizontal axes represent  $x_i = 0$  (for state of less than major damage) and  $x_i = 1$  (for state of major damage) in relation to (A-1) for Bridge M1 under the eighty earthquakes generated. The corresponding fragility curve is derived on the basis of these diamonds and replotted in figure 5-6 to demonstrate more easily how well the corresponding fragility curves fit to the input damage data. Similar eighty diamonds associated with the state of minor damage for Bridge M1 are plotted in figure 5-7 together with the corresponding fragility curve.

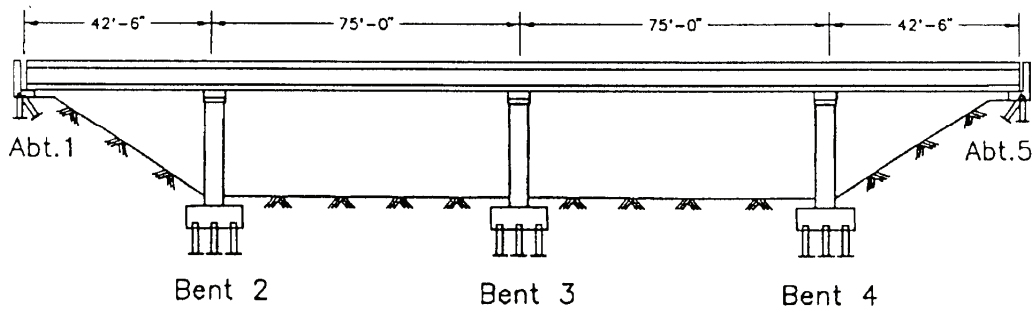
Figures 5-8 and 5-9 plot the fragility curves for Bridge M1 associated with at least minor damage and with major damage, respectively with solid curves based on 80 earthquakes and dashed curves on 60 earthquakes (in accordance with the pseudo-hyper Latin cube procedure described earlier). The results suggest that the reduction of sample size from 80 to 60 may be tolerable for the fragility curve development. Caution should be exercised, however, to recognize that the key to develop a reasonable fragility curve is not only to have an adequate sample size (a minimum of 30 or so) but also to have the sample covering appropriately the three ranges of PGA for no damage, damage and variable fragility (e.g.,  $PGA \leq 0.20g$ ,  $PGA \geq 0.35g$  and  $PGA$  between the two in figure 5-9). The intermediate range is where the fragility value rises from zero to unity. Unfortunately, the adequacy of such a coverage can only be judged after the fact. Hence, depending on the simulation result at hand, decision must be made whether to terminate or continue with the simulation primarily on the basis of judgment. It is mentioned in passing that this option of increasing the sample size at the expense of additional computational effort does not exist for the empirical fragility curve development in the sense that the source of data is

limited to the damage report. The analysis performed under the ground motion in the transverse direction produced states of lesser damage and hence not given in this report.

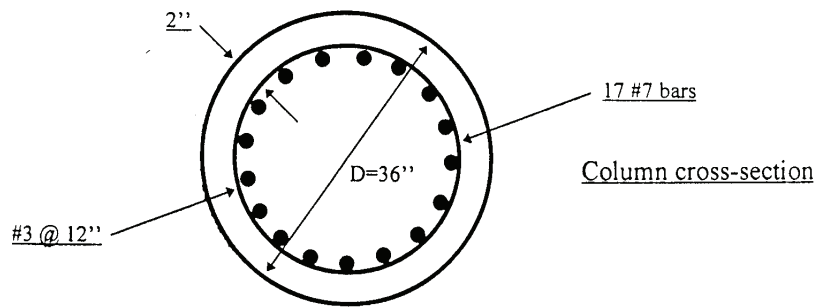
It is important to recognize that mixed modes of failure can occur simultaneously as well as sequentially depending on the specific process of dynamic response each bridge experiences. The following modes of failure are more obvious examples to which due consideration must be given. The columns can fail not only in a single mode under bending or under shear, but also in a mixed bending and shear. Prior to these serious failures that could induce a state of collapse of a bridge, however, bearings located on bents could fail when bridge columns and decks are not monolithically constructed. The bearing failure can not only induce states of physical damage such as unseating and falling-off of the decks, but also potentially result in traffic closure by creating abrupt deck surface irregularity even when essential bridge structural components such as decks themselves, columns and abutments suffer from little damage. Similar failures including those arising from pounding between adjacent decks could occur, particularly at expansion joints. At present, however, these modes of failure present a significant technical challenge to be included in the dynamic analysis in the sequence they occur. Indeed, it is one thing to analytically formulate the failure criteria, but it is entirely another to reproduce computationally the sequence of these failures. Quasi-static and related approaches may provide additional information to circumvent this difficulty.



Plan



Elevation



Column cross-section

**FIGURE 5-1 A Representative Memphis Bridge**

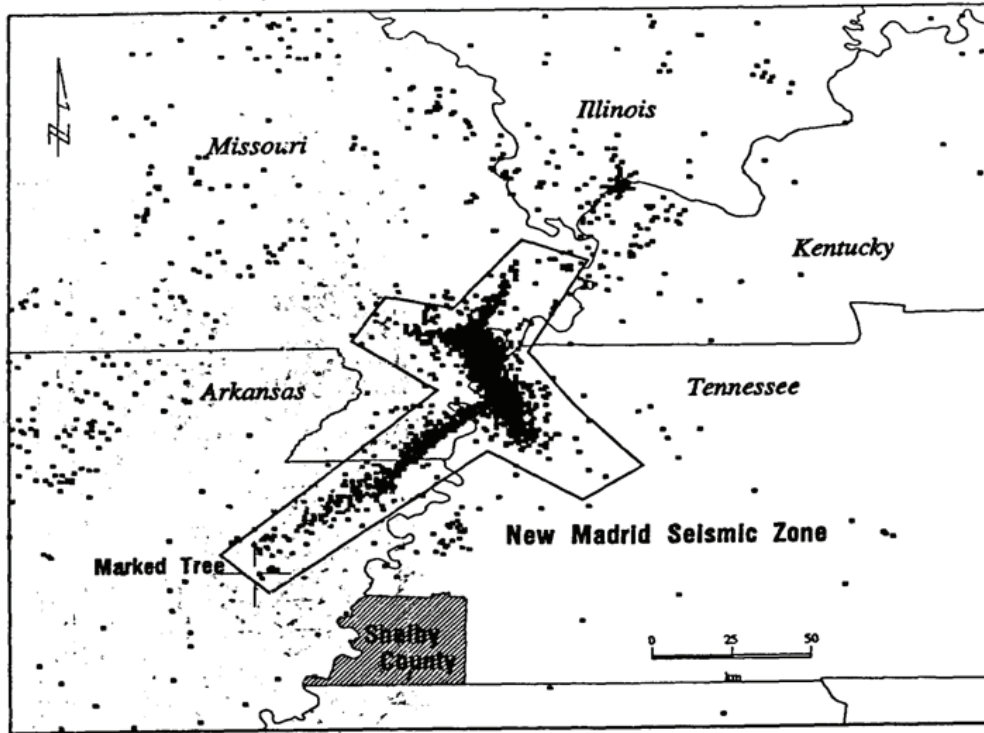


**FIGURE 5-2 New Madrid Seismic Zone and Marked Tree, AR**

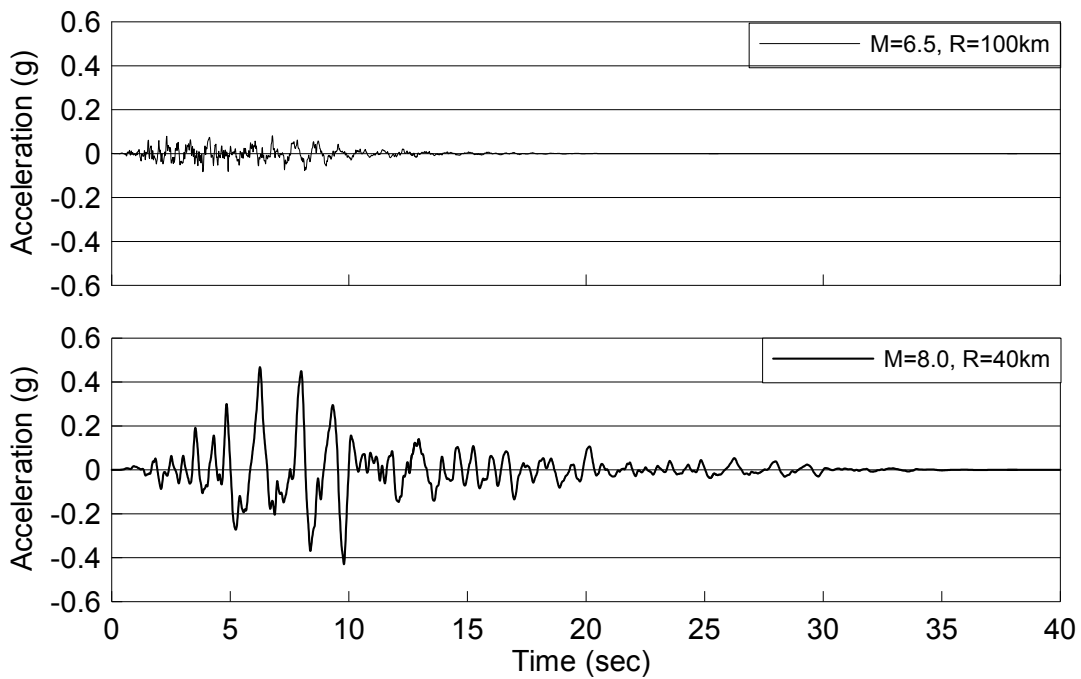


**FIGURE 5-3 Typical Ground Acceleration Time Histories in the Memphis Area**

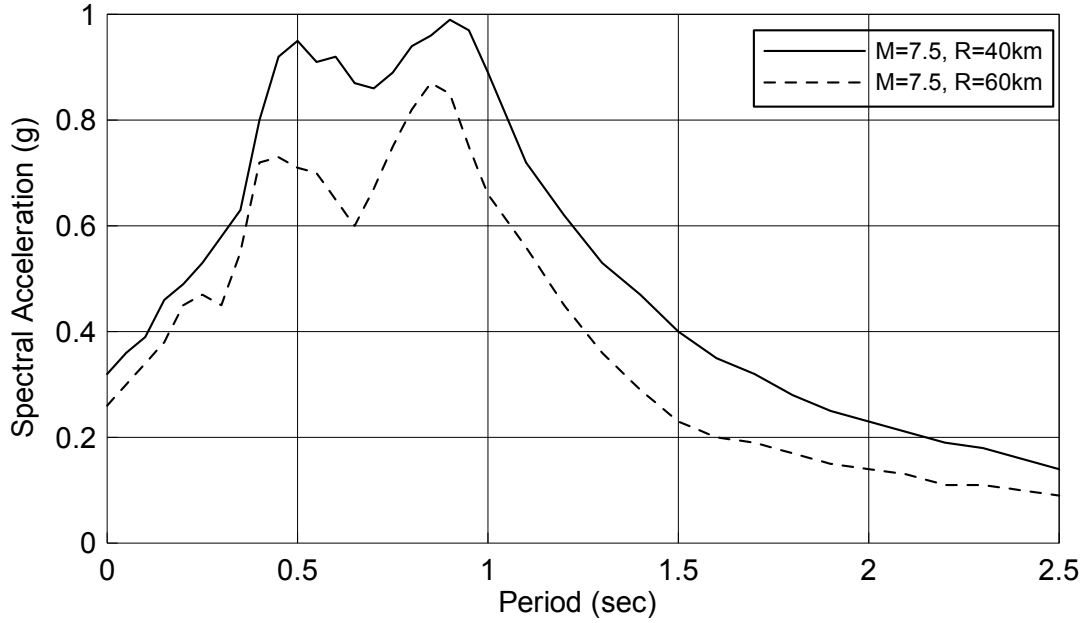


**FIGURE 5-4 Average Spectral Accelerations in the Memphis Area**

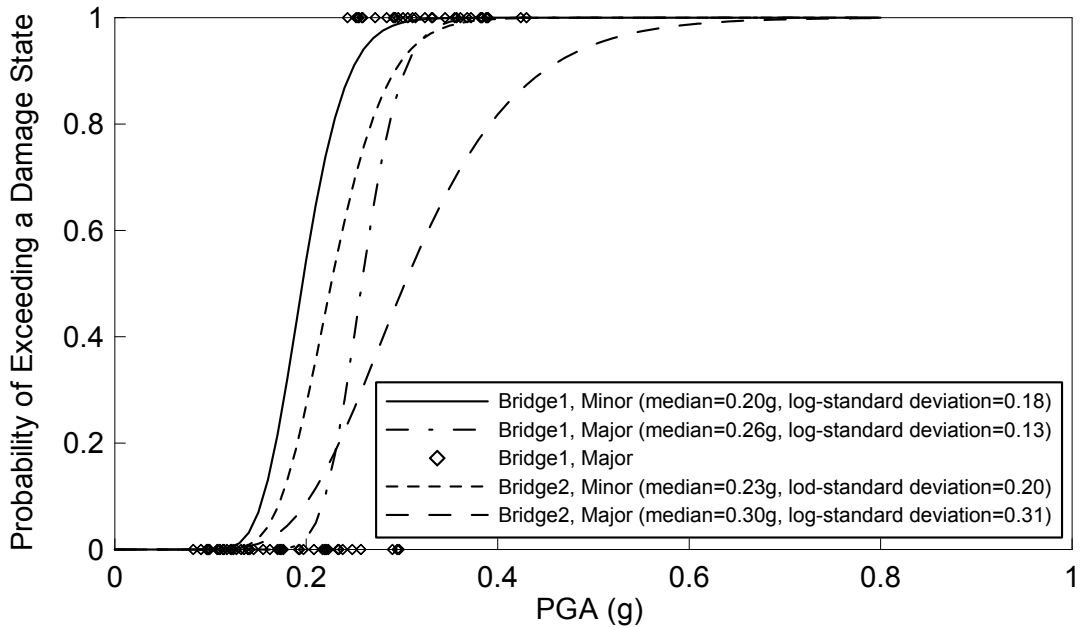


**FIGURE 5-5 Fragility Curves for Memphis Bridges M1 and M2**

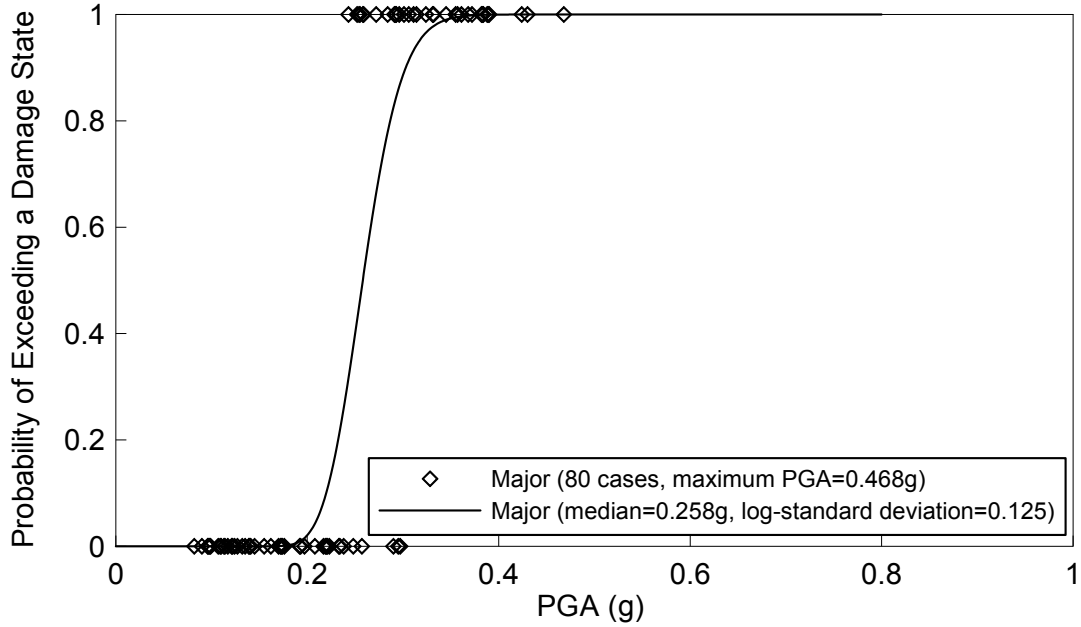


**FIGURE 5-6 Fragility Curve for Bridge M1 with Major Damage and Input Damage Data**

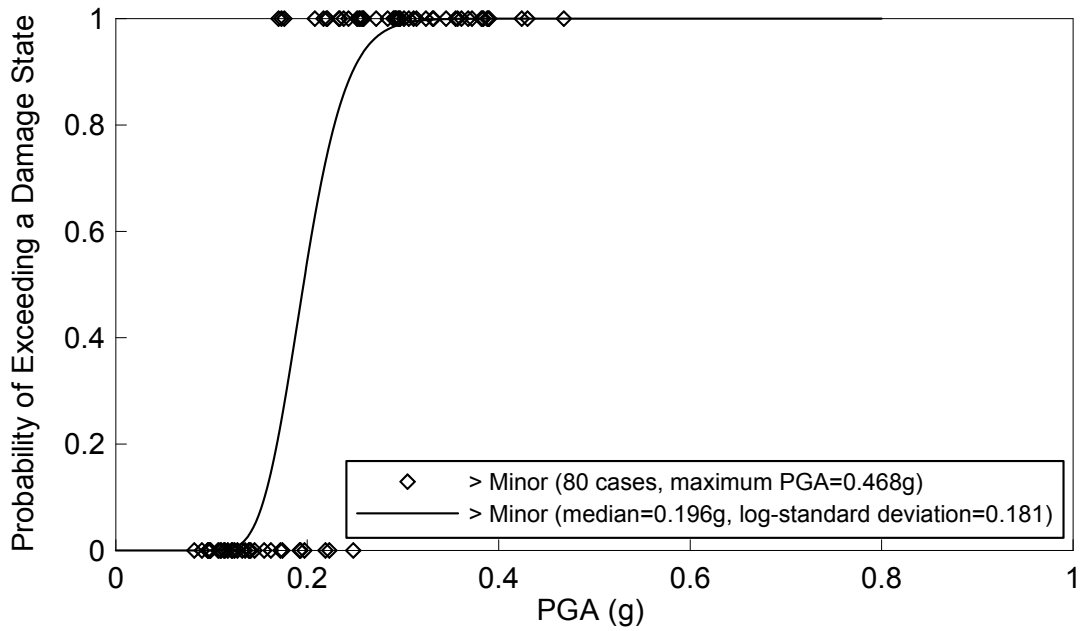


**FIGURE 5-7 Fragility Curve for Bridge M1 with at least Minor Damage and Input Damage Data**

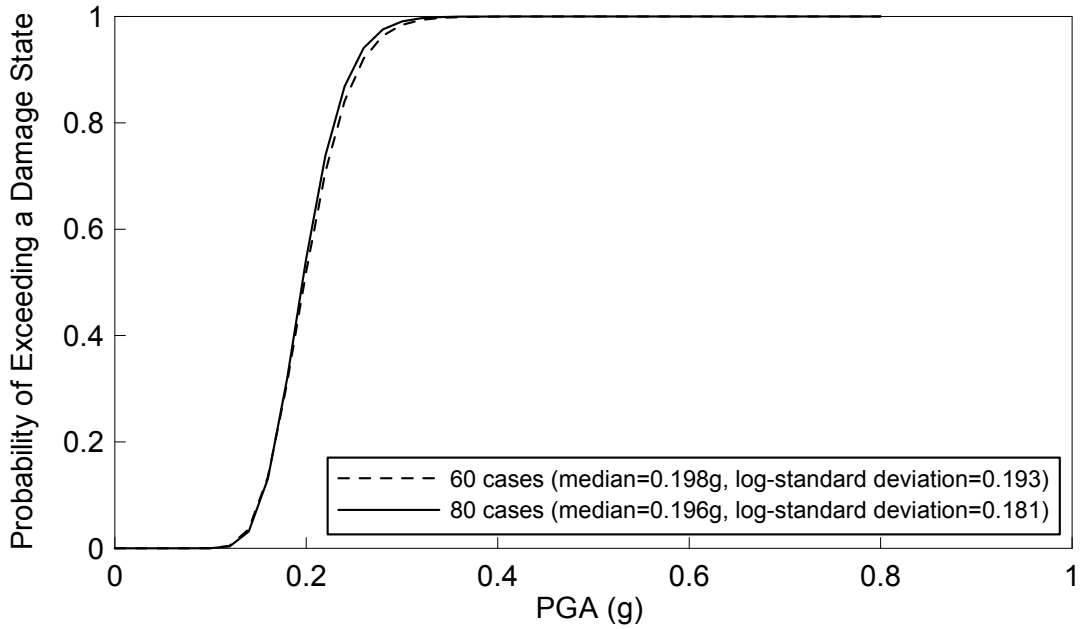


**FIGURE 5-8 Comparison of Fragility Curves based on Sample Size 80 and 60 (Bridge M1 with at least Minor Damage)**

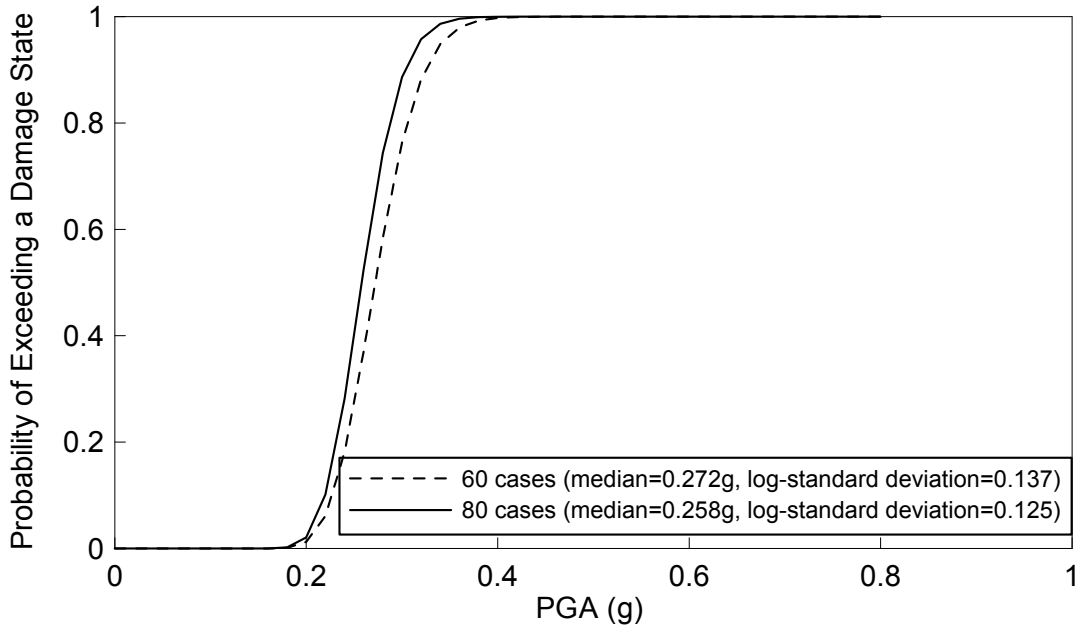


**FIGURE 5-9 Comparison of Fragility Curves based on Sample Size 80 and 60 (Bridge M1 with Major Damage)**



## SECTION 6 COMPARISON OF FRAGILITY CURVES

### 6.1 Comparison of Analytical Fragility Curves with other Fragility Curves

HAZUS (1999) documented five damage states of highway bridges as ‘No’, ‘Slight/Minor’, ‘Moderate’, ‘Extensive’ and ‘Complete’ damage which are equivalent to the five damage states as reported by Caltrans. Following the theoretical background presented in Basöz and Mander (1999), HAZUS categorized a total of 28 bridge classes (HWB1 through HWB28) in accordance with bridge design, configuration and functional characteristics. These fragility curves are used to compare analytical fragility curves those obtained after calibrating with empirical damage data. For this purpose, bridge class HWB9 (National Bridge Inventory (NBI) Class: 205 – 206) is selected for comparison, which has closest resemblance with the example bridges among 28 classes described in HAZUS. The median spectral accelerations (SA) of damage states ‘Slight/Minor’, ‘Moderate’, ‘Extensive’ (Major) and ‘Complete’ (Collapse) for class HWB9 are obtained from Table 7.7 of the HAZUS technical manual (1999) and modified further to incorporate 3D effect ( $k_{3D}$ ) for total number of span, amplification factor (S) for soil type and modification factor for skewness ( $k_{skew}$ ). According to the example bridges, the following modification factors are implied:  $S = 1.3$  for soil type ‘C’,  $k_{skew} = 1.0$  for zero skewness and  $k_{3D} = 1.08, 1.04$  and  $1.03$  for Bridge 2, 4 and 5, respectively. As  $I_{shape} = 0$  for HWB9 (Table 7.7 of HAZUS manual),  $k_{shape}$  does not apply in modifying SA. Modified SAs are used to generate bridge specific fragility curves for different damage levels.

The median PGA values for NBI class 205 – 206 are also obtained from Basöz and Mander (1999). These median PGA values are suggested to use as SA (natural period = 1 sec) for long period structures, and thereafter modified according to the analytical bridge model as indicated in the previous paragraph. A set of fragility curves for different damage levels are obtained using these modified SAs.

For the purpose of comparison, the analytical fragility curves are converted for ground motion intensity parameter SA, and plotted in the same figure along with the fragility curves from HAZUS and Basöz and Mander (1999). Figures 6-1 ~ 6-9 show the fragility curves of Bridge 2, 4 and 5 for minor, moderate and major damage states and table 6-1 represents the corresponding median SA values. Comparison indicates that in moderate and major damage states analytical fragility curves are consistent with HAZUS for Bridge 2, although these are weaker than HAZUS for other two bridges. In case of minor damage, analysis produces stronger fragility curves than HAZUS for all bridges.

In all cases, fragility curves from Basöz and Mander (1999) are substantially conservative than other fragility curves. In comparison with HAZUS, they do not produce good consistency which is mainly due to the different approaches used in these two methods to imply soil type modification factor. Also, the median fragility parameters mentioned here are slightly different though both considered same bridge class.

**TABLE 6-1 Median Spectral Accelerations (SA)**

Damage State	Modified median SA from HAZUS (1999) (g)	Modified median SA from Basöz and Mander (1999) (g)	Median SA for Bridge 2 (g)
Bridge 2			
Minor	0.60	0.42	0.72
Moderate	0.97	0.73	0.89
Major	1.41	1.02	1.33
Bridge 4			
Minor	0.60	0.42	0.69
Moderate	0.93	0.70	0.79
Major	1.33	0.96	1.08
Bridge 5			
Minor	0.60	0.42	0.68
Moderate	0.93	0.70	0.86
Major	1.34	0.96	1.08

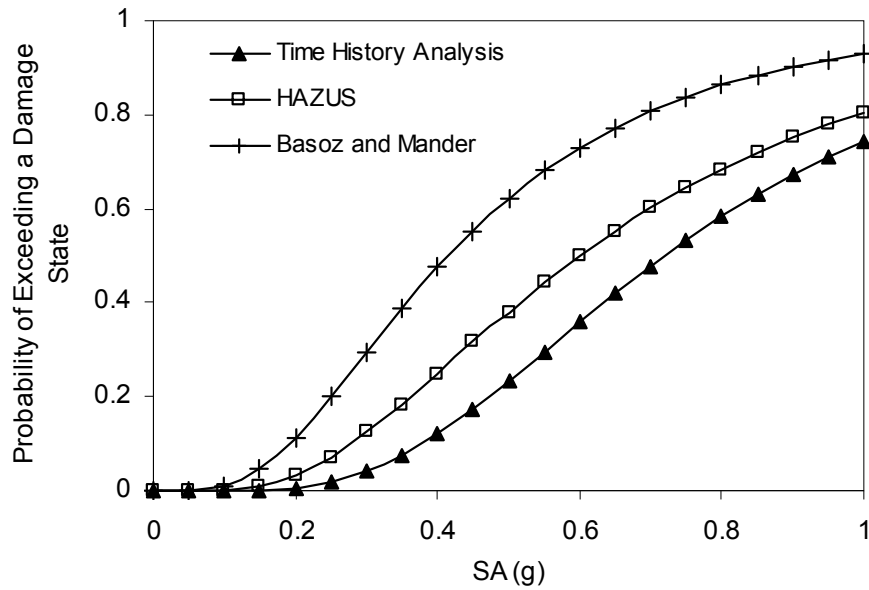


**FIGURE 6-1 Comparison of Fragility Curves of Bridge 2 at Minor Damage**

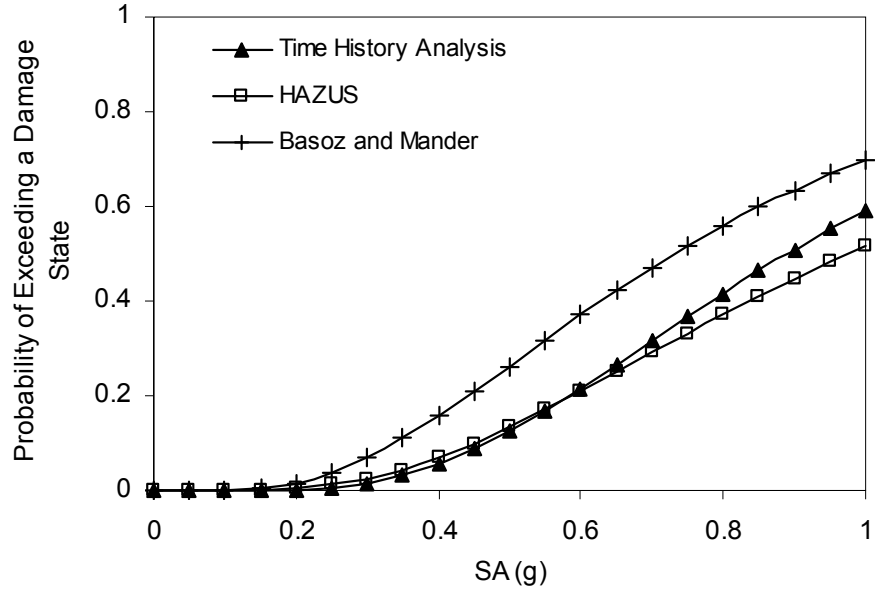


**FIGURE 6-2 Comparison of Fragility Curves of Bridge 2 at Moderate Damage**

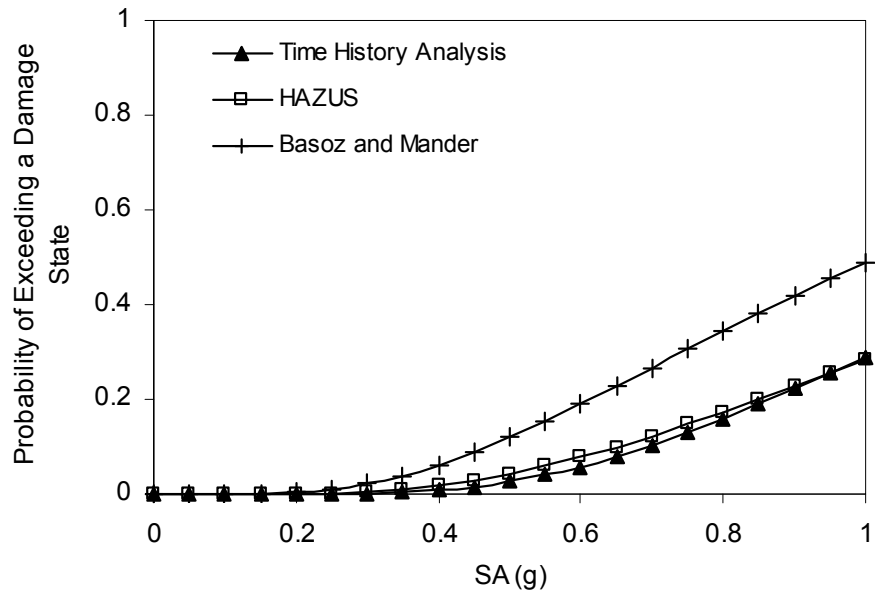


**FIGURE 6-3 Comparison of Fragility Curves of Bridge 2 at Major Damage**

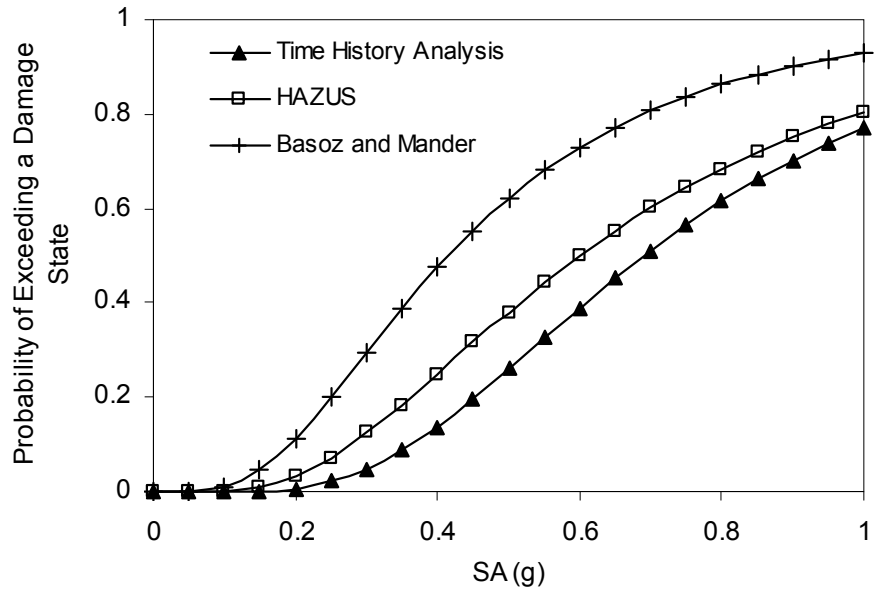


**FIGURE 6-4 Comparison of Fragility Curves of Bridge 4 at Minor Damage**

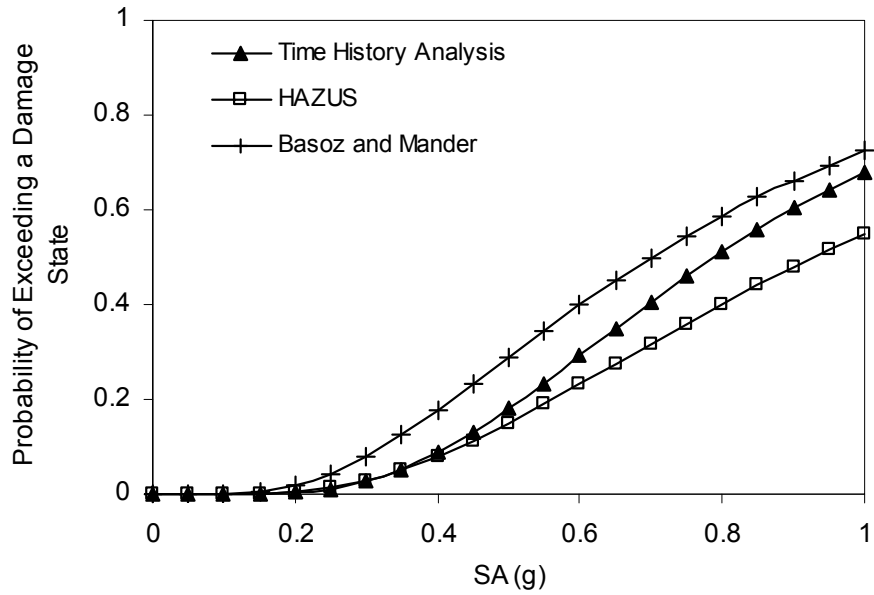


**FIGURE 6-5 Comparison of Fragility Curves of Bridge 4 at Moderate Damage**

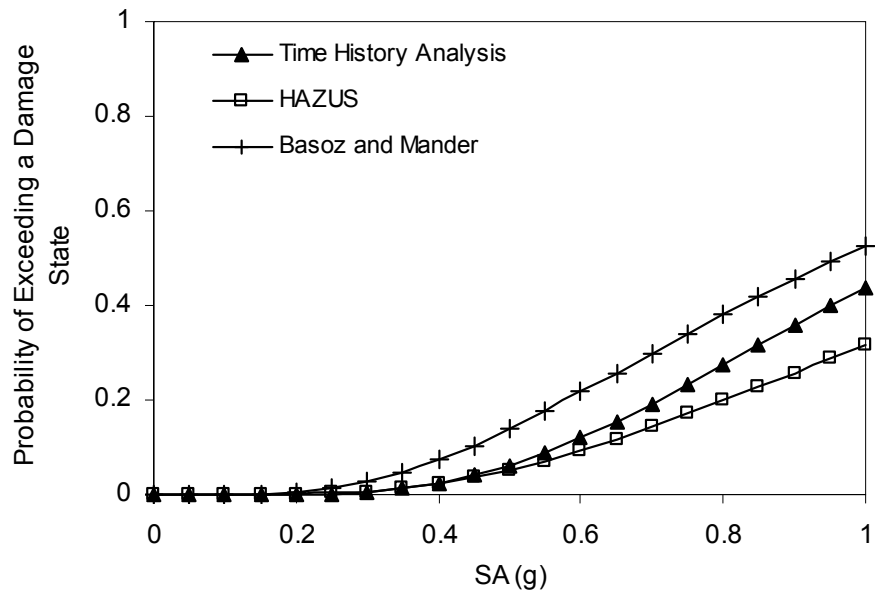


**FIGURE 6-6 Comparison of Fragility Curves of Bridge 4 at Major Damage**

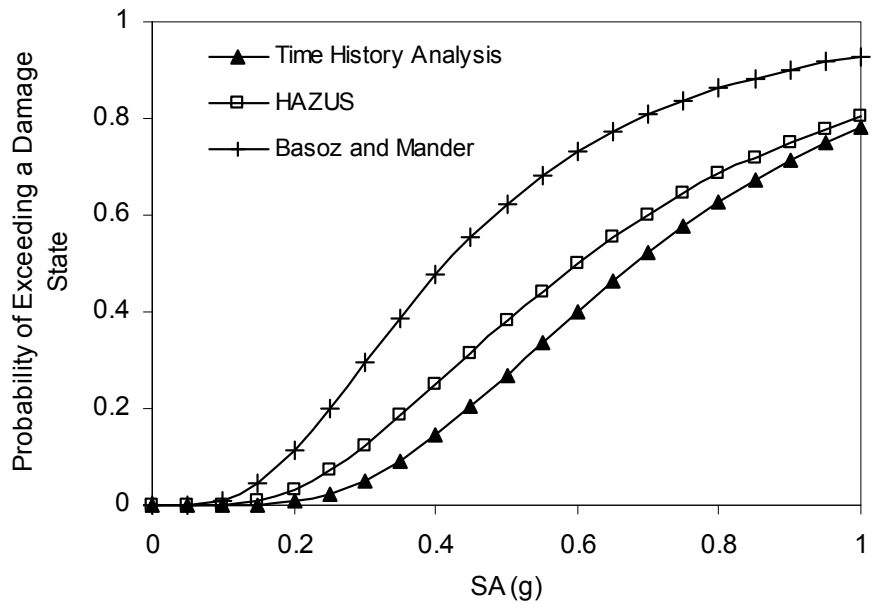


**FIGURE 6-7 Comparison of Fragility Curves of Bridge 5 at Minor Damage**

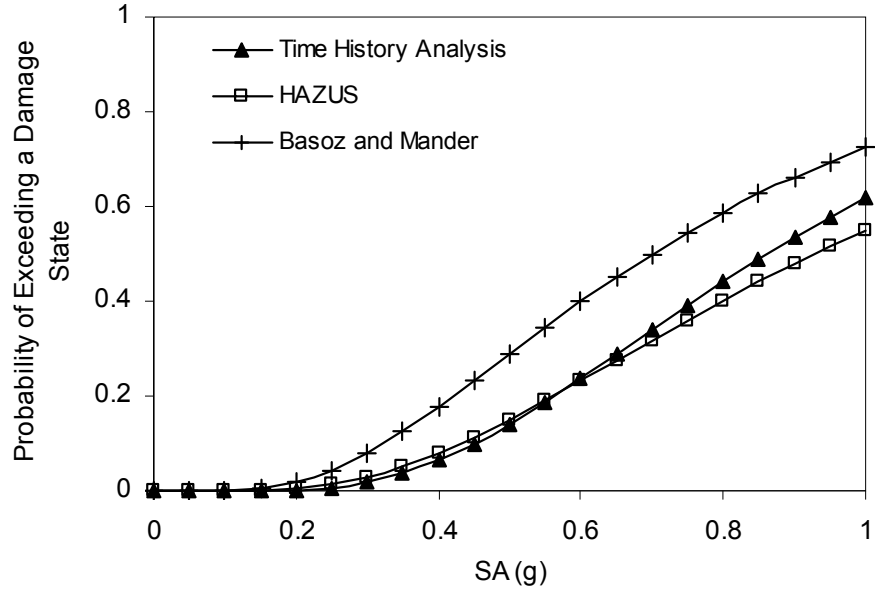


**FIGURE 6-8 Comparison of Fragility Curves of Bridge 5 at Moderate Damage**

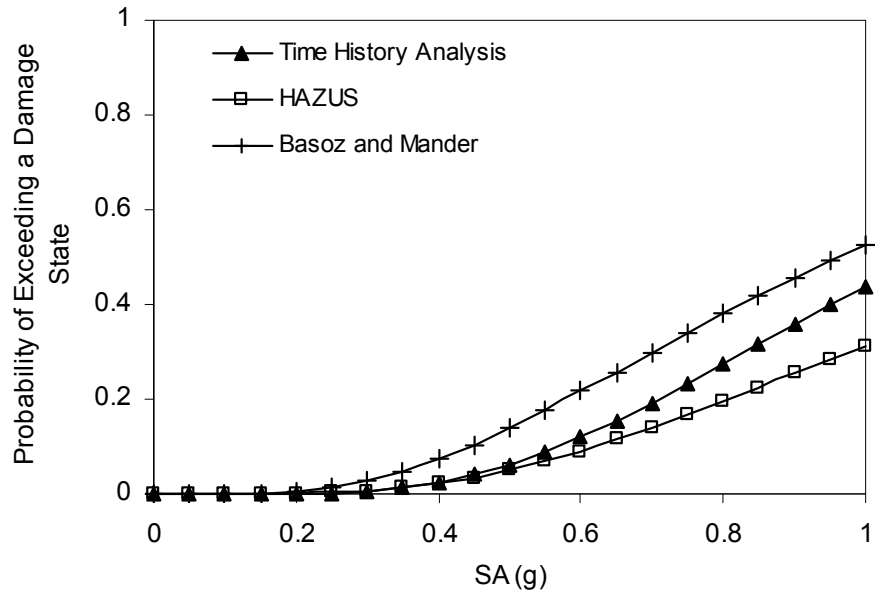


**FIGURE 6-9 Comparison of Fragility Curves of Bridge 5 at Major Damage**

## 6.2 Comparison of Empirical Fragility Curves with HAZUS

As discussed in chapter 2, empirical fragility curves are developed from the bridge damage data from Northridge earthquake. The damaged bridges are categorized into different sub-sets according to the bridge attribute and configurations and empirical fragility curves are developed in each sub-set. Tables 6-2 and 6-3 documented the fragility parameters of Caltrans bridges when they are classified according to skewness and number of span, respectively. The number of damaged bridges falls in a particular category is represented as “Sample Size”.

HAZUS documented the modification factor for bridge skewness and number of span. In order to make a comparison with HAZUS recommendations, empirical fragility parameters are used to compute these modification factors. In case of skewed bridges, the modification factor for certain skew angle is computed by dividing the median fragility parameter corresponding to this skew angle with that corresponding to zero skew angle (table 6-2). Figure 6-10 represents the modification factors for skew angle obtained from empirical fragility curves and HAZUS documentation.

Figure 6-11 shows the modification factors for number of bridge span obtained from empirical fragility curves and HAZUS documentation. The empirical modification factor for number of bridge span is computed by dividing the median fragility parameter obtained for some category with that obtained for number of bridge span > 10 (table 6-3).

**TABLE 6-2 Empirical Fragility Parameters of Caltrans’ Bridges with Different Skewness**

Sample Size	562	666	384	235	42
Median PGA (g)	Skew Angle (Deg.)				
	0	1 ~ 20	21 ~ 40	41 ~ 60	> 60
$C_{minor}$	1.18	0.88	0.60	0.77	0.49
$C_{moderate}$	1.66	1.14	0.74	0.86	0.65
$C_{major}$	3.17	1.61	1.12	1.36	0.83

**TABLE 6-3 Empirical Fragility Parameters of Caltrans’ Bridges with Different Numbers of Span**

Sample Size	548	474	517	323	193	91	69
Median PGA (g)	Number of Span						
	1	2	3	4	5,6,7	8,9,10	> 10
$C_{minor}$	0.93	0.8	0.77	0.63	0.46	0.37	0.34
$C_{moderate}$	1.14	0.95	1.02	0.80	0.60	0.42	0.39
$C_{major}$	1.51	1.50	1.52	1.22	0.88	0.59	0.69

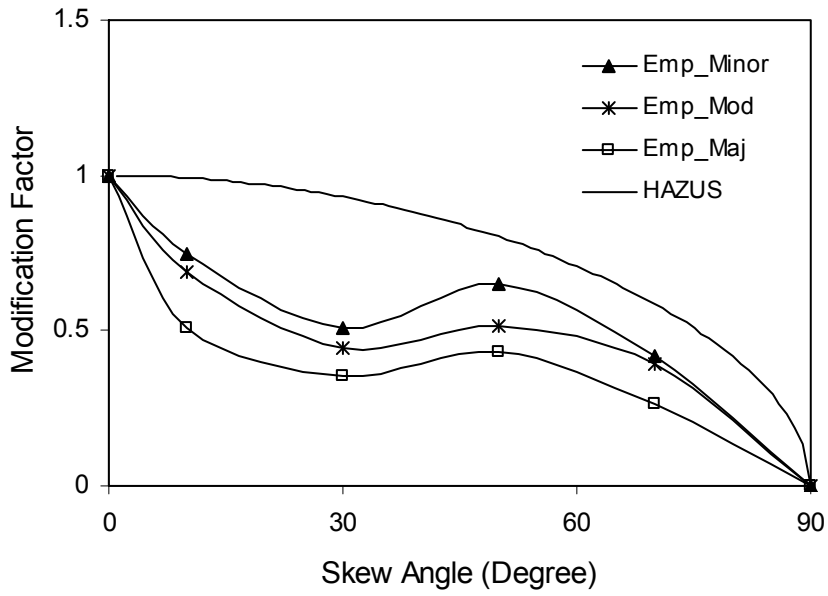


**FIGURE 6-10 Comparison of Modification Factors for Different Skew Angles**

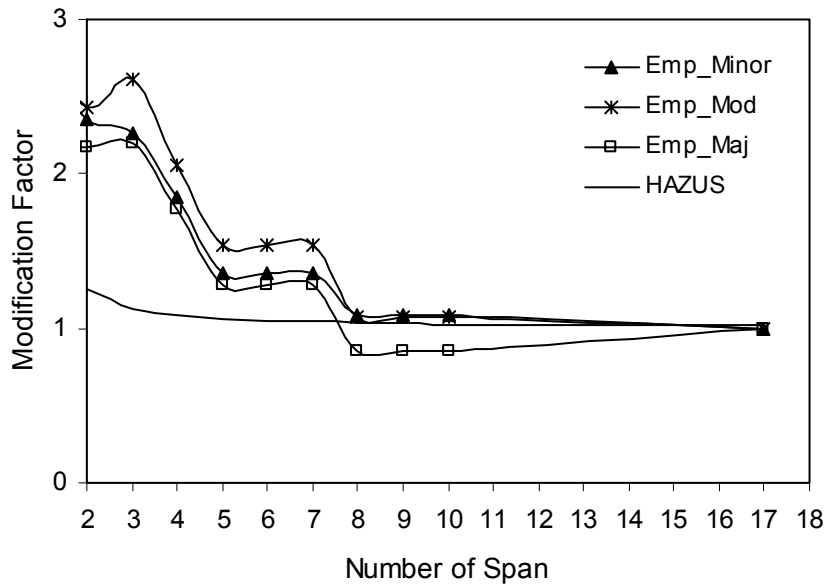


**FIGURE 6-11 Comparison of Modification Factors for Different Numbers of Bridge Spans**



## **SECTION 7**

### **VERIFICATION OF BRIDGE DAMAGE STATE DEFINITIONS THROUGH EXPERIMENTAL DATA**

As discussed in earlier, bridge damage state definitions are quantified by mechanistically calibrating analytical bridge damage data, generated through numerical simulation of bridge dynamic characteristics, with that obtained from the 1994 Northridge earthquake. Thus derived bridge damage state definitions quantify the physical descriptions presented in HAZUS (1999). However, it is always desirable to compare these definitions with available experimental data from full scale bridge model testing. For this purpose, the current section deals with the bridge damage data observed from a large scale shaking table test conducted at the University of Nevada, Reno (Johnson et al. 2006) in which a research team from University of California, Irvine was participated. This experimental study provides bridge response and its progressive failure nature under ground motions with various intensity levels. Damage data from this experiment are studied here and analyzed further to produce relevant result so that these results can be utilized in a straightforward comparative study involving analytical result. Following sections describes this experimental study and comparison between analytical and experimental results.

#### **7.1 Experimental Study**

A large-scale shaking table test of a 20.5 m long two-span reinforced concrete bridge model was conducted at the University of Nevada, Reno (Johnson et al. 2006). Main objective of this experimental research was to determine the seismic response of a bridge under different levels of excitation. Total height of this specimen was 3.28 m from the bottom of the footing block to the top of the superstructure. Bridge spans, each 9.14 m long, were supported on three column bents with the tallest one at middle. Clear heights of these bents were 1.83 m, 2.44 m and 1.52 m. Each bent was consisting of two columns of same cross-sectional and material properties. A solid slab was composed as bridge deck that was post-tensioned in both longitudinal and transverse directions of the bridge. Cast-in-place drilled pile shafts were assumed as substructure. Figures 7-1 and 7-2 show the bridge model and experimental set up. From this model, axial force is estimated as 219.2 kN on bent 1 and 3, and 182.2 kN on bent 2.



**FIGURE 7-1 Experimental Model of a Two-Span Reinforced Concrete Bridge (Johnson et al. 2006)**

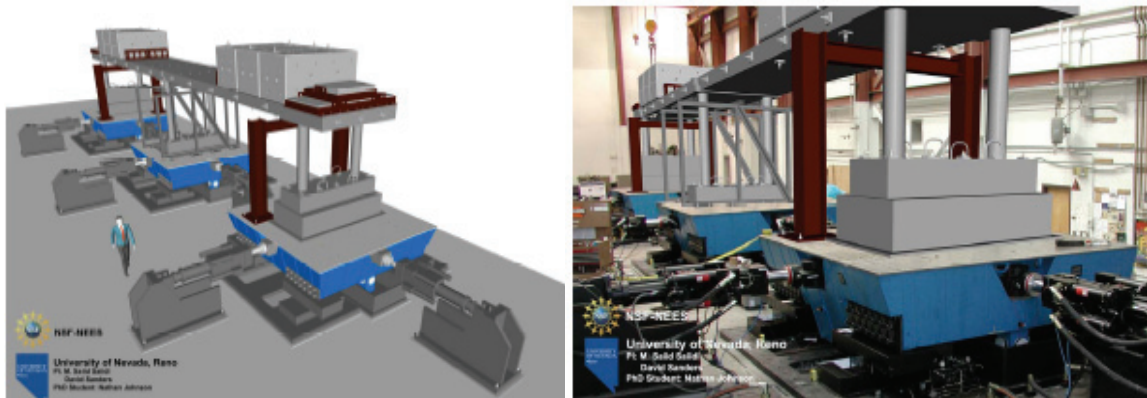


**FIGURE 7-2 Experimental Bridge Model on Shake Tables (Johnson et al. 2006)**

### 7.1.1 Low and High Amplitude Tests

This bridge model was excited with both low and high amplitude earthquakes by placing it on three shaking tables as shown in figure 7-2. Earthquake ground motions used in this study were calculated from the motion recorded at the Century City Country Club during the 1994 Northridge earthquake. In this experiment, ground motions were applied along the transverse direction of the bridge. Bridge movement in the longitudinal direction was not studied as in this direction in-span hinges and boundary conditions of the bridge were not modeled in order to keep the experimental model ‘reasonably simple’. Although transverse movement produced some response in the longitudinal direction of the bridge, that was accurate only up to the closure of prototype hinge gap. Therefore bridge response only in the transverse direction is considered here for further analysis.

Before high amplitude tests, 11 tests were conducted such a way that longitudinal reinforcement in bridge columns did not yield. These tests are referred to as low amplitude tests. Following these, 9 high amplitude tests were performed (test 12 to 20) by gradually increasing ground motion intensity. Main purpose of these high amplitude tests was to excite the bridge model so that bridge columns failed in the transverse direction. To investigate the nature of progressive failure, bridge response was recorded in each step from yielding to buckling of longitudinal reinforcements. In doing so, ground motion with very low amplitude was applied during test 12 and gradually scaled up in consecutive tests. Table 7-1 lists target PGAs at shaking table during high amplitude tests. During test 19, this bridge model was regarded to have failed when columns of bent 3 failed in flexure, though no major damage was observed in other two bents. Afterwards, upon completion of test 20 two additional tests were performed with reduced amplitude to produce more damage in bents 1 and 2.

**TABLE 7-1 High Amplitude Tests and Target PGAs**

High Amplitude Test #	Bed Rock Excitation (g)	Target PGA at Shaking Table (g)
12	0.40	0.075
13	0.40	0.15
14	0.40	0.25
15	0.40	0.50
16	0.40	0.75
17	0.40	1.00
18	0.40	1.33
19	0.40	1.66
20	0.40	1.00

### 7.1.2 Bridge Response and Progressive Damage in Columns

Prior to testing, shake table model was instrumented with displacement transducers, accelerometers and strain gauges in order to record bridge seismic response. Johnson et al. (2006) documented bridge response in terms of displacement and acceleration of superstructure, curvature at column ends, strain in the column reinforcement, etc. They verified these response quantities by making analytical model of this two-span bridge using SAP2000 Nonlinear and Drain-3DX (Prakash and Campbell, 1994) computer code.

Recorded response during high amplitude tests indicates the progressive failure pattern of the bridge. During tests 12 and 13, no damage was observed in any of the bridge columns. Gradually hairline cracks started to form during test 14 though no significant damage was noticed at that time. During tests 15 and 16, cover concrete in bridge columns started to spill out

which became significant during test 17. During test 19, both columns of bent 3 failed in flexure due to the buckling of longitudinal reinforcing bars. A detail description of this progressive failure and observed bridge response are documented in Johnson et al. (2006).

## 7.2 Comparison Between Experimental and Analytical Result

As stated before, damage data observed in this experiment (Johnson et al., 2006) is a valuable source of information about bridge response under seismic ground motions with various intensity levels. This set of data is utilized in this research to compare these with the analytical result discussed in one of the preceding chapters of this report. For this purpose, bridge damage states are introduced as no such definition was indicated in the experimental study. Then experimental damage data are categorized into these newly incorporated damage states. Following sections describe this procedure in detail.

### 7.2.1 Bridge Damage States

According to the nature of damage observed in columns during high amplitude tests, bridge damage can be categorized into four damage levels starting from no damage to major damage. This categorization is done in accordance with the damage state description presented in HAZUS (1999). Table 7-2 lists these damage states and corresponding damage in bridge columns.

**TABLE 7-2 Description of Bridge Damage States as Observed from the Experiment**

Damage States	Descriptions of Physical Damage
No Damage	No damage in bridge columns
Minor Damage	Height of column flaking/spalling $\leq 80$ mm
Moderate Damage	Height of column spalling $> 80$ mm or exposure of column reinforcement
Major Damage	Buckling of reinforcing bar(s)

At the beginning of high amplitude tests (during tests 12 to 14), no damage was observed in bridge columns. Therefore, observed curvatures at column ends during these tests represent the state of no damage. In the similar fashion, recorded curvatures during tests at which bridge columns experienced minor, moderate and major damage represent these damage states. Table 7-3 lists curvatures at column ends observed during high amplitude tests and corresponding damage levels of this bridge.

**TABLE 7-3 Recorded Curvatures at Column Ends and Corresponding Damage Levels**

Location	Test #	Curvature rad/mm	Damage	Location	Test #	Curvature rad/mm	Damage
Bent 1, East Col, Top	12	$1.1 \times 10^{-5}$	No	Bent 1, East Col, Top	16	$1.8 \times 10^{-4}$	Minor
	14	$4.4 \times 10^{-5}$	No		17	$1.4 \times 10^{-4}$	Minor
Bent 1, East Col, Bottom	12	$1.3 \times 10^{-5}$	No	Bent 1, East Col, Bottom	16	$2.2 \times 10^{-4}$	Minor
	15	$1.0 \times 10^{-4}$	No		17	$1.7 \times 10^{-4}$	Minor
Bent 1, West Col, Top	12	$1.3 \times 10^{-5}$	No	Bent 1, West Col, Top	16	$2.0 \times 10^{-4}$	Minor
	14	$4.5 \times 10^{-5}$	No		18	$2.3 \times 10^{-4}$	Minor
Bent 1, West Col, Bottom	12	$1.4 \times 10^{-5}$	No	Bent 1, West Col, Bottom	16	$2.1 \times 10^{-4}$	Minor
	15	$1.2 \times 10^{-4}$	No		17	$1.5 \times 10^{-4}$	Minor
Bent 2, East Col, Top	12	$5.4 \times 10^{-6}$	No	Bent 2, East Col, Top	18	$2.0 \times 10^{-4}$	Minor
	15	$4.2 \times 10^{-5}$	No				
Bent 2, East Col, Bottom	12	$8.8 \times 10^{-6}$	No	Bent 2, East Col, Bottom	18	$1.7 \times 10^{-4}$	Minor
	15	$5.2 \times 10^{-5}$	No				
Bent 2, West Col, Top	12	$6.0 \times 10^{-6}$	No	Bent 2, West Col, Top	19	$2.4 \times 10^{-4}$	Minor
	15	$4.8 \times 10^{-5}$	No				
Bent 2, West Col, Bottom	12	$7.4 \times 10^{-6}$	No	Bent 2, West Col, Bottom	18	$1.9 \times 10^{-4}$	Minor
	16	$1.3 \times 10^{-4}$	No				
Bent 3, East Col, Top	12	$9.8 \times 10^{-6}$	No	Bent 3, East Col, Top	15	$1.3 \times 10^{-4}$	Minor
	14	$3.9 \times 10^{-5}$	No		16	$1.9 \times 10^{-4}$	Minor
Bent 3, East Col, Bottom	12	$1.0 \times 10^{-5}$	No	Bent 3, East Col, Bottom	15	$1.4 \times 10^{-4}$	Minor
	14	$4.0 \times 10^{-5}$	No		16	$2.0 \times 10^{-4}$	Minor
Bent 3, West Col, Top	12	$9.0 \times 10^{-6}$	No	Bent 3, West Col, Top	16	$1.5 \times 10^{-4}$	Minor
	15	$7.3 \times 10^{-5}$	No				
Bent 3, West Col, Bottom	12	$1.1 \times 10^{-5}$	No	Bent 3, West Col, Bottom	16	$2.0 \times 10^{-4}$	Minor
	14	$4.0 \times 10^{-5}$	No		15	$1.5 \times 10^{-4}$	Minor
Bent 1, East Col, Top	19	$2.7 \times 10^{-4}$	Moderate	Bent 3, East Col, Top	18	$3.4 \times 10^{-4}$	Moderate
	21	$2.4 \times 10^{-4}$	Moderate				

**TABLE 7-3 Recorded Curvatures at Column Ends and Corresponding Damage Levels  
(Cont'd)**

Bent 1, East Col, Bottom	19	$3.2 \times 10^{-4}$	Moderate	Bent 3, East Col, Bottom	18	$3.7 \times 10^{-4}$	Moderate
	21	$2.4 \times 10^{-4}$	Moderate				
Bent 1, West Col, Top	19	$2.9 \times 10^{-4}$	Moderate	Bent 3, West Col, Top	18	$2.6 \times 10^{-4}$	Moderate
Bent 1, West Col, Bottom	19	$3.0 \times 10^{-4}$	Moderate	Bent 3, West Col, Bottom	18	$3.2 \times 10^{-4}$	Moderate
Bent 2, East Col, Top	22	$2.8 \times 10^{-4}$	Moderate	Bent 3, East Col, Top	19	$5.3 \times 10^{-4}$	Major
					21	$3.9 \times 10^{-4}$	Major
Bent 2, East Col, Bottom	22	$2.5 \times 10^{-4}$	Moderate	Bent 3, East Col, Bottom	19	$5.0 \times 10^{-4}$	Major
					21	$4.0 \times 10^{-4}$	Major
Bent 2, West Col, Top	22	$3.0 \times 10^{-4}$	Moderate	Bent 3, West Col, Top	19	$4.6 \times 10^{-4}$	Major
					20	$3.8 \times 10^{-4}$	Major
Bent 2, West Col, Bottom	22	$3.2 \times 10^{-4}$	Moderate	Bent 3, West Col, Bottom	19	$5.9 \times 10^{-4}$	Major
					20	$4.6 \times 10^{-4}$	Major

### 7.2.2 Moment-Rotation Analysis

From the abovementioned experimental study, one only can get bridge response (in terms of rotation, displacement, acceleration etc.) as tabulated in table 7-3. Although to perform a comparative study involving analytical result, it is necessary to evaluate rotational ductility from these observed curvatures. In doing so, the moment-curvature relation of bridge columns presented in Johnson et al. (2006) cannot be used as it provides conservative estimation in comparison with that observed from the experimental investigation. From the moment-curvature curve of Johnson et al. (2006), ultimate curvature is computed as 0.00028 rad/mm while a maximum curvature of 0.00037 rad/mm is observed in columns of Bent 3 during test 18. Again, in test 19 when these columns are having major damage in the sense that they buckled in flexure, observed curvature is nearly twice as big as ultimate curvature obtained from the moment-curvature analysis by Johnson et al. (2006).

Therefore to compute rotational ductility, moment-rotation relations of bridge columns are developed by utilizing the program given by Kushiyama (2002) (Appendix A). For this purpose, following properties of the bridge are obtained from the experimental model. It should be noted here that the effective column height is taken from the bottom of the superstructure soffit to the half depth point of the bridge deck. Figures 7-3 and 7-4 show moment-rotation curve of column bents.

- Effective depth of the member: 2.58 m (Bent 1 and 3), 3.19 m (Bent 2)
- Diameter of bridge columns: 0.3048 m
- Axial force by dead load: 209.2 kN (Bent 1 and 3), 182.2 kN (Bent 2)
- Compressive strength of unconfined concrete: 34.42 MPa
- Yield stress of longitudinal reinforcement: 457.85 MPa
- Yield stress of hoop reinforcement: 461.30 MPa
- Concrete cover to confine longitudinal reinforcement: 19 mm
- Number of longitudinal reinforcement: 16
- Diameter of longitudinal reinforcement: 9.525 mm (#3)
- Diameter of hoops: 4.88 mm (W2.9)
- Spacing of hoops: 31.75 mm

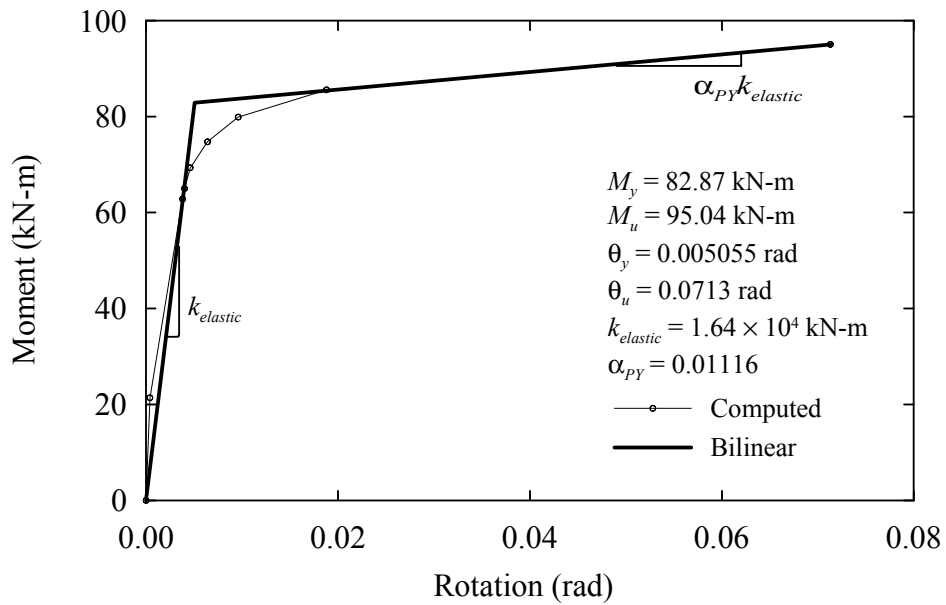


**FIGURE 7-3 Moment-Rotation Curve of Bent 1 and 3**

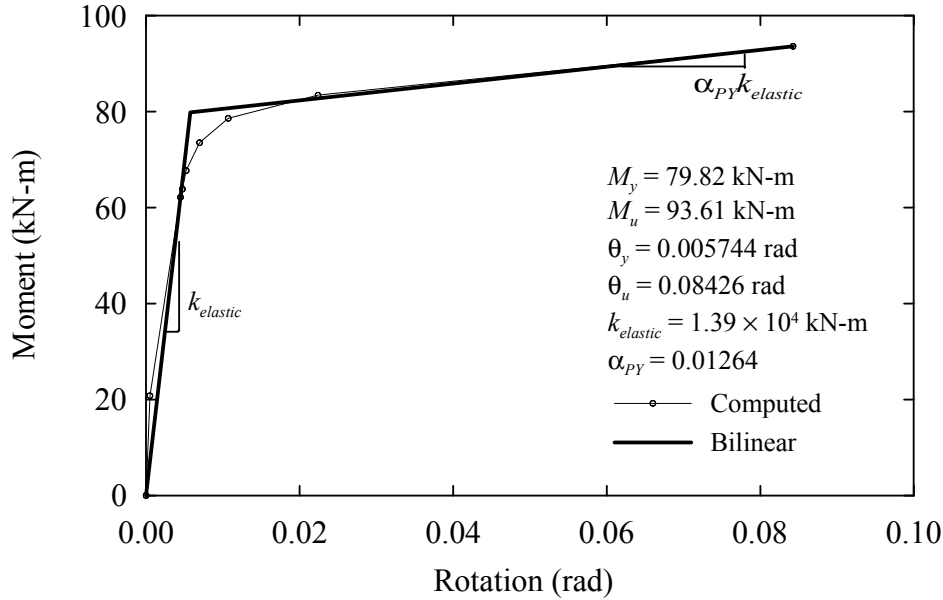


**FIGURE 7-4 Moment-Rotation Curve of Bent 2**

### 7.2.3 Rotational Ductility of Bridge Columns at Various Damage States

According to the experimental set-up, rotations at bridge column ends can be obtained by multiplying measured curvature with gauge length (127 mm) which is the interval between curvature rod and fixity. Hence, rotational ductility is computed by dividing these rotations with yield rotations obtained from moment-rotation relation of column bents (figures 7-3 and 7-4). Table 7-4 presents rotations at column ends and their corresponding rotational ductility values. In this table, values in bold and italic letters represent maximum or minimum rotational ductility obtained at different bridge damage states.

Figure 7-5 plots these rotational ductilities and corresponding bridge damage states in which damage state index 0, 1, 2 and 3 respectively represent no, minor, moderate and major damage. Eventually, threshold damage limits are estimated by averaging minimum and maximum rotational ductilities obtained in two successive damage states. For example, minimum rotational ductility observed in minor damage is 3.27 while the maximum rotational ductility observe in no damage is 3.01. Therefore, lower bound of rotational ductility for the state of minor damage is computed as 3.14. Similar values for moderate and major damage are estimated as 5.90 and 9.42, respectively. It should be noted here that these values of threshold limits are obtained considering all column bents in a same statistical population.



**TABLE 7-4 Rotational Ductility of Bridge Columns at Different Damage Levels**

Location	Curvature rad/mm	Rotation rad	Rot. Ductility	Location	Curvature rad/mm	Rotation rad	Rot. Ductility
No Damage				No Damage			
Bent 1	$1.1 \times 10^{-5}$	0.0014	0.28	Bent 1	$1.3 \times 10^{-5}$	0.0017	0.33
Bent 1	$4.4 \times 10^{-5}$	0.0056	1.11	Bent 1	$4.5 \times 10^{-5}$	0.0057	1.13
Bent 1	$1.3 \times 10^{-5}$	0.0017	0.33	Bent 1	$1.4 \times 10^{-5}$	0.0018	0.35
Bent 1	$1.0 \times 10^{-4}$	0.0127	2.51	Bent 1	$1.2 \times 10^{-4}$	0.0152	<b>3.01</b>
Bent 2	$5.4 \times 10^{-6}$	0.0007	0.12	Bent 2	$6.0 \times 10^{-6}$	0.0008	0.13
Bent 2	$4.2 \times 10^{-5}$	0.0053	0.93	Bent 2	$4.8 \times 10^{-5}$	0.0061	1.06
Bent 2	$8.8 \times 10^{-6}$	0.0011	0.19	Bent 2	$7.4 \times 10^{-6}$	0.0009	0.16
Bent 2	$5.2 \times 10^{-5}$	0.0066	1.15	Bent 2	$1.3 \times 10^{-4}$	0.0165	2.87
Bent 3	$9.8 \times 10^{-6}$	0.0012	0.25	Bent 3	$9.0 \times 10^{-6}$	0.0011	0.23
Bent 3	$3.9 \times 10^{-5}$	0.0050	0.98	Bent 3	$7.3 \times 10^{-5}$	0.0093	1.83
Bent 3	$1.0 \times 10^{-5}$	0.0013	0.25	Bent 3	$1.1 \times 10^{-5}$	0.0014	0.28
Bent 3	$4.0 \times 10^{-5}$	0.0051	1.00	Bent 3	$4.0 \times 10^{-5}$	0.0051	1.00
Minor Damage				Minor Damage			
Bent 1	$1.8 \times 10^{-4}$	0.0229	4.52	Bent 1	$2.0 \times 10^{-4}$	0.0254	5.02
Bent 1	$1.4 \times 10^{-4}$	0.0178	3.52	Bent 1	$2.3 \times 10^{-4}$	0.0292	<b>5.78</b>
Bent 1	$2.2 \times 10^{-4}$	0.0279	5.53	Bent 1	$2.1 \times 10^{-4}$	0.0267	5.28
Bent 1	$1.7 \times 10^{-4}$	0.0216	4.27	Bent 1	$1.5 \times 10^{-4}$	0.0191	3.77
Bent 2	$2.0 \times 10^{-4}$	0.0254	4.42	Bent 2	$2.4 \times 10^{-4}$	0.0305	5.31
Bent 2	$1.7 \times 10^{-4}$	0.0216	3.76	Bent 2	$1.9 \times 10^{-4}$	0.0241	4.20
Bent 3	$1.3 \times 10^{-4}$	0.0165	<b>3.27</b>	Bent 3	$1.5 \times 10^{-4}$	0.0191	3.77
Bent 3	$1.9 \times 10^{-4}$	0.0241	4.77	Bent 3	$2.0 \times 10^{-4}$	0.0254	5.02
Bent 3	$1.4 \times 10^{-4}$	0.0178	3.52	Bent 3	$1.5 \times 10^{-4}$	0.0191	3.77
Bent 3	$2.0 \times 10^{-4}$	0.0254	5.02				
Moderate Damage				Moderate Damage			
Bent 1	$2.7 \times 10^{-4}$	0.0343	6.78	Bent 1	$2.4 \times 10^{-4}$	0.0305	<b>6.03</b>
Bent 1	$2.4 \times 10^{-4}$	0.0305	6.03	Bent 1	$2.9 \times 10^{-4}$	0.0368	7.29
Bent 1	$3.2 \times 10^{-4}$	0.0406	8.04	Bent 1	$3.0 \times 10^{-4}$	0.0381	7.54

**TABLE 7-4 Rotational Ductility of Bridge Columns at Different Damage Levels (Cont'd)**

Bent 2	$2.8 \times 10^{-4}$	0.0356	6.19	Bent 2	$3.0 \times 10^{-4}$	0.0381	6.63
Bent 2	$2.5 \times 10^{-4}$	0.0318	5.53	Bent 2	$3.2 \times 10^{-4}$	0.0406	7.08
Bent 3	$3.4 \times 10^{-4}$	0.0432	8.54	Bent 3	$2.6 \times 10^{-4}$	0.0330	6.53
Bent 3	$3.7 \times 10^{-4}$	0.0470	<b>9.30</b>	Bent 3	$3.2 \times 10^{-4}$	0.0406	8.04
Major Damage				Major Damage			
Bent 3	$5.3 \times 10^{-4}$	0.0673	13.32	Bent 3	$4.6 \times 10^{-4}$	0.0584	11.56
Bent 3	$3.2 \times 10^{-4}$	0.0495	9.80	Bent 3	$3.8 \times 10^{-4}$	0.0483	<b>9.55</b>
Bent 3	$5.0 \times 10^{-4}$	0.0635	12.56	Bent 3	$4.6 \times 10^{-4}$	0.0584	11.56
Bent 3	$4.0 \times 10^{-4}$	0.0508	10.05				

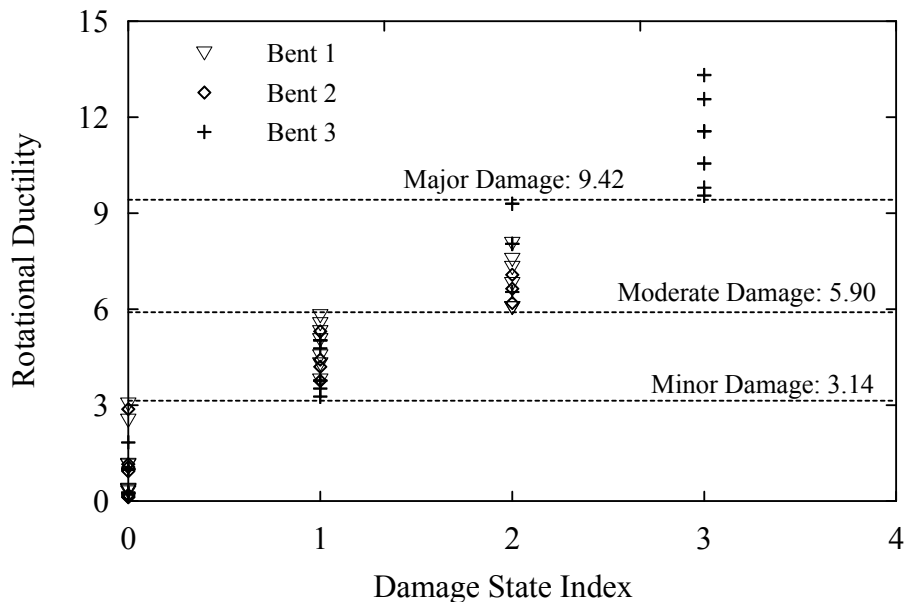


**Figure 7-5 Estimated Rotational Ductilities from Experimental Data**

#### 7.2.4 Comparison of Threshold Damage Limits

Objective of the current study is to compare the threshold limits of bridge damage as presented in Figure 7-5 with those obtained from analytical study in Chapter 4. The experimental model represents a two-span bridge with zero skewness and thus comparable with analytical bridge models. For the purpose of comparison, damage limits obtained through experiment are plotted in figure 7-6 together with that derived by mechanistically calibrating analytical bridge damage models. Comparison indicates that damage limits obtained from experimental result correspond satisfactorily with that previously obtained by utilizing three analytical bridges. Moreover, experimental result helps to update the trend of damage limits which is developed on the basis of least square fit as shown in figure 7-6.

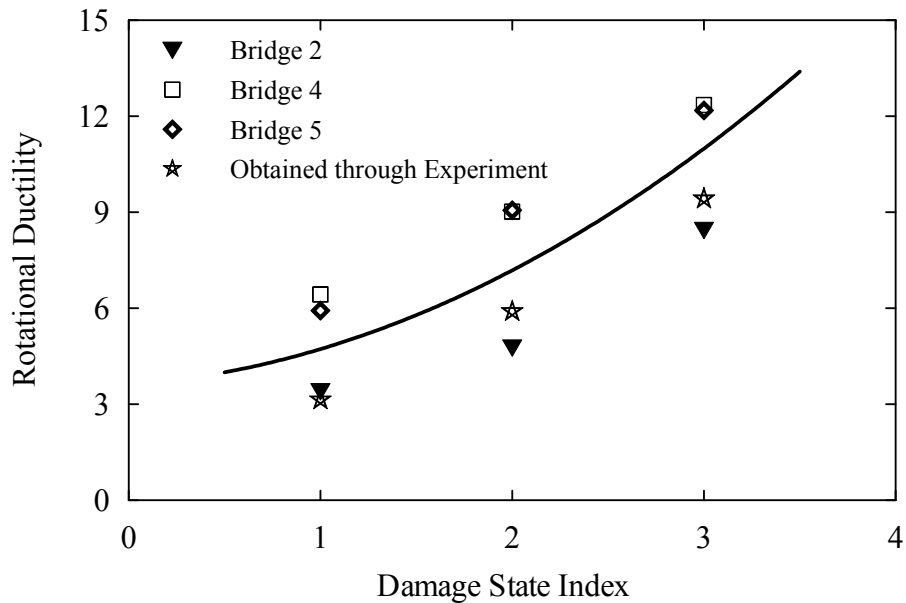


**Figure 7-6 Rotational Ductilities Representing Threshold Limits of Bridge Damage**

### 7.3 Discussion of Results

This chapter integrates empirical, analytical and experimental seismic damage data of bridges in order to compare threshold damage limits. Comparison indicates good correspondence of threshold damage limits obtained by calibrating analytical model with empirical data and generated from experimental observation.

It should be noted here that threshold rotational ductility values obtained through experiment are for the transverse direction of the bridge while these for analytical bridges are for the longitudinal direction. Even then, this comparison is valid as experimental bridge model had columns with circular cross-section. In previous chapters it is mentioned that threshold damage limits in terms of rotational ductility in the longitudinal and transverse directions are same for bridges with circular columns (applied for Bridge 1 and 2). On this basis, it can be stated that this comparison confirms the consistency of bridge damage limits quantified by calibrating analytically simulated bridge damage with past earthquake damage data. Obviously, these definitions can be updated by utilizing more damage data generated through experimental study with relevant bridge configuration and/or observed during earthquake in real-time.



## SECTION 8 DEVELOPMENT OF DESIGN STRATEGY

In general, performance-based design methodology is controlled through the relationship between earthquake ground motions described by their return periods and intensities, and the seismic performance of structural systems. A structural design should not be accepted if it does not satisfy the performance criteria set for design. In this context, this section recommends a guideline for the design verification of a newly designed bridge that can be analyzed utilizing the nonlinear analytical tool described in the preceding section of this report.

It appears reasonable to suggest that the five bridge damage states mentioned above are considered as equivalent to, respectively, “Operational”, “Immediate Occupancy”, “Life Safety” and “Collapse Prevention” of ‘Performance-Based Design of Buildings’ (FEMA 356, 2000), except for “Collapse” which does not have any counterpart. It is assumed that these performance levels can be evaluated by comparing the computed rotational ductility (RD) at plastic hinge regions of bridge columns with the rotational ductility limits (RDL) at each damage state. These RDLs are obtained from the calibration of analytical bridge damage with empirical data. As discussed in the earlier section of this report, calibration is performed in terms of comparison of the fragility parameters. Therefore, this is a major application of fragility curves in performing bridge design verification. Figure 8-1 schematically describes the performance levels and threshold RDLs.

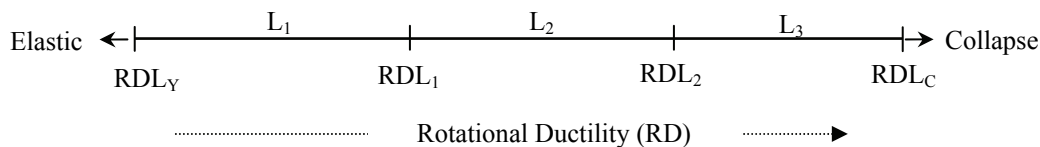


**FIGURE 8-1 Performance Levels of Bridge under Seismic Excitation**

$L_1$  represents both ‘No’ and ‘Minor’ damage of bridges which are equivalent to respectively, ‘Operational’ and ‘Immediate Occupancy’ performance levels for building;  $L_2$  indicates ‘Moderate’ damage which is equivalent to ‘Life Safety’ performance level for building; and  $L_3$  defines ‘Major’ (Extensive) damage which is equivalent to ‘Collapse Prevention’ performance level for building. RDL’s are the rotational ductility limits in which  $RDL_Y$  and  $RDL_C$  represent, respectively, the yield and collapse states of the bridge. The following section describes the utilization of these threshold performance levels (RDLs) to examine the performance of the bridge after analyzing it under certain earthquake ground motion.

For different input ground motions, the following figures (figures 8-2, 8-3 and 8-4) describe 3 different methods to perform the analysis. Method 1 and Method 2 are straightforward and deal with one earthquake ground motion with specific hazard level and one target performance level. As described in figure 8-2, ground motion input is in the form of response spectrum. Rotational ductility (RD) of the bridge can be obtained using nonlinear dynamic and static procedures. In case of nonlinear dynamic analysis, RD is computed directly from the response time history whereas, in nonlinear static analysis performance displacement ( $S_d$ ) of the structure is computed

first (Appendix B, Section B.8) and then converted to rotation at plastic hinge  $\theta$  from which RD can be estimated. The design is acceptable if desired performance level is achieved, otherwise design should be modified. Method 2 (figure 8-3) is the same as Method 1 except for the input ground motion. Here, time history of the ground motion is used as an input and it needs to be converted to elastic response spectra in case of nonlinear static analysis.

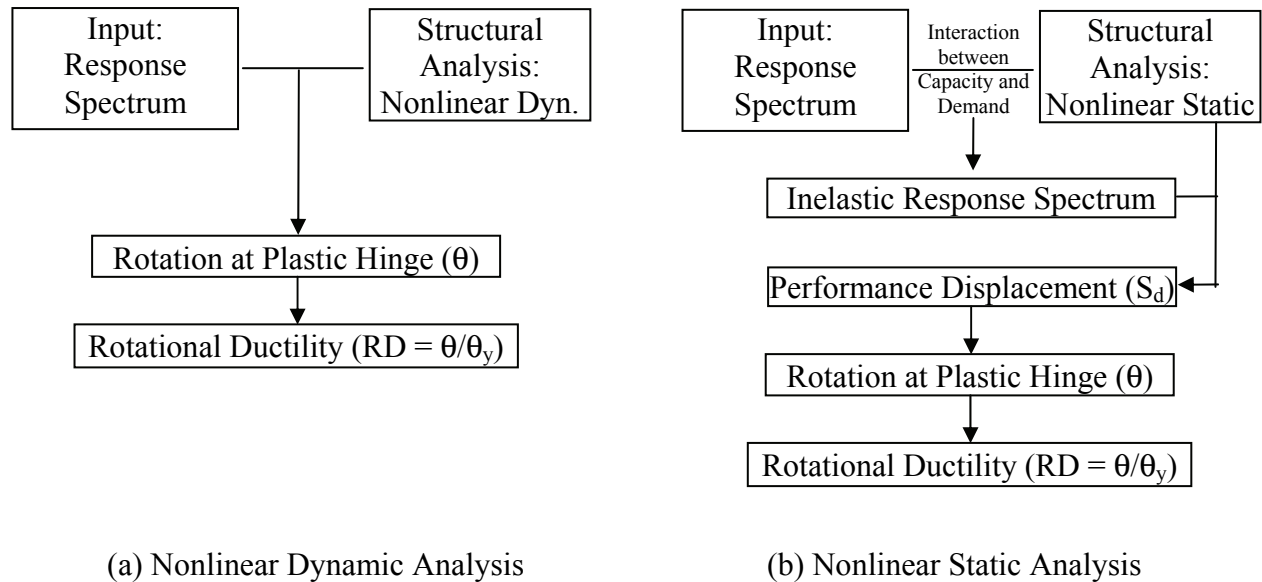


**FIGURE 8-2 Flow Chart: Method 1**

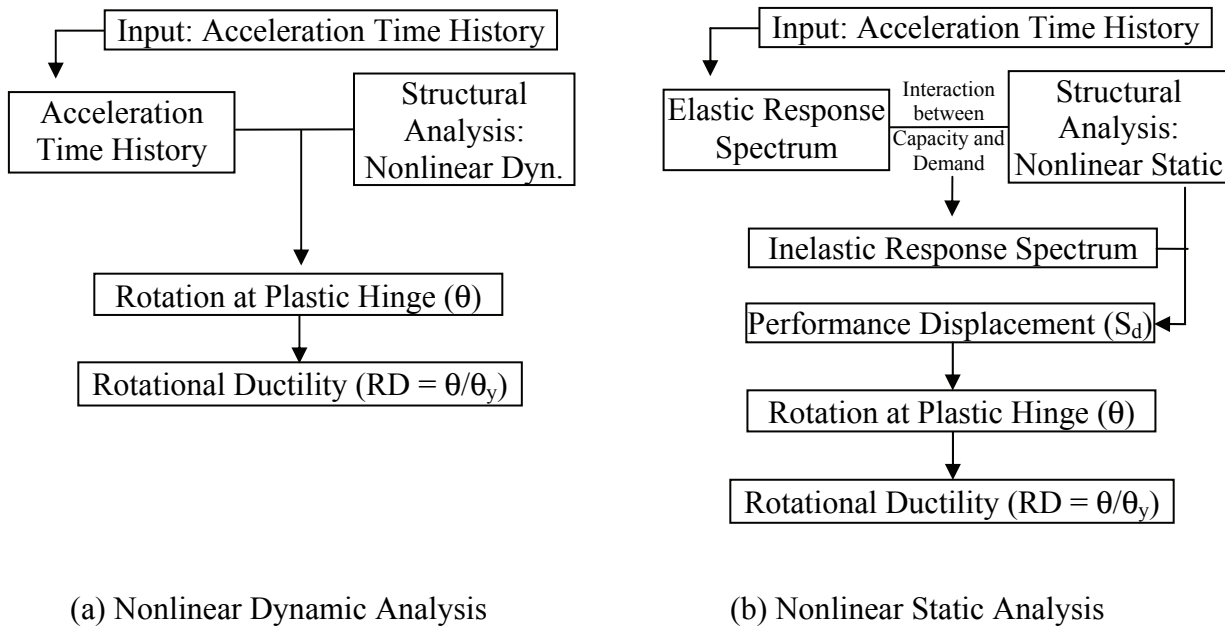
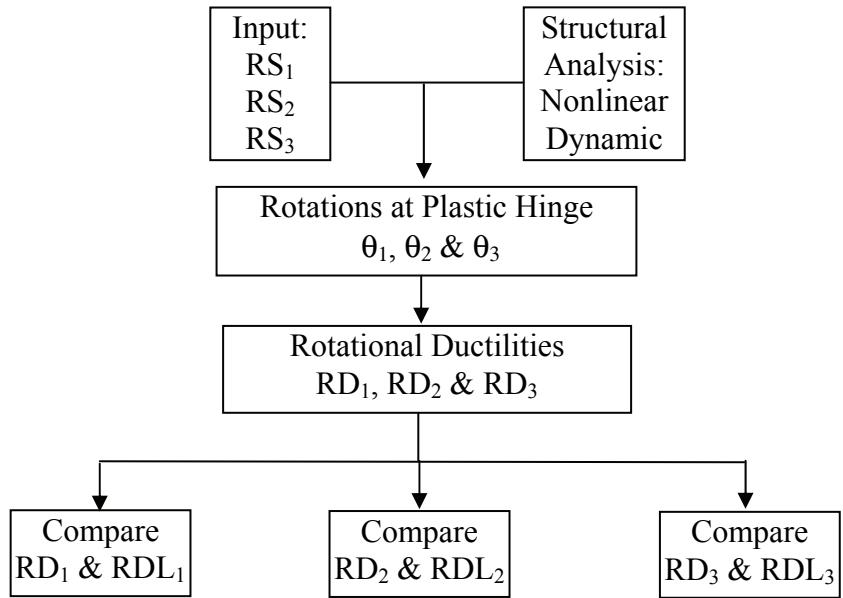


**FIGURE 8-3 Flow Chart: Method 2**

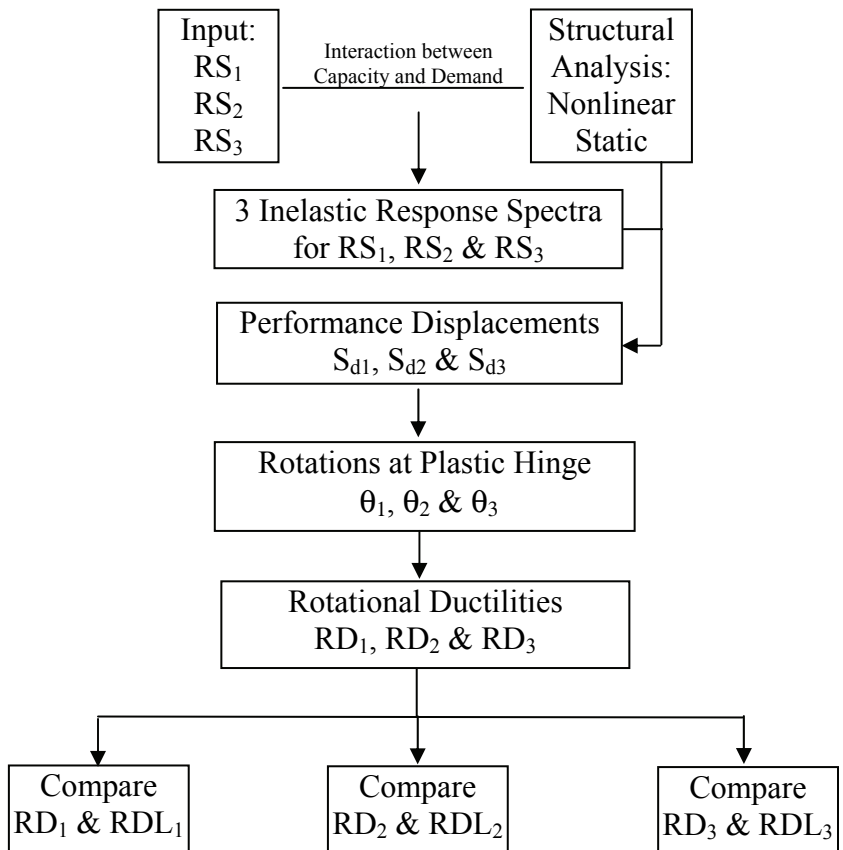
Method 3 deals with more than one ground motions with specific return period and corresponding target performance level (figure 8-4). The bridge will be designed for three response spectra  $RS_1$ ,  $RS_2$  and  $RS_3$  having return periods respectively of 2500 yrs, 475 yrs and 72 yrs. For example, a newly designed bridge must satisfy the following criteria.

1. Level  $L_1$ ; Under  $RS_1$  with return period 72 yrs (exceedance probability 50% in 50 yrs) compute rotational ductility  $RD_1 (= \theta_1/\theta_Y)$  where  $RDL_Y \leq RD_1 \leq RDL_1$
2. Level  $L_2$ ; Under  $RS_2$  with return period 475 yrs (exceedance probability 10% in 50 yrs) compute rotational ductility  $RD_2 (= \theta_2/\theta_Y)$  where  $RDL_1 \leq RD_2 \leq RDL_2$
3. Level  $L_3$ ; Under  $RS_4$  with return period 2500 yrs (exceedance probability 2% in 50 yrs) compute rotational ductility  $RD_3 (= \theta_3/\theta_Y)$  where  $RDL_2 \leq RD_3 \leq RDL_C$

If, (1)  $RD_1 \leq RDL_1$ , (2)  $RD_2 \leq RDL_2$  and (3)  $RD_3 \leq RDL_C$ , the design satisfies the criteria and it is accepted. But, design should be revised if any one among these three fails. It is important to note that the number of performance levels and corresponding return periods can be set differently. Here, Method 3 only demonstrates the methodology. Similar analysis must be performed for retrofitted bridges.



(a) Nonlinear Dynamic Analysis



(b) Nonlinear Static Analysis

**FIGURE 8-4 Flow Chart: Method 3**



## **SECTION 9 CONCLUSIONS**

This synthesis report combines statistical, empirical and mechanistic aspects of fragility analysis of reinforced concrete bridges. The empirical fragility curves are developed from the past earthquake damage data from the 1994 Northridge Earthquake. Two-parameter lognormal distribution functions are used to represent the fragility curves where these two-parameters (referred to as fragility parameters) are estimated by means of maximum likelihood method. In addition, this report also includes statistical procedures of testing goodness of fit of the fragility curves and of estimating the confidence intervals of the fragility parameters.

For analytical fragility curve development, nonlinear time history analyses of five (5) Caltrans' bridges are performed before and after column retrofit with steel jacketing. Also, some parametric study is carried out in order to assess the individual and combined effect of various factors such as pounding and restrainer at expansion joint, and soil effects at the column bases. A substantial improvement in bridge fragility characteristics is observed due to seismic retrofit of bridge columns. In conjunction with the dynamic analysis, nonlinear static analysis is also conducted. Comparison of analytical fragility curves obtained from dynamic and static analyses shows a good agreement in fragility curves for all damage states. Therefore, static nonlinear analysis can be considered as a good alternative to the nonlinear time history analysis.

To be consistent with empirical fragility curves, damage state definitions are established by mechanistically calibrating the analytical bridge damage data with that from past earthquakes. This makes the analytical fragility curves consistent with empirical ones. Thus, the developed analytical fragility curves are used to compare with that from HAZUS.

This report also addresses the issue of directionality effect of earthquake ground motion on structures based on the fact that an earthquake can come from any arbitrary direction to the structure. Result indicates that in seismic performance analysis, consideration of ground motion acting only along longitudinal and/or transverse directions of the bridge may underestimate the maximum seismic demand. Furthermore, on the basis of the suggested nonlinear static procedure, a general guideline for bridge design verification is recommended that integrates bridge damage states with ground motion return periods.



## **SECTION 10 REFERENCES**

- Abeyasinghe, R. S., Gavaise, E., Rosignoli, M. and Tzavas, T., (2002), “Pushover Analysis of Inelastic Seismic Behavior of Grevniotikos Bridge”, *Journal of Bridge Engineering*, ASCE, 7(2), 115-126.
- Applied Technology Council (ATC), (1996), “ATC-40, Seismic Evaluation and Retrofit of Concrete Buildings”, Redwood City, California.
- Basöz, N., and Kiremidjian, A. S., (1998), “Evaluation of Bridge Damage Data from the Loma Prieta and Northridge, California Earthquake”, Technical Report MCEER-98-0004.
- Basöz, N., and Mander, J.B., (1999), “Enhancement of the Highway Transportation Lifeline Module in HAZUS”, Final Pre-Publication Draft (#7), Nation Institute of Building Sciences.
- Boore, D. M., (1983), “Stochastic Simulation of High-frequency Ground Motions Based on Seismological Models of the Radiation Spectra”, *Bulletin of the Seismological Society of America*, 73, 1865-1894.
- California Department of Transportation, (2004), Bridge Design Criteria.
- California Department of Transportation (Caltrans), (1994a), “The Northridge Earthquake”, Caltrans PEQIT Report, Division of Structures, Sacramento, CA.
- California Department of Transportation (Caltrans), (1994b), “Supplementary Bridge Damage Reports”, Division of Structures, Sacramento, CA.
- Chai, Y.H., Priestley, M.J.N. and Seible F., (1991), “Seismic Retrofit of Circular Bridge Columns for Enhanced Flexural Performance”, *ACI Structural Journal*, V. 88 (No. 5), 572-584.
- Choi, E., DesRoches, R. and Nielson, B. (2004), “Seismic Fragility of Typical Bridges in Moderate Seismic Zones”, *Engineering Structures*, 26, 187–199.
- Computer and Structures, Inc., (2002), SAP2000/Nonlinear Users Manual, Berkeley, CA.
- Dutta, A. and Mander, J.B., (1998), “Seismic Fragility Analysis of Highway Bridges”, Proc., INCEDE-MCEER Center-to-Center Workshop on Earthquake Engineering Frontiers in Transportation Systems, Tokyo, Japan, 311-325.
- Fajfar, P., Gaspersic, P. and Drobnic, D., (1997), “A Simplified Nonlinear Method for Seismic Damage Analysis of Structures”, *Seismic Design Methodologies for the Next Generation of Codes*, Edited by P. Fajfar and H. Krawinkler, A.A. Balkema Publishers, Rotterdam, 183-194.
- Fajfar, P., (1999), “Capacity Spectrum Method Based on Inelastic Demand Spectra”, *Earthquake Engineering and Structural Dynamics*, 28, 979-993.

Federal Highway Administration (1996), Seismic Design of Bridges, Design Example No. 9 FHWA-SA-97-006.

Federal Emergency Management Agency (FEMA), (2000), “Prestandard and Commentary for the Seismic Rehabilitation of Buildings”, FEMA 356, Washington, D.C.

Fukushima, S., Kai, Y. and Yashiro, K., (1996), “Study on the Fragility of System — Part 1: Structure with Brittle Elements in its Stories”, in Proceedings of the 11th World Conference on Earthquake Engineering, Pergamon, Elsevier Science Ltd., Oxford, UK, Paper No. 333.

Gardoni, P., Der Kiureghian, A. and Mosalam, K. M., (2002), “Probabilistic Models and Fragility Estimates for Bridge Components and Systems”, Technical Report PEER 2002/13, Pacific Earthquake Engineering Research Center, University of California, Berkeley, CA.

HAZUS (1999), “Earthquake Loss Estimation Methodology”, Technical Manual HAZUS99-SR2, National Institute of Building for the Federal Emergency Management Agency, Washington, D.C.

Hwang, H. M., and Huo, J. R., (1996), “Simulation of Earthquake Acceleration Time Histories”, Center for Earthquake Research and Information, The University of Memphis, Technical Report.

Idriss, I. M., and Sun, J. I., (1992), “SHAKE91, A Computer Program for Conducting Equivalent Linear Seismic Response Analyses of Horizontally Layered Soil Deposits, User's manual”, Center for Geotechnical Modeling, Department of Civil and Environmental Engineering, University of California, Davis, CA.

Isakovic, T. and Fischinger, M., (2006), “Higher Modes in Simplified Inelastic Seismic Analysis of Single Column Bent Viaducts”, Earthquake Engineering and Structural Dynamics, 35(1), 95–114.

Jernigan, J. B., and Hwang, H. M., (1997), “Inventory and Fragility Analysis of Memphis Bridges”, Center for Earthquake Research and Information”, The University of Memphis, Technical Report.

Johnson, N.S., Saiidi, M. and Sanders, D.H. (2006), “Large-Scale Experimental and Analytical Seismic Studies of a Two-Span Reinforced Concrete Bridge System”, Report No. CCEER-06-02, Center for Earthquake Engineering Research, University of Nevada, Reno, NV.

Kai, Y. and Fukushima, S., (1996), “Study on the Fragility of System — Part 2: System with Ductile Elements in its Stories” Proceedings of the 11th World Conference on Earthquake Engineering, Pergamon, Elsevier Science Ltd., Oxford, UK, 1, Paper No. 334.

Karim, K. R. and Yamazaki, F., (2001), “Effect of Earthquake Ground Motions on Fragility Curves of Highway Bridge Piers Based on Numerical Simulation”, Earthquake Engineering and Structural Dynamics, 30(12), 1839–1856.

Kim, S-H., (2003), “Fragility Analysis of Bridges under Ground Motion with Spatial Variation”, Ph.D. Dissertation, Department of Civil and Environmental Engineering, University of California, Irvine, CA.

Kim, S-H., and Shinozuka, M., (2003), “Effects of Seismically Induced Pounding at Expansion Joints of Concrete Bridges”, *J. Engrg. Mech., ASCE*, 129(11), 1225-1234.

Krawinkler, H. and Nasser, A.A., (1992) “Seismic Design Based on Ductility and Cumulative Damage Demands and Capacities”, *Nonlinear Seismic Analysis and Design of Reinforced Concrete Buildings*, Edited by Peter Fajfar and Helmut Krawinkler, Elsevier Science Publisher Ltd., New York, N.Y., 23-40.

Kushiyama, S., (2002), “Calculation Moment-Rotation Relationship of Reinforced Concrete Member with/without Steel Jacket”, Unpublished Report at University of Southern California, CA, USA.

Lopez, O. A., and Torres, R., (1997), “The Critical Angle of Seismic Incidence and the Maximum Structural Response”, *Earthquake Engineering and Structural Dynamics*, 26, 881–894.

Lopez, O. A., Chopra, A. K., and Hernandez, J. J., (2000), “Response to Three-Component Seismic Motion of Arbitrary Direction”, *Earthquake Engineering and Structural Dynamics*, 31, 55–77.

Mander, J. B. and Basoz, N., (1999), “Seismic Fragility Curve Theory for Highway Bridges”, in *Proceedings of the 5th U.S. Conference on Lifeline Earthquake Engineering*, Reston, Virginia, 31–40.

Miranda, E., and Bertero, V. V., (1994), “Evaluation of Strength Reduction Factors for Earthquake-resistance Design”, *Earthquake Spectra*, 10(1), 357-379.

Paraskeva, T.S., Kappos, A.J. and Sextos, A.G., (2006), “Extension of Modal Pushover Analysis to Seismic Assessment of Bridges”, *Earthquake Engineering and Structural Dynamics*, 35(10), 1269–1293.

Prakash, V. and Campbell, S. (1994), “Drain-3DX: Static and Dynamic Analysis of Inelastic 3D Structures”, Department of Civil Engineering, University of California, Berkeley.

Priestley, M. J. N., Seible, F., and Calvi, G. M., (1996), *Seismic Design and Retrofit of Bridges*, John Wiley and Sons, Inc., NY.

Reinhorn, A.M., (1997), “Inelastic Analysis Techniques in Seismic Evaluation”, *Seismic Design Methodologies for the Next Generation of Codes*, Edited by Peter Fajfar and Helmut Krawinkler, A.A. Balkema Publishers, Rotterdam, 277-287.

Shinozuka, M. and Deodatis, G., (1991), “Simulation of Stochastic Processes by Spectral Representation”, *Applied Mechanics Reviews*, Vol. 44, No. 4, 191-204.

Shinozuka, M. and Deodatis, G., (1996), “Simulation of Multi-Dimensional Gaussian Stochastic Fields by Spectral Representation”, *Applied Mechanics Review* Vol. 49, No. 1, 29-53.

Shinozuka, M., Feng, M.Q., Lee, J., and Naganuma, T. (2000a). *Statistical Analysis of Fragility Curves*”, *Journal of Engineering Mechanics, ASCE*, 126(12): 1224-1231.

Shinozuka, M., Feng, M. Q, Kim, H.-K. and Kim, S.-H., (2000b), “Nonlinear Static Procedure for Fragility Curve Development”, *Journal of Engineering Mechanics, ASCE*, Vol.126, No.12, 1287-1295.

Shinozuka, M., Feng, M. Q, Kim, H., Uzawa, T., and Uada, T., (2003), “Statistical Analysis of Fragility Curves”, Technical Report MCEER-03-0002, Multidisciplinary Center for Earthquake Engineering Research, The State University of New York at Buffalo.

Shinozuka, M., Zhou, Y., Kim, S.-H., Murachi, Y., Banerjee, S., Cho, S. and Chung, H., (2005), “Socio-Economic Effect of Seismic Retrofit Implemented on Bridges in the Los Angeles Highway Network”, Final Report RTA-59A0304, California Department of Transportation, Sacramento, CA.

Shinozuka, M., Banerjee, S., and Kim, S.-H., (2006), “Statistical and Mechanistic Fragility Analysis of Reinforced Concrete Bridges”, MCEER Technical Report Submitted for Review, Multidisciplinary Center for Earthquake Engineering Research, The State University of New York at Buffalo.

Singhal, A. and Kiremidjian, A., (1998), “Bayesian Updating of Fragilities with Application to RC Frames”, *Journal of Structural Engineering, ASCE*, 124 (8), 922–929.

U.S. Nuclear Regulatory Commission (NRC), (1983), “PRA Procedures Guide”, NUREG/CR-2300, Vol. 2, 11-46.

Wilson, E. L., and Butten, M. R., (1982), “Three-dimensional Dynamic Analysis for Multi-component Earthquake Spectra”, *J. Earthquake Engineering and Structural Dynamics*, 10, 471–476.

Wilson, E. L., Suharwardy, I., and Habibullah, A., (1995), “A Clarification of Orthogonal Effects in a Three-dimensional Seismic Analysis”, *Earthquake Spectra*, 11(4), 659–666.

Zheng, Y., Usami, T. and Ge, H., (2003), “Seismic Response Predictions of Multi-span Steel Bridges Through Pushover Analysis”, *Earthquake Engineering and Structural Dynamics*, 32, 1259-1274.

## APPENDIX A

According to Shinozuka et al. (2003), the parameter estimation, hypotheses testing and confidence interval estimation related to the fragility curves are carried out in different ways. The following describes the methods.

### A.1 Estimation of Fragility Parameters

#### A.1.1 Method 1

In Method 1, the parameters of each fragility curve are independently estimated by means of the maximum likelihood procedure as described below. The likelihood function for the present purpose is expressed as

$$L = \prod_{i=1}^N [F(a_i)]^{x_i} [1 - F(a_i)]^{1-x_i} \quad (\text{A-1})$$

where  $F(\cdot)$  represents the fragility curve for a specific state of damage,  $a_i$  is the PGA value to which bridge  $i$  is subjected,  $x_i$  represents realizations of the Bernoulli random variable  $X_i$  and  $x_i=1$  or  $0$  depending on whether or not the bridge sustains the state of damage under  $\text{PGA} = a_i$ , and  $N$  is the total number of bridges inspected after the earthquake. Under the current lognormal assumption,  $F(a)$  takes the following analytical form

$$F(a) = \Phi \left[ \frac{\ln\left(\frac{a}{c}\right)}{\zeta} \right] \quad (\text{A-2})$$

in which “ $a$ ” represents PGA and  $\Phi[\cdot]$  is the standardized normal distribution function. Figure A-1 schematically shows the development of fragility curve using Method 1. Abscissa represents ground motion intensity (in this case, PGA) and ordinate presents probability of failure ( $P_f$ ) is presented. Circles at  $P_f = 0.0$  and  $1.0$  indicate, respectively ‘Not Damaged’ and ‘Damaged’ conditions of bridges under PGA values. Two-parameters  $c$  and  $\zeta$  in (A-2) are computed as  $c_0$  and  $\zeta_0$  satisfying the following equations to maximize  $\ln L$  and hence  $L$ ;

$$\frac{d \ln L}{dc} = \frac{d \ln L}{d\zeta} = 0 \quad (\text{A-3})$$

This computation is performed by implementing a straightforward optimization algorithm.

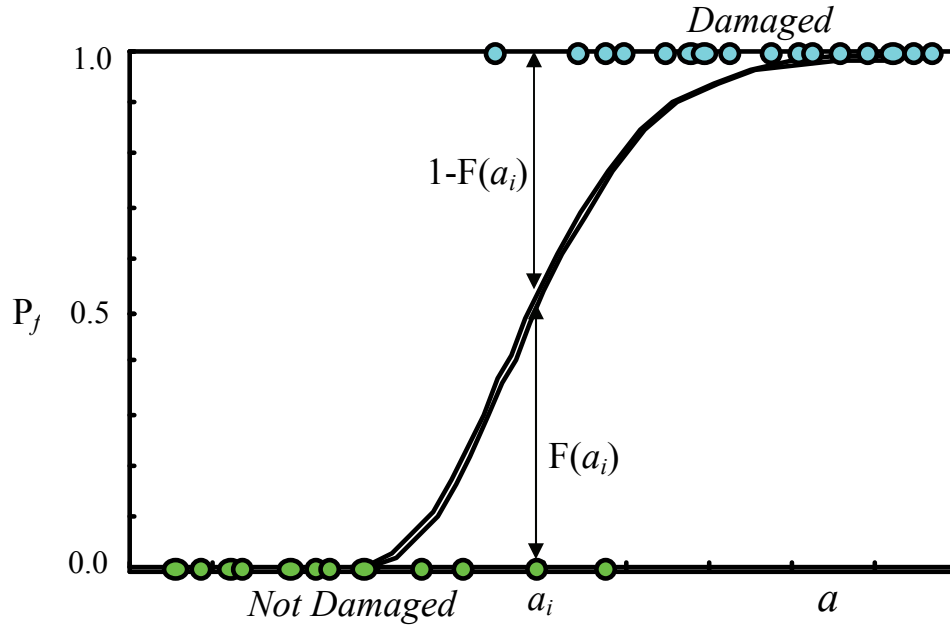


**FIGURE A-1 Schematics of Fragility Curve in Method 1**

In the following part of this report, only fragility curves are shown that represents bridge damageability. Bridge damage states (either no damage or damage) are not shown in following plots.

### A.1.2 Method 2

Although Method 2 can be used for any number of damage states, it is assumed here for the ease of demonstration of analytical procedure that there are four states of damage including the state of no damage. A family of three (3) fragility curves exist in this case exist as schematically shown in figure A-2 where events  $E_1$ ,  $E_2$ ,  $E_3$  and  $E_4$  respectively indicate the state of no, at least minor, at least moderate and major damage.  $P_{ik} = P(a_i, E_k)$  in turn indicates the probability that a bridge  $i$  selected randomly from the sample will be in the damage state  $E_k$  when subjected to ground motion intensity expressed by PGA =  $a_i$ . All fragility curves are represented by two-parameter lognormal distribution functions

$$F_j(a_i; c_j, \zeta_j) = \Phi \left[ \frac{\ln(a_i / c_j)}{\zeta_j} \right] \quad (\text{A-4})$$

where  $c_j$  and  $\zeta_j$  are the median and log-standard deviation of the fragility curves for the damage state of “at least minor”, “at least moderate” and “major” identified by  $j = 1, 2$  and  $3$  respectively. From this definition of fragility curves, and under the assumption that the log-standard deviation is equal to  $\zeta$  common to all the fragility curves, one obtains:



$$P(E1) = P_{i1} = P(a_i, E_1) = 1 - F_1(a_i; c_1, \zeta) \quad (\text{A-5})$$

$$P(E2) = P_{i2} = P(a_i, E_2) = F_1(a_i; c_1, \zeta) - F_2(a_i; c_2, \zeta) \quad (\text{A-6})$$

$$P(E3) = P_{i3} = P(a_i, E_3) = F_2(a_i; c_2, \zeta) - F_2(a_i; c_3, \zeta) \quad (\text{A-7})$$

$$P(E4) = P_{i4} = P(a_i, E_4) = F_3(a_i; c_3, \zeta) \quad (\text{A-8})$$

The likelihood function can then be introduced as

$$L(c_1, c_2, c_3, \zeta) = \prod_{i=1}^n \prod_{k=1}^4 P_k(a_i; E_k)^{x_{ik}} \quad (\text{A-9})$$

where

$$x_{ik} = 1 \quad (\text{A-10})$$

if the damage state  $E_k$  occurs for the  $i$ -th bridge subjected to  $a = a_i$ , and

$$x_{ik} = 0 \quad (\text{A-11})$$

otherwise. The maximum likelihood estimates  $c_{0j}$  for  $c_j$  and  $\zeta_0$  for  $\zeta$  are obtained by solving the following equations,

$$\frac{\partial \ln L(c_1, c_2, c_3, \zeta)}{\partial c_j} = \frac{\partial \ln L(c_1, c_2, c_3, \zeta)}{\partial \zeta} = 0 \quad (j = 1, 2, 3) \quad (\text{A-12})$$

by again implementing a straightforward optimization algorithm.

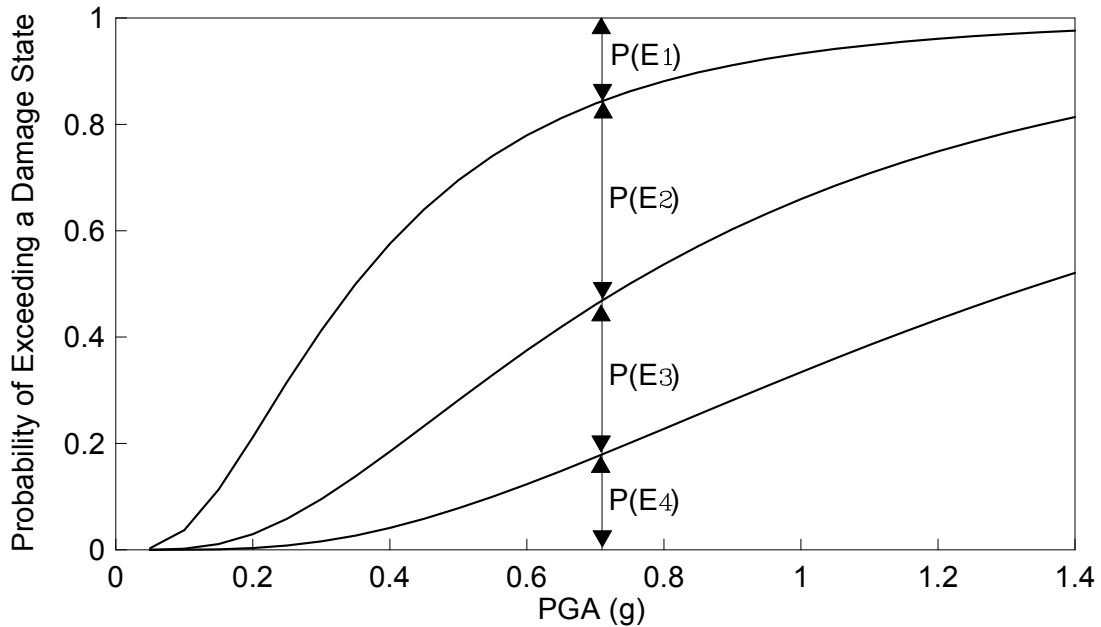


**FIGURE A-2 Schematics of Fragility Curves in Method 2**

### A.1.3 Fragility Curves for Caltrans' Bridges in Method 1 and Method 2

Damage data of Caltrans bridges can be obtained from Caltrans (1994a, 1994b). For the construction of fragility curves these damage data are rearranged for computational convenience (Shinozuka et al., 2003). Four fragility curves for Caltrans' bridges associated with 'at least minor', 'at least moderate', 'at least major' and 'collapse' are plotted in figures A-3 and A-4, upon estimating the parameters involved by Methods 1 and 2 respectively (with their respective median and log-standard deviation values also indicated).

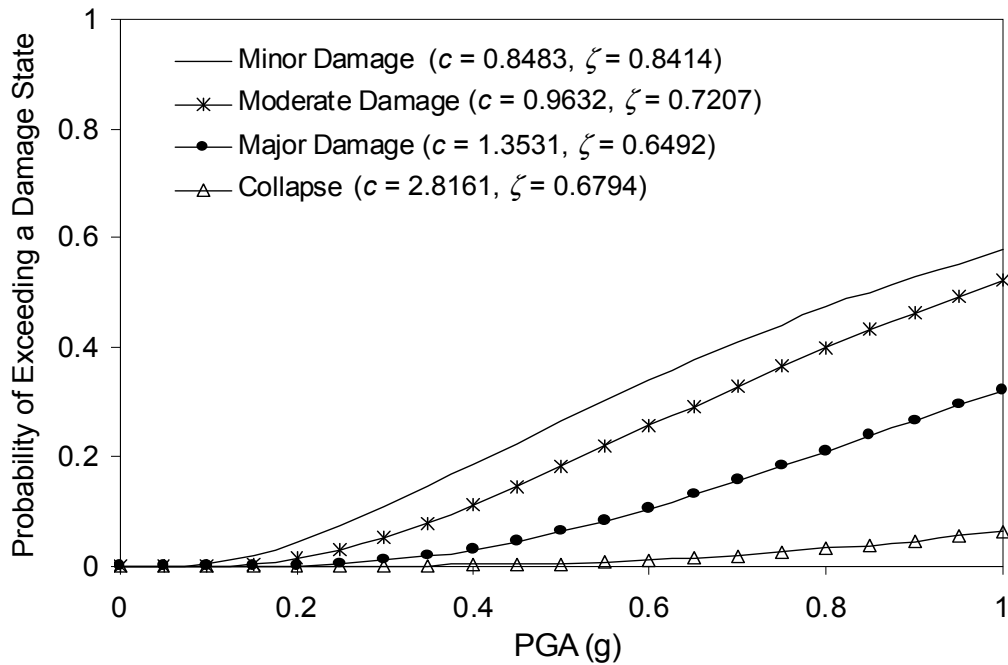


FIGURE A-3 Fragility Curves for Caltrans' Bridges (Method 1)

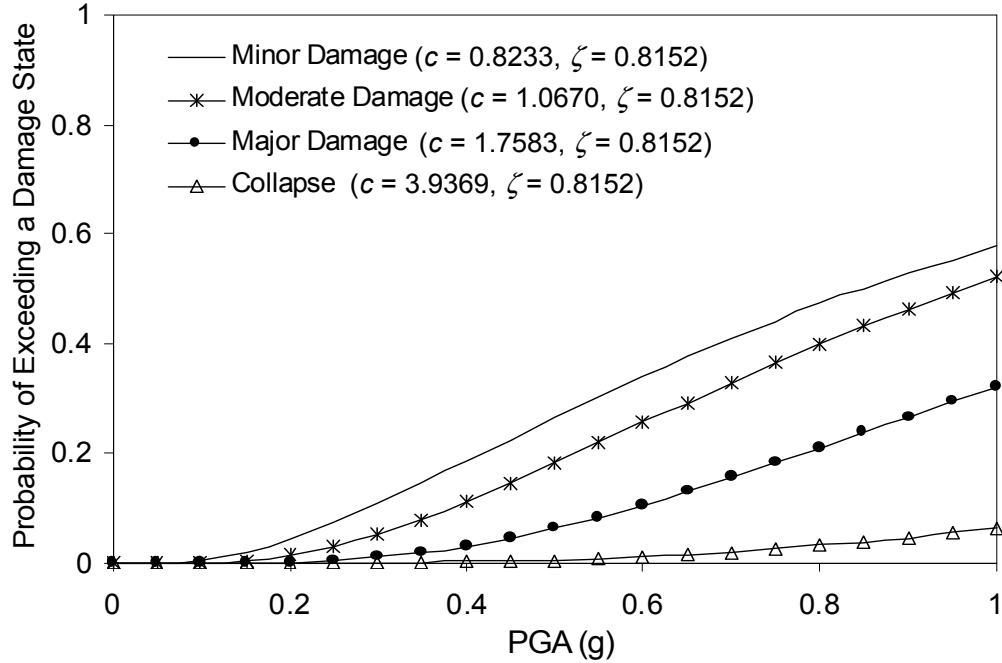


FIGURE A-4 Fragility Curves for Caltrans' Bridges (Method 2)

## A.2 Test of Goodness of Fit

### A.2.1 Method 1

The fundamental probabilistic interpretation of a fragility curve  $F(a)$  as a function of “ $a$ ” suggests that a bridge will sustain a designated state of damage with probability  $F(a)$  and will not sustain the damage state with probability  $1 - F(a)$  under the earthquake intensity represented by PGA equal to “ $a$ ”. This means that, under each PGA value, the probabilistic phenomena one deals with can be described by random variable  $X_i$  following the Bernoulli distribution such that  $X_i = 1$  when the state of damage is reached under  $PGA = a_i$ , and  $X_i = 0$  otherwise. Then,

$$Y_i^2 = (X_i - p_i)^2 \quad (\text{A-13})$$

has mean and variance equal to

$$\mu_{Y_i^2} = p_i(1 - p_i) \quad (\text{A-14})$$

and

$$\sigma_{Y_i^2}^2 = \text{Var}(Y_i^2) = p_i(1 - p_i)(1 - 2p_i)^2 \quad (\text{A-15})$$

respectively, where  $p_i = F(a_i)$ .

The sum of  $Y_i^2$  shown below

$$Y^2 = \sum_{i=1}^N (X_i - p_i)^2 \quad (\text{A-16})$$

approaches asymptotically Gaussian as  $N$  becomes large under the assumption that each Bernoulli event is independent, where  $N$  is the sample size (the total number of the bridges inspected) and in this analysis it is indeed a large value ( $\gg 1$ ).

Recalling that  $X_i$  is independent of  $X_j$  ( $i \neq j$ ) and governed by the Bernoulli distribution, a straightforward analysis shows that the expected value  $\mu_{Y^2} = E(Y^2)$  and the variance  $\sigma^2_{Y^2} = Var(Y^2)$  can be written as

$$\mu_{Y^2} = E(Y^2) = \sum_{i=1}^N p_i (1 - p_i) \quad (\text{A-17})$$

and

$$\sigma^2_{Y^2} = Var(Y^2) = \sum_{i=1}^N p_i (1 - p_i) (1 - 2p_i)^2 \quad (\text{A-18})$$

On the other hand, if  $x_i$  represents the realization (observation) of  $X_i$  as defined in the likelihood function given by (A-1),

$$y^2 = \sum_{i=1}^N (x_i - p_i)^2 \quad (\text{A-19})$$

is the realization of  $Y^2$ .

Since  $p_i$  depends on the values of  $c_0$  and  $\zeta_0$ , the standard procedure of hypothesis testing suggests that if  $\alpha$  represents the level of statistical significance such that

$$P_{y^2} = \Phi \left( \frac{y^2 - \mu_{y^2}}{\sigma_{y^2}} \right) \leq 1 - \alpha \quad (\text{A-20})$$

then, the hypothesis that  $c_0$  and  $\zeta_0$  are indeed the true values of  $c$  and  $\zeta$  cannot be rejected with the significance level  $\alpha$  usually set equal to 0.05 or 0.10.

### A.2.2 Method 2

The probability  $P_{y^2}$  for the test of goodness of fit with respect to the fragility curves developed on the basis of the parameters estimated by Method 2 must be derived in a manner consistent with the probabilistic nature of Method 2. The essential derivation is given as follows.

Let  $m$  = the number of damage states and  $N$  = the total sample size, and define

$$Y_i^2 = \sum_{k=1}^m (X_{ik} - p_{ik})^2 \quad (\text{A-21})$$

where  $X_{ik}$  is the multi-outcome Bernoulli type random variable whose realizations  $x_{ik}$  are introduced in Section 2.2 in such a way that  $x_{ik} = 1$  when the damage state  $k$  occurs and  $x_{ik} = 0$  otherwise, and  $p_{ik} = F_k(a_i) =$  probability of occurrence of the damage state  $k$  under  $\text{PGA} = a_i$ . The function  $F_k(a_i)$  represents the fragility curve associated with the damage state  $k$  and estimated at  $\text{PGA} = a_i$ . It can be shown that the mean value of  $Y_i^2$  is

$$\mu_{Y_i^2} = 1 - \sum_{k=1}^m p_{ik}^2 \quad (\text{A-22})$$

and the variance of  $Y_i^2$  is

$$\sigma_{Y_i^2} = \text{Var} (Y_i^2) = 4 \left\{ \sum_{k=1}^m p_{ik}^3 - \left( \sum_{k=1}^m p_{ik}^2 \right)^2 \right\} \quad (\text{A-23})$$

The sum of  $Y_i^2$  shown below

$$Y^2 = \sum_{i=1}^N \sum_{k=1}^m (X_{ik} - p_{ik})^2 \quad (\text{A-24})$$

has the mean value and the variance, respectively equal to

$$\mu_{Y^2} = N - \sum_{i=1}^N \sum_{k=1}^m p_{ik}^2 \quad (\text{A-25})$$

and

$$\sigma_{Y^2} = 4 \sum_{i=1}^N \sum_{k=1}^m p_{ik}^3 - 4 \sum_{i=1}^N \left( \sum_{k=1}^m p_{ik}^2 \right)^2 \quad (\text{A-26})$$

The realization  $y^2$  of  $Y^2$  is obtained by

$$y^2 = \sum_{i=1}^N \sum_{k=1}^m (x_{ik} - p_{ik})^2 \quad (\text{A-27})$$

As in the case of  $Y^2$  defined in Section A.2.1, the random variable  $Y^2$  given in (A-24) is also asymptotically normal and, as  $N \rightarrow \infty$ , its distribution approaches the normal distribution function as shown in (A-20) with  $\mu_{Y^2}$  and  $\sigma_{Y^2}$  provided by (A-25) and (A-26), respectively.



## APPENDIX B

### B.1 Bridge Description

A short description of the five (5) sample bridges used for analysis is given in table B-1. Bridge 1 is a three span bridge having overall length of 34 m. The superstructure consists of a longitudinally reinforced concrete deck slab of 10 m width. The bridge is supported on two pairs of three circular columns of 0.8 m diameter and an abutment at each end. Bridge 2 has an overall length of 242 m and an expansion joint. This bridge is supported on four 21 m high identical circular columns of diameter 2.4 m. The deck has a 3-cell concrete box girder (13 m x 2 m). Bridge 3 has an overall length of 226 m consisting of three frames separated by two expansion joints. The superstructure consists of a RC box girder in the outer spans and a prestressed box girder in the interior (central) span. The deck has a 6-cell box girder (20 m x 2.6 m). The columns are octagonal in shape and with varying lengths. Bridge 4 is of 483 m long and it has four expansion joints. This bridge is supported on nine columns of all different heights. Each column has a rectangular cross section (1.2 m x 3.7 m). The deck has a 5-cell concrete box type girder section (17 m x 2 m). Bridge 5 has an overall length of 500 m with twelve spans and an expansion joint. It is supported on eleven oblong columns of equal height (12.8 m) and cross-sections. The deck is consisting of 4-cell concrete box type girder section (15 m x 2 m).

**TABLE B-1 Description of Five (5) Sample Bridges**

Bridges	Overall Length	Number of Spans	Number of Hinges	Column Height
1	34 m	3	0	4.7 m
2	242 m	5	1	21.0 m
3	226 m	5	2	9.5 ~ 24.7 m
4	483 m	10	4	9.5 ~ 34.4 m
5	500 m	12	1	12.8 m

### B.2 Nonlinear Modeling of Bridges

Finite element computer code SAP2000 Nonlinear (Computer and Structures, 2002) is used in the ensuing time history analysis. The bridge deck is integrated with the column bents, so full continuity is considered at its girder-column joints. The bridge superstructure is free to rotate at the abutment locations for longitudinal excitation, although the translational motion is limited to the initially provided gap between the bridge girder and abutment. If the relative displacement of the bridge girder at abutment locations exceeds this gap, axial force develops at the interface due to the passive earth pressure of embankment soil. According to Caltrans recommendation (Bridge Design Criteria, 2004), the longitudinal abutment stiffness is

$$K_{abut} = K_i \times w \times \left( \frac{h}{5.5} \right) \quad \text{in U.S. units} \quad (\text{B-1})$$

where  $K_i$  is the initial embankment stiffness (= 20 kip/in/ft),  $w$  is the width of the backfill in ft and  $h$  is the height of the backfill in ft. During transverse out-of-plane motion, it can rotate freely while movement is restrained by wingwalls and concrete shear keys which are, in general, assumed to be rigidly connected with abutments and not to dissipate any energy through yielding (Federal Highway Administration, 1996). Therefore, during transverse motion, the bridge end and the abutment move together as rigidly joined. To incorporate the soil effects behind wingwalls at abutments, translational (linear) springs are attached at the end of bridge girder. Spring stiffness is determined according to Caltrans recommendation for abutment stiffness in transverse direction.

Bridges with expansion joint(s) are modeled such that the two ends of an expansion joint can move independently in longitudinal direction and rotate in longitudinal plane while they have no relative vertical movement. During out-of-plane motion, they are assumed as pin connections as the lateral translations of the two ends of bridge deck at expansion joint are same.

Due to the seismic excitation, bending moment is generated in columns which may lead to the formation of plastic hinges at both ends of the columns. The approximate nonlinearities in a bridge are shown in figure B-1 and as described immediately below. Moment-curvature relationship at the plastic hinges can generate a complex hysteretic behavior. For the sake of simplicity and design compatibility, however, rotational springs with bilinear moment-curvature relationship are introduced to represent the nonlinearity at both ends of bridge columns. Also linear translational and rotational springs are introduced at the bases of the columns to account for soil effect in longitudinal and transverse directions. An effective moment of inertia is considered to take care of the cracked state of concrete bridge columns.

The computer code (SAP 2000) permits the use of a gap element to take care of the effect of pounding between two adjacent bridge decks at expansion joints and abutment locations during longitudinal movement of the bridge. At abutment locations, an initial gap of 0.0508 m (2 in) is provided between the bridge deck and abutment (figure B-2a). The gap element at expansion joint is modeled as a linear spring having stiffness not more than 1000 times of that of the adjacent element (Kim and Shinozuka, 2003). Here the initially provided gap is 0.0254 m (1 in) (figure B-2b) and during oscillation, pounding develops (compressive force) at the interface of the two adjacent bridge decks when relative displacement exhausts this initial gap width. The hook element represents the restraining bar or cable that can be severed under excessive tensile stress, or producing failure of anchorages through which restrainers are tied to decks. Figure B-2c shows that the initial slack in the restrainer is 0.013 m (0.5 in) and axial force generates when the restrainer gets engaged by losing this initial slack.



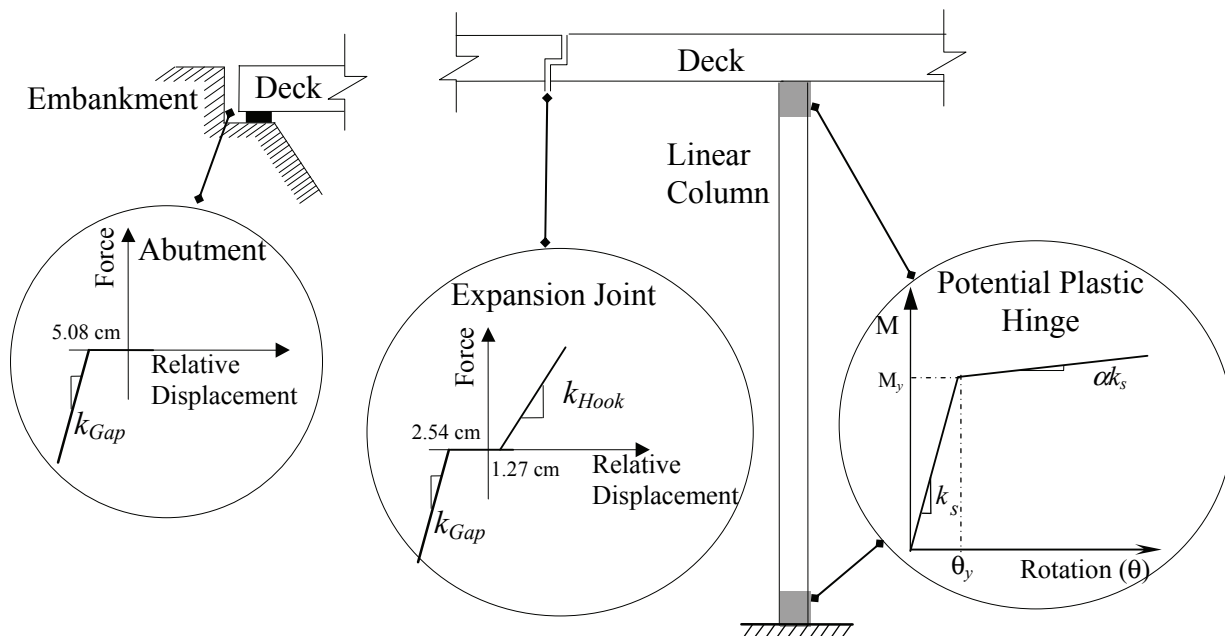


**FIGURE B-1 Nonlinearities in Bridge Model**

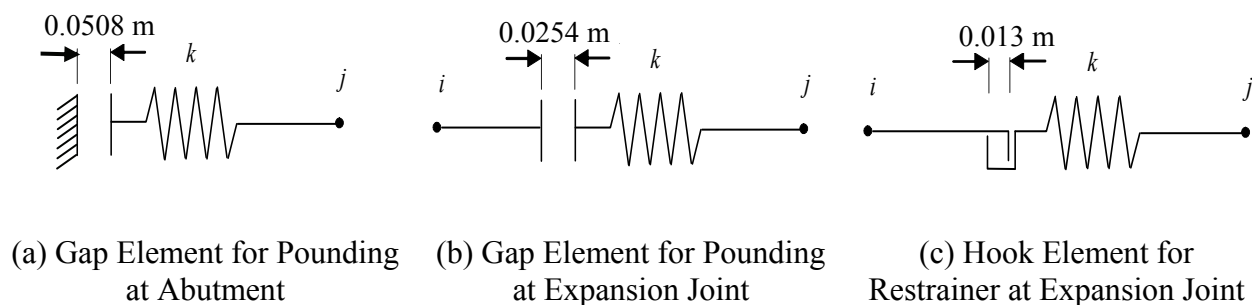


**FIGURE B-2 Nonlinear Modeling of Gap and Hook Elements**

### B.3 Retrofit of Reinforced Concrete Columns by Steel Jacketing

During seismic excitation, concrete columns often lack flexural strength, flexural ductility and shear strength. One of the main causes for these structural inadequacies is lap splices in critical regions and/or premature breakdown of longitudinal reinforcement. A number of column-retrofit techniques, such as steel jacketing, wire pre-stressing and composite material jacketing, have been developed and tested. Among all these, the steel jacketing has been widely applied to bridge retrofit as the most common retrofit technique. The present study focuses on the steel jacketing technique for retrofitting existing bridge columns to improve their seismic performance.

Chai et al. (1991) performed an experiment to investigate the retrofit of circular columns with steel jacketing. In this experiment with circular columns, two half shells of steel plate rolled to a radius slightly larger than that of the column. These plates are site-welded along the vertical plane, and placed over the area to be retrofitted to provide a continuous tube with a small annular gap around the column. This gap is grouted with pure cement. Typically the jacket is cut to provide a space of about 0.05 m between the jacket and any supporting member. It is noted that the jacket is effective only in passive confinement and the level of confinement depends on the hoop strength and stiffness of the steel jacket.

The thickness of steel jacket is calculated from the following equation (Priestley et al., 1996).

$$t_j = \frac{0.18(\varepsilon_{cm} - 0.004)Df'_{cc}}{f_{yj}\varepsilon_{sm}} \quad (\text{B-2})$$

where  $\varepsilon_{cm}$  is the strain at maximum stress in concrete,  $\varepsilon_{sm}$  the strain at maximum stress in steel jacket,  $D$  the diameter of circular column,  $f'_{cc}$  the compressive strength of confined concrete and  $f_{yj}$  the yield stress of steel jacket.

#### **B.4 Moment Curvature Relationship**

The moment-curvature relationship of each bridge column is obtained using the column ductility program developed by Kushiyama (2002) that follows the concept and equations given in Priestley et al. (1996). The rotational ductility demand at each column end is defined as  $\theta/\theta_y$ , where  $\theta$  is the rotation of a bridge column in its plastic hinge region and  $\theta_y$  is the corresponding yield rotation. Figure B-3 shows the cross-section of column 1 of Bridge 2 and their bilinear hysteretic behavior before and after retrofit as obtained from the column ductility program. The moment rotation curves before and after retrofit of bridge columns of Bridge 1 to 5 in both longitudinal and transverse directions are shown in Shinozuka et al. (2005) and Shinozuka et al. (2006).

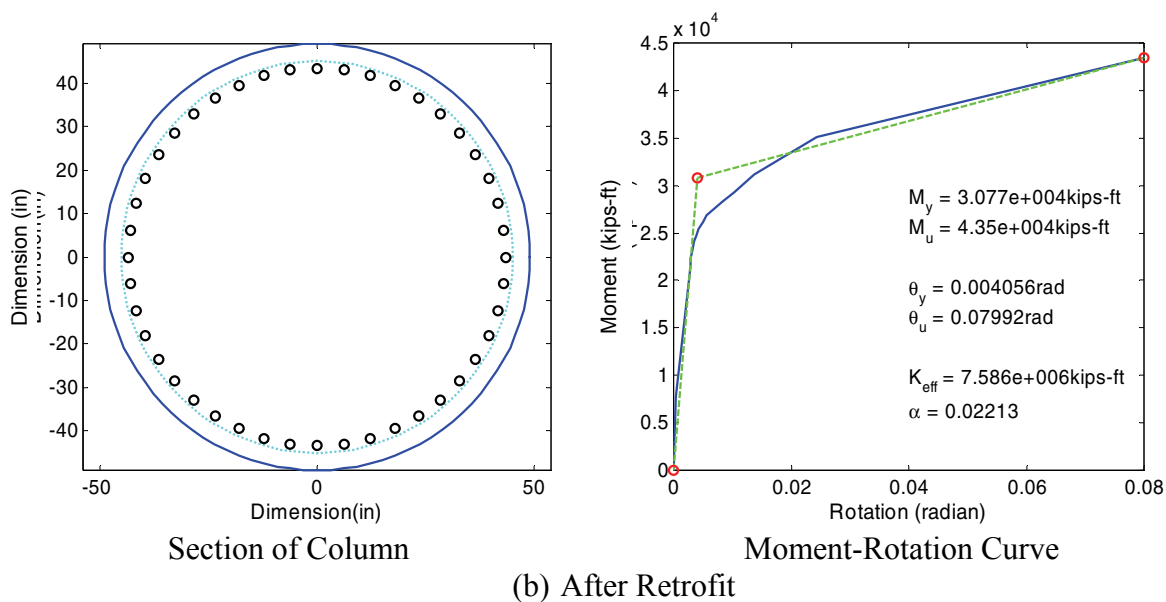
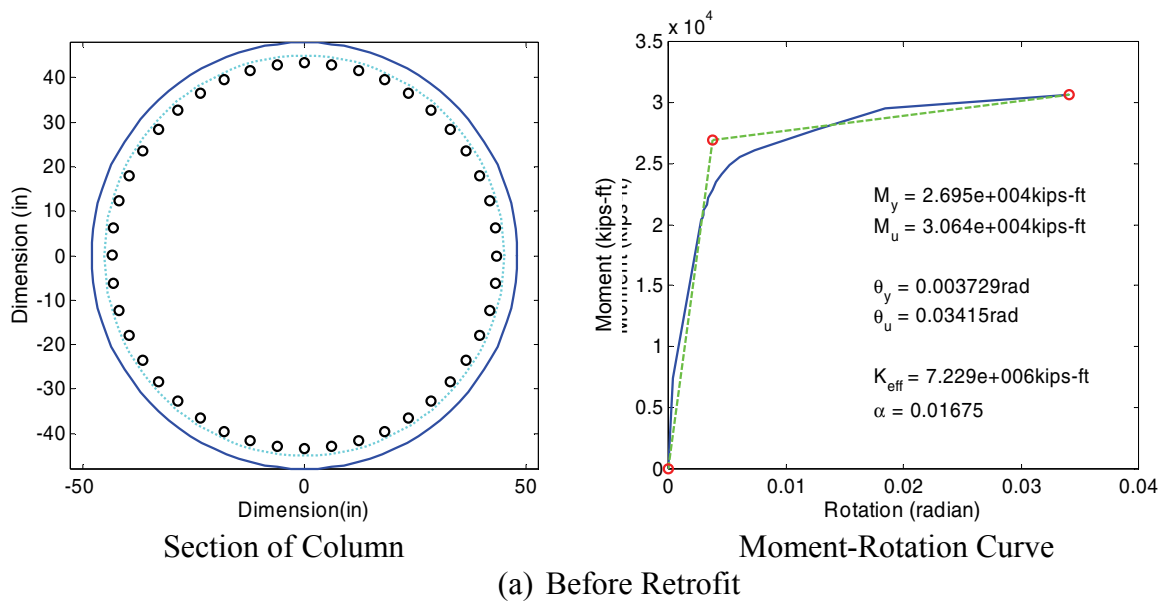


**FIGURE B-3 Moment-Curvature Analysis of Column 1 of Bridge 2**

### B.5 Bridge Damage States

By definition rotational ductility demand is the ratio of rotation ( $\theta$ ) of the column end, modeled as nonlinear spring, to the yield rotation ( $\theta_y$ ). Hence, according to the moment curvature result of bridge column of Bridge 2 before retrofit, rotational ductility at yield and ultimate points are 1.0 ( $= \theta_y/\theta_y$ ) and 9.16 ( $= \theta_u/\theta_y$ ), respectively. Following the recommendation given by Dutta and Mander (1998), five different damage states namely ‘Almost no’, ‘Minor’, ‘Moderate’, ‘Major’ and ‘Collapse’ can be defined and quantified on the basis of column drifts as given in table B-2. Priestley et al. (1996) recommended that yield drift = 0.005. Therefore, the rotational ductility at

yield (1.00) and ultimate (9.16) are corresponding to the drift limits, respectively of 0.005 and 0.075. Rotational ductility in other damage states such as Minor, Moderate and Major are computed in proportional to the variation in drift limit. This procedure is repeated for each column of each bridge. Obtained rotational ductility demands for one particular column are used to define the state of damage of that column under seismic excitation. Tables B-3 and B-4 list the ductility capacities at two ends of only the first left column of five (5) example bridges where plastic hinges are likely to form during longitudinal and transverse movement.

**Table B-2 Damage States and Ductility Capacities for the Bridge Columns**

Damage state	Description	Drift Limits
Almost no	First yield	Yield
Minor	Cracking, spalling	0.01
Moderate	Loss of anchorage	0.025
Major	Incipient column collapse	0.050
Complete	Column collapse	0.075

**TABLE B-3 Peak Ductility Demand of First Left Column of Example Bridges During Longitudinal Motion**

Damage States	Bridge 1	Bridge 2	Bridge 3	Bridge 4	Bridge 5
Almost no	1.00	1.00	1.00	1.00	1.00
Minor	1.52	1.58	1.40	1.82	2.05
Moderate	3.10	3.33	2.58	4.27	5.20
Major	5.72	6.24	4.56	8.36	10.45
Complete	8.34	9.16	6.54	12.44	15.70

**TABLE B-4 Peak Ductility Demand of First Left Column of Sample Bridges During Transverse Motion**

Damage States	Bridge 1	Bridge 2	Bridge 3	Bridge 4	Bridge 5
Almost no	1.00	1.00	1.00	1.00	1.00
Minor	1.52	1.58	1.30	1.56	1.82
Moderate	3.10	3.33	2.19	3.25	4.27
Major	5.72	6.24	3.69	6.07	8.36
Complete	8.34	9.16	5.18	8.89	12.44

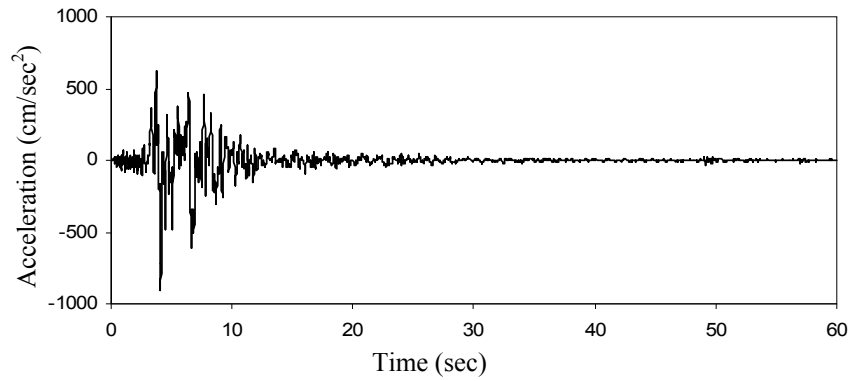
## B.6 Input Ground Motions

Sixty (60) earthquake time histories in Los Angeles area (originally developed for FEMA/SAC project; [http://nisee.berkeley.edu/data/strong\\_motion/sacsteel/ground\\_motions.html](http://nisee.berkeley.edu/data/strong_motion/sacsteel/ground_motions.html)), listed in table B-5, are utilized in this study. They consists of 3 sets of 20 actual earthquake records, each set are scaled linearly so as to have return periods of 2500 yrs, 475 yrs and 72 yrs that are representative of earthquakes with exceedance probabilities, respectively of 2, 10 and 50% in 50 years. Among these 60 records, three representative earthquakes one from each set, observed during 1994 Northridge earthquake (LA27; PGA: 908.70cm/sec<sup>2</sup>), 1940 El Centro Earthquake (LA02; PGA: 662.88cm/sec<sup>2</sup>), and 1979 Imperial Valley Earthquake (LA44; PGA: 109.45cm/sec<sup>2</sup>), are shown in figure B-4.

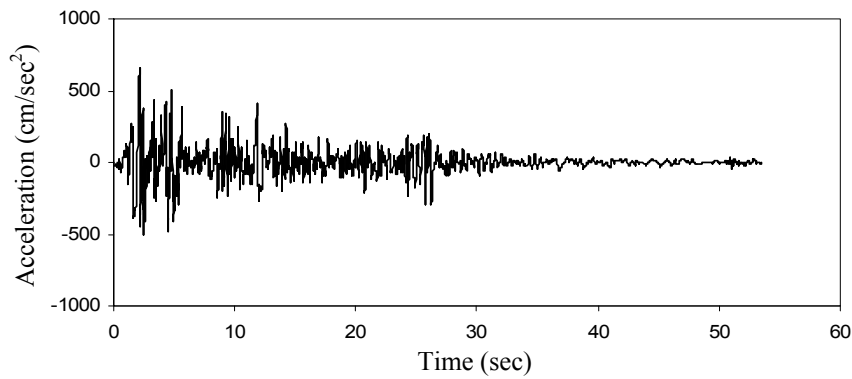
Kim (2003) showed that assumption of identical support ground motions underestimates the peak ductility demands of the bridge columns. According to his research, ground motions are scaled accordingly for different bridges in order to estimate the accurate response.

**TABLE B-5 Description of Los Angeles Ground Motions**

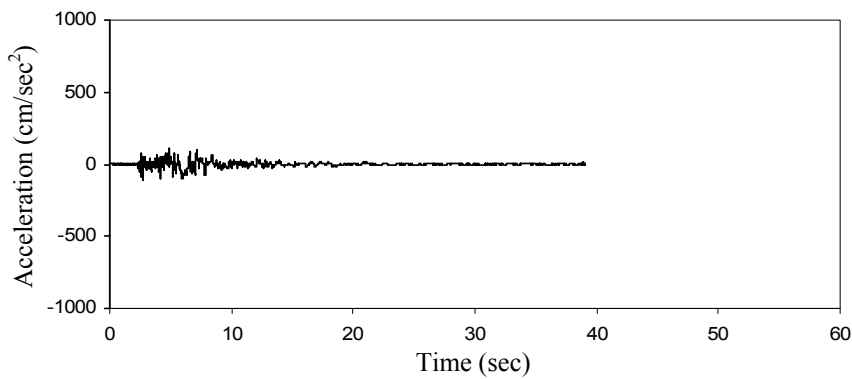
10% Exceedence in 50 yr				2% Exceedence in 50 yr				50% Exceedence in 50 yr			
SAC Name	DT (sec)	Duration (sec)	PGA (cm/sec <sup>2</sup> )	SAC Name	DT (sec)	Duration (sec)	PGA (cm/sec <sup>2</sup> )	SAC Name	DT (sec)	Duration (sec)	PGA (cm/sec <sup>2</sup> )
LA01	0.02	39.38	452.03	LA21	0.02	59.98	1258.00	LA41	0.01	39.38	578.34
LA02	0.02	39.38	662.88	LA22	0.02	59.98	902.75	LA42	0.01	39.38	326.81
LA03	0.01	39.38	386.04	LA23	0.01	24.99	409.95	LA43	0.01	39.08	140.67
LA04	0.01	39.38	478.65	LA24	0.01	24.99	463.76	LA44	0.01	39.08	109.45
LA05	0.01	39.38	295.69	LA25	0.005	14.945	851.62	LA45	0.02	78.60	141.49
LA06	0.01	39.38	230.08	LA26	0.005	14.945	925.29	LA46	0.02	78.60	156.02
LA07	0.02	79.98	412.98	LA27	0.02	59.98	908.70	LA47	0.02	79.98	331.22
LA08	0.02	79.98	417.49	LA28	0.02	59.98	1304.10	LA48	0.02	79.98	301.74
LA09	0.02	79.98	509.70	LA29	0.02	49.98	793.45	LA49	0.02	59.98	312.41
LA10	0.02	79.98	353.35	LA30	0.02	49.98	972.58	LA50	0.02	59.98	535.88
LA11	0.02	39.38	652.49	LA31	0.01	29.99	1271.20	LA51	0.02	43.92	765.65
LA12	0.02	39.38	950.93	LA32	0.01	29.99	1163.50	LA52	0.02	43.92	619.36
LA13	0.02	59.98	664.93	LA33	0.01	29.99	767.26	LA53	0.02	26.14	680.01
LA14	0.02	59.98	644.49	LA34	0.01	29.99	667.59	LA54	0.02	26.14	775.05
LA15	0.005	14.945	523.30	LA35	0.01	29.99	973.16	LA55	0.02	59.98	507.58
LA16	0.005	14.945	568.58	LA36	0.01	29.99	1079.30	LA56	0.02	59.98	371.66
LA17	0.02	59.98	558.43	LA37	0.02	59.98	697.84	LA57	0.02	79.46	248.14
LA18	0.02	59.98	801.44	LA38	0.02	59.98	761.31	LA58	0.02	79.46	226.54
LA19	0.02	59.98	999.43	LA39	0.02	59.98	490.58	LA59	0.02	39.98	753.70
LA20	0.02	59.98	967.61	LA40	0.02	59.98	613.28	LA60	0.02	39.98	469.07



(a) Ground Motion 1  
 (1994 Northridge earthquake (LA27) with exceedance Probability 2% in 50 yrs)



(b) Ground Motion 2  
 (1940 El Centro Earthquake (LA02) with exceedance Probability 10% in 50 yrs)



(c) Ground Motion 3  
 (1979 Imperial Valley Earthquake (LA44) with exceedance Probability 50% in 50 yrs)

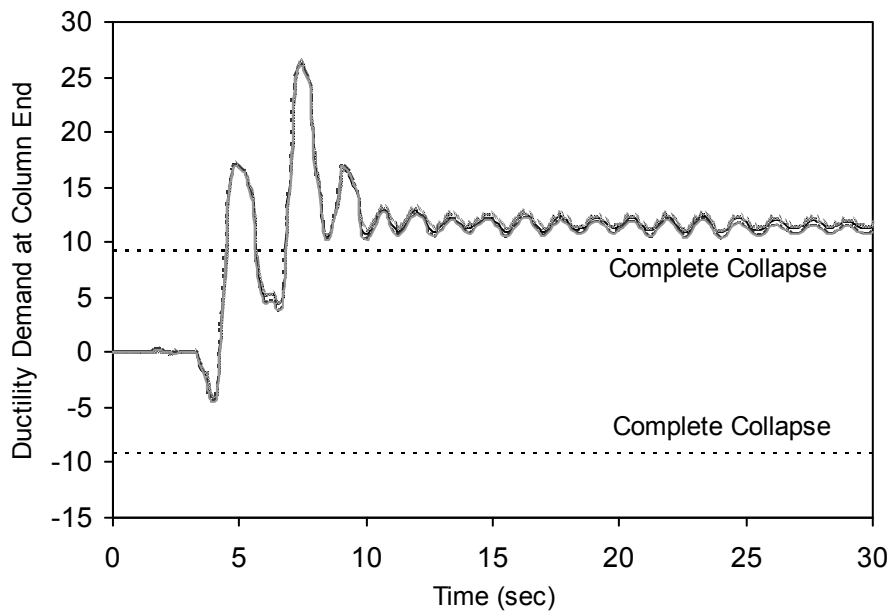
**FIGURE B-4 Acceleration Time Histories Generated for Los Angeles**

## **B.7 Bridge Response from Nonlinear Time History Analysis**

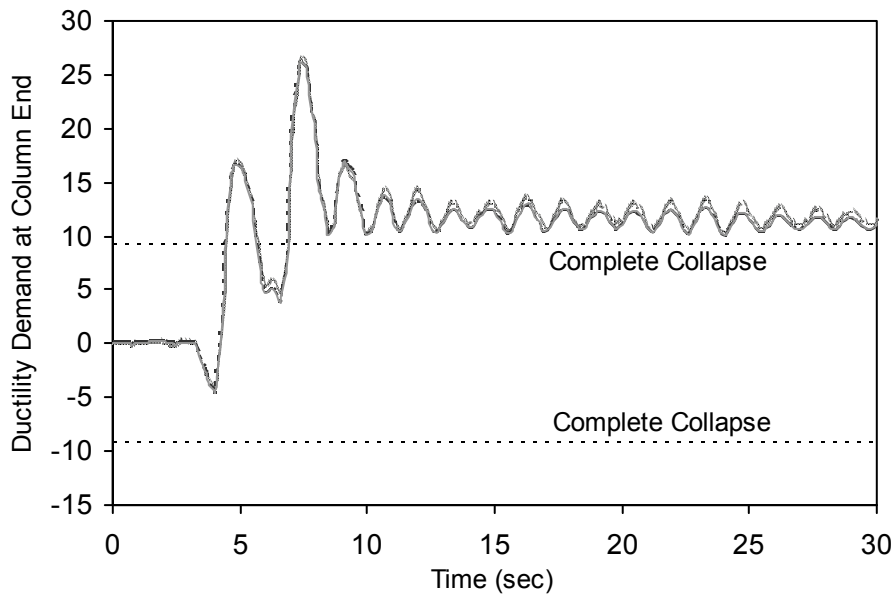
Nonlinear time history analysis of example bridges are performed under 60 earthquake ground motions. Responses are measured at column ends in terms of ductility demand and in the interface of adjacent bridge decks in terms of axial force in restrainer and the pounding force due to impact. Also, generated shear force in plastic hinge regions is estimated to check for premature shear failure of bridge columns. It should be noted that bridge failure due to liquefaction is not considered here. The following section demonstrates different failure modes of Bridge 2 under ground motion 1 (figure B-4).

### **B.7.1 Rotation at Column Ends**

Figures B-5(a) and B-5(b) show the different damage states and variation of ductility demand with time for four column tops and bottoms respectively under ground motion 1. These figures indicate that the variation of ductility factors at all column ends is same as all columns are identical. Though this bridge has one expansion joint, but the stiffness of the hook element (restrainer) is considerably high and no out-of-phase motion is observed between right and left subsystems of the bridge separated by the joint during longitudinal excitation of the bridge. The two column ends have same nature of variation of ductility demand with time.



(a) All Column Tops



(b) All Column Bottoms

**FIGURE B-5 Ductility Demand at Column Ends**



### B.7.2 Pounding and Restrainer Failure

The relative displacement time history at the two ends of expansion joint is plotted in figure B-6. Impact force develops at the interface of the adjacent bridge decks when the relative displacement becomes zero exhausting the initially provided gap equal to 0.0254 m and hence causing the pounding. Figure B-7 depicts that pounding force generates only at that time instance when relative inward movement of decks is more than the specified value. The bridge experiences a maximum of 10870 kN impact force at 15.4 sec. The outward movement between the adjacent bridge decks at the expansion joint results in the development of the axial force in restrainer as the hook element gets engaged by losing initially provided slack equal to 0.013 m. This axial force in the restrainer is transmitted to the nearby concrete block through anchors that hold the restrainer in position. Figure B-8 shows the development of axial force in the restrainer. The anchors fail when the axial force exceeds the anchor design capacity and this failure is assumed conservatively to lead to the collapse of bridge. Depending on the design, however, the restrainer itself fails before anchorage fails. This also is assumed to result in the bridge collapse.

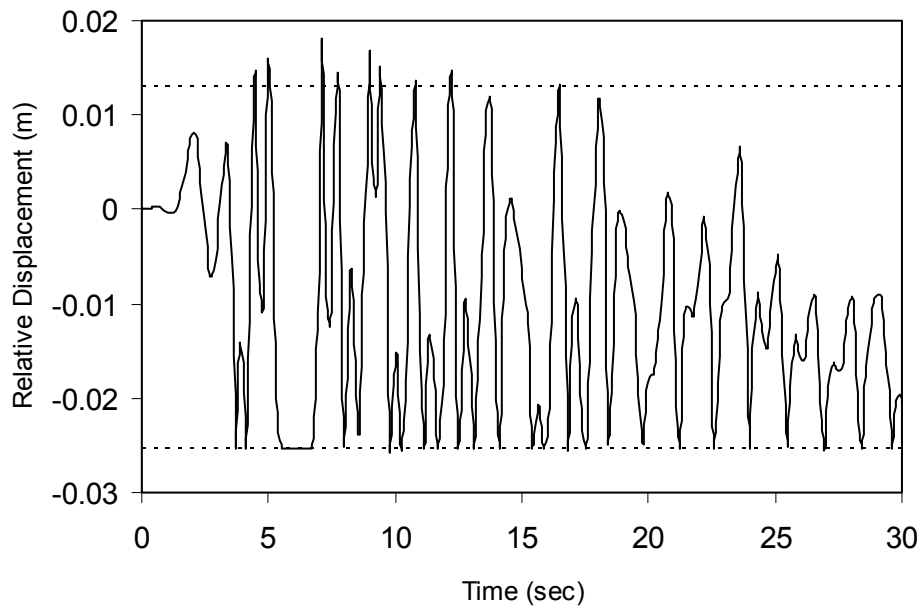


**FIGURE B-6 Relative Displacement at Expansion Joint**

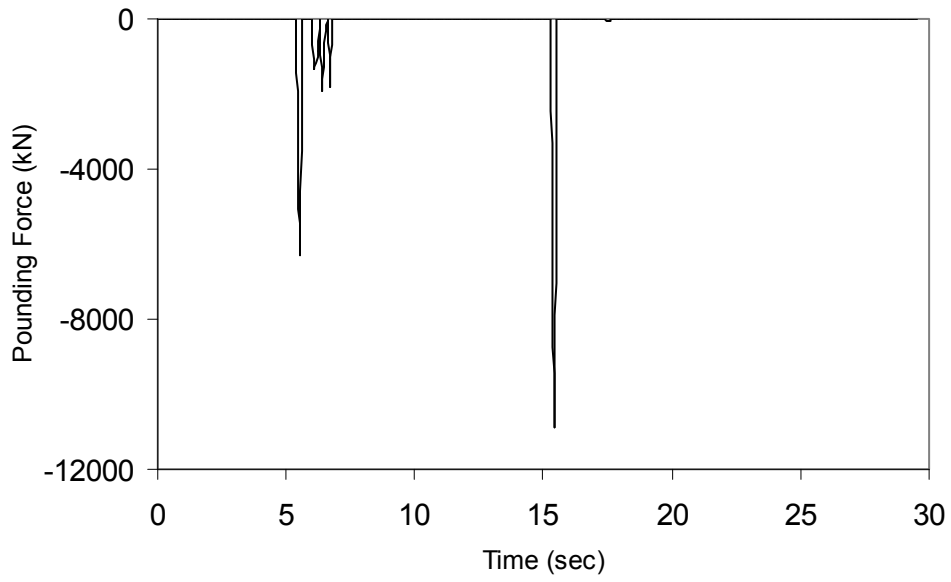


**FIGURE B-7 Pounding Force Developed at Expansion Joint**

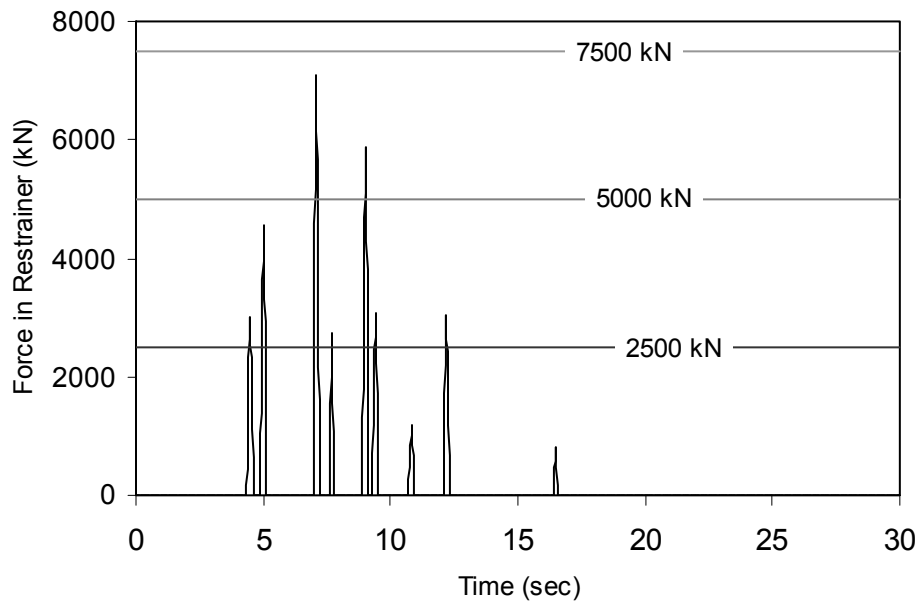


**FIGURE B-8 Axial Force in Restrainer**

### B.7.3 Premature Shear Failure

Development of shear force in the region of plastic hinges of column may lead to premature shear failure preventing flexural ductility capacity at those regions from full utilization. Priestley et al. (1996) focused on this issue and prescribed the analytical estimation of shear capacity in the plastic hinge regions in relation to the curvature ductility factor at those regions. They expressed the nominal shear capacity of concrete,  $V_c = k(\sqrt{f'_c})A_e$  where  $A_e$  is 0.8 times the gross area of column,  $f'_c$  is the compressive strength of unconfined concrete, and  $k$  is presented graphically as a function of curvature ductility factor  $\mu_\phi$ . Outside the plastic hinge regions, value of  $k$  for  $\mu_\phi = 1$  is suggested. To check the possibility of having a premature shear failure, they compared shear strength (capacity) of column with the flexural strength – ductility relationship in the plastic hinge regions. For convenience, the flexural moment – curvature relationship is expressed as equivalent shear force – curvature relationships (shear demand). Following this procedure, the shear capacity and equivalent shear force (i.e. demand) at the plastic hinge regions of Bridge 2 are estimated and presented in figures B-9 and B-10 respectively.

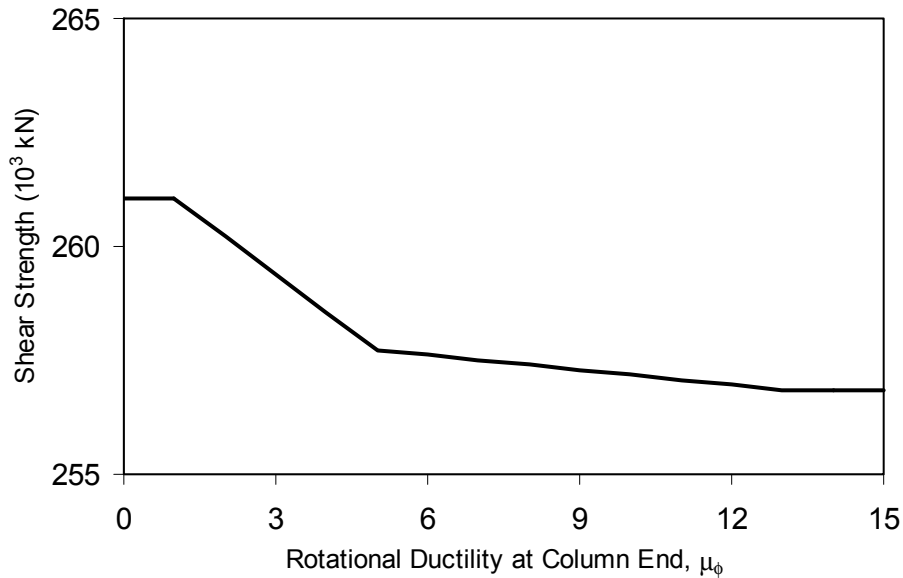


**FIGURE B-9 Shear Strength Envelope: Shear Strength in Column at Plastic Hinge Locations**

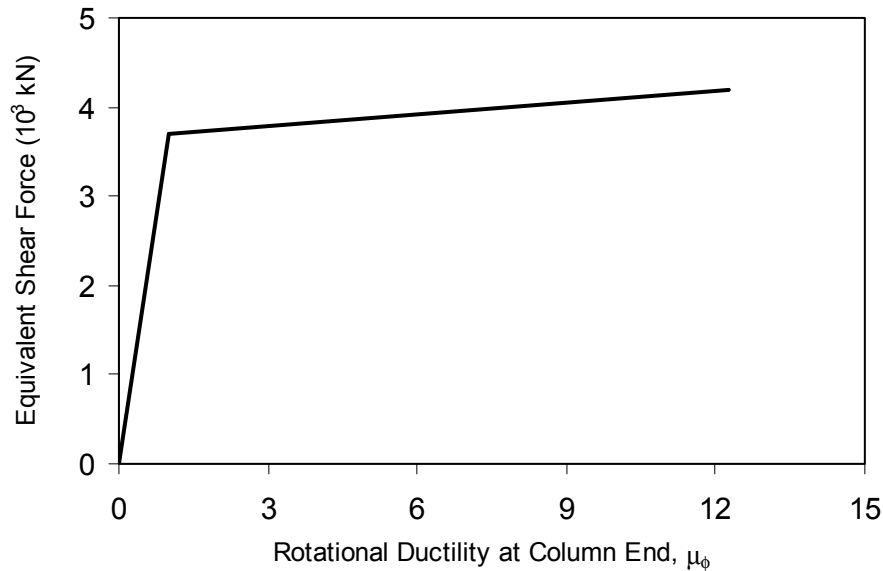


**FIGURE B-10 Equivalent Shear Force-Curvature Relation from Moment-Curvature Relation**

## **B.8 Bridge Response from Capacity Spectrum Method (CSM)**

Over past few years, CSM has been studied and applied for the seismic evaluation of structures, mainly RC buildings. Applied Technology Council (ATC-40, 1996) documented nonlinear static analysis procedures including CSM for seismic evaluation of concrete buildings. The same concept is currently under investigation for the use in bridge analysis, design and seismic evaluation (Fajfar et al., 1997, Shinozuka et al., 2000b, Abeyasinghe et al., 2002 and Zheng et al., 2003, Isakovic and Fischinger, 2006 and Paraskeva et al., 2006). For the purpose of vulnerability assessment of bridges, this section focuses to establish the nonlinear static procedure involving CSM that incorporates performance-based engineering concept.

In this context, this section aims to develop a general procedure utilizing nonlinear static analysis for the seismic vulnerability assessment of bridges considering the whole bridge as a system. For the demonstration of the methodology, Bridge 2 is analyzed under sixty (60) ground acceleration time histories mentioned earlier. The following section elaborates the methodology.

### **B.8.1 Development of Capacity Spectrum**

Capacity curve is given in terms of the force-displacement curve that represents the capacity of the structure within and beyond elastic limit. Computation of total shear force generated at bridge supports as a function of displacement of the superstructure constitutes the capacity curve by definition. This procedure is also referred to as pushover analysis. To generate the capacity curve for building structures, the horizontal displacement at roof level is considered as a most critical displacement component. However, for bridge structures the displacements of the bridge

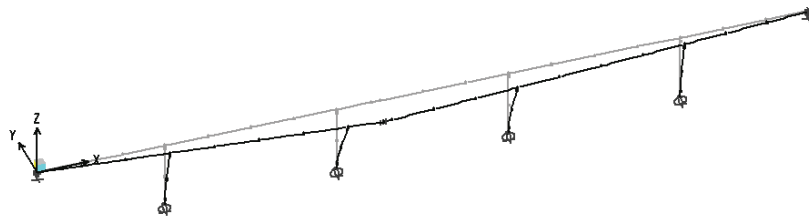
girder in longitudinal direction is used to develop the capacity curve. To develop this plot, static nonlinear analysis (pushover analysis) is performed using SAP2000 Nonlinear computer code.

As stated in ATC-40 (1996) the ‘lateral’ forces (i.e., force in a horizontal plane acting along longitudinal/transverse direction) are applied in proportion to the fundamental mode shape, and is described as

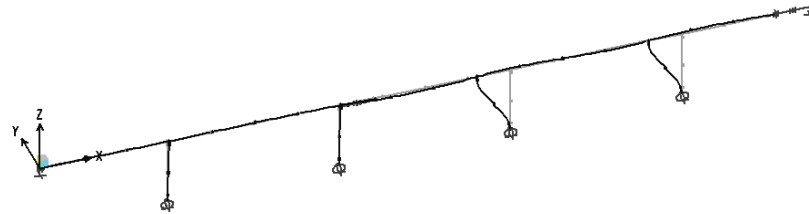
$$F_i = \left( w_i \phi_i / \sum_{i=1}^N w_i \phi_i \right) V \quad (\text{B-3})$$

where  $F_i$  is the ‘lateral’ force on node  $i$  ( $i = 1, 2, \dots, N$ ),  $w_i$  is the dead weight assigned to node  $i$ ,  $\phi_i$  is the amplitude of the fundamental mode at node  $i$ ,  $V$  the total base shear and  $N$  the number of nodes.

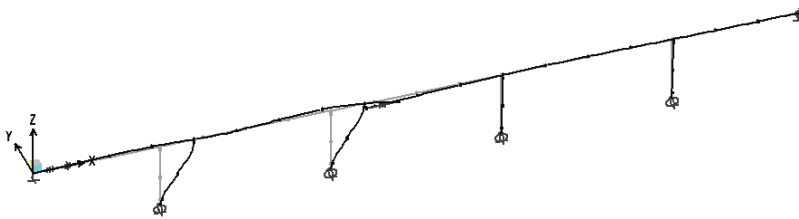
Bridge 2 has 1<sup>st</sup> mode ( $T_1 = 1.94$  sec) of vibration in transverse direction and the next two modes ( $T_2 = 1.56$  sec and  $T_3 = 1.39$  sec) are in longitudinal direction as shown in figure B-11. As second (2<sup>nd</sup>) and third (3<sup>rd</sup>) modes are very close to each other, SRSS rule is applied for these two modes to determine the ‘lateral’ forces at each node of the bridge for longitudinal pushover analysis. Figures B-12a and B-12b show the capacity curves of the bridge obtained from longitudinal pushover analysis which represent, respectively, the overall base shear force as a function of the bridge girder displacement and rotation at plastic hinge region of bridge column.



(a) Mode 1 in Transverse Direction



(b) Mode 2 in Longitudinal Direction

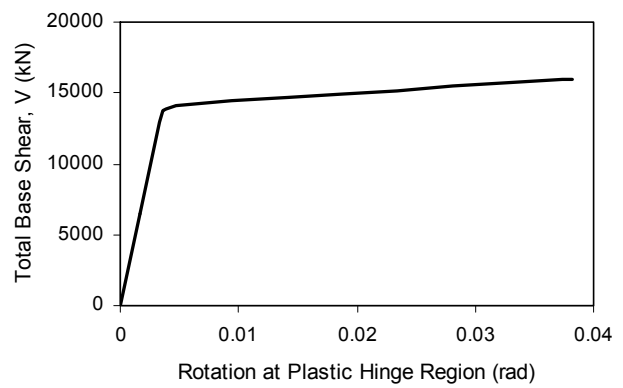


(b) Mode 3 in Longitudinal Direction

**FIGURE B-11 Mode Shapes of Bridge 2 in First 3 Modes**



(a)



(b)

**FIGURE B-12 Capacity Curves of Bridge 2 from Longitudinal Pushover Analysis**

According to the general trend of CSM, it is required to convert the capacity curve to the capacity spectrum in ADRS (Acceleration-Displacement Response Spectra) format. Two measures of capacity spectrum, spectral acceleration  $S_a$  and spectral displacement  $S_d$ , can be estimated as:

$$S_a = \frac{V/W}{\alpha} \quad (\text{B-4})$$

$$S_d = \frac{\Delta_{girder}}{PF\phi_{girder}} \quad (\text{B-5})$$

where  $W$  overall dead weight of bridge,  $\Delta_{girder}$  is the horizontal displacement at girder,  $\phi_{girder}$  is the amplitude of the fundamental mode at girder,  $\alpha$  and  $PF$  are modal mass coefficient and modal participation factor of the fundamental mode defined as follows

$$\alpha = \frac{\left[ \sum_{i=1}^N (w_i \phi_i) / g \right]^2}{\left[ \sum_{i=1}^N w_i / g \right] \left[ \sum_{i=1}^N (w_i \phi_i^2) / g \right]} \quad (\text{B-6})$$

$$PF = \frac{\left[ \sum_{i=1}^N (w_i \phi_i) / g \right]}{\left[ \sum_{i=1}^N (w_i \phi_i^2) / g \right]} \quad (\text{B-7})$$

For longitudinal pushover analysis, SRSS rule is also applied to obtain  $\alpha$  and  $PF$ . Figures B-13 and B-14 show capacity spectrum of Bridge 2 in longitudinal and transverse directions.

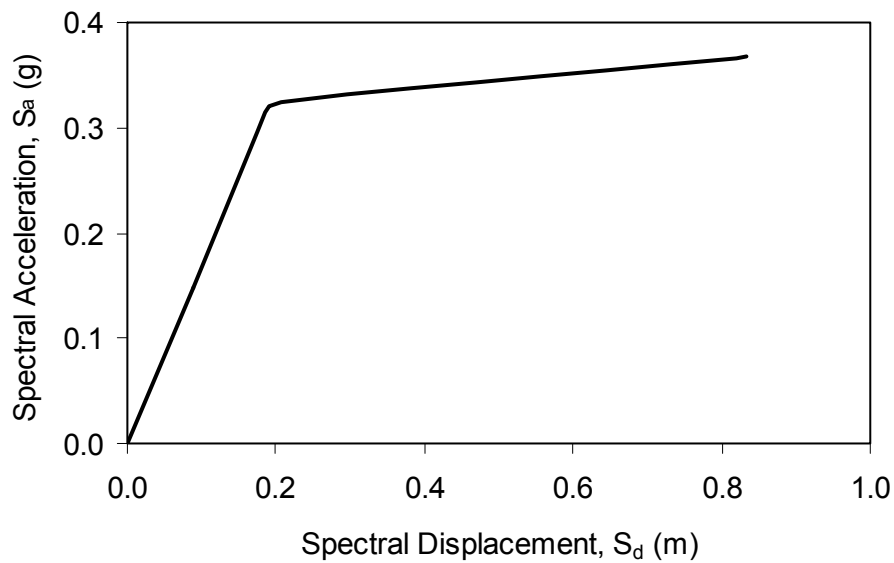


**FIGURE B-13 Capacity Spectrum of Bridge 2 in Longitudinal Direction**

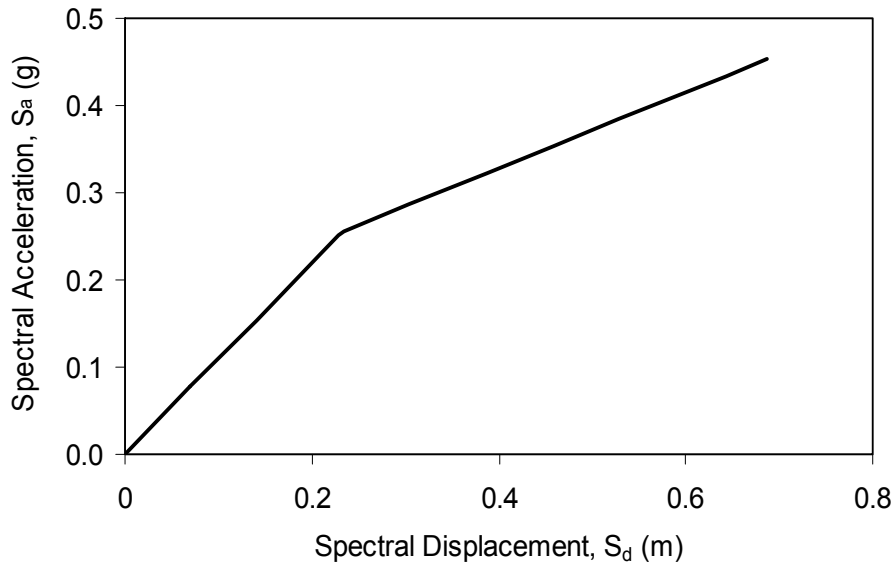


**FIGURE B-14 Capacity Spectrum of Bridge 2 in Transverse Direction**

### B.8.2 Development of Demand Spectrum

Sixty elastic acceleration response spectra (5% damped) are generated from ground motion time histories (table B-5). To use the CSM, these are converted to ADRS format as follows

$$S_d = \frac{T^2}{4\pi^2} S_a g \quad (\text{B-8})$$

Figures B-15 and B-16 show the elastic acceleration response spectrum and corresponding demand spectrum for ground motion LA01.

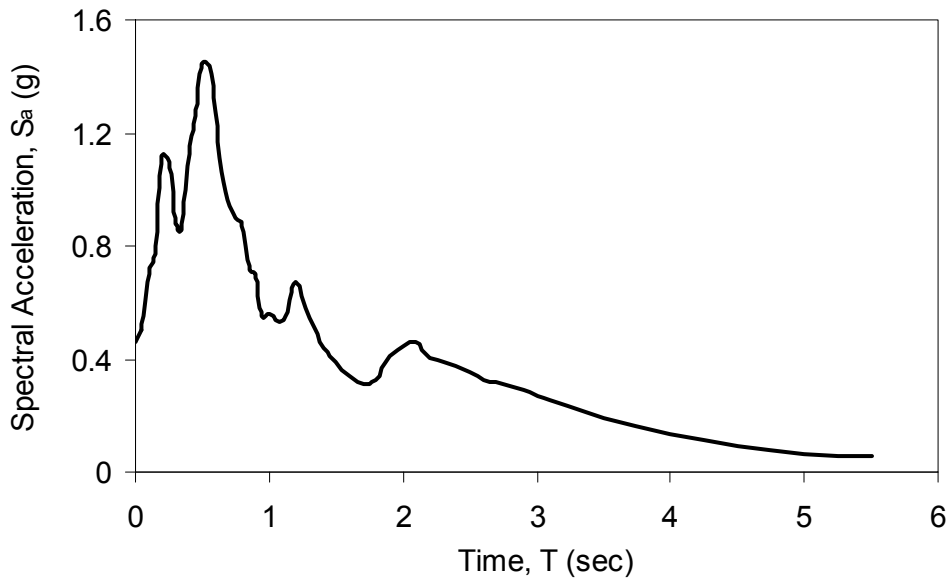


**FIGURE B-15 Elastic Acceleration Response Spectrum (5% Damped)**



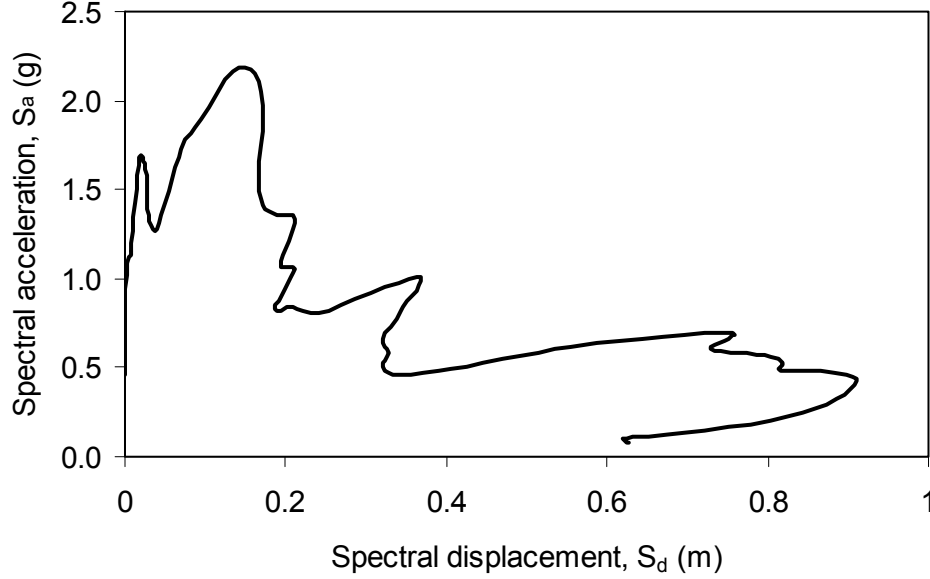


**FIGURE B-16 Acceleration-Displacement Response Spectrum**

### B.8.3 Computation of Performance Point

Performance point is the intersecting point of capacity spectrum with demand spectrum. To incorporate the energy dissipation of the structure through hysteretic behavior beyond yield, the elastic demand curve of the earthquake ground motion should be reduced. In a variation of ATC-40 (1996), recent studies developed few methods to determine inelastic demand spectra from elastic spectra (Fajfar, 1999, Miranda and Bertero, 1994, Reinhorn, 1997). In this study, the procedure given by Reinhorn (1997) is used to produce the inelastic demand spectrum and, hence the inelastic response. According to this procedure, the inelastic spectral displacement ( $S_d^{in}$ ) and inelastic spectral acceleration ( $S_a^{in}$ ) can be expressed as

$$S_d^{in} = \frac{S_d^e}{R} \left\{ 1 + \frac{1}{c} (R^c - 1) \right\} \geq \frac{S_d^e}{R} \quad (\text{B-9})$$

$$S_a^{in} = \frac{S_a^e}{R} \left[ 1 + \alpha_{PY} \left\{ \frac{1}{c} (R^c - 1) \right\} \right] \quad (\text{B-10})$$

where  $S_d^e$  and  $S_a^e$ , respectively are the elastic spectral displacement and acceleration,  $R$  is the reduction factor,  $c$  is a constant and  $\alpha_{PY}$  is the post-yield hardening coefficient of the structure. The reduction factor  $R$  is defined as the ratio of maximum elastic force ( $Q^e/W$ ) to the yield force ( $Q^y/W$ ) as shown in figure B-17. The constant  $c$  can be computed according to the following equation

$$c = \frac{T_o^a}{1 + T_o^a} + \frac{b}{T_o} \quad (\text{B-11})$$

where  $T_o$  is the initial time period of the capacity spectrum,  $a$  and  $b$  are factors as given in table B-6 (Krawinkler and Nasser, 1992).

**TABLE B-6 Coefficients as Given in Krawinkler and Nasser (1992)**

$\alpha_{py}$	$a$	$b$
0%	1.0	0.42
2%	1.0	0.37
10%	0.80	0.29

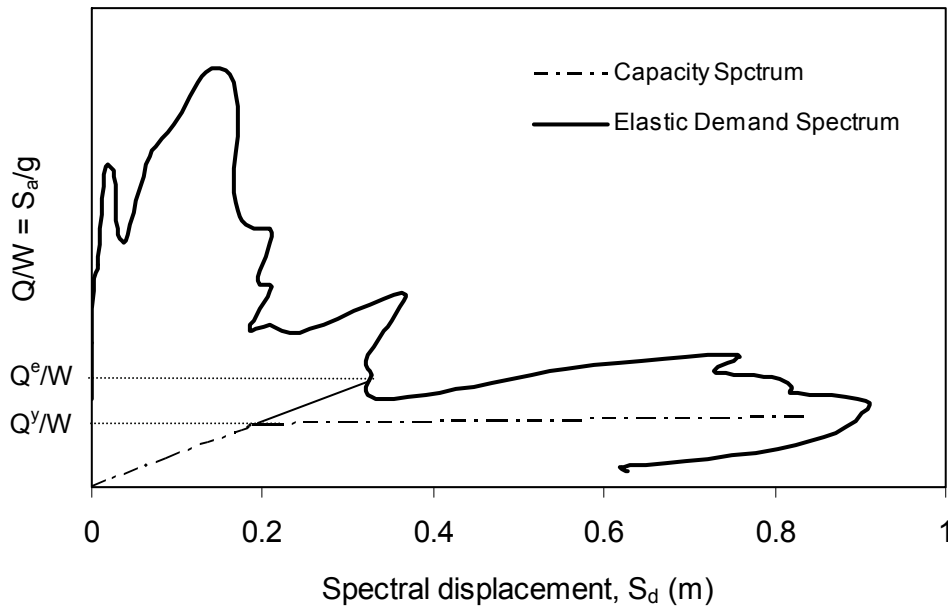


**FIGURE B-17 Estimation of Spectral Reduction Factor,  $R$**

Following this procedure, 60 inelastic demand spectra are generated from corresponding elastic demand spectra. Figure B-18 shows the inelastic demand spectrum generated from the elastic spectrum of LA01.

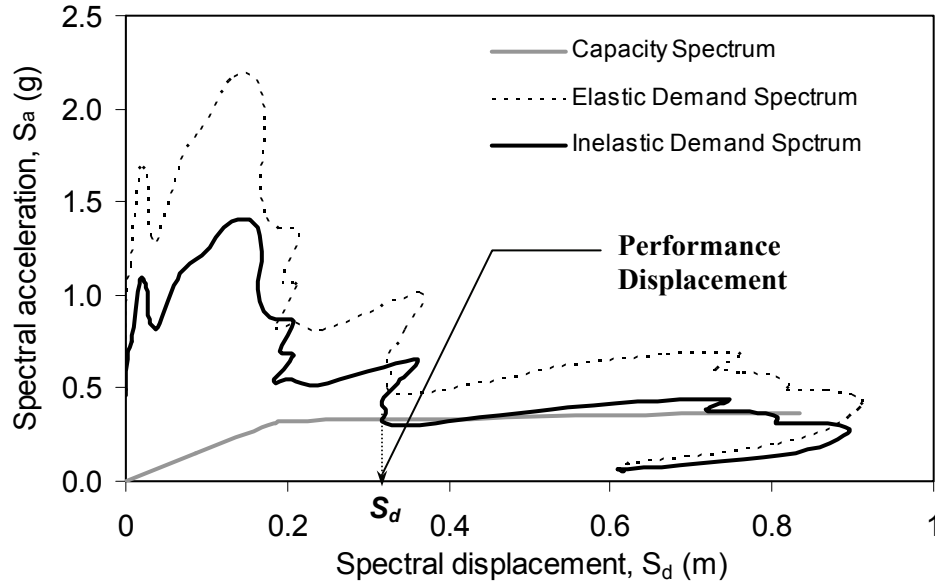


**FIGURE B-18 Calculation of Performance Displacement for LA01**

The intersecting point of capacity and inelastic demand spectra represents structural performance under that particular ground motion (figure B-17). It should be noted that the reduction factor  $R$  depends on the capacity curve of the structure as well as on the elastic demand curve of the ground motion under consideration. Hence, it is obvious that  $R$  will vary with different structures and earthquake ground motions.

#### **B.8.4 Computation of Structural Response**

For sixty earthquake ground motions, sixty performance (spectral) displacements ( $S_d$ ) are obtained separately and converted to the displacement of the bridge girder with the aid of following equation.

$$\Delta_{girder} = S_d \times PF \times \phi_{girder} \quad (B-12)$$

#### **B.9 Effect of Ground Motion Directionality**

Wilson and Button (1982) and Wilson et al. (1995) proposed a methodology to estimate the maximum structural response under multi-component earthquake input assuming the input spectra as statistically independent because of the complex nature of three-dimensional wave propagation. Lopez and Torres (1997) and Lopez et al. (2000) calculated the critical angle of seismic incidence and the maximum structural response under uncorrelated multi-component seismic motions. Following the concept presented in these previous studies, this section presents a practice-oriented technique to compute the effect of directionality of earthquake ground motion on seismic performance of highway bridges. The methodology is demonstrated utilizing structural response obtained from nonlinear time history analysis. It should be noted that the

definition of ‘directionality’ is used here as opposed to ‘directivity’ used in seismology with a specific definition related to fault motion unique to that discipline.

### B.9.1 Estimation of Structural Response

To investigate the effect of directionality of two orthogonal components of earthquake ground motion, it is considered that one component,  $GM_1$  acts at an angle  $\theta$  with respect to the longitudinal (x) axis and at the same time the other component,  $GM_2$  acts at an angle of  $90+\theta$ . Figure B-19 schematically shows these motions and relative position of the bridge. In the present study, time histories of structural responses are first estimated assuming that accelerations are acting on the structure along the longitudinal and transverse directions. Then, directionality effect is assessed by projecting the computed response components on the inclined plane along which the ground motions actually proceed.

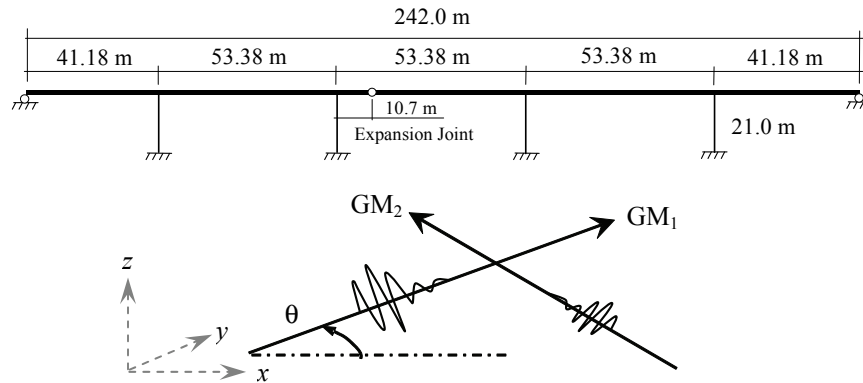


**FIGURE B-19 Bridge under Two Horizontal Orthogonal Components of Earthquake Ground Motions**

For the purpose of demonstration of the above procedure it is assumed that at any time instance ‘t’, the ground motion  $GM_i$  produces response  $(R_{ij})_t$  at a location ‘A’ of the bridge if comes along the j direction of the bridge, where i takes 1 and 2 and j stands for x (longitudinal) and y (transverse). Structural response is expressed here in terms of a deformation function (such as displacement, rotation) or a resultant force (such as moment, force). Figure B-20 represents the response components for  $GM_1$  and  $GM_2$  at any time instance ‘t’. Therefore, the response of the bridge at ‘A’ due to  $GM_1$  when acting with an angle  $\theta$  can be computed by taking projections of  $(R_{1x})_t$  and  $(R_{1y})_t$  on  $\theta$  axis as shown in figures B-20(a) and (b). Hence, the response  $(R_{1\theta})_t$  is

$$(R_{1\theta})_t = (R_{1x})_t \cos \theta + (R_{1y})_t \sin \theta \quad (\text{B-13})$$

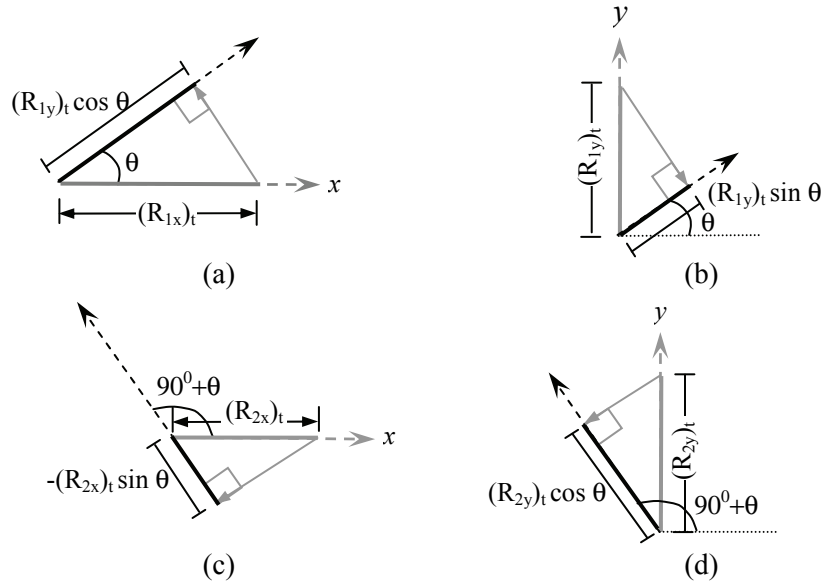


**FIGURE B-20 Structural Response at any Time Instance ‘t’ under Two Orthogonal Components of Ground Motion (Plan View); (a) Longitudinal Response and Projection on  $\theta$  Axis under  $GM_1$ , (b) Transverse Response and Projection on  $\theta$  Axis under  $GM_1$ , (c) Longitudinal Response and Projection on  $90+\theta$  axis under  $GM_2$  and (d) Transverse Response and Projection on  $90+\theta$  Axis under  $GM_2$**

Similarly, the response of the bridge at ‘A’ due to  $GM_2$  when acting with an angle  $90+\theta$  can be computed by taking projections of  $(R_{2x})_t$  and  $(R_{2y})_t$  on  $90+\theta$  axis (figures B-20(c) and (d)), and hence, the response  $(R_{2\theta})_t$  becomes

$$(R_{2\theta})_t = -(R_{2x})_t \sin \theta + (R_{2y})_t \cos \theta \quad (B-14)$$

As these orthogonal components are assumed to be statistically independent, SRSS rule is applied to estimate the resultant response at any time instance ‘t’,  $(R_\theta)_t$  of the bridge at location ‘A’. Therefore,  $(R_\theta)_t$  can be expressed in the following format as a combination of  $(R_{1\theta})_t$  and  $(R_{2\theta})_t$ .

$$\begin{aligned} (R_\theta)_t &= \sqrt{(R_{1\theta})_t^2 + (R_{2\theta})_t^2} \\ &= \sqrt{\left\{ (R_{1x})_t \cos \theta + (R_{1y})_t \sin \theta \right\}^2 + \left\{ -(R_{2x})_t \sin \theta + (R_{2y})_t \cos \theta \right\}^2} \end{aligned} \quad (B-15)$$

Utilizing (B-15), the maximum resultant response over the whole time history, obtained for one particular value of  $\theta$ , is

$$R_\theta = \max\{(R_\theta)_t\} \quad (B-16)$$

In case that only one inclined ground motion exists or a set of two orthogonal components in which one component is negligible, the maximum resultant response becomes

$$R_{\theta} = \max\{(R_{\theta})_t\} = \max\{(R_x)_t \cos \theta + (R_y)_t \sin \theta\} \quad (\text{B-17})$$

where  $(R_j)_t$  is the response of the bridge at time instance 't' and location 'A' due to a ground GM acting with an angle  $\theta$  with the longitudinal axis of bridge and j stands for x (longitudinal) and y (transverse).

Clearly, this maximum resultant response  $R_{\theta}$  is a function of the inclination  $\theta$  of the horizontal ground motion components. Therefore, variation in ground motion inclination ( $\theta$ ) results in variation in  $R_{\theta}$ .

## APPENDIX C

### STIFFNESS AND STRENGTH DEGRADATION OF MOMENT-ROTATION RELATIONSHIP

In this study, Bridge 1 is analyzed under 60 ground motions for the following models of moment-rotation relation; elastic-plastic, bi-linear, stiffness degradation, and stiffness and strength degradation. For all cases, the same yield moment and yield rotation are used. The above four moment-rotation relationships at plastic hinge locations are plotted in Figure C-1.

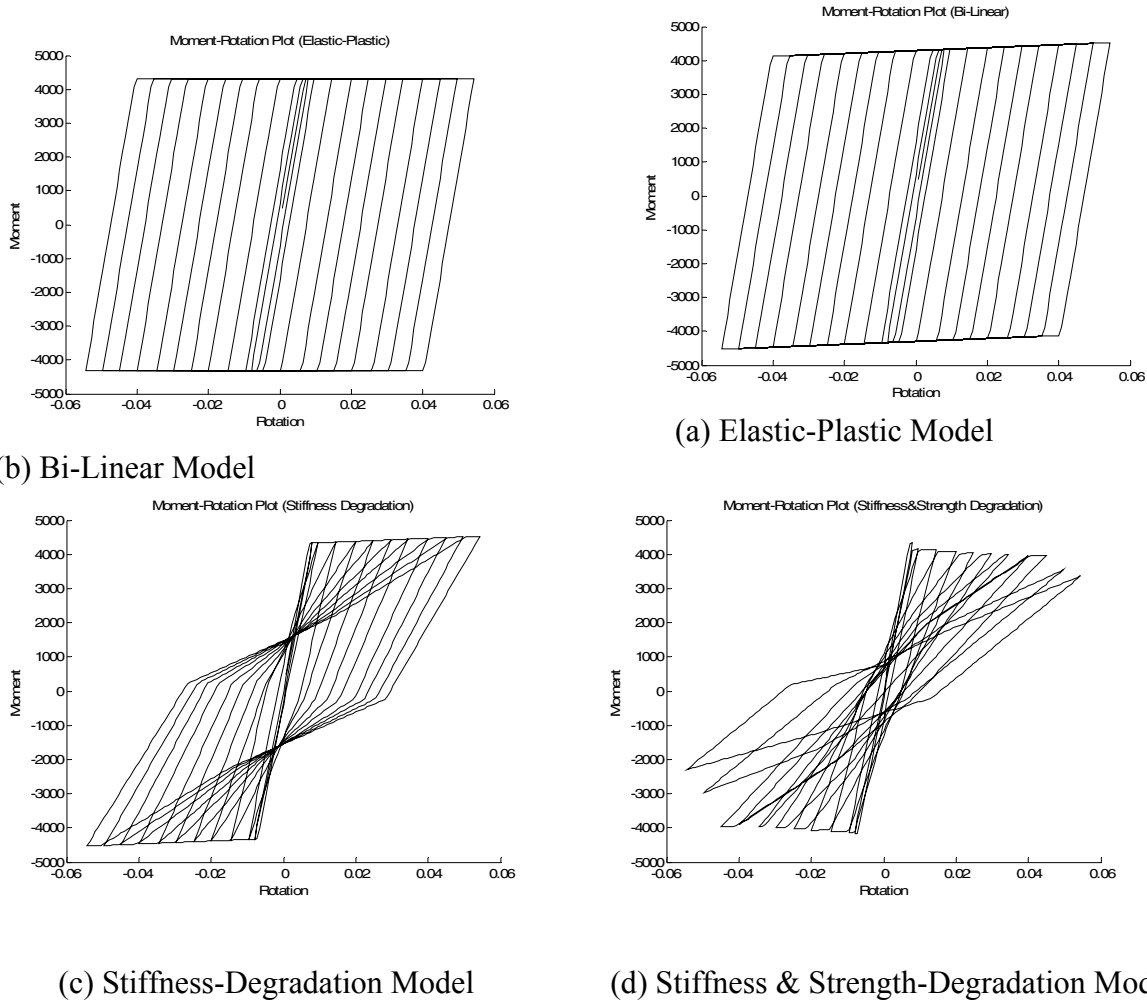


**FIGURE C-1 Moment-Rotation Relationship**

Figures C-2, C-3, C-4 and C-5 represent fragility curves computed with these nonlinear models respectively for almost no, minor, moderate and major damage states. Result indicates that fragility curves at almost no damage are nearly the same for these four models. In other three damage states, fragility curves using stiffness and strength degradation model are the weakest among all curves.

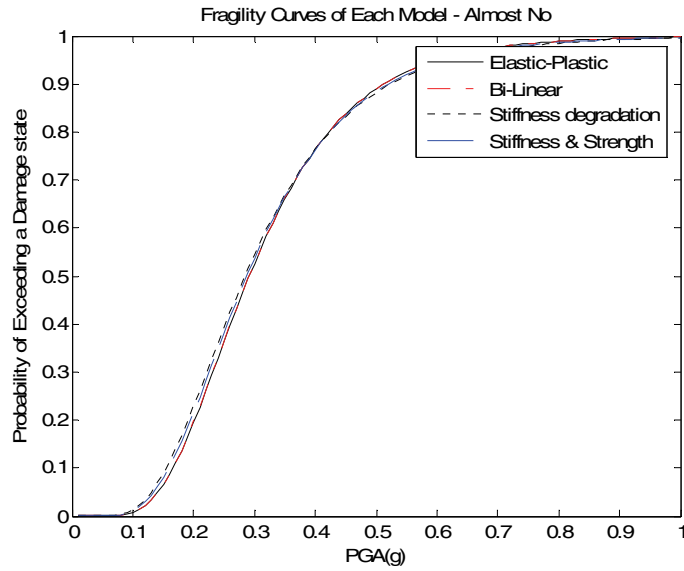


**FIGURE C-2 Fragility Curves in Almost No Damage State**

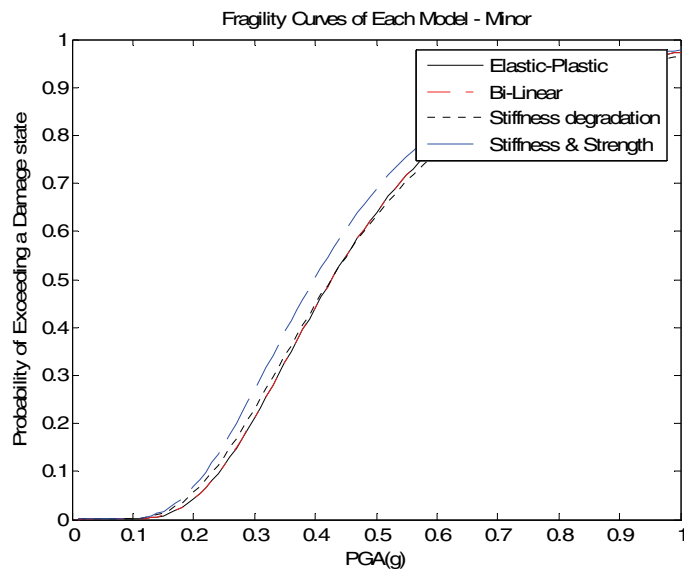


**FIGURE C-3 Fragility Curves in Minor Damage State**



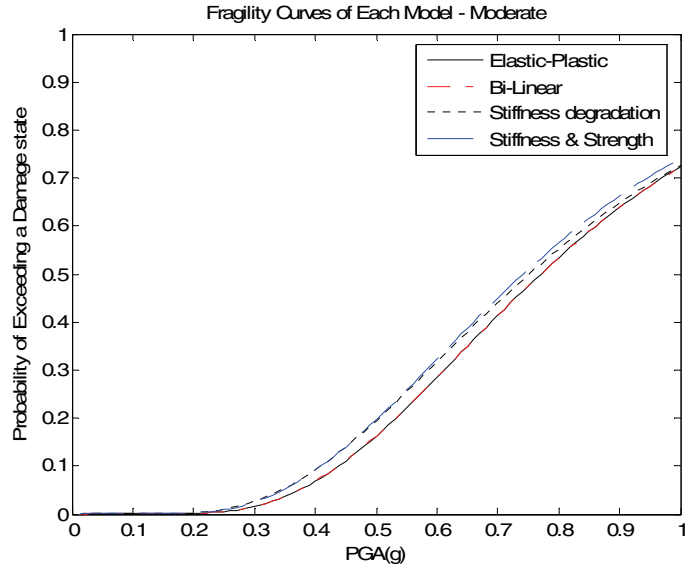


**FIGURE C-4 Fragility Curves in Moderate Damage State**

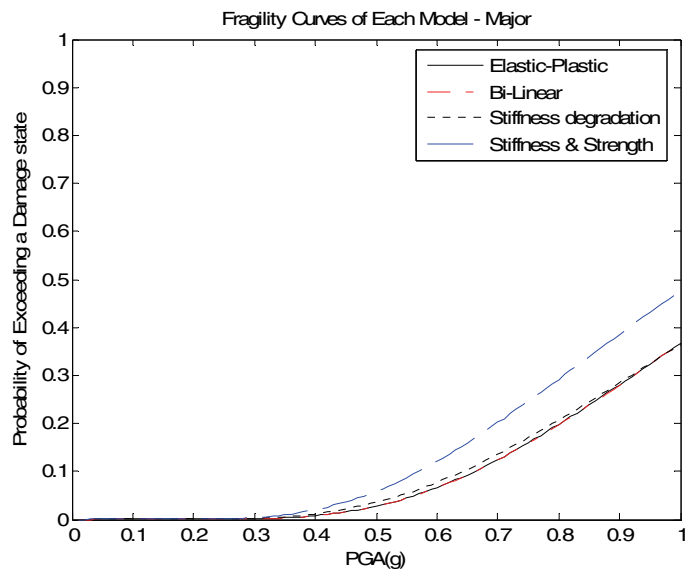


**FIGURE C-5 Fragility Curves in Major Damage State**



## MCEER Technical Reports

MCEER publishes technical reports on a variety of subjects written by authors funded through MCEER. These reports are available from both MCEER Publications and the National Technical Information Service (NTIS). Requests for reports should be directed to MCEER Publications, MCEER, University at Buffalo, State University of New York, Red Jacket Quadrangle, Buffalo, New York 14261. Reports can also be requested through NTIS, 5285 Port Royal Road, Springfield, Virginia 22161. NTIS accession numbers are shown in parenthesis, if available.

- NCEER-87-0001 "First-Year Program in Research, Education and Technology Transfer," 3/5/87, (PB88-134275, A04, MF-A01).
- NCEER-87-0002 "Experimental Evaluation of Instantaneous Optimal Algorithms for Structural Control," by R.C. Lin, T.T. Soong and A.M. Reinhorn, 4/20/87, (PB88-134341, A04, MF-A01).
- NCEER-87-0003 "Experimentation Using the Earthquake Simulation Facilities at University at Buffalo," by A.M. Reinhorn and R.L. Ketter, to be published.
- NCEER-87-0004 "The System Characteristics and Performance of a Shaking Table," by J.S. Hwang, K.C. Chang and G.C. Lee, 6/1/87, (PB88-134259, A03, MF-A01). This report is available only through NTIS (see address given above).
- NCEER-87-0005 "A Finite Element Formulation for Nonlinear Viscoplastic Material Using a Q Model," by O. Gyebe and G. Dasgupta, 11/2/87, (PB88-213764, A08, MF-A01).
- NCEER-87-0006 "Symbolic Manipulation Program (SMP) - Algebraic Codes for Two and Three Dimensional Finite Element Formulations," by X. Lee and G. Dasgupta, 11/9/87, (PB88-218522, A05, MF-A01).
- NCEER-87-0007 "Instantaneous Optimal Control Laws for Tall Buildings Under Seismic Excitations," by J.N. Yang, A. Akbarpour and P. Ghaemmaghami, 6/10/87, (PB88-134333, A06, MF-A01). This report is only available through NTIS (see address given above).
- NCEER-87-0008 "IDARC: Inelastic Damage Analysis of Reinforced Concrete Frame - Shear-Wall Structures," by Y.J. Park, A.M. Reinhorn and S.K. Kunnath, 7/20/87, (PB88-134325, A09, MF-A01). This report is only available through NTIS (see address given above).
- NCEER-87-0009 "Liquefaction Potential for New York State: A Preliminary Report on Sites in Manhattan and Buffalo," by M. Budhu, V. Vijayakumar, R.F. Giese and L. Baumgras, 8/31/87, (PB88-163704, A03, MF-A01). This report is available only through NTIS (see address given above).
- NCEER-87-0010 "Vertical and Torsional Vibration of Foundations in Inhomogeneous Media," by A.S. Veletsos and K.W. Dotson, 6/1/87, (PB88-134291, A03, MF-A01). This report is only available through NTIS (see address given above).
- NCEER-87-0011 "Seismic Probabilistic Risk Assessment and Seismic Margins Studies for Nuclear Power Plants," by Howard H.M. Hwang, 6/15/87, (PB88-134267, A03, MF-A01). This report is only available through NTIS (see address given above).
- NCEER-87-0012 "Parametric Studies of Frequency Response of Secondary Systems Under Ground-Acceleration Excitations," by Y. Yong and Y.K. Lin, 6/10/87, (PB88-134309, A03, MF-A01). This report is only available through NTIS (see address given above).
- NCEER-87-0013 "Frequency Response of Secondary Systems Under Seismic Excitation," by J.A. HoLung, J. Cai and Y.K. Lin, 7/31/87, (PB88-134317, A05, MF-A01). This report is only available through NTIS (see address given above).
- NCEER-87-0014 "Modelling Earthquake Ground Motions in Seismically Active Regions Using Parametric Time Series Methods," by G.W. Ellis and A.S. Cakmak, 8/25/87, (PB88-134283, A08, MF-A01). This report is only available through NTIS (see address given above).
- NCEER-87-0015 "Detection and Assessment of Seismic Structural Damage," by E. DiPasquale and A.S. Cakmak, 8/25/87, (PB88-163712, A05, MF-A01). This report is only available through NTIS (see address given above).

- NCEER-87-0016 "Pipeline Experiment at Parkfield, California," by J. Isenberg and E. Richardson, 9/15/87, (PB88-163720, A03, MF-A01). This report is available only through NTIS (see address given above).
- NCEER-87-0017 "Digital Simulation of Seismic Ground Motion," by M. Shinozuka, G. Deodatis and T. Harada, 8/31/87, (PB88-155197, A04, MF-A01). This report is available only through NTIS (see address given above).
- NCEER-87-0018 "Practical Considerations for Structural Control: System Uncertainty, System Time Delay and Truncation of Small Control Forces," J.N. Yang and A. Akbarpour, 8/10/87, (PB88-163738, A08, MF-A01). This report is only available through NTIS (see address given above).
- NCEER-87-0019 "Modal Analysis of Nonclassically Damped Structural Systems Using Canonical Transformation," by J.N. Yang, S. Sarkani and F.X. Long, 9/27/87, (PB88-187851, A04, MF-A01).
- NCEER-87-0020 "A Nonstationary Solution in Random Vibration Theory," by J.R. Red-Horse and P.D. Spanos, 11/3/87, (PB88-163746, A03, MF-A01).
- NCEER-87-0021 "Horizontal Impedances for Radially Inhomogeneous Viscoelastic Soil Layers," by A.S. Veletsos and K.W. Dotson, 10/15/87, (PB88-150859, A04, MF-A01).
- NCEER-87-0022 "Seismic Damage Assessment of Reinforced Concrete Members," by Y.S. Chung, C. Meyer and M. Shinozuka, 10/9/87, (PB88-150867, A05, MF-A01). This report is available only through NTIS (see address given above).
- NCEER-87-0023 "Active Structural Control in Civil Engineering," by T.T. Soong, 11/11/87, (PB88-187778, A03, MF-A01).
- NCEER-87-0024 "Vertical and Torsional Impedances for Radially Inhomogeneous Viscoelastic Soil Layers," by K.W. Dotson and A.S. Veletsos, 12/87, (PB88-187786, A03, MF-A01).
- NCEER-87-0025 "Proceedings from the Symposium on Seismic Hazards, Ground Motions, Soil-Liquefaction and Engineering Practice in Eastern North America," October 20-22, 1987, edited by K.H. Jacob, 12/87, (PB88-188115, A23, MF-A01). This report is available only through NTIS (see address given above).
- NCEER-87-0026 "Report on the Whittier-Narrows, California, Earthquake of October 1, 1987," by J. Pantelic and A. Reinhorn, 11/87, (PB88-187752, A03, MF-A01). This report is available only through NTIS (see address given above).
- NCEER-87-0027 "Design of a Modular Program for Transient Nonlinear Analysis of Large 3-D Building Structures," by S. Srivastav and J.F. Abel, 12/30/87, (PB88-187950, A05, MF-A01). This report is only available through NTIS (see address given above).
- NCEER-87-0028 "Second-Year Program in Research, Education and Technology Transfer," 3/8/88, (PB88-219480, A04, MF-A01).
- NCEER-88-0001 "Workshop on Seismic Computer Analysis and Design of Buildings With Interactive Graphics," by W. McGuire, J.F. Abel and C.H. Conley, 1/18/88, (PB88-187760, A03, MF-A01). This report is only available through NTIS (see address given above).
- NCEER-88-0002 "Optimal Control of Nonlinear Flexible Structures," by J.N. Yang, F.X. Long and D. Wong, 1/22/88, (PB88-213772, A06, MF-A01).
- NCEER-88-0003 "Substructuring Techniques in the Time Domain for Primary-Secondary Structural Systems," by G.D. Manolis and G. Juhn, 2/10/88, (PB88-213780, A04, MF-A01).
- NCEER-88-0004 "Iterative Seismic Analysis of Primary-Secondary Systems," by A. Singhal, L.D. Lutes and P.D. Spanos, 2/23/88, (PB88-213798, A04, MF-A01).
- NCEER-88-0005 "Stochastic Finite Element Expansion for Random Media," by P.D. Spanos and R. Ghanem, 3/14/88, (PB88-213806, A03, MF-A01).

- NCEER-88-0006 "Combining Structural Optimization and Structural Control," by F.Y. Cheng and C.P. Pantelides, 1/10/88, (PB88-213814, A05, MF-A01).
- NCEER-88-0007 "Seismic Performance Assessment of Code-Designed Structures," by H.H-M. Hwang, J-W. Jaw and H-J. Shau, 3/20/88, (PB88-219423, A04, MF-A01). This report is only available through NTIS (see address given above).
- NCEER-88-0008 "Reliability Analysis of Code-Designed Structures Under Natural Hazards," by H.H-M. Hwang, H. Ushiba and M. Shinozuka, 2/29/88, (PB88-229471, A07, MF-A01). This report is only available through NTIS (see address given above).
- NCEER-88-0009 "Seismic Fragility Analysis of Shear Wall Structures," by J-W Jaw and H.H-M. Hwang, 4/30/88, (PB89-102867, A04, MF-A01).
- NCEER-88-0010 "Base Isolation of a Multi-Story Building Under a Harmonic Ground Motion - A Comparison of Performances of Various Systems," by F-G Fan, G. Ahmadi and I.G. Tadjbakhsh, 5/18/88, (PB89-122238, A06, MF-A01). This report is only available through NTIS (see address given above).
- NCEER-88-0011 "Seismic Floor Response Spectra for a Combined System by Green's Functions," by F.M. Lavelle, L.A. Bergman and P.D. Spanos, 5/1/88, (PB89-102875, A03, MF-A01).
- NCEER-88-0012 "A New Solution Technique for Randomly Excited Hysteretic Structures," by G.Q. Cai and Y.K. Lin, 5/16/88, (PB89-102883, A03, MF-A01).
- NCEER-88-0013 "A Study of Radiation Damping and Soil-Structure Interaction Effects in the Centrifuge," by K. Weissman, supervised by J.H. Prevost, 5/24/88, (PB89-144703, A06, MF-A01).
- NCEER-88-0014 "Parameter Identification and Implementation of a Kinematic Plasticity Model for Frictional Soils," by J.H. Prevost and D.V. Griffiths, to be published.
- NCEER-88-0015 "Two- and Three- Dimensional Dynamic Finite Element Analyses of the Long Valley Dam," by D.V. Griffiths and J.H. Prevost, 6/17/88, (PB89-144711, A04, MF-A01).
- NCEER-88-0016 "Damage Assessment of Reinforced Concrete Structures in Eastern United States," by A.M. Reinhorn, M.J. Seidel, S.K. Kunnath and Y.J. Park, 6/15/88, (PB89-122220, A04, MF-A01). This report is only available through NTIS (see address given above).
- NCEER-88-0017 "Dynamic Compliance of Vertically Loaded Strip Foundations in Multilayered Viscoelastic Soils," by S. Ahmad and A.S.M. Israil, 6/17/88, (PB89-102891, A04, MF-A01).
- NCEER-88-0018 "An Experimental Study of Seismic Structural Response With Added Viscoelastic Dampers," by R.C. Lin, Z. Liang, T.T. Soong and R.H. Zhang, 6/30/88, (PB89-122212, A05, MF-A01). This report is available only through NTIS (see address given above).
- NCEER-88-0019 "Experimental Investigation of Primary - Secondary System Interaction," by G.D. Manolis, G. Juhn and A.M. Reinhorn, 5/27/88, (PB89-122204, A04, MF-A01).
- NCEER-88-0020 "A Response Spectrum Approach For Analysis of Nonclassically Damped Structures," by J.N. Yang, S. Sarkani and F.X. Long, 4/22/88, (PB89-102909, A04, MF-A01).
- NCEER-88-0021 "Seismic Interaction of Structures and Soils: Stochastic Approach," by A.S. Veletsos and A.M. Prasad, 7/21/88, (PB89-122196, A04, MF-A01). This report is only available through NTIS (see address given above).
- NCEER-88-0022 "Identification of the Serviceability Limit State and Detection of Seismic Structural Damage," by E. DiPasquale and A.S. Cakmak, 6/15/88, (PB89-122188, A05, MF-A01). This report is available only through NTIS (see address given above).
- NCEER-88-0023 "Multi-Hazard Risk Analysis: Case of a Simple Offshore Structure," by B.K. Bhartia and E.H. Vanmarcke, 7/21/88, (PB89-145213, A05, MF-A01).

- NCEER-88-0024 "Automated Seismic Design of Reinforced Concrete Buildings," by Y.S. Chung, C. Meyer and M. Shinozuka, 7/5/88, (PB89-122170, A06, MF-A01). This report is available only through NTIS (see address given above).
- NCEER-88-0025 "Experimental Study of Active Control of MDOF Structures Under Seismic Excitations," by L.L. Chung, R.C. Lin, T.T. Soong and A.M. Reinhorn, 7/10/88, (PB89-122600, A04, MF-A01).
- NCEER-88-0026 "Earthquake Simulation Tests of a Low-Rise Metal Structure," by J.S. Hwang, K.C. Chang, G.C. Lee and R.L. Ketter, 8/1/88, (PB89-102917, A04, MF-A01).
- NCEER-88-0027 "Systems Study of Urban Response and Reconstruction Due to Catastrophic Earthquakes," by F. Kozin and H.K. Zhou, 9/22/88, (PB90-162348, A04, MF-A01).
- NCEER-88-0028 "Seismic Fragility Analysis of Plane Frame Structures," by H.H-M. Hwang and Y.K. Low, 7/31/88, (PB89-131445, A06, MF-A01).
- NCEER-88-0029 "Response Analysis of Stochastic Structures," by A. Kardara, C. Bucher and M. Shinozuka, 9/22/88, (PB89-174429, A04, MF-A01).
- NCEER-88-0030 "Nonnormal Accelerations Due to Yielding in a Primary Structure," by D.C.K. Chen and L.D. Lutes, 9/19/88, (PB89-131437, A04, MF-A01).
- NCEER-88-0031 "Design Approaches for Soil-Structure Interaction," by A.S. Veletsos, A.M. Prasad and Y. Tang, 12/30/88, (PB89-174437, A03, MF-A01). This report is available only through NTIS (see address given above).
- NCEER-88-0032 "A Re-evaluation of Design Spectra for Seismic Damage Control," by C.J. Turkstra and A.G. Tallin, 11/7/88, (PB89-145221, A05, MF-A01).
- NCEER-88-0033 "The Behavior and Design of Noncontact Lap Splices Subjected to Repeated Inelastic Tensile Loading," by V.E. Sagan, P. Gergely and R.N. White, 12/8/88, (PB89-163737, A08, MF-A01).
- NCEER-88-0034 "Seismic Response of Pile Foundations," by S.M. Mamoon, P.K. Banerjee and S. Ahmad, 11/1/88, (PB89-145239, A04, MF-A01).
- NCEER-88-0035 "Modeling of R/C Building Structures With Flexible Floor Diaphragms (IDARC2)," by A.M. Reinhorn, S.K. Kunnath and N. Panahshahi, 9/7/88, (PB89-207153, A07, MF-A01).
- NCEER-88-0036 "Solution of the Dam-Reservoir Interaction Problem Using a Combination of FEM, BEM with Particular Integrals, Modal Analysis, and Substructuring," by C-S. Tsai, G.C. Lee and R.L. Ketter, 12/31/88, (PB89-207146, A04, MF-A01).
- NCEER-88-0037 "Optimal Placement of Actuators for Structural Control," by F.Y. Cheng and C.P. Pantelides, 8/15/88, (PB89-162846, A05, MF-A01).
- NCEER-88-0038 "Teflon Bearings in Aseismic Base Isolation: Experimental Studies and Mathematical Modeling," by A. Mokha, M.C. Constantinou and A.M. Reinhorn, 12/5/88, (PB89-218457, A10, MF-A01). This report is available only through NTIS (see address given above).
- NCEER-88-0039 "Seismic Behavior of Flat Slab High-Rise Buildings in the New York City Area," by P. Weidlinger and M. Ettouney, 10/15/88, (PB90-145681, A04, MF-A01).
- NCEER-88-0040 "Evaluation of the Earthquake Resistance of Existing Buildings in New York City," by P. Weidlinger and M. Ettouney, 10/15/88, to be published.
- NCEER-88-0041 "Small-Scale Modeling Techniques for Reinforced Concrete Structures Subjected to Seismic Loads," by W. Kim, A. El-Attar and R.N. White, 11/22/88, (PB89-189625, A05, MF-A01).
- NCEER-88-0042 "Modeling Strong Ground Motion from Multiple Event Earthquakes," by G.W. Ellis and A.S. Cakmak, 10/15/88, (PB89-174445, A03, MF-A01).

- NCEER-88-0043 "Nonstationary Models of Seismic Ground Acceleration," by M. Grigoriu, S.E. Ruiz and E. Rosenblueth, 7/15/88, (PB89-189617, A04, MF-A01).
- NCEER-88-0044 "SARCF User's Guide: Seismic Analysis of Reinforced Concrete Frames," by Y.S. Chung, C. Meyer and M. Shinozuka, 11/9/88, (PB89-174452, A08, MF-A01).
- NCEER-88-0045 "First Expert Panel Meeting on Disaster Research and Planning," edited by J. Pantelic and J. Stoyke, 9/15/88, (PB89-174460, A05, MF-A01).
- NCEER-88-0046 "Preliminary Studies of the Effect of Degrading Infill Walls on the Nonlinear Seismic Response of Steel Frames," by C.Z. Chrysostomou, P. Gergely and J.F. Abel, 12/19/88, (PB89-208383, A05, MF-A01).
- NCEER-88-0047 "Reinforced Concrete Frame Component Testing Facility - Design, Construction, Instrumentation and Operation," by S.P. Pessiki, C. Conley, T. Bond, P. Gergely and R.N. White, 12/16/88, (PB89-174478, A04, MF-A01).
- NCEER-89-0001 "Effects of Protective Cushion and Soil Compliancy on the Response of Equipment Within a Seismically Excited Building," by J.A. HoLung, 2/16/89, (PB89-207179, A04, MF-A01).
- NCEER-89-0002 "Statistical Evaluation of Response Modification Factors for Reinforced Concrete Structures," by H.H-M. Hwang and J-W. Jaw, 2/17/89, (PB89-207187, A05, MF-A01).
- NCEER-89-0003 "Hysteretic Columns Under Random Excitation," by G-Q. Cai and Y.K. Lin, 1/9/89, (PB89-196513, A03, MF-A01).
- NCEER-89-0004 "Experimental Study of 'Elephant Foot Bulge' Instability of Thin-Walled Metal Tanks," by Z-H. Jia and R.L. Ketter, 2/22/89, (PB89-207195, A03, MF-A01).
- NCEER-89-0005 "Experiment on Performance of Buried Pipelines Across San Andreas Fault," by J. Isenberg, E. Richardson and T.D. O'Rourke, 3/10/89, (PB89-218440, A04, MF-A01). This report is available only through NTIS (see address given above).
- NCEER-89-0006 "A Knowledge-Based Approach to Structural Design of Earthquake-Resistant Buildings," by M. Subramani, P. Gergely, C.H. Conley, J.F. Abel and A.H. Zaghaw, 1/15/89, (PB89-218465, A06, MF-A01).
- NCEER-89-0007 "Liquefaction Hazards and Their Effects on Buried Pipelines," by T.D. O'Rourke and P.A. Lane, 2/1/89, (PB89-218481, A09, MF-A01).
- NCEER-89-0008 "Fundamentals of System Identification in Structural Dynamics," by H. Imai, C-B. Yun, O. Maruyama and M. Shinozuka, 1/26/89, (PB89-207211, A04, MF-A01).
- NCEER-89-0009 "Effects of the 1985 Michoacan Earthquake on Water Systems and Other Buried Lifelines in Mexico," by A.G. Ayala and M.J. O'Rourke, 3/8/89, (PB89-207229, A06, MF-A01).
- NCEER-89-R010 "NCEER Bibliography of Earthquake Education Materials," by K.E.K. Ross, Second Revision, 9/1/89, (PB90-125352, A05, MF-A01). This report is replaced by NCEER-92-0018.
- NCEER-89-0011 "Inelastic Three-Dimensional Response Analysis of Reinforced Concrete Building Structures (IDARC-3D), Part I - Modeling," by S.K. Kunnath and A.M. Reinhorn, 4/17/89, (PB90-114612, A07, MF-A01). This report is available only through NTIS (see address given above).
- NCEER-89-0012 "Recommended Modifications to ATC-14," by C.D. Poland and J.O. Malley, 4/12/89, (PB90-108648, A15, MF-A01).
- NCEER-89-0013 "Repair and Strengthening of Beam-to-Column Connections Subjected to Earthquake Loading," by M. Corazao and A.J. Durrani, 2/28/89, (PB90-109885, A06, MF-A01).
- NCEER-89-0014 "Program EXKAL2 for Identification of Structural Dynamic Systems," by O. Maruyama, C-B. Yun, M. Hoshiya and M. Shinozuka, 5/19/89, (PB90-109877, A09, MF-A01).

- NCEER-89-0015 "Response of Frames With Bolted Semi-Rigid Connections, Part I - Experimental Study and Analytical Predictions," by P.J. DiCorso, A.M. Reinhorn, J.R. Dickerson, J.B. Radzinski and W.L. Harper, 6/1/89, to be published.
- NCEER-89-0016 "ARMA Monte Carlo Simulation in Probabilistic Structural Analysis," by P.D. Spanos and M.P. Mignolet, 7/10/89, (PB90-109893, A03, MF-A01).
- NCEER-89-P017 "Preliminary Proceedings from the Conference on Disaster Preparedness - The Place of Earthquake Education in Our Schools," Edited by K.E.K. Ross, 6/23/89, (PB90-108606, A03, MF-A01).
- NCEER-89-0017 "Proceedings from the Conference on Disaster Preparedness - The Place of Earthquake Education in Our Schools," Edited by K.E.K. Ross, 12/31/89, (PB90-207895, A012, MF-A02). This report is available only through NTIS (see address given above).
- NCEER-89-0018 "Multidimensional Models of Hysteretic Material Behavior for Vibration Analysis of Shape Memory Energy Absorbing Devices, by E.J. Graesser and F.A. Cozzarelli, 6/7/89, (PB90-164146, A04, MF-A01).
- NCEER-89-0019 "Nonlinear Dynamic Analysis of Three-Dimensional Base Isolated Structures (3D-BASIS)," by S. Nagarajaiah, A.M. Reinhorn and M.C. Constantinou, 8/3/89, (PB90-161936, A06, MF-A01). This report has been replaced by NCEER-93-0011.
- NCEER-89-0020 "Structural Control Considering Time-Rate of Control Forces and Control Rate Constraints," by F.Y. Cheng and C.P. Pantelides, 8/3/89, (PB90-120445, A04, MF-A01).
- NCEER-89-0021 "Subsurface Conditions of Memphis and Shelby County," by K.W. Ng, T-S. Chang and H-H.M. Hwang, 7/26/89, (PB90-120437, A03, MF-A01).
- NCEER-89-0022 "Seismic Wave Propagation Effects on Straight Jointed Buried Pipelines," by K. Elhadi and M.J. O'Rourke, 8/24/89, (PB90-162322, A10, MF-A02).
- NCEER-89-0023 "Workshop on Serviceability Analysis of Water Delivery Systems," edited by M. Grigoriu, 3/6/89, (PB90-127424, A03, MF-A01).
- NCEER-89-0024 "Shaking Table Study of a 1/5 Scale Steel Frame Composed of Tapered Members," by K.C. Chang, J.S. Hwang and G.C. Lee, 9/18/89, (PB90-160169, A04, MF-A01).
- NCEER-89-0025 "DYNA1D: A Computer Program for Nonlinear Seismic Site Response Analysis - Technical Documentation," by Jean H. Prevost, 9/14/89, (PB90-161944, A07, MF-A01). This report is available only through NTIS (see address given above).
- NCEER-89-0026 "1:4 Scale Model Studies of Active Tendon Systems and Active Mass Dampers for Aseismic Protection," by A.M. Reinhorn, T.T. Soong, R.C. Lin, Y.P. Yang, Y. Fukao, H. Abe and M. Nakai, 9/15/89, (PB90-173246, A10, MF-A02). This report is available only through NTIS (see address given above).
- NCEER-89-0027 "Scattering of Waves by Inclusions in a Nonhomogeneous Elastic Half Space Solved by Boundary Element Methods," by P.K. Hadley, A. Askar and A.S. Cakmak, 6/15/89, (PB90-145699, A07, MF-A01).
- NCEER-89-0028 "Statistical Evaluation of Deflection Amplification Factors for Reinforced Concrete Structures," by H.H.M. Hwang, J-W. Jaw and A.L. Ch'ng, 8/31/89, (PB90-164633, A05, MF-A01).
- NCEER-89-0029 "Bedrock Accelerations in Memphis Area Due to Large New Madrid Earthquakes," by H.H.M. Hwang, C.H.S. Chen and G. Yu, 11/7/89, (PB90-162330, A04, MF-A01).
- NCEER-89-0030 "Seismic Behavior and Response Sensitivity of Secondary Structural Systems," by Y.Q. Chen and T.T. Soong, 10/23/89, (PB90-164658, A08, MF-A01).
- NCEER-89-0031 "Random Vibration and Reliability Analysis of Primary-Secondary Structural Systems," by Y. Ibrahim, M. Grigoriu and T.T. Soong, 11/10/89, (PB90-161951, A04, MF-A01).



- NCEER-89-0032 "Proceedings from the Second U.S. - Japan Workshop on Liquefaction, Large Ground Deformation and Their Effects on Lifelines, September 26-29, 1989," Edited by T.D. O'Rourke and M. Hamada, 12/1/89, (PB90-209388, A22, MF-A03).
- NCEER-89-0033 "Deterministic Model for Seismic Damage Evaluation of Reinforced Concrete Structures," by J.M. Bracci, A.M. Reinhorn, J.B. Mander and S.K. Kunnath, 9/27/89, (PB91-108803, A06, MF-A01).
- NCEER-89-0034 "On the Relation Between Local and Global Damage Indices," by E. DiPasquale and A.S. Cakmak, 8/15/89, (PB90-173865, A05, MF-A01).
- NCEER-89-0035 "Cyclic Undrained Behavior of Nonplastic and Low Plasticity Silts," by A.J. Walker and H.E. Stewart, 7/26/89, (PB90-183518, A10, MF-A01).
- NCEER-89-0036 "Liquefaction Potential of Surficial Deposits in the City of Buffalo, New York," by M. Budhu, R. Giese and L. Baumgrass, 1/17/89, (PB90-208455, A04, MF-A01).
- NCEER-89-0037 "A Deterministic Assessment of Effects of Ground Motion Incoherence," by A.S. Veletsos and Y. Tang, 7/15/89, (PB90-164294, A03, MF-A01).
- NCEER-89-0038 "Workshop on Ground Motion Parameters for Seismic Hazard Mapping," July 17-18, 1989, edited by R.V. Whitman, 12/1/89, (PB90-173923, A04, MF-A01).
- NCEER-89-0039 "Seismic Effects on Elevated Transit Lines of the New York City Transit Authority," by C.J. Costantino, C.A. Miller and E. Heymsfield, 12/26/89, (PB90-207887, A06, MF-A01).
- NCEER-89-0040 "Centrifugal Modeling of Dynamic Soil-Structure Interaction," by K. Weissman, Supervised by J.H. Prevost, 5/10/89, (PB90-207879, A07, MF-A01).
- NCEER-89-0041 "Linearized Identification of Buildings With Cores for Seismic Vulnerability Assessment," by I-K. Ho and A.E. Aktan, 11/1/89, (PB90-251943, A07, MF-A01).
- NCEER-90-0001 "Geotechnical and Lifeline Aspects of the October 17, 1989 Loma Prieta Earthquake in San Francisco," by T.D. O'Rourke, H.E. Stewart, F.T. Blackburn and T.S. Dickerman, 1/90, (PB90-208596, A05, MF-A01).
- NCEER-90-0002 "Nonnormal Secondary Response Due to Yielding in a Primary Structure," by D.C.K. Chen and L.D. Lutes, 2/28/90, (PB90-251976, A07, MF-A01).
- NCEER-90-0003 "Earthquake Education Materials for Grades K-12," by K.E.K. Ross, 4/16/90, (PB91-251984, A05, MF-A05). This report has been replaced by NCEER-92-0018.
- NCEER-90-0004 "Catalog of Strong Motion Stations in Eastern North America," by R.W. Busby, 4/3/90, (PB90-251984, A05, MF-A01).
- NCEER-90-0005 "NCEER Strong-Motion Data Base: A User Manual for the GeoBase Release (Version 1.0 for the Sun3)," by P. Friberg and K. Jacob, 3/31/90 (PB90-258062, A04, MF-A01).
- NCEER-90-0006 "Seismic Hazard Along a Crude Oil Pipeline in the Event of an 1811-1812 Type New Madrid Earthquake," by H.H.M. Hwang and C-H.S. Chen, 4/16/90, (PB90-258054, A04, MF-A01).
- NCEER-90-0007 "Site-Specific Response Spectra for Memphis Sheahan Pumping Station," by H.H.M. Hwang and C.S. Lee, 5/15/90, (PB91-108811, A05, MF-A01).
- NCEER-90-0008 "Pilot Study on Seismic Vulnerability of Crude Oil Transmission Systems," by T. Ariman, R. Dobry, M. Grigoriu, F. Kozin, M. O'Rourke, T. O'Rourke and M. Shinozuka, 5/25/90, (PB91-108837, A06, MF-A01).
- NCEER-90-0009 "A Program to Generate Site Dependent Time Histories: EQGEN," by G.W. Ellis, M. Srinivasan and A.S. Cakmak, 1/30/90, (PB91-108829, A04, MF-A01).
- NCEER-90-0010 "Active Isolation for Seismic Protection of Operating Rooms," by M.E. Talbott, Supervised by M. Shinozuka, 6/8/9, (PB91-110205, A05, MF-A01).

- NCEER-90-0011 "Program LINEARID for Identification of Linear Structural Dynamic Systems," by C-B. Yun and M. Shinozuka, 6/25/90, (PB91-110312, A08, MF-A01).
- NCEER-90-0012 "Two-Dimensional Two-Phase Elasto-Plastic Seismic Response of Earth Dams," by A.N. Yiagos, Supervised by J.H. Prevost, 6/20/90, (PB91-110197, A13, MF-A02).
- NCEER-90-0013 "Secondary Systems in Base-Isolated Structures: Experimental Investigation, Stochastic Response and Stochastic Sensitivity," by G.D. Manolis, G. Juhn, M.C. Constantinou and A.M. Reinhorn, 7/1/90, (PB91-110320, A08, MF-A01).
- NCEER-90-0014 "Seismic Behavior of Lightly-Reinforced Concrete Column and Beam-Column Joint Details," by S.P. Pessiki, C.H. Conley, P. Gergely and R.N. White, 8/22/90, (PB91-108795, A11, MF-A02).
- NCEER-90-0015 "Two Hybrid Control Systems for Building Structures Under Strong Earthquakes," by J.N. Yang and A. Daniellians, 6/29/90, (PB91-125393, A04, MF-A01).
- NCEER-90-0016 "Instantaneous Optimal Control with Acceleration and Velocity Feedback," by J.N. Yang and Z. Li, 6/29/90, (PB91-125401, A03, MF-A01).
- NCEER-90-0017 "Reconnaissance Report on the Northern Iran Earthquake of June 21, 1990," by M. Mehrain, 10/4/90, (PB91-125377, A03, MF-A01).
- NCEER-90-0018 "Evaluation of Liquefaction Potential in Memphis and Shelby County," by T.S. Chang, P.S. Tang, C.S. Lee and H. Hwang, 8/10/90, (PB91-125427, A09, MF-A01).
- NCEER-90-0019 "Experimental and Analytical Study of a Combined Sliding Disc Bearing and Helical Steel Spring Isolation System," by M.C. Constantinou, A.S. Mokha and A.M. Reinhorn, 10/4/90, (PB91-125385, A06, MF-A01). This report is available only through NTIS (see address given above).
- NCEER-90-0020 "Experimental Study and Analytical Prediction of Earthquake Response of a Sliding Isolation System with a Spherical Surface," by A.S. Mokha, M.C. Constantinou and A.M. Reinhorn, 10/11/90, (PB91-125419, A05, MF-A01).
- NCEER-90-0021 "Dynamic Interaction Factors for Floating Pile Groups," by G. Gazetas, K. Fan, A. Kaynia and E. Kausel, 9/10/90, (PB91-170381, A05, MF-A01).
- NCEER-90-0022 "Evaluation of Seismic Damage Indices for Reinforced Concrete Structures," by S. Rodriguez-Gomez and A.S. Cakmak, 9/30/90, PB91-171322, A06, MF-A01).
- NCEER-90-0023 "Study of Site Response at a Selected Memphis Site," by H. Desai, S. Ahmad, E.S. Gazetas and M.R. Oh, 10/11/90, (PB91-196857, A03, MF-A01).
- NCEER-90-0024 "A User's Guide to Strongmo: Version 1.0 of NCEER's Strong-Motion Data Access Tool for PCs and Terminals," by P.A. Friberg and C.A.T. Susch, 11/15/90, (PB91-171272, A03, MF-A01).
- NCEER-90-0025 "A Three-Dimensional Analytical Study of Spatial Variability of Seismic Ground Motions," by L-L. Hong and A.H.-S. Ang, 10/30/90, (PB91-170399, A09, MF-A01).
- NCEER-90-0026 "MUMOID User's Guide - A Program for the Identification of Modal Parameters," by S. Rodriguez-Gomez and E. DiPasquale, 9/30/90, (PB91-171298, A04, MF-A01).
- NCEER-90-0027 "SARCF-II User's Guide - Seismic Analysis of Reinforced Concrete Frames," by S. Rodriguez-Gomez, Y.S. Chung and C. Meyer, 9/30/90, (PB91-171280, A05, MF-A01).
- NCEER-90-0028 "Viscous Dampers: Testing, Modeling and Application in Vibration and Seismic Isolation," by N. Makris and M.C. Constantinou, 12/20/90 (PB91-190561, A06, MF-A01).
- NCEER-90-0029 "Soil Effects on Earthquake Ground Motions in the Memphis Area," by H. Hwang, C.S. Lee, K.W. Ng and T.S. Chang, 8/2/90, (PB91-190751, A05, MF-A01).

- NCEER-91-0001 "Proceedings from the Third Japan-U.S. Workshop on Earthquake Resistant Design of Lifeline Facilities and Countermeasures for Soil Liquefaction, December 17-19, 1990," edited by T.D. O'Rourke and M. Hamada, 2/1/91, (PB91-179259, A99, MF-A04).
- NCEER-91-0002 "Physical Space Solutions of Non-Proportionally Damped Systems," by M. Tong, Z. Liang and G.C. Lee, 1/15/91, (PB91-179242, A04, MF-A01).
- NCEER-91-0003 "Seismic Response of Single Piles and Pile Groups," by K. Fan and G. Gazetas, 1/10/91, (PB92-174994, A04, MF-A01).
- NCEER-91-0004 "Damping of Structures: Part 1 - Theory of Complex Damping," by Z. Liang and G. Lee, 10/10/91, (PB92-197235, A12, MF-A03).
- NCEER-91-0005 "3D-BASIS - Nonlinear Dynamic Analysis of Three Dimensional Base Isolated Structures: Part II," by S. Nagarajaiah, A.M. Reinhorn and M.C. Constantinou, 2/28/91, (PB91-190553, A07, MF-A01). This report has been replaced by NCEER-93-0011.
- NCEER-91-0006 "A Multidimensional Hysteretic Model for Plasticity Deforming Metals in Energy Absorbing Devices," by E.J. Graesser and F.A. Cozzarelli, 4/9/91, (PB92-108364, A04, MF-A01).
- NCEER-91-0007 "A Framework for Customizable Knowledge-Based Expert Systems with an Application to a KBES for Evaluating the Seismic Resistance of Existing Buildings," by E.G. Ibarra-Anaya and S.J. Fennes, 4/9/91, (PB91-210930, A08, MF-A01).
- NCEER-91-0008 "Nonlinear Analysis of Steel Frames with Semi-Rigid Connections Using the Capacity Spectrum Method," by G.G. Deierlein, S-H. Hsieh, Y-J. Shen and J.F. Abel, 7/2/91, (PB92-113828, A05, MF-A01).
- NCEER-91-0009 "Earthquake Education Materials for Grades K-12," by K.E.K. Ross, 4/30/91, (PB91-212142, A06, MF-A01). This report has been replaced by NCEER-92-0018.
- NCEER-91-0010 "Phase Wave Velocities and Displacement Phase Differences in a Harmonically Oscillating Pile," by N. Makris and G. Gazetas, 7/8/91, (PB92-108356, A04, MF-A01).
- NCEER-91-0011 "Dynamic Characteristics of a Full-Size Five-Story Steel Structure and a 2/5 Scale Model," by K.C. Chang, G.C. Yao, G.C. Lee, D.S. Hao and Y.C. Yeh," 7/2/91, (PB93-116648, A06, MF-A02).
- NCEER-91-0012 "Seismic Response of a 2/5 Scale Steel Structure with Added Viscoelastic Dampers," by K.C. Chang, T.T. Soong, S-T. Oh and M.L. Lai, 5/17/91, (PB92-110816, A05, MF-A01).
- NCEER-91-0013 "Earthquake Response of Retaining Walls; Full-Scale Testing and Computational Modeling," by S. Alampalli and A-W.M. Elgamal, 6/20/91, to be published.
- NCEER-91-0014 "3D-BASIS-M: Nonlinear Dynamic Analysis of Multiple Building Base Isolated Structures," by P.C. Tsopelas, S. Nagarajaiah, M.C. Constantinou and A.M. Reinhorn, 5/28/91, (PB92-113885, A09, MF-A02).
- NCEER-91-0015 "Evaluation of SEAOC Design Requirements for Sliding Isolated Structures," by D. Theodossiou and M.C. Constantinou, 6/10/91, (PB92-114602, A11, MF-A03).
- NCEER-91-0016 "Closed-Loop Modal Testing of a 27-Story Reinforced Concrete Flat Plate-Core Building," by H.R. Somaprasad, T. Toksoy, H. Yoshiyuki and A.E. Aktan, 7/15/91, (PB92-129980, A07, MF-A02).
- NCEER-91-0017 "Shake Table Test of a 1/6 Scale Two-Story Lightly Reinforced Concrete Building," by A.G. El-Attar, R.N. White and P. Gergely, 2/28/91, (PB92-222447, A06, MF-A02).
- NCEER-91-0018 "Shake Table Test of a 1/8 Scale Three-Story Lightly Reinforced Concrete Building," by A.G. El-Attar, R.N. White and P. Gergely, 2/28/91, (PB93-116630, A08, MF-A02).
- NCEER-91-0019 "Transfer Functions for Rigid Rectangular Foundations," by A.S. Veletsos, A.M. Prasad and W.H. Wu, 7/31/91, to be published.

- NCEER-91-0020 "Hybrid Control of Seismic-Excited Nonlinear and Inelastic Structural Systems," by J.N. Yang, Z. Li and A. Daniellians, 8/1/91, (PB92-143171, A06, MF-A02).
- NCEER-91-0021 "The NCEER-91 Earthquake Catalog: Improved Intensity-Based Magnitudes and Recurrence Relations for U.S. Earthquakes East of New Madrid," by L. Seeber and J.G. Armbruster, 8/28/91, (PB92-176742, A06, MF-A02).
- NCEER-91-0022 "Proceedings from the Implementation of Earthquake Planning and Education in Schools: The Need for Change - The Roles of the Changemakers," by K.E.K. Ross and F. Winslow, 7/23/91, (PB92-129998, A12, MF-A03).
- NCEER-91-0023 "A Study of Reliability-Based Criteria for Seismic Design of Reinforced Concrete Frame Buildings," by H.H.M. Hwang and H-M. Hsu, 8/10/91, (PB92-140235, A09, MF-A02).
- NCEER-91-0024 "Experimental Verification of a Number of Structural System Identification Algorithms," by R.G. Ghanem, H. Gavin and M. Shinozuka, 9/18/91, (PB92-176577, A18, MF-A04).
- NCEER-91-0025 "Probabilistic Evaluation of Liquefaction Potential," by H.H.M. Hwang and C.S. Lee, 11/25/91, (PB92-143429, A05, MF-A01).
- NCEER-91-0026 "Instantaneous Optimal Control for Linear, Nonlinear and Hysteretic Structures - Stable Controllers," by J.N. Yang and Z. Li, 11/15/91, (PB92-163807, A04, MF-A01).
- NCEER-91-0027 "Experimental and Theoretical Study of a Sliding Isolation System for Bridges," by M.C. Constantinou, A. Kartoum, A.M. Reinhorn and P. Bradford, 11/15/91, (PB92-176973, A10, MF-A03).
- NCEER-92-0001 "Case Studies of Liquefaction and Lifeline Performance During Past Earthquakes, Volume 1: Japanese Case Studies," Edited by M. Hamada and T. O'Rourke, 2/17/92, (PB92-197243, A18, MF-A04).
- NCEER-92-0002 "Case Studies of Liquefaction and Lifeline Performance During Past Earthquakes, Volume 2: United States Case Studies," Edited by T. O'Rourke and M. Hamada, 2/17/92, (PB92-197250, A20, MF-A04).
- NCEER-92-0003 "Issues in Earthquake Education," Edited by K. Ross, 2/3/92, (PB92-222389, A07, MF-A02).
- NCEER-92-0004 "Proceedings from the First U.S. - Japan Workshop on Earthquake Protective Systems for Bridges," Edited by I.G. Buckle, 2/4/92, (PB94-142239, A99, MF-A06).
- NCEER-92-0005 "Seismic Ground Motion from a Haskell-Type Source in a Multiple-Layered Half-Space," A.P. Theoharis, G. Deodatis and M. Shinozuka, 1/2/92, to be published.
- NCEER-92-0006 "Proceedings from the Site Effects Workshop," Edited by R. Whitman, 2/29/92, (PB92-197201, A04, MF-A01).
- NCEER-92-0007 "Engineering Evaluation of Permanent Ground Deformations Due to Seismically-Induced Liquefaction," by M.H. Baziar, R. Dobry and A-W.M. Elgamal, 3/24/92, (PB92-222421, A13, MF-A03).
- NCEER-92-0008 "A Procedure for the Seismic Evaluation of Buildings in the Central and Eastern United States," by C.D. Poland and J.O. Malley, 4/2/92, (PB92-222439, A20, MF-A04).
- NCEER-92-0009 "Experimental and Analytical Study of a Hybrid Isolation System Using Friction Controllable Sliding Bearings," by M.Q. Feng, S. Fujii and M. Shinozuka, 5/15/92, (PB93-150282, A06, MF-A02).
- NCEER-92-0010 "Seismic Resistance of Slab-Column Connections in Existing Non-Ductile Flat-Plate Buildings," by A.J. Durrani and Y. Du, 5/18/92, (PB93-116812, A06, MF-A02).
- NCEER-92-0011 "The Hysteretic and Dynamic Behavior of Brick Masonry Walls Upgraded by Ferrocement Coatings Under Cyclic Loading and Strong Simulated Ground Motion," by H. Lee and S.P. Prawl, 5/11/92, to be published.
- NCEER-92-0012 "Study of Wire Rope Systems for Seismic Protection of Equipment in Buildings," by G.F. Demetriades, M.C. Constantinou and A.M. Reinhorn, 5/20/92, (PB93-116655, A08, MF-A02).

- NCEER-92-0013 "Shape Memory Structural Dampers: Material Properties, Design and Seismic Testing," by P.R. Witting and F.A. Cozzarelli, 5/26/92, (PB93-116663, A05, MF-A01).
- NCEER-92-0014 "Longitudinal Permanent Ground Deformation Effects on Buried Continuous Pipelines," by M.J. O'Rourke, and C. Nordberg, 6/15/92, (PB93-116671, A08, MF-A02).
- NCEER-92-0015 "A Simulation Method for Stationary Gaussian Random Functions Based on the Sampling Theorem," by M. Grigoriu and S. Balopoulou, 6/11/92, (PB93-127496, A05, MF-A01).
- NCEER-92-0016 "Gravity-Load-Designed Reinforced Concrete Buildings: Seismic Evaluation of Existing Construction and Detailing Strategies for Improved Seismic Resistance," by G.W. Hoffmann, S.K. Kunnath, A.M. Reinhorn and J.B. Mander, 7/15/92, (PB94-142007, A08, MF-A02).
- NCEER-92-0017 "Observations on Water System and Pipeline Performance in the Limón Area of Costa Rica Due to the April 22, 1991 Earthquake," by M. O'Rourke and D. Ballantyne, 6/30/92, (PB93-126811, A06, MF-A02).
- NCEER-92-0018 "Fourth Edition of Earthquake Education Materials for Grades K-12," Edited by K.E.K. Ross, 8/10/92, (PB93-114023, A07, MF-A02).
- NCEER-92-0019 "Proceedings from the Fourth Japan-U.S. Workshop on Earthquake Resistant Design of Lifeline Facilities and Countermeasures for Soil Liquefaction," Edited by M. Hamada and T.D. O'Rourke, 8/12/92, (PB93-163939, A99, MF-E11).
- NCEER-92-0020 "Active Bracing System: A Full Scale Implementation of Active Control," by A.M. Reinhorn, T.T. Soong, R.C. Lin, M.A. Riley, Y.P. Wang, S. Aizawa and M. Higashino, 8/14/92, (PB93-127512, A06, MF-A02).
- NCEER-92-0021 "Empirical Analysis of Horizontal Ground Displacement Generated by Liquefaction-Induced Lateral Spreads," by S.F. Bartlett and T.L. Youd, 8/17/92, (PB93-188241, A06, MF-A02).
- NCEER-92-0022 "IDARC Version 3.0: Inelastic Damage Analysis of Reinforced Concrete Structures," by S.K. Kunnath, A.M. Reinhorn and R.F. Lobo, 8/31/92, (PB93-227502, A07, MF-A02).
- NCEER-92-0023 "A Semi-Empirical Analysis of Strong-Motion Peaks in Terms of Seismic Source, Propagation Path and Local Site Conditions, by M. Kamiyama, M.J. O'Rourke and R. Flores-Berrones, 9/9/92, (PB93-150266, A08, MF-A02).
- NCEER-92-0024 "Seismic Behavior of Reinforced Concrete Frame Structures with Nonductile Details, Part I: Summary of Experimental Findings of Full Scale Beam-Column Joint Tests," by A. Beres, R.N. White and P. Gergely, 9/30/92, (PB93-227783, A05, MF-A01).
- NCEER-92-0025 "Experimental Results of Repaired and Retrofitted Beam-Column Joint Tests in Lightly Reinforced Concrete Frame Buildings," by A. Beres, S. El-Borgi, R.N. White and P. Gergely, 10/29/92, (PB93-227791, A05, MF-A01).
- NCEER-92-0026 "A Generalization of Optimal Control Theory: Linear and Nonlinear Structures," by J.N. Yang, Z. Li and S. Vongchavalitkul, 11/2/92, (PB93-188621, A05, MF-A01).
- NCEER-92-0027 "Seismic Resistance of Reinforced Concrete Frame Structures Designed Only for Gravity Loads: Part I - Design and Properties of a One-Third Scale Model Structure," by J.M. Bracci, A.M. Reinhorn and J.B. Mander, 12/1/92, (PB94-104502, A08, MF-A02).
- NCEER-92-0028 "Seismic Resistance of Reinforced Concrete Frame Structures Designed Only for Gravity Loads: Part II - Experimental Performance of Subassemblages," by L.E. Aycaardi, J.B. Mander and A.M. Reinhorn, 12/1/92, (PB94-104510, A08, MF-A02).
- NCEER-92-0029 "Seismic Resistance of Reinforced Concrete Frame Structures Designed Only for Gravity Loads: Part III - Experimental Performance and Analytical Study of a Structural Model," by J.M. Bracci, A.M. Reinhorn and J.B. Mander, 12/1/92, (PB93-227528, A09, MF-A01).

- NCEER-92-0030 "Evaluation of Seismic Retrofit of Reinforced Concrete Frame Structures: Part I - Experimental Performance of Retrofitted Subassemblages," by D. Choudhuri, J.B. Mander and A.M. Reinhorn, 12/8/92, (PB93-198307, A07, MF-A02).
- NCEER-92-0031 "Evaluation of Seismic Retrofit of Reinforced Concrete Frame Structures: Part II - Experimental Performance and Analytical Study of a Retrofitted Structural Model," by J.M. Bracci, A.M. Reinhorn and J.B. Mander, 12/8/92, (PB93-198315, A09, MF-A03).
- NCEER-92-0032 "Experimental and Analytical Investigation of Seismic Response of Structures with Supplemental Fluid Viscous Dampers," by M.C. Constantinou and M.D. Symans, 12/21/92, (PB93-191435, A10, MF-A03). This report is available only through NTIS (see address given above).
- NCEER-92-0033 "Reconnaissance Report on the Cairo, Egypt Earthquake of October 12, 1992," by M. Khater, 12/23/92, (PB93-188621, A03, MF-A01).
- NCEER-92-0034 "Low-Level Dynamic Characteristics of Four Tall Flat-Plate Buildings in New York City," by H. Gavin, S. Yuan, J. Grossman, E. Pekelis and K. Jacob, 12/28/92, (PB93-188217, A07, MF-A02).
- NCEER-93-0001 "An Experimental Study on the Seismic Performance of Brick-Infilled Steel Frames With and Without Retrofit," by J.B. Mander, B. Nair, K. Wojtkowski and J. Ma, 1/29/93, (PB93-227510, A07, MF-A02).
- NCEER-93-0002 "Social Accounting for Disaster Preparedness and Recovery Planning," by S. Cole, E. Pantoja and V. Razak, 2/22/93, (PB94-142114, A12, MF-A03).
- NCEER-93-0003 "Assessment of 1991 NEHRP Provisions for Nonstructural Components and Recommended Revisions," by T.T. Soong, G. Chen, Z. Wu, R-H. Zhang and M. Grigoriu, 3/1/93, (PB93-188639, A06, MF-A02).
- NCEER-93-0004 "Evaluation of Static and Response Spectrum Analysis Procedures of SEAOC/UBC for Seismic Isolated Structures," by C.W. Winters and M.C. Constantinou, 3/23/93, (PB93-198299, A10, MF-A03).
- NCEER-93-0005 "Earthquakes in the Northeast - Are We Ignoring the Hazard? A Workshop on Earthquake Science and Safety for Educators," edited by K.E.K. Ross, 4/2/93, (PB94-103066, A09, MF-A02).
- NCEER-93-0006 "Inelastic Response of Reinforced Concrete Structures with Viscoelastic Braces," by R.F. Lobo, J.M. Bracci, K.L. Shen, A.M. Reinhorn and T.T. Soong, 4/5/93, (PB93-227486, A05, MF-A02).
- NCEER-93-0007 "Seismic Testing of Installation Methods for Computers and Data Processing Equipment," by K. Kosar, T.T. Soong, K.L. Shen, J.A. HoLung and Y.K. Lin, 4/12/93, (PB93-198299, A07, MF-A02).
- NCEER-93-0008 "Retrofit of Reinforced Concrete Frames Using Added Dampers," by A. Reinhorn, M. Constantinou and C. Li, to be published.
- NCEER-93-0009 "Seismic Behavior and Design Guidelines for Steel Frame Structures with Added Viscoelastic Dampers," by K.C. Chang, M.L. Lai, T.T. Soong, D.S. Hao and Y.C. Yeh, 5/1/93, (PB94-141959, A07, MF-A02).
- NCEER-93-0010 "Seismic Performance of Shear-Critical Reinforced Concrete Bridge Piers," by J.B. Mander, S.M. Waheed, M.T.A. Chaudhary and S.S. Chen, 5/12/93, (PB93-227494, A08, MF-A02).
- NCEER-93-0011 "3D-BASIS-TABS: Computer Program for Nonlinear Dynamic Analysis of Three Dimensional Base Isolated Structures," by S. Nagarajaiah, C. Li, A.M. Reinhorn and M.C. Constantinou, 8/2/93, (PB94-141819, A09, MF-A02).
- NCEER-93-0012 "Effects of Hydrocarbon Spills from an Oil Pipeline Break on Ground Water," by O.J. Helweg and H.H.M. Hwang, 8/3/93, (PB94-141942, A06, MF-A02).
- NCEER-93-0013 "Simplified Procedures for Seismic Design of Nonstructural Components and Assessment of Current Code Provisions," by M.P. Singh, L.E. Suarez, E.E. Matheu and G.O. Maldonado, 8/4/93, (PB94-141827, A09, MF-A02).
- NCEER-93-0014 "An Energy Approach to Seismic Analysis and Design of Secondary Systems," by G. Chen and T.T. Soong, 8/6/93, (PB94-142767, A11, MF-A03).

- NCEER-93-0015 "Proceedings from School Sites: Becoming Prepared for Earthquakes - Commemorating the Third Anniversary of the Loma Prieta Earthquake," Edited by F.E. Winslow and K.E.K. Ross, 8/16/93, (PB94-154275, A16, MF-A02).
- NCEER-93-0016 "Reconnaissance Report of Damage to Historic Monuments in Cairo, Egypt Following the October 12, 1992 Dahshur Earthquake," by D. Sykora, D. Look, G. Croci, E. Karaesmen and E. Karaesmen, 8/19/93, (PB94-142221, A08, MF-A02).
- NCEER-93-0017 "The Island of Guam Earthquake of August 8, 1993," by S.W. Swan and S.K. Harris, 9/30/93, (PB94-141843, A04, MF-A01).
- NCEER-93-0018 "Engineering Aspects of the October 12, 1992 Egyptian Earthquake," by A.W. Elgamal, M. Amer, K. Adalier and A. Abul-Fadl, 10/7/93, (PB94-141983, A05, MF-A01).
- NCEER-93-0019 "Development of an Earthquake Motion Simulator and its Application in Dynamic Centrifuge Testing," by I. Krstelj, Supervised by J.H. Prevost, 10/23/93, (PB94-181773, A-10, MF-A03).
- NCEER-93-0020 "NCEER-Taisei Corporation Research Program on Sliding Seismic Isolation Systems for Bridges: Experimental and Analytical Study of a Friction Pendulum System (FPS)," by M.C. Constantinou, P. Tsopelas, Y-S. Kim and S. Okamoto, 11/1/93, (PB94-142775, A08, MF-A02).
- NCEER-93-0021 "Finite Element Modeling of Elastomeric Seismic Isolation Bearings," by L.J. Billings, Supervised by R. Shepherd, 11/8/93, to be published.
- NCEER-93-0022 "Seismic Vulnerability of Equipment in Critical Facilities: Life-Safety and Operational Consequences," by K. Porter, G.S. Johnson, M.M. Zadeh, C. Scawthorn and S. Eder, 11/24/93, (PB94-181765, A16, MF-A03).
- NCEER-93-0023 "Hokkaido Nansei-oki, Japan Earthquake of July 12, 1993, by P.I. Yanev and C.R. Scawthorn, 12/23/93, (PB94-181500, A07, MF-A01).
- NCEER-94-0001 "An Evaluation of Seismic Serviceability of Water Supply Networks with Application to the San Francisco Auxiliary Water Supply System," by I. Markov, Supervised by M. Grigoriu and T. O'Rourke, 1/21/94, (PB94-204013, A07, MF-A02).
- NCEER-94-0002 "NCEER-Taisei Corporation Research Program on Sliding Seismic Isolation Systems for Bridges: Experimental and Analytical Study of Systems Consisting of Sliding Bearings, Rubber Restoring Force Devices and Fluid Dampers," Volumes I and II, by P. Tsopelas, S. Okamoto, M.C. Constantinou, D. Ozaki and S. Fujii, 2/4/94, (PB94-181740, A09, MF-A02 and PB94-181757, A12, MF-A03).
- NCEER-94-0003 "A Markov Model for Local and Global Damage Indices in Seismic Analysis," by S. Rahman and M. Grigoriu, 2/18/94, (PB94-206000, A12, MF-A03).
- NCEER-94-0004 "Proceedings from the NCEER Workshop on Seismic Response of Masonry Infills," edited by D.P. Abrams, 3/1/94, (PB94-180783, A07, MF-A02).
- NCEER-94-0005 "The Northridge, California Earthquake of January 17, 1994: General Reconnaissance Report," edited by J.D. Goltz, 3/11/94, (PB94-193943, A10, MF-A03).
- NCEER-94-0006 "Seismic Energy Based Fatigue Damage Analysis of Bridge Columns: Part I - Evaluation of Seismic Capacity," by G.A. Chang and J.B. Mander, 3/14/94, (PB94-219185, A11, MF-A03).
- NCEER-94-0007 "Seismic Isolation of Multi-Story Frame Structures Using Spherical Sliding Isolation Systems," by T.M. Al-Hussaini, V.A. Zayas and M.C. Constantinou, 3/17/94, (PB94-193745, A09, MF-A02).
- NCEER-94-0008 "The Northridge, California Earthquake of January 17, 1994: Performance of Highway Bridges," edited by I.G. Buckle, 3/24/94, (PB94-193851, A06, MF-A02).
- NCEER-94-0009 "Proceedings of the Third U.S.-Japan Workshop on Earthquake Protective Systems for Bridges," edited by I.G. Buckle and I. Friedland, 3/31/94, (PB94-195815, A99, MF-A06).

- NCEER-94-0010 "3D-BASIS-ME: Computer Program for Nonlinear Dynamic Analysis of Seismically Isolated Single and Multiple Structures and Liquid Storage Tanks," by P.C. Tsopelas, M.C. Constantinou and A.M. Reinhorn, 4/12/94, (PB94-204922, A09, MF-A02).
- NCEER-94-0011 "The Northridge, California Earthquake of January 17, 1994: Performance of Gas Transmission Pipelines," by T.D. O'Rourke and M.C. Palmer, 5/16/94, (PB94-204989, A05, MF-A01).
- NCEER-94-0012 "Feasibility Study of Replacement Procedures and Earthquake Performance Related to Gas Transmission Pipelines," by T.D. O'Rourke and M.C. Palmer, 5/25/94, (PB94-206638, A09, MF-A02).
- NCEER-94-0013 "Seismic Energy Based Fatigue Damage Analysis of Bridge Columns: Part II - Evaluation of Seismic Demand," by G.A. Chang and J.B. Mander, 6/1/94, (PB95-18106, A08, MF-A02).
- NCEER-94-0014 "NCEER-Taisei Corporation Research Program on Sliding Seismic Isolation Systems for Bridges: Experimental and Analytical Study of a System Consisting of Sliding Bearings and Fluid Restoring Force/Damping Devices," by P. Tsopelas and M.C. Constantinou, 6/13/94, (PB94-219144, A10, MF-A03).
- NCEER-94-0015 "Generation of Hazard-Consistent Fragility Curves for Seismic Loss Estimation Studies," by H. Hwang and J-R. Huo, 6/14/94, (PB95-181996, A09, MF-A02).
- NCEER-94-0016 "Seismic Study of Building Frames with Added Energy-Absorbing Devices," by W.S. Pong, C.S. Tsai and G.C. Lee, 6/20/94, (PB94-219136, A10, A03).
- NCEER-94-0017 "Sliding Mode Control for Seismic-Excited Linear and Nonlinear Civil Engineering Structures," by J. Yang, J. Wu, A. Agrawal and Z. Li, 6/21/94, (PB95-138483, A06, MF-A02).
- NCEER-94-0018 "3D-BASIS-TABS Version 2.0: Computer Program for Nonlinear Dynamic Analysis of Three Dimensional Base Isolated Structures," by A.M. Reinhorn, S. Nagarajaiah, M.C. Constantinou, P. Tsopelas and R. Li, 6/22/94, (PB95-182176, A08, MF-A02).
- NCEER-94-0019 "Proceedings of the International Workshop on Civil Infrastructure Systems: Application of Intelligent Systems and Advanced Materials on Bridge Systems," Edited by G.C. Lee and K.C. Chang, 7/18/94, (PB95-252474, A20, MF-A04).
- NCEER-94-0020 "Study of Seismic Isolation Systems for Computer Floors," by V. Lambrou and M.C. Constantinou, 7/19/94, (PB95-138533, A10, MF-A03).
- NCEER-94-0021 "Proceedings of the U.S.-Italian Workshop on Guidelines for Seismic Evaluation and Rehabilitation of Unreinforced Masonry Buildings," Edited by D.P. Abrams and G.M. Calvi, 7/20/94, (PB95-138749, A13, MF-A03).
- NCEER-94-0022 "NCEER-Taisei Corporation Research Program on Sliding Seismic Isolation Systems for Bridges: Experimental and Analytical Study of a System Consisting of Lubricated PTFE Sliding Bearings and Mild Steel Dampers," by P. Tsopelas and M.C. Constantinou, 7/22/94, (PB95-182184, A08, MF-A02).
- NCEER-94-0023 "Development of Reliability-Based Design Criteria for Buildings Under Seismic Load," by Y.K. Wen, H. Hwang and M. Shinozuka, 8/1/94, (PB95-211934, A08, MF-A02).
- NCEER-94-0024 "Experimental Verification of Acceleration Feedback Control Strategies for an Active Tendon System," by S.J. Dyke, B.F. Spencer, Jr., P. Quast, M.K. Sain, D.C. Kaspari, Jr. and T.T. Soong, 8/29/94, (PB95-212320, A05, MF-A01).
- NCEER-94-0025 "Seismic Retrofitting Manual for Highway Bridges," Edited by I.G. Buckle and I.F. Friedland, published by the Federal Highway Administration (PB95-212676, A15, MF-A03).
- NCEER-94-0026 "Proceedings from the Fifth U.S.-Japan Workshop on Earthquake Resistant Design of Lifeline Facilities and Countermeasures Against Soil Liquefaction," Edited by T.D. O'Rourke and M. Hamada, 11/7/94, (PB95-220802, A99, MF-E08).



- NCEER-95-0001 “Experimental and Analytical Investigation of Seismic Retrofit of Structures with Supplemental Damping: Part 1 - Fluid Viscous Damping Devices,” by A.M. Reinhorn, C. Li and M.C. Constantinou, 1/3/95, (PB95-266599, A09, MF-A02).
- NCEER-95-0002 “Experimental and Analytical Study of Low-Cycle Fatigue Behavior of Semi-Rigid Top-And-Seat Angle Connections,” by G. Pekcan, J.B. Mander and S.S. Chen, 1/5/95, (PB95-220042, A07, MF-A02).
- NCEER-95-0003 “NCEER-ATC Joint Study on Fragility of Buildings,” by T. Anagnos, C. Rojahn and A.S. Kiremidjian, 1/20/95, (PB95-220026, A06, MF-A02).
- NCEER-95-0004 “Nonlinear Control Algorithms for Peak Response Reduction,” by Z. Wu, T.T. Soong, V. Gattulli and R.C. Lin, 2/16/95, (PB95-220349, A05, MF-A01).
- NCEER-95-0005 “Pipeline Replacement Feasibility Study: A Methodology for Minimizing Seismic and Corrosion Risks to Underground Natural Gas Pipelines,” by R.T. Eguchi, H.A. Seligson and D.G. Honegger, 3/2/95, (PB95-252326, A06, MF-A02).
- NCEER-95-0006 “Evaluation of Seismic Performance of an 11-Story Frame Building During the 1994 Northridge Earthquake,” by F. Naeim, R. DiSulio, K. Benuska, A. Reinhorn and C. Li, to be published.
- NCEER-95-0007 “Prioritization of Bridges for Seismic Retrofitting,” by N. Basöz and A.S. Kiremidjian, 4/24/95, (PB95-252300, A08, MF-A02).
- NCEER-95-0008 “Method for Developing Motion Damage Relationships for Reinforced Concrete Frames,” by A. Singhal and A.S. Kiremidjian, 5/11/95, (PB95-266607, A06, MF-A02).
- NCEER-95-0009 “Experimental and Analytical Investigation of Seismic Retrofit of Structures with Supplemental Damping: Part II - Friction Devices,” by C. Li and A.M. Reinhorn, 7/6/95, (PB96-128087, A11, MF-A03).
- NCEER-95-0010 “Experimental Performance and Analytical Study of a Non-Ductile Reinforced Concrete Frame Structure Retrofitted with Elastomeric Spring Dampers,” by G. Pekcan, J.B. Mander and S.S. Chen, 7/14/95, (PB96-137161, A08, MF-A02).
- NCEER-95-0011 “Development and Experimental Study of Semi-Active Fluid Damping Devices for Seismic Protection of Structures,” by M.D. Symans and M.C. Constantinou, 8/3/95, (PB96-136940, A23, MF-A04).
- NCEER-95-0012 “Real-Time Structural Parameter Modification (RSPM): Development of Innervated Structures,” by Z. Liang, M. Tong and G.C. Lee, 4/11/95, (PB96-137153, A06, MF-A01).
- NCEER-95-0013 “Experimental and Analytical Investigation of Seismic Retrofit of Structures with Supplemental Damping: Part III - Viscous Damping Walls,” by A.M. Reinhorn and C. Li, 10/1/95, (PB96-176409, A11, MF-A03).
- NCEER-95-0014 “Seismic Fragility Analysis of Equipment and Structures in a Memphis Electric Substation,” by J-R. Huo and H.H.M. Hwang, 8/10/95, (PB96-128087, A09, MF-A02).
- NCEER-95-0015 “The Hanshin-Awaji Earthquake of January 17, 1995: Performance of Lifelines,” Edited by M. Shinozuka, 11/3/95, (PB96-176383, A15, MF-A03).
- NCEER-95-0016 “Highway Culvert Performance During Earthquakes,” by T.L. Youd and C.J. Beckman, available as NCEER-96-0015.
- NCEER-95-0017 “The Hanshin-Awaji Earthquake of January 17, 1995: Performance of Highway Bridges,” Edited by I.G. Buckle, 12/1/95, to be published.
- NCEER-95-0018 “Modeling of Masonry Infill Panels for Structural Analysis,” by A.M. Reinhorn, A. Madan, R.E. Valles, Y. Reichmann and J.B. Mander, 12/8/95, (PB97-110886, MF-A01, A06).
- NCEER-95-0019 “Optimal Polynomial Control for Linear and Nonlinear Structures,” by A.K. Agrawal and J.N. Yang, 12/11/95, (PB96-168737, A07, MF-A02).

- NCEER-95-0020 “Retrofit of Non-Ductile Reinforced Concrete Frames Using Friction Dampers,” by R.S. Rao, P. Gergely and R.N. White, 12/22/95, (PB97-133508, A10, MF-A02).
- NCEER-95-0021 “Parametric Results for Seismic Response of Pile-Supported Bridge Bents,” by G. Mylonakis, A. Nikolaou and G. Gazetas, 12/22/95, (PB97-100242, A12, MF-A03).
- NCEER-95-0022 “Kinematic Bending Moments in Seismically Stressed Piles,” by A. Nikolaou, G. Mylonakis and G. Gazetas, 12/23/95, (PB97-113914, MF-A03, A13).
- NCEER-96-0001 “Dynamic Response of Unreinforced Masonry Buildings with Flexible Diaphragms,” by A.C. Costley and D.P. Abrams, 10/10/96, (PB97-133573, MF-A03, A15).
- NCEER-96-0002 “State of the Art Review: Foundations and Retaining Structures,” by I. Po Lam, to be published.
- NCEER-96-0003 “Ductility of Rectangular Reinforced Concrete Bridge Columns with Moderate Confinement,” by N. Wehbe, M. Saiidi, D. Sanders and B. Douglas, 11/7/96, (PB97-133557, A06, MF-A02).
- NCEER-96-0004 “Proceedings of the Long-Span Bridge Seismic Research Workshop,” edited by I.G. Buckle and I.M. Friedland, to be published.
- NCEER-96-0005 “Establish Representative Pier Types for Comprehensive Study: Eastern United States,” by J. Kulicki and Z. Prucz, 5/28/96, (PB98-119217, A07, MF-A02).
- NCEER-96-0006 “Establish Representative Pier Types for Comprehensive Study: Western United States,” by R. Imbsen, R.A. Schamber and T.A. Osterkamp, 5/28/96, (PB98-118607, A07, MF-A02).
- NCEER-96-0007 “Nonlinear Control Techniques for Dynamical Systems with Uncertain Parameters,” by R.G. Ghanem and M.I. Bujakov, 5/27/96, (PB97-100259, A17, MF-A03).
- NCEER-96-0008 “Seismic Evaluation of a 30-Year Old Non-Ductile Highway Bridge Pier and Its Retrofit,” by J.B. Mander, B. Mahmoodzadegan, S. Bhadra and S.S. Chen, 5/31/96, (PB97-110902, MF-A03, A10).
- NCEER-96-0009 “Seismic Performance of a Model Reinforced Concrete Bridge Pier Before and After Retrofit,” by J.B. Mander, J.H. Kim and C.A. Ligozio, 5/31/96, (PB97-110910, MF-A02, A10).
- NCEER-96-0010 “IDARC2D Version 4.0: A Computer Program for the Inelastic Damage Analysis of Buildings,” by R.E. Valles, A.M. Reinhorn, S.K. Kunnath, C. Li and A. Madan, 6/3/96, (PB97-100234, A17, MF-A03).
- NCEER-96-0011 “Estimation of the Economic Impact of Multiple Lifeline Disruption: Memphis Light, Gas and Water Division Case Study,” by S.E. Chang, H.A. Seligson and R.T. Eguchi, 8/16/96, (PB97-133490, A11, MF-A03).
- NCEER-96-0012 “Proceedings from the Sixth Japan-U.S. Workshop on Earthquake Resistant Design of Lifeline Facilities and Countermeasures Against Soil Liquefaction, Edited by M. Hamada and T. O’Rourke, 9/11/96, (PB97-133581, A99, MF-A06).
- NCEER-96-0013 “Chemical Hazards, Mitigation and Preparedness in Areas of High Seismic Risk: A Methodology for Estimating the Risk of Post-Earthquake Hazardous Materials Release,” by H.A. Seligson, R.T. Eguchi, K.J. Tierney and K. Richmond, 11/7/96, (PB97-133565, MF-A02, A08).
- NCEER-96-0014 “Response of Steel Bridge Bearings to Reversed Cyclic Loading,” by J.B. Mander, D-K. Kim, S.S. Chen and G.J. Premus, 11/13/96, (PB97-140735, A12, MF-A03).
- NCEER-96-0015 “Highway Culvert Performance During Past Earthquakes,” by T.L. Youd and C.J. Beckman, 11/25/96, (PB97-133532, A06, MF-A01).
- NCEER-97-0001 “Evaluation, Prevention and Mitigation of Pounding Effects in Building Structures,” by R.E. Valles and A.M. Reinhorn, 2/20/97, (PB97-159552, A14, MF-A03).
- NCEER-97-0002 “Seismic Design Criteria for Bridges and Other Highway Structures,” by C. Rojahn, R. Mayes, D.G. Anderson, J. Clark, J.H. Hom, R.V. Nutt and M.J. O’Rourke, 4/30/97, (PB97-194658, A06, MF-A03).

- NCEER-97-0003 "Proceedings of the U.S.-Italian Workshop on Seismic Evaluation and Retrofit," Edited by D.P. Abrams and G.M. Calvi, 3/19/97, (PB97-194666, A13, MF-A03).
- NCEER-97-0004 "Investigation of Seismic Response of Buildings with Linear and Nonlinear Fluid Viscous Dampers," by A.A. Seleemah and M.C. Constantinou, 5/21/97, (PB98-109002, A15, MF-A03).
- NCEER-97-0005 "Proceedings of the Workshop on Earthquake Engineering Frontiers in Transportation Facilities," edited by G.C. Lee and I.M. Friedland, 8/29/97, (PB98-128911, A25, MR-A04).
- NCEER-97-0006 "Cumulative Seismic Damage of Reinforced Concrete Bridge Piers," by S.K. Kunnath, A. El-Bahy, A. Taylor and W. Stone, 9/2/97, (PB98-108814, A11, MF-A03).
- NCEER-97-0007 "Structural Details to Accommodate Seismic Movements of Highway Bridges and Retaining Walls," by R.A. Imbsen, R.A. Schamber, E. Thorkildsen, A. Kartoum, B.T. Martin, T.N. Rosser and J.M. Kulicki, 9/3/97, (PB98-108996, A09, MF-A02).
- NCEER-97-0008 "A Method for Earthquake Motion-Damage Relationships with Application to Reinforced Concrete Frames," by A. Singhal and A.S. Kiremidjian, 9/10/97, (PB98-108988, A13, MF-A03).
- NCEER-97-0009 "Seismic Analysis and Design of Bridge Abutments Considering Sliding and Rotation," by K. Fishman and R. Richards, Jr., 9/15/97, (PB98-108897, A06, MF-A02).
- NCEER-97-0010 "Proceedings of the FHWA/NCEER Workshop on the National Representation of Seismic Ground Motion for New and Existing Highway Facilities," edited by I.M. Friedland, M.S. Power and R.L. Mayes, 9/22/97, (PB98-128903, A21, MF-A04).
- NCEER-97-0011 "Seismic Analysis for Design or Retrofit of Gravity Bridge Abutments," by K.L. Fishman, R. Richards, Jr. and R.C. Divito, 10/2/97, (PB98-128937, A08, MF-A02).
- NCEER-97-0012 "Evaluation of Simplified Methods of Analysis for Yielding Structures," by P. Tsopelas, M.C. Constantinou, C.A. Kircher and A.S. Whittaker, 10/31/97, (PB98-128929, A10, MF-A03).
- NCEER-97-0013 "Seismic Design of Bridge Columns Based on Control and Repairability of Damage," by C-T. Cheng and J.B. Mander, 12/8/97, (PB98-144249, A11, MF-A03).
- NCEER-97-0014 "Seismic Resistance of Bridge Piers Based on Damage Avoidance Design," by J.B. Mander and C-T. Cheng, 12/10/97, (PB98-144223, A09, MF-A02).
- NCEER-97-0015 "Seismic Response of Nominally Symmetric Systems with Strength Uncertainty," by S. Balopoulou and M. Grigoriu, 12/23/97, (PB98-153422, A11, MF-A03).
- NCEER-97-0016 "Evaluation of Seismic Retrofit Methods for Reinforced Concrete Bridge Columns," by T.J. Wipf, F.W. Klaiber and F.M. Russo, 12/28/97, (PB98-144215, A12, MF-A03).
- NCEER-97-0017 "Seismic Fragility of Existing Conventional Reinforced Concrete Highway Bridges," by C.L. Mullen and A.S. Cakmak, 12/30/97, (PB98-153406, A08, MF-A02).
- NCEER-97-0018 "Loss Assessment of Memphis Buildings," edited by D.P. Abrams and M. Shinozuka, 12/31/97, (PB98-144231, A13, MF-A03).
- NCEER-97-0019 "Seismic Evaluation of Frames with Infill Walls Using Quasi-static Experiments," by K.M. Mosalam, R.N. White and P. Gergely, 12/31/97, (PB98-153455, A07, MF-A02).
- NCEER-97-0020 "Seismic Evaluation of Frames with Infill Walls Using Pseudo-dynamic Experiments," by K.M. Mosalam, R.N. White and P. Gergely, 12/31/97, (PB98-153430, A07, MF-A02).
- NCEER-97-0021 "Computational Strategies for Frames with Infill Walls: Discrete and Smeared Crack Analyses and Seismic Fragility," by K.M. Mosalam, R.N. White and P. Gergely, 12/31/97, (PB98-153414, A10, MF-A02).

- NCEER-97-0022 "Proceedings of the NCEER Workshop on Evaluation of Liquefaction Resistance of Soils," edited by T.L. Youd and I.M. Idriss, 12/31/97, (PB98-155617, A15, MF-A03).
- MCEER-98-0001 "Extraction of Nonlinear Hysteretic Properties of Seismically Isolated Bridges from Quick-Release Field Tests," by Q. Chen, B.M. Douglas, E.M. Maragakis and I.G. Buckle, 5/26/98, (PB99-118838, A06, MF-A01).
- MCEER-98-0002 "Methodologies for Evaluating the Importance of Highway Bridges," by A. Thomas, S. Eshenaur and J. Kulicki, 5/29/98, (PB99-118846, A10, MF-A02).
- MCEER-98-0003 "Capacity Design of Bridge Piers and the Analysis of Overstrength," by J.B. Mander, A. Dutta and P. Goel, 6/1/98, (PB99-118853, A09, MF-A02).
- MCEER-98-0004 "Evaluation of Bridge Damage Data from the Loma Prieta and Northridge, California Earthquakes," by N. Basoz and A. Kiremidjian, 6/2/98, (PB99-118861, A15, MF-A03).
- MCEER-98-0005 "Screening Guide for Rapid Assessment of Liquefaction Hazard at Highway Bridge Sites," by T. L. Youd, 6/16/98, (PB99-118879, A06, not available on microfiche).
- MCEER-98-0006 "Structural Steel and Steel/Concrete Interface Details for Bridges," by P. Ritchie, N. Kaulh and J. Kulicki, 7/13/98, (PB99-118945, A06, MF-A01).
- MCEER-98-0007 "Capacity Design and Fatigue Analysis of Confined Concrete Columns," by A. Dutta and J.B. Mander, 7/14/98, (PB99-118960, A14, MF-A03).
- MCEER-98-0008 "Proceedings of the Workshop on Performance Criteria for Telecommunication Services Under Earthquake Conditions," edited by A.J. Schiff, 7/15/98, (PB99-118952, A08, MF-A02).
- MCEER-98-0009 "Fatigue Analysis of Unconfined Concrete Columns," by J.B. Mander, A. Dutta and J.H. Kim, 9/12/98, (PB99-123655, A10, MF-A02).
- MCEER-98-0010 "Centrifuge Modeling of Cyclic Lateral Response of Pile-Cap Systems and Seat-Type Abutments in Dry Sands," by A.D. Gadre and R. Dobry, 10/2/98, (PB99-123606, A13, MF-A03).
- MCEER-98-0011 "IDARC-BRIDGE: A Computational Platform for Seismic Damage Assessment of Bridge Structures," by A.M. Reinhorn, V. Simeonov, G. Mylonakis and Y. Reichman, 10/2/98, (PB99-162919, A15, MF-A03).
- MCEER-98-0012 "Experimental Investigation of the Dynamic Response of Two Bridges Before and After Retrofitting with Elastomeric Bearings," by D.A. Wendichansky, S.S. Chen and J.B. Mander, 10/2/98, (PB99-162927, A15, MF-A03).
- MCEER-98-0013 "Design Procedures for Hinge Restrainers and Hinge Sear Width for Multiple-Frame Bridges," by R. Des Roches and G.L. Fenves, 11/3/98, (PB99-140477, A13, MF-A03).
- MCEER-98-0014 "Response Modification Factors for Seismically Isolated Bridges," by M.C. Constantinou and J.K. Quarshie, 11/3/98, (PB99-140485, A14, MF-A03).
- MCEER-98-0015 "Proceedings of the U.S.-Italy Workshop on Seismic Protective Systems for Bridges," edited by I.M. Friedland and M.C. Constantinou, 11/3/98, (PB2000-101711, A22, MF-A04).
- MCEER-98-0016 "Appropriate Seismic Reliability for Critical Equipment Systems: Recommendations Based on Regional Analysis of Financial and Life Loss," by K. Porter, C. Scawthorn, C. Taylor and N. Blais, 11/10/98, (PB99-157265, A08, MF-A02).
- MCEER-98-0017 "Proceedings of the U.S. Japan Joint Seminar on Civil Infrastructure Systems Research," edited by M. Shinozuka and A. Rose, 11/12/98, (PB99-156713, A16, MF-A03).
- MCEER-98-0018 "Modeling of Pile Footings and Drilled Shafts for Seismic Design," by I. PoLam, M. Kapuskar and D. Chaudhuri, 12/21/98, (PB99-157257, A09, MF-A02).

- MCEER-99-0001 "Seismic Evaluation of a Masonry Infilled Reinforced Concrete Frame by Pseudodynamic Testing," by S.G. Buonopane and R.N. White, 2/16/99, (PB99-162851, A09, MF-A02).
- MCEER-99-0002 "Response History Analysis of Structures with Seismic Isolation and Energy Dissipation Systems: Verification Examples for Program SAP2000," by J. Scheller and M.C. Constantinou, 2/22/99, (PB99-162869, A08, MF-A02).
- MCEER-99-0003 "Experimental Study on the Seismic Design and Retrofit of Bridge Columns Including Axial Load Effects," by A. Dutta, T. Kokorina and J.B. Mander, 2/22/99, (PB99-162877, A09, MF-A02).
- MCEER-99-0004 "Experimental Study of Bridge Elastomeric and Other Isolation and Energy Dissipation Systems with Emphasis on Uplift Prevention and High Velocity Near-source Seismic Excitation," by A. Kasalanati and M. C. Constantinou, 2/26/99, (PB99-162885, A12, MF-A03).
- MCEER-99-0005 "Truss Modeling of Reinforced Concrete Shear-flexure Behavior," by J.H. Kim and J.B. Mander, 3/8/99, (PB99-163693, A12, MF-A03).
- MCEER-99-0006 "Experimental Investigation and Computational Modeling of Seismic Response of a 1:4 Scale Model Steel Structure with a Load Balancing Supplemental Damping System," by G. Pekcan, J.B. Mander and S.S. Chen, 4/2/99, (PB99-162893, A11, MF-A03).
- MCEER-99-0007 "Effect of Vertical Ground Motions on the Structural Response of Highway Bridges," by M.R. Button, C.J. Cronin and R.L. Mayes, 4/10/99, (PB2000-101411, A10, MF-A03).
- MCEER-99-0008 "Seismic Reliability Assessment of Critical Facilities: A Handbook, Supporting Documentation, and Model Code Provisions," by G.S. Johnson, R.E. Sheppard, M.D. Quilici, S.J. Eder and C.R. Scawthorn, 4/12/99, (PB2000-101701, A18, MF-A04).
- MCEER-99-0009 "Impact Assessment of Selected MCEER Highway Project Research on the Seismic Design of Highway Structures," by C. Rojahn, R. Mayes, D.G. Anderson, J.H. Clark, D'Appolonia Engineering, S. Gloyd and R.V. Nutt, 4/14/99, (PB99-162901, A10, MF-A02).
- MCEER-99-0010 "Site Factors and Site Categories in Seismic Codes," by R. Dobry, R. Ramos and M.S. Power, 7/19/99, (PB2000-101705, A08, MF-A02).
- MCEER-99-0011 "Restrainer Design Procedures for Multi-Span Simply-Supported Bridges," by M.J. Randall, M. Saiidi, E. Maragakis and T. Isakovic, 7/20/99, (PB2000-101702, A10, MF-A02).
- MCEER-99-0012 "Property Modification Factors for Seismic Isolation Bearings," by M.C. Constantinou, P. Tsopelas, A. Kasalanati and E. Wolff, 7/20/99, (PB2000-103387, A11, MF-A03).
- MCEER-99-0013 "Critical Seismic Issues for Existing Steel Bridges," by P. Ritchie, N. Kauh and J. Kulicki, 7/20/99, (PB2000-101697, A09, MF-A02).
- MCEER-99-0014 "Nonstructural Damage Database," by A. Kao, T.T. Soong and A. Vender, 7/24/99, (PB2000-101407, A06, MF-A01).
- MCEER-99-0015 "Guide to Remedial Measures for Liquefaction Mitigation at Existing Highway Bridge Sites," by H.G. Cooke and J. K. Mitchell, 7/26/99, (PB2000-101703, A11, MF-A03).
- MCEER-99-0016 "Proceedings of the MCEER Workshop on Ground Motion Methodologies for the Eastern United States," edited by N. Abrahamson and A. Becker, 8/11/99, (PB2000-103385, A07, MF-A02).
- MCEER-99-0017 "Quindío, Colombia Earthquake of January 25, 1999: Reconnaissance Report," by A.P. Asfura and P.J. Flores, 10/4/99, (PB2000-106893, A06, MF-A01).
- MCEER-99-0018 "Hysteretic Models for Cyclic Behavior of Deteriorating Inelastic Structures," by M.V. Sivaselvan and A.M. Reinhorn, 11/5/99, (PB2000-103386, A08, MF-A02).

- MCEER-99-0019 "Proceedings of the 7<sup>th</sup> U.S.- Japan Workshop on Earthquake Resistant Design of Lifeline Facilities and Countermeasures Against Soil Liquefaction," edited by T.D. O'Rourke, J.P. Bardet and M. Hamada, 11/19/99, (PB2000-103354, A99, MF-A06).
- MCEER-99-0020 "Development of Measurement Capability for Micro-Vibration Evaluations with Application to Chip Fabrication Facilities," by G.C. Lee, Z. Liang, J.W. Song, J.D. Shen and W.C. Liu, 12/1/99, (PB2000-105993, A08, MF-A02).
- MCEER-99-0021 "Design and Retrofit Methodology for Building Structures with Supplemental Energy Dissipating Systems," by G. Pekcan, J.B. Mander and S.S. Chen, 12/31/99, (PB2000-105994, A11, MF-A03).
- MCEER-00-0001 "The Marmara, Turkey Earthquake of August 17, 1999: Reconnaissance Report," edited by C. Scawthorn; with major contributions by M. Bruneau, R. Eguchi, T. Holzer, G. Johnson, J. Mander, J. Mitchell, W. Mitchell, A. Papageorgiou, C. Scaethorn, and G. Webb, 3/23/00, (PB2000-106200, A11, MF-A03).
- MCEER-00-0002 "Proceedings of the MCEER Workshop for Seismic Hazard Mitigation of Health Care Facilities," edited by G.C. Lee, M. Ettouney, M. Grigoriu, J. Hauer and J. Nigg, 3/29/00, (PB2000-106892, A08, MF-A02).
- MCEER-00-0003 "The Chi-Chi, Taiwan Earthquake of September 21, 1999: Reconnaissance Report," edited by G.C. Lee and C.H. Loh, with major contributions by G.C. Lee, M. Bruneau, I.G. Buckle, S.E. Chang, P.J. Flores, T.D. O'Rourke, M. Shinozuka, T.T. Soong, C-H. Loh, K-C. Chang, Z-J. Chen, J-S. Hwang, M-L. Lin, G-Y. Liu, K-C. Tsai, G.C. Yao and C-L. Yen, 4/30/00, (PB2001-100980, A10, MF-A02).
- MCEER-00-0004 "Seismic Retrofit of End-Sway Frames of Steel Deck-Truss Bridges with a Supplemental Tendon System: Experimental and Analytical Investigation," by G. Pekcan, J.B. Mander and S.S. Chen, 7/1/00, (PB2001-100982, A10, MF-A02).
- MCEER-00-0005 "Sliding Fragility of Unrestrained Equipment in Critical Facilities," by W.H. Chong and T.T. Soong, 7/5/00, (PB2001-100983, A08, MF-A02).
- MCEER-00-0006 "Seismic Response of Reinforced Concrete Bridge Pier Walls in the Weak Direction," by N. Abo-Shadi, M. Saiidi and D. Sanders, 7/17/00, (PB2001-100981, A17, MF-A03).
- MCEER-00-0007 "Low-Cycle Fatigue Behavior of Longitudinal Reinforcement in Reinforced Concrete Bridge Columns," by J. Brown and S.K. Kunnath, 7/23/00, (PB2001-104392, A08, MF-A02).
- MCEER-00-0008 "Soil Structure Interaction of Bridges for Seismic Analysis," I. PoLam and H. Law, 9/25/00, (PB2001-105397, A08, MF-A02).
- MCEER-00-0009 "Proceedings of the First MCEER Workshop on Mitigation of Earthquake Disaster by Advanced Technologies (MEDAT-1), edited by M. Shinozuka, D.J. Inman and T.D. O'Rourke, 11/10/00, (PB2001-105399, A14, MF-A03).
- MCEER-00-0010 "Development and Evaluation of Simplified Procedures for Analysis and Design of Buildings with Passive Energy Dissipation Systems, Revision 01," by O.M. Ramirez, M.C. Constantinou, C.A. Kircher, A.S. Whittaker, M.W. Johnson, J.D. Gomez and C. Chrysostomou, 11/16/01, (PB2001-105523, A23, MF-A04).
- MCEER-00-0011 "Dynamic Soil-Foundation-Structure Interaction Analyses of Large Caissons," by C-Y. Chang, C-M. Mok, Z-L. Wang, R. Settgast, F. Waggoner, M.A. Ketchum, H.M. Gonnermann and C-C. Chin, 12/30/00, (PB2001-104373, A07, MF-A02).
- MCEER-00-0012 "Experimental Evaluation of Seismic Performance of Bridge Restrainers," by A.G. Vlassis, E.M. Maragakis and M. Saiid Saiidi, 12/30/00, (PB2001-104354, A09, MF-A02).
- MCEER-00-0013 "Effect of Spatial Variation of Ground Motion on Highway Structures," by M. Shinozuka, V. Saxena and G. Deodatis, 12/31/00, (PB2001-108755, A13, MF-A03).
- MCEER-00-0014 "A Risk-Based Methodology for Assessing the Seismic Performance of Highway Systems," by S.D. Werner, C.E. Taylor, J.E. Moore, II, J.S. Walton and S. Cho, 12/31/00, (PB2001-108756, A14, MF-A03).

- MCEER-01-0001 "Experimental Investigation of P-Delta Effects to Collapse During Earthquakes," by D. Vian and M. Bruneau, 6/25/01, (PB2002-100534, A17, MF-A03).
- MCEER-01-0002 "Proceedings of the Second MCEER Workshop on Mitigation of Earthquake Disaster by Advanced Technologies (MEDAT-2)," edited by M. Bruneau and D.J. Inman, 7/23/01, (PB2002-100434, A16, MF-A03).
- MCEER-01-0003 "Sensitivity Analysis of Dynamic Systems Subjected to Seismic Loads," by C. Roth and M. Grigoriu, 9/18/01, (PB2003-100884, A12, MF-A03).
- MCEER-01-0004 "Overcoming Obstacles to Implementing Earthquake Hazard Mitigation Policies: Stage 1 Report," by D.J. Alesch and W.J. Petak, 12/17/01, (PB2002-107949, A07, MF-A02).
- MCEER-01-0005 "Updating Real-Time Earthquake Loss Estimates: Methods, Problems and Insights," by C.E. Taylor, S.E. Chang and R.T. Eguchi, 12/17/01, (PB2002-107948, A05, MF-A01).
- MCEER-01-0006 "Experimental Investigation and Retrofit of Steel Pile Foundations and Pile Bents Under Cyclic Lateral Loadings," by A. Shama, J. Mander, B. Blabac and S. Chen, 12/31/01, (PB2002-107950, A13, MF-A03).
- MCEER-02-0001 "Assessment of Performance of Bolu Viaduct in the 1999 Duzce Earthquake in Turkey" by P.C. Roussis, M.C. Constantinou, M. Erdik, E. Durukal and M. Dicleli, 5/8/02, (PB2003-100883, A08, MF-A02).
- MCEER-02-0002 "Seismic Behavior of Rail Counterweight Systems of Elevators in Buildings," by M.P. Singh, Rildova and L.E. Suarez, 5/27/02. (PB2003-100882, A11, MF-A03).
- MCEER-02-0003 "Development of Analysis and Design Procedures for Spread Footings," by G. Mylonakis, G. Gazetas, S. Nikolaou and A. Chauncey, 10/02/02, (PB2004-101636, A13, MF-A03, CD-A13).
- MCEER-02-0004 "Bare-Earth Algorithms for Use with SAR and LIDAR Digital Elevation Models," by C.K. Huyck, R.T. Eguchi and B. Houshmand, 10/16/02, (PB2004-101637, A07, CD-A07).
- MCEER-02-0005 "Review of Energy Dissipation of Compression Members in Concentrically Braced Frames," by K.Lee and M. Bruneau, 10/18/02, (PB2004-101638, A10, CD-A10).
- MCEER-03-0001 "Experimental Investigation of Light-Gauge Steel Plate Shear Walls for the Seismic Retrofit of Buildings" by J. Berman and M. Bruneau, 5/2/03, (PB2004-101622, A10, MF-A03, CD-A10).
- MCEER-03-0002 "Statistical Analysis of Fragility Curves," by M. Shinozuka, M.Q. Feng, H. Kim, T. Uzawa and T. Ueda, 6/16/03, (PB2004-101849, A09, CD-A09).
- MCEER-03-0003 "Proceedings of the Eighth U.S.-Japan Workshop on Earthquake Resistant Design of Lifeline Facilities and Countermeasures Against Liquefaction," edited by M. Hamada, J.P. Bardet and T.D. O'Rourke, 6/30/03, (PB2004-104386, A99, CD-A99).
- MCEER-03-0004 "Proceedings of the PRC-US Workshop on Seismic Analysis and Design of Special Bridges," edited by L.C. Fan and G.C. Lee, 7/15/03, (PB2004-104387, A14, CD-A14).
- MCEER-03-0005 "Urban Disaster Recovery: A Framework and Simulation Model," by S.B. Miles and S.E. Chang, 7/25/03, (PB2004-104388, A07, CD-A07).
- MCEER-03-0006 "Behavior of Underground Piping Joints Due to Static and Dynamic Loading," by R.D. Meis, M. Maragakis and R. Siddharthan, 11/17/03, (PB2005-102194, A13, MF-A03, CD-A00).
- MCEER-03-0007 "Seismic Vulnerability of Timber Bridges and Timber Substructures," by A.A. Shama, J.B. Mander, I.M. Friedland and D.R. Allicock, 12/15/03.
- MCEER-04-0001 "Experimental Study of Seismic Isolation Systems with Emphasis on Secondary System Response and Verification of Accuracy of Dynamic Response History Analysis Methods," by E. Wolff and M. Constantinou, 1/16/04 (PB2005-102195, A99, MF-E08, CD-A00).


- MCEER-04-0002 “Tension, Compression and Cyclic Testing of Engineered Cementitious Composite Materials,” by K. Kesner and S.L. Billington, 3/1/04, (PB2005-102196, A08, CD-A08).
- MCEER-04-0003 “Cyclic Testing of Braces Laterally Restrained by Steel Studs to Enhance Performance During Earthquakes,” by O.C. Celik, J.W. Berman and M. Bruneau, 3/16/04, (PB2005-102197, A13, MF-A03, CD-A00).
- MCEER-04-0004 “Methodologies for Post Earthquake Building Damage Detection Using SAR and Optical Remote Sensing: Application to the August 17, 1999 Marmara, Turkey Earthquake,” by C.K. Huyck, B.J. Adams, S. Cho, R.T. Eguchi, B. Mansouri and B. Houshmand, 6/15/04, (PB2005-104888, A10, CD-A00).
- MCEER-04-0005 “Nonlinear Structural Analysis Towards Collapse Simulation: A Dynamical Systems Approach,” by M.V. Sivaselvan and A.M. Reinhorn, 6/16/04, (PB2005-104889, A11, MF-A03, CD-A00).
- MCEER-04-0006 “Proceedings of the Second PRC-US Workshop on Seismic Analysis and Design of Special Bridges,” edited by G.C. Lee and L.C. Fan, 6/25/04, (PB2005-104890, A16, CD-A00).
- MCEER-04-0007 “Seismic Vulnerability Evaluation of Axially Loaded Steel Built-up Laced Members,” by K. Lee and M. Bruneau, 6/30/04, (PB2005-104891, A16, CD-A00).
- MCEER-04-0008 “Evaluation of Accuracy of Simplified Methods of Analysis and Design of Buildings with Damping Systems for Near-Fault and for Soft-Soil Seismic Motions,” by E.A. Pavlou and M.C. Constantinou, 8/16/04, (PB2005-104892, A08, MF-A02, CD-A00).
- MCEER-04-0009 “Assessment of Geotechnical Issues in Acute Care Facilities in California,” by M. Lew, T.D. O’Rourke, R. Dobry and M. Koch, 9/15/04, (PB2005-104893, A08, CD-A00).
- MCEER-04-0010 “Scissor-Jack-Damper Energy Dissipation System,” by A.N. Sigaher-Boyle and M.C. Constantinou, 12/1/04 (PB2005-108221).
- MCEER-04-0011 “Seismic Retrofit of Bridge Steel Truss Piers Using a Controlled Rocking Approach,” by M. Pollino and M. Bruneau, 12/20/04 (PB2006-105795).
- MCEER-05-0001 “Experimental and Analytical Studies of Structures Seismically Isolated with an Uplift-Restraint Isolation System,” by P.C. Roussis and M.C. Constantinou, 1/10/05 (PB2005-108222).
- MCEER-05-0002 “A Versatile Experimentation Model for Study of Structures Near Collapse Applied to Seismic Evaluation of Irregular Structures,” by D. Kusumastuti, A.M. Reinhorn and A. Rutenberg, 3/31/05 (PB2006-101523).
- MCEER-05-0003 “Proceedings of the Third PRC-US Workshop on Seismic Analysis and Design of Special Bridges,” edited by L.C. Fan and G.C. Lee, 4/20/05, (PB2006-105796).
- MCEER-05-0004 “Approaches for the Seismic Retrofit of Braced Steel Bridge Piers and Proof-of-Concept Testing of an Eccentrically Braced Frame with Tubular Link,” by J.W. Berman and M. Bruneau, 4/21/05 (PB2006-101524).
- MCEER-05-0005 “Simulation of Strong Ground Motions for Seismic Fragility Evaluation of Nonstructural Components in Hospitals,” by A. Wanitkorkul and A. Filiatrault, 5/26/05 (PB2006-500027).
- MCEER-05-0006 “Seismic Safety in California Hospitals: Assessing an Attempt to Accelerate the Replacement or Seismic Retrofit of Older Hospital Facilities,” by D.J. Alesch, L.A. Arendt and W.J. Petak, 6/6/05 (PB2006-105794).
- MCEER-05-0007 “Development of Seismic Strengthening and Retrofit Strategies for Critical Facilities Using Engineered Cementitious Composite Materials,” by K. Kesner and S.L. Billington, 8/29/05 (PB2006-111701).
- MCEER-05-0008 “Experimental and Analytical Studies of Base Isolation Systems for Seismic Protection of Power Transformers,” by N. Murota, M.Q. Feng and G-Y. Liu, 9/30/05 (PB2006-111702).
- MCEER-05-0009 “3D-BASIS-ME-MB: Computer Program for Nonlinear Dynamic Analysis of Seismically Isolated Structures,” by P.C. Tsopelas, P.C. Roussis, M.C. Constantinou, R. Buchanan and A.M. Reinhorn, 10/3/05 (PB2006-111703).



- MCEER-05-0010 "Steel Plate Shear Walls for Seismic Design and Retrofit of Building Structures," by D. Vian and M. Bruneau, 12/15/05 (PB2006-111704).
- MCEER-05-0011 "The Performance-Based Design Paradigm," by M.J. Astrella and A. Whittaker, 12/15/05 (PB2006-111705).
- MCEER-06-0001 "Seismic Fragility of Suspended Ceiling Systems," H. Badillo-Almaraz, A.S. Whittaker, A.M. Reinhorn and G.P. Cimellaro, 2/4/06 (PB2006-111706).
- MCEER-06-0002 "Multi-Dimensional Fragility of Structures," by G.P. Cimellaro, A.M. Reinhorn and M. Bruneau, 3/1/06 (PB2007-106974, A09, MF-A02, CD A00).
- MCEER-06-0003 "Built-Up Shear Links as Energy Dissipators for Seismic Protection of Bridges," by P. Dusicka, A.M. Itani and I.G. Buckle, 3/15/06 (PB2006-111708).
- MCEER-06-0004 "Analytical Investigation of the Structural Fuse Concept," by R.E. Vargas and M. Bruneau, 3/16/06 (PB2006-111709).
- MCEER-06-0005 "Experimental Investigation of the Structural Fuse Concept," by R.E. Vargas and M. Bruneau, 3/17/06 (PB2006-111710).
- MCEER-06-0006 "Further Development of Tubular Eccentrically Braced Frame Links for the Seismic Retrofit of Braced Steel Truss Bridge Piers," by J.W. Berman and M. Bruneau, 3/27/06 (PB2007-105147).
- MCEER-06-0007 "REDARS Validation Report," by S. Cho, C.K. Huyck, S. Ghosh and R.T. Eguchi, 8/8/06 (PB2007-106983).
- MCEER-06-0008 "Review of Current NDE Technologies for Post-Earthquake Assessment of Retrofitted Bridge Columns," by J.W. Song, Z. Liang and G.C. Lee, 8/21/06 06 (PB2007-106984).
- MCEER-06-0009 "Liquefaction Remediation in Silty Soils Using Dynamic Compaction and Stone Columns," by S. Thevanayagam, G.R. Martin, R. Nashed, T. Shenthan, T. Kanagalingam and N. Ecemis, 8/28/06 06 (PB2007-106985).
- MCEER-06-0010 "Conceptual Design and Experimental Investigation of Polymer Matrix Composite Infill Panels for Seismic Retrofitting," by W. Jung, M. Chiewanichakorn and A.J. Aref, 9/21/06 (PB2007-106986).
- MCEER-06-0011 "A Study of the Coupled Horizontal-Vertical Behavior of Elastomeric and Lead-Rubber Seismic Isolation Bearings," by G.P. Warn and A.S. Whittaker, 9/22/06 (PB2007-108679).
- MCEER-06-0012 "Proceedings of the Fourth PRC-US Workshop on Seismic Analysis and Design of Special Bridges: Advancing Bridge Technologies in Research, Design, Construction and Preservation," Edited by L.C. Fan, G.C. Lee and L. Ziang, 10/12/06 (PB2007-109042).
- MCEER-06-0013 "Cyclic Response and Low Cycle Fatigue Characteristics of Plate Steels," by P. Dusicka, A.M. Itani and I.G. Buckle, 11/1/06 06 (PB2007-106987).
- MCEER-06-0014 "Proceedings of the Second US-Taiwan Bridge Engineering Workshop," edited by W.P. Yen, J. Shen, J-Y. Chen and M. Wang, 11/15/06.
- MCEER-06-0015 "User Manual and Technical Documentation for the REDARS<sup>TM</sup> Import Wizard," by S. Cho, S. Ghosh, C.K. Huyck and S.D. Werner, 11/30/06 (PB2007-114766).
- MCEER-06-0016 "Hazard Mitigation Strategy and Monitoring Technologies for Urban and Infrastructure Public Buildings: Proceedings of the China-US Workshops," edited by X.Y. Zhou, A.L. Zhang, G.C. Lee and M. Tong, 12/12/06.
- MCEER-07-0001 "Static and Kinetic Coefficients of Friction for Rigid Blocks," by C. Kafali, S. Fathali, M. Grigoriu and A.S. Whittaker, 3/20/07 (PB2007-114767).
- MCEER-07-0002 "Hazard Mitigation Investment Decision Making: Organizational Response to Legislative Mandate," by L.A. Arendt, D.J. Alesch and W.J. Petak, 4/9/07 (PB2007-114768).


- MCEER-07-0003 “Seismic Behavior of Bidirectional-Resistant Ductile End Diaphragms with Unbonded Braces in Straight or Skewed Steel Bridges,” by O. Celik and M. Bruneau, 4/11/07 (PB2008-105141).
- MCEER-07-0004 “Modeling Pile Behavior in Large Pile Groups Under Lateral Loading,” by A.M. Dodds and G.R. Martin, 4/16/07(PB2008-105142).
- MCEER-07-0005 “Experimental Investigation of Blast Performance of Seismically Resistant Concrete-Filled Steel Tube Bridge Piers,” by S. Fujikura, M. Bruneau and D. Lopez-Garcia, 4/20/07 (PB2008-105143).
- MCEER-07-0006 “Seismic Analysis of Conventional and Isolated Liquefied Natural Gas Tanks Using Mechanical Analogs,” by I.P. Christovasilis and A.S. Whittaker, 5/1/07.
- MCEER-07-0007 “Experimental Seismic Performance Evaluation of Isolation/Restraint Systems for Mechanical Equipment – Part 1: Heavy Equipment Study,” by S. Fathali and A. Filiatrault, 6/6/07 (PB2008-105144).
- MCEER-07-0008 “Seismic Vulnerability of Timber Bridges and Timber Substructures,” by A.A. Sharma, J.B. Mander, I.M. Friedland and D.R. Allicock, 6/7/07 (PB2008-105145).
- MCEER-07-0009 “Experimental and Analytical Study of the XY-Friction Pendulum (XY-FP) Bearing for Bridge Applications,” by C.C. Marin-Artieda, A.S. Whittaker and M.C. Constantinou, 6/7/07.
- MCEER-07-0010 “Proceedings of the PRC-US Earthquake Engineering Forum for Young Researchers,” Edited by G.C. Lee and X.Z. Qi, 6/8/07.
- MCEER-07-0011 “Design Recommendations for Perforated Steel Plate Shear Walls,” by R. Purba and M. Bruneau, 6/18/07.
- MCEER-07-0012 “Performance of Seismic Isolation Hardware Under Service and Seismic Loading,” by M.C. Constantinou, A.S. Whittaker, Y. Kalpakidis, D.M. Fenz and G.P. Warn, 8/27/07.
- MCEER-07-0013 “Experimental Evaluation of the Seismic Performance of Hospital Piping Subassemblies,” by E.R. Goodwin, E. Maragakis and A.M. Itani, 9/4/07.
- MCEER-07-0014 “A Simulation Model of Urban Disaster Recovery and Resilience: Implementation for the 1994 Northridge Earthquake,” by S. Miles and S.E. Chang, 9/7/07.
- MCEER-07-0015 “Statistical and Mechanistic Fragility Analysis of Concrete Bridges,” by M. Shinozuka, S. Banerjee and S-H. Kim, 9/10/07.
- MCEER-07-0016 “Three-Dimensional Modeling of Inelastic Buckling in Frame Structures,” by M. Schachter and AM. Reinhorn, 9/13/07.
- MCEER-07-0017 “Modeling of Seismic Wave Scattering on Pile Groups and Caissons,” by I. Po Lam, H. Law and C.T. Yang, 9/17/07.
- MCEER-07-0018 “Bridge Foundations: Modeling Large Pile Groups and Caissons for Seismic Design,” by I. Po Lam, H. Law and G.R. Martin (Coordinating Author), 12/1/07.
- MCEER-07-0019 “Principles and Performance of Roller Seismic Isolation Bearings for Highway Bridges,” by G.C. Lee, Y.C. Ou, Z. Liang, T.C. Niu and J. Song, 12/10/07.
- MCEER-07-0020 “Centrifuge Modeling of Permeability and Pinning Reinforcement Effects on Pile Response to Lateral Spreading,” by L.L. Gonzalez-Lagos, T. Abdoun and R. Dobry, 12/10/07.
- MCEER-07-0021 “Damage to the Highway System from the Pisco, Perú Earthquake of August 15, 2007,” by J.S. O’Connor, L. Mesa and M. Nykamp, 12/10/07.
- MCEER-07-0022 “Experimental Seismic Performance Evaluation of Isolation/Restraint Systems for Mechanical Equipment – Part 2: Light Equipment Study,” by S. Fathali and A. Filiatrault, 12/13/07.
- MCEER-07-0023 “Fragility Considerations in Highway Bridge Design,” by M. Shinozuka, S. Banerjee and S.H. Kim, 12/14/07.





**EARTHQUAKE ENGINEERING TO EXTREME EVENTS**

University at Buffalo, The State University of New York  
Red Jacket Quadrangle ▪ Buffalo, New York 14261  
Phone: (716) 645-3391 ▪ Fax: (716) 645-3399  
E-mail: [mceer@buffalo.edu](mailto:mceer@buffalo.edu) ▪ WWW Site <http://mceer.buffalo.edu>



University at Buffalo *The State University of New York*

ISSN 1520-295X